SHORT-TERM AIR QUALITY FORECASTS FOR THE PACIFIC NORTHWEST AND LONG-RANGE GLOBAL CHANGE PREDICTIONS FOR THE U.S.

By

JACK CHI-MOU CHEN

A dissertation submitted in partial fulfillment of
the requirements for the degree of

DOCTOR OF PHILOSOPHY

WASHINGTON STATE UNIVERSITY
Department of Civil and Environmental Engineering

MAY 2007

To the Faculty of Washington State University:

The members of the Committee appointed to examine the dissertation of JACK CHI-MOU CHEN find it satisfactory and recommend that it be accepted.

Chair

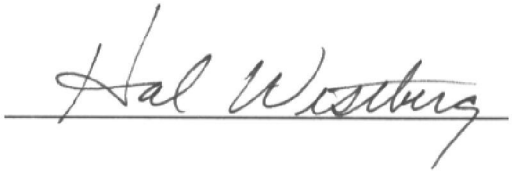

ACKNOWLEDGMENT

I would like to express my deepest gratitude to my graduate advisor and chair, Dr. Brian Lamb, for his guidance, support and encouragement during my years at the Washington State University. He has inspired me not just professionally but also personally. I thank him for showing me the field of air quality modeling. I lookup to him on what I would do if I become an academic professor, and I am learning from him on the ability to balance family, work and fun.

I would like to thank my committee Dr. Hal Westberg, Dr. George Mount and Dr. Alex Guenther for their guidance over the years, and their comments and suggestions on the research work.

I would like to thank Dr. Alex Guenther and Dr. Christine Wiedinmyer for offering me the valuable opportunity to work at NCAR in the summer of 2005. It was a wonderful experience. Special thank to Dr. Christine Wiedinmyer for not just her professional help in this research, but also her cheerfulness and hospitality.

I would like to acknowledge the financial support from the Boeing Endowment, the NW-AIRQUEST Consortium and the US EPA Science to Achieve Results (STAR) research grant. I thank the Washington State Ecology for facilitating the funding of the AIRPACT project, especially Clint Bowman and Sally Otterson for helping with various data inquiries. Many thanks to the collaborators: University of Washington, Puget Sound Clean Air Agency and USDA Forest Service for sharing their expertise, resources and data.

I would like to thank the professional staff in the WSU Civil & Environmental Engineering Department for their administrative assistance: Tom Weber, Maureen Clausen, Lola Gillespie, Cyndi Whitmore, and Vicki Ruddick.

I would also like to express my appreciation to the past and present members of the LAR graduate students. They are the ones that made graduate studentship fun and interesting. Thank go to the “AQ modelers”: Dr. Joe Vaughan, Jeremy Avise, Ying Xie, Matt Porter and Farren Thrope. I appreciate the collaboration with Jeremy Avise on various projects; we make a great team. Special thank to the “Goddesses” of LAR – Dr. Susan O’Neill, Dr. Shelley Pressley and Dr. Tara Strand. It had been wonderful and enjoyable experiences sharing the lovely office – Dana 334 – with you.

Finally, and most importantly, I would like to thank my family for their endless love, support, and encouragement throughout my student life: the Chen family and the Tam family. No words can express my sincere gratitude to my parents for their guidance and upbringing, and to my marriage parents for their understanding and support. I also thank my wife, Maggie, for her persistence, encouragement, and understanding throughout the wonderful time we had in Pullman, WA, USA.

SHORT-TERM AIR QUALITY FORECASTS FOR THE PACIFIC NORTHWEST AND LONG-RANGE GLOBAL CHANGE PREDICTIONS FOR THE U.S.

Abstract

by Jack Chi-Mou Chen, Ph.D.

Washington State University
May 2007

Chair: Brian K. Lamb

This dissertation presents the development and evaluation of a comprehensive numerical air quality modeling system designed to provide daily forecasts in the Pacific Northwest. The system was also applied to predict the impact of global change upon air quality in the future for the US. This system employs the EPA Community Multi-scale Air Quality (CMAQ) model to treat photochemical gas and aerosol formation, transport and deposition.

For short-term regional air quality forecasts, CMAQ was coupled with the University of Washington meteorological forecast operations using the MM5 weather model to create a regional system called AIRPACT-3. An important aspect of the development was the use of an automated, dynamic emissions processing system. The detailed evaluation of the system against observational data covering a four month period showed the system performed well. For ozone, it correctly predicted high episodic conditions, but over-predicted lower observed concentrations. For $PM_{2.5}$, it captured concentration variations between urban and rural regions, and concentrations of nitrate and ammonium $PM_{2.5}$ components, but under-predicted sulfate $PM_{2.5}$.

For global change impacts on US regional air quality, the CMAQ model was employed along with MM5 to downscale results from the Parallel Climate Model and the MOZART2 global

chemistry model based upon the IPCC A2 'business as usual' scenario. US anthropogenic emissions were projected using the EPA EGAS economic model and biogenic emissions were projected using the MEGAN model with adjusted land use. Evaluation using a decade of ozone measurements showed that the system reproduced episodic conditions (defined as the 98th percentile of daily maximum 8-hr concentration) with a predicted average US concentration of 93 ppbv and a measured concentration of 90 ppbv. Predictions for 2045-2054 indicated poorer air quality for the selected future scenario. The results showed that the future average daily maximum 8-hour ozone concentration will increase 8 ppbv, and larger areas of the US will be impacted at ozone levels greater than 80 ppbv. Additional simulations showed changing future land use and land cover scenarios significantly reduced the magnitude and spatial distributions of future biogenic emissions, which subsequently reduced ozone and secondary organic aerosol levels in the future.

TABLE OF CONTENTS

LIST OF TABLES

CHAPTER TWO:

CHAPTER THREE:

CHAPTER FOUR:

LIST OF FIGURES

CHAPTER TWO:

CHAPTER THREE:

CHAPTER FOUR:

ATTRIBUTION

This dissertation consists of five chapters. Chapter 1 is an overall introduction to the research work and an overview of the model system used in the study, Chapters 2, 3 and 4 are independent manuscripts that will be submitted for publication. Chapter 5 contains the general summary and conclusions from the research.

I am the primary author of the entire dissertation, and conducted essentially all the numerical model experiments and data analyses. However, this work is made possible by the collaborative ideas and efforts from many people. All the research work was performed under the scientific guidance of Dr. Brian Lamb. Additional manuscript authorship detail and individual project financial support are given below:

- **Chapter 2: Enhancement and Evaluation of the AIRPACT Ozone and PM2.5 Forecast System for the Pacific Northwest**

  Jack Chen, Joe Vaughan, Jeremy Avise, Brian Lamb
  Washington State University, Department of Civil and Environmental Research

  Susan O'Neill
  United States Department of Agriculture, Natural Resources Conservation Service

This is a continuation of the AIRPACT real-time numerical air quality forecast project initiated in 2000 through the NW-AIRQUEST consortium. Dr. Brian Lamb is the principal investigator of the project. Dr. Joe Vaughan built the initial AIRPACT system, and maintains the daily operations of the current AIRPACT forecast system. Jeremy Avise assisted in the development and compilations of boundary conditions for the modeling system. Dr. Susan O'Neill assisted in the development of the real-time wild and prescribed fire emission processing system, and provided input data for used in the evaluation work. Funding for this project was provided through the NW-AIRQUEST Consortium, and the Boeing Corporation Endowment.

- **Chapter 3: Global Change Impacts on Future Regional Air Quality in the United States**

Jack Chen, Jeremy Avise, Brian Lamb
Washington State University, Department of Civil and Environmental Research

Clifford Mass, Eric Salathé
University of Washington

Alex Guenther, Christine Wiedinmyer
National Center for Atmospheric Research

Donald McKenzie, Narasimhan Larkin
United States Department of Agriculture, Forest Service

Susan O'Neill
United States Department of Agriculture, Natural Resources Conservation Service

The project is a collaborative work by researchers from many institutes. Dr. Brian Lamb is the principal investigator of the project. Jeremy Avise developed the interface and processed chemical boundary conditions from global chemistry models. He also assisted in running the long-term numerical simulations. Dr. Alex Guenther and Dr. Christine Wiedinmyer provided future land use, land cover information, and biogenic emissions input for the system. Dr. Christine Wiedinmyer also assisted in obtaining the global climate and chemistry model results. Dr. Clifford Mass and Dr. Eric Salathé developed the meteorological interface between the global climate models and the regional meteorological model. They also performed the regional meteorological model simulations. Dr. Donald McKenzie, Dr. Narasimhan Larkin and Dr. Susan O'Neill provided fire emissions for the system, as well as computational resources for performing the numerical simulations. Funding for the project was provided by US Environmental Protection Agency (EPA) Science to Achieve Results (STAR) Program (Grant # RD83096201).

- **Chapter 4: Impact of Future Land Use and Land Cover Changes on Regional Air Quality in the United States**

  Jack Chen, Jeremy Avise, Brian Lamb
  Washington State University, Department of Civil and Environmental Research

  Alex Guenther, Christine Wiedinmyer
  National Center for Atmospheric Research

This project is a continuation of the work on global change impacts on regional air quality. Dr. Brian Lamb is the principal investigator of the project. Jeremy Avise assisted in performing the numerical simulations. Dr. Alex Guenther and Dr. Christine Wideinmyer provided the future land use and land cover scenarios and assisted in the construction of the biogenic emissions input. Funding for the project was provided by US Environmental Protection Agency (EPA) Science to Achieve Results (STAR) Program (Grant # RD83096201).

CHAPTER ONE

Introduction

Ground level ozone (O_3) and fine particulate matter (PM) in the ambient atmosphere are pollutants known to cause severe health problems in humans and damage surrounding ecosystems (Folinsbee, 1993; Brauer et al., 2001). Increased exposures to these pollutants can significantly increase the nation's economical burden through increased health care expenses, decreased national productivity and degradation of natural resources (Benner, 2004; Rabl et al., 1999). To protect the public health and welfare, the US Environmental Protection Agency (EPA) established the National Ambient Air Quality Standards (NAAQS) for ozone, and for PM with aerodynamic diameters less than 10 μm (PM_{10}) and 2.5 μm ($PM_{2.5}$). The current NAAQS for ozone is 80 ppbv over an 8-hour averaging period, and for $PM_{2.5}$, the standard was revised in 2006, from 65 $\mu g/m^3$ to 35 $\mu g/m^3$ over a 24-hour averaging period.

An important aspect of regulating pollutant concentrations is the development of ways to forecast air quality conditions in the future. The knowledge of future air quality conditions has tremendous benefit to the society. In the near term, air quality forecasts for the next day are valuable information for air managers who issue early warnings to the public for precautionary actions. In the far term, air quality simulations for the next decade are valuable resources for governments making future economic and healthcare decisions.

This dissertation contains three manuscripts that describe the current research and results in building and analyzing numerical air quality systems for short-term forecasts and long-range predictions. The goals of the two modeling frameworks are to provide insights into future

US air quality conditions, evaluate new approaches to simulate air quality dynamics, as well as understand the current limitations of the numerical air quality modeling system.

Short-term numerical air quality forecast systems are aimed at providing air pollution concentration predictions over the next 24 to 48 hours. These systems simulate transport and formation of atmospheric pollutants with forecast meteorology and estimated emission activities. The spatial coverage is usually centered over small, highly populated urban areas. Recently, several such systems have been implemented around the world, and in the US; examples include: the Australian AAQFS (http://www.epa.vic.gov.au/air/aaqfs/), the Canadian CHRONOS (http://www.msc-smc.ec.gc.ca/aq_smog, Pudykiewicz et al., 2001), the France regional scale modeling system (http://www.airparif.asso.fr/pages/modelisation/regionale), the UK NAME-III system (http://www.airquality.co.uk), and several systems in the US, such as the AIRNow inter-agency network (www.airnow.gov, Eder et al., 2006a), and five systems for the Eastern US recently reviewed by McKeen et al. (2005).

In the Pacific Northwest, as part of the Northwest International Air Quality Environmental Science & Technology Consortium (NW-AIRQUEST), the Air Indicator Report for Public Access and Community Tracking (AIRPACT) real-time numerical air quality forecast system was constructed in 2000 to provide hourly ozone forecasts (Vaughan et al., 2004). In this dissertation, the AIRPACT system was revised with a new numerical modeling framework, and used to demonstrate the ability to accurately predict the onset of ozone and $PM_{2.5}$ pollution events for the region. The implementation and evaluation of this system (AIRPACT-3) is presented in Chapter 2 as an independent manuscript entitled:

- **Enhancement and Evaluation of the AIRPACT Ozone and $PM_{2.5}$ Forecast System for the Pacific Northwest**

In addition to short-term air quality forecasts, long-range numerical air quality predictions are aimed at understanding and quantifying air quality conditions in the future from direct and indirect effects of global changes. Many recent researchers have unequivocally indicated that large scale global changes are inevitable in the future. Global environmental changes such as climate change, land use, land cover (LULC) alterations, and the associated regional emission changes can significantly modify the chemistry and physics of the future atmosphere. To quantify future air quality impacts, several studies have employed global scale models to simulate tropospheric ozone responses to future environments (e.g. Prather et al., 2003; Dentener et al., 2006; Horowitz, 2006; Shindell et al., 2006). Results from most studies generally showed higher global ozone burdens in year 2030 – 2100 compared to present conditions. The predicted changes differ depending on the assumed future climate and emission scenarios.

In this study, the construction of a coupled global and regional scale model system provides a more in depth look at ozone pollution conditions over the US continent fifty years in the future: 2045-2054. The model system accounts for the collective effects of global climate change, regional LULC changes, differences in global chemical pollutant background concentrations, and projected future regional emissions within the US. The results were analyzed in terms of changes in future ozone concentrations, variability of extreme pollution events, and spatiotemporal extent of future air pollution episodes. The implementation, evaluation and analyses of the long term air quality forecast system are presented in Chapter 3 entitled:

- **Global Change Impacts on Future Regional Air Quality in the United States**

To further look at the future regional air quality conditions, Chapter 4 emphasizes future LULC scenario impacts on regional biogenic emissions, and how the changes in biogenic emissions influence ozone and biogenic secondary organic aerosol formations within the continental US.

The effects of human-induced LULC changes such as deforestation, urbanization and increases in agricultural land have been shown to impact future global climate as well as global atmospheric chemistry (Feddema et al., 2005; Foley et al., 2005). In the US, future climate change and continuous human agricultural expansion can alter dominant plant species, and change the magnitudes and spatial distributions of biogenic emissions. Plants emit large amounts of volatile organic compounds (VOC) with estimated annual emissions exceeding combined anthropogenic sources (Lamb et al., 1993). Changes in future biogenic emissions from changing LULC can, therefore, alter regional atmospheric chemistry and influence the formation of secondary pollutants. For quantitative investigation of such effects, this study implements the new MEGAN biogenic emissions model (Guenther et al., 2006) and the long term regional air quality forecast system to examine biogenic emissions and air quality conditions in the future. The results demonstrate the interconnectivity of global change and anthropogenic influences toward changing biogenic emissions and regional air pollution. The manuscript in Chapter 4 is entitled:

- **Impact of Future Land Use and Land Cover Changes on Regional Air Quality in the United States**

Numerical Simulations of Regional Air Quality

General Review

A major part of this research work is based on the implementation and analyses of computational numerical models in simulating air quality conditions of present and future environments. An air quality model is a collection of mathematical relationships and algorithms that calculates the behavior of chemical compounds in the atmosphere over space and time. It offers a systematic approach for understanding processes affecting regional atmospheric chemistry and physics, and provides quantitative estimates on the spatiotemporal extent of pollution changes. In recent years, air quality models have increased in complexity along with our understanding of atmospheric processes and the aid of advanced computational technology. The systems have demonstrated skill in capturing the status of atmospheric conditions and are indispensable tools in the study of atmospheric sciences.

In this research, the main photochemical model common to all manuscripts is the Community Multi-scale Air Quality Model (CMAQ). The model was developed by the US EPA following the 'one-atmosphere' paradigm (Byun et al., 1999). The paradigm addresses the complex relationships between multiple chemical compounds from different sources and physical states simultaneous within the modeling framework. Since its inception in 1990s, the system has undergone continuous community development and support, with updated scientific algorithms and physical parameterizations (see: Community Modeling and Analysis System – http://www.cmascenter.org). The latest revision (version 4.6) was released in October 2006 and was implemented for the AIRPACT-3 short-term air quality forecast system. The model accounts for chemical interactions from gas-phase mechanisms, as well as aqueous and aerosol phase chemical compounds. The system represents the latest state-of-science in regional environmental air quality modeling.

The CMAQ model has been applied in various atmospheric studies for different geographical regions. In several studies, it was used to examine the detailed chemistry of coupled ozone and $PM_{2.5}$ pollution episodes (e.g. O'Neill et al., 2006; Eder et al., 2006b; Smyth et al., 2006). The algorithms in CMAQ also allowed the study of visibility degradation from regional haze in the atmosphere (Choi et al., 2006; Pun et al., 2006; Mebust et al., 2003; Mebust et al., 2003). In addition, the model has been used to simulate formation and transport of other atmospheric pollutants such as mercury (Bullock et al., 2002; Gbor et al., 2007; Gbor et al., 2006), hazardous air toxics (Seigneur et al., 2000; Luecken et al., 2006) pollution deposition on surface ecosystems (Nenes et al., 1999; Davis et al., 2006), air quality impacts from forest wild-fires (Roy et al., 2007; Lamb et al., 2007), fine particle number concentrations in the US (Park et al., 2006; Elleman, 2007) and long-range transport of pollutants (Zhang et al., 2006).

Furthermore, the CMAQ model is also being adopted by research institutes as the core photochemical model in numerical forecast systems. In addition to the AIRPACT-3 system for the Pacific Northwest, Monache et al., (2006) used the CMAQ model as part of an ensemble air quality forecast framework in Vancouver, Canada. Yu et al., (2006) applied it in the New England region in support of a field study, and recently scientists at the University of Houston have used it to implement a real-time numerical air quality forecast system for Eastern Texas in an operational setting (http://www.imaqs.uh.edu/aqfmain.htm).

One major proponent of the CMAQ short-term air quality forecast in the US is the interagency collaboration of EPA and NOAA (National Oceanic and Atmospheric Administration). The group implemented CMAQ as the operational forecast system with forecast meteorology from the National Center for Environmental Prediction (NCEP) large-scale modeling system. The national air quality forecast covers the entire eastern US continent at 12-km grid resolution, with planned expansion over the western US states in the near future (http://www.weather.gov/ost/air_quality, Otte et al., 2005). The results from this numerical

forecast are now part of the US government public Internet resources for national air quality (http://airnow.gov).

In addition to real-time air quality forecasts, the CMAQ model was recently used to study the effects of climate change on future regional air quality. The studies examined the sensitivity of ozone concentrations due to predicted variations in temperature, relative humidity, projected regional emissions and future global pollution conditions.

For example, Hogrefe et al. (2004) first applied the CMAQ system to investigate ozone pollution as a result of climate change for the Eastern US. The study did not account for dynamic variations in future background chemical conditions with global chemistry models. They found daily maximum 8-hr ozone to increase by 2.7 to 5.0 ppbv with future emissions and climate. The results were subsequently used to assess future health impacts (Knowlton et al., 2004), and effects of urbanization on future meteorology and ozone within New York City (Civerolo et al., 2000). More recently, Steiner et al. (2006) used the CMAQ model to examine future ozone concentrations in California due to independent changes in model inputs such as, temperature, water vapor, biogenic emissions, anthropogenic emissions and chemical boundary conditions. They found changing anthropogenic emissions to have the largest effect in reducing future urban ozone levels (10 ppbv - 20 ppbv decrease) followed by changing boundary conditions. One weakness, however, in this study was that meteorological conditions were decoupled and applied for the future scenarios. The study isolated the temperature change from the model input, and thus ignored the associated thermodynamic influences such as planetary boundary layer (PBL) changes, wind speed and wind direction variations on resulting ozone predictions.

In this research work, the long-range air quality prediction incorporates the coupled global and regional scale models, to address the dynamics between global forcings toward

regional air quality changes. In addition, long term simulations of 10-year periods ensure that the system represents future variations in meteorological conditions, chemical concentration backgrounds, and regional emission changes collectively to better simulate the future air pollution environment.

Eularian Grid Model

The CMAQ model follows the Eularian modeling framework to simulate the atmospheric processes of chemical compounds. Like all Eularian grid models, CMAQ represents a spatial region – simulation domain – with 3-dimensional computational grid volumes and solves the conservation equation for each chemical species, for each grid volume for each time step. Detailed CMAQ numerical formulations can be found in Byun et al. (2006). Following is the generalized species conservation equation that is common in most Eularian air quality models:

$$\frac{\partial C_i}{\partial t} + U\frac{\partial C_i}{\partial x} + V\frac{\partial C_i}{\partial y} + W\frac{\partial C_i}{\partial z} = \frac{\partial}{\partial x}\left(K_x\frac{\partial C_i}{\partial x}\right) + \frac{\partial}{\partial y}\left(K_y\frac{\partial C_i}{\partial y}\right) + \frac{\partial}{\partial z}\left(K_z\frac{\partial C_i}{\partial z}\right) + R + D + S \qquad \text{(E1)}$$

(A) (B1) (B2) (B3) (C1) (C2) (C3) (D) (E) (F)

where,

(A) ..... is the time rate of change of chemical specie *i*
(B1, B2) ..... are horizontal advection components of specie *i*
(B3) ..... is the vertical advection transport of specie *i*
(C1,C2) ..... are the horizontal atmospheric turbulent diffusion components of specie *i*
(C3) ..... is the vertical atmospheric turbulent diffusion of specie *i*
(D) ..... is a general term for chemical reactions of the specie *i*
(E) ..... is a general term for deposition processes of specie *i*
(F) ..... is a general term for source emissions of the specie *i*

The species conservation equation, E1, divides physical transport processes (terms B and C) and chemical processes (terms D, E and F) into individual numerical problems, and solves each term iteratively. The system assumes quasi-steady-state conditions such that, the processes of other terms remain unchanged within each numerical synchronization time step.

In Equation E1, the CMAQ model obtains the mean *U*, *V* and *W* wind components from the input meteorological data, and calculates turbulent diffusion coefficients *Kx*, *Ky*, and *Kz* with modeled atmospheric stability conditions, height within the PBL, as well as domain grid structures and simulation numerical time steps.

In recent model revisions, the parameterization of vertical turbulent diffusivity (*Kz*) was updated to better represent the influences of urban landuse (Pleim et al., 2005). This enables *Kz* to increase in urban grids with higher surface roughness, and decrease in non-urban regions with lower vertical mixing. The revised *Kz* resulted in better night time ozone simulations in urban areas from higher vertical mixing. The parameterizations of horizontal turbulent diffusivity (*Kx* and *Ky*) are simpler, but also less understood due to inadequate measurement studies. The CMAQ horizontal diffusivity algorithms are based on earlier studies by Smagorinsky (1963) and vary primarily by domain grid structures.

For chemical processes, the model handles individual gas and aerosol phase species by separate modules. The system accounts for multi-phase chemical reactions, surface emissions, as well as wet and dry deposition. The following sections describe the ozone gas-phase and aerosol-phase chemistry in the CMAQ model in greater detail.

Chemistry of Tropospheric Ozone

The CMAQ model offers a choice of different chemical mechanisms in simulating atmospheric gas-phase interactions: CB-IV, SAPRC-99 and RADM2. In this study the SAPRC-99 mechanism (Carter, 2000) was chosen because of the more explicit representation of organic chemical species. The mechanism uses the 'lumped-molecule' approach to simplify atmospheric VOC by combining compounds with similar hydroxyl radical ($OH^{\cdot}$) reactivities and functional groups together. Inorganic gas-phase species in SAPRC-99 are explicitly defined since these are better understood and have fewer species compared to VOC. The SAPRC-99

mechanism, excluding aerosol and aqueous components, contains 72 mechanism species, and 214 chemical reactions, of which 30 reactions are photolytic. Appendix A lists the SAPRC99 mechanism species and their descriptions.

Simulating the onset of ozone events is highly challenging due to the non-linear chemistry between ozone and its precursor emissions, NOx (NO + NO_2) and VOC. In the troposphere, ozone is formed from the photolysis reaction of NO_2 in the presence of sunlight:

$$NO_2 + h\nu \rightarrow NO + O \qquad \text{(R1)}$$

$$O + O_2 \rightarrow O_3 + M \qquad \text{(R2)}$$

The wavelength of NO_2 photolysis in R1 is $h\nu < 424$ nm. The M in reaction R2 represents neutral molecules that absorb excess energy to stabilize the O_3 reaction product. Once ozone is formed, it is also continuously removed via:

$$O_3 + NO \rightarrow NO_2 + O_2 \qquad \text{(R3)}$$

In an unpolluted atmosphere, the ozone concentration is regulated by the constant formation and removal reactions. The chemical cycle R1, R2, and R3 establishes steady state surface ozone concentrations of approximately 20-30 ppbv.

Ground level ozone chemistry differs greatly in polluted environments. Ozone concentrations can increase several fold with elevated VOC and NOx emissions. Anthropogenic NOx are mainly from sources such as automobiles and power plants. VOC are released from wider range of sources, such as automobiles, industrial processes and vegetation. NOx from automobiles consist of approximately 90% NO and 10% NO_2.

In an urban plume, high NO emissions from automobile exhaust initially reduces ozone concentration through R3, a process called ozone NO titration. However once the urban plume expands, it dilutes the NO concentrations and picks up surrounding VOC emissions. Under

correct meteorological conditions, the system can rapidly increase ozone chemical production via catalytic conversion of NO to NO_2:

$$R\text{-}H + OH\cdot + 2\ O_2 \rightarrow\rightarrow RO_2\cdot + HO_2\cdot + H_2O + R'CHO \qquad (R4)$$

$$RO_2\cdot + NO \rightarrow NO_2 + RO\cdot \qquad (R5)$$

$$HO_2\cdot + NO \rightarrow NO_2 + OH\cdot \qquad (R6)$$

The R-H in R4 denotes carbon-hydrogen bonds from VOC. The oxidations of VOC by OH· in R4 produce peroxy radicals ($RO_2\cdot$) and hydroperoxy radicals ($HO_2\cdot$). These two highly reactive radicals can rapidly convert the abundant NO to NO_2 via R5 and R6, bypassing the ozone removal reaction of R3. In the presence of sunlight, the addition of NO_2 in the air can rapidly form ozone via reactions R1 and R2.

The generalized reactions showed one molecule of VOC to catalyze the formation of at least 2 molecules of NO_2. This, in turn, produces 2 molecules of ozone. The chemical mix of urban pollution provides continuous ozone production mechanisms, and results in accumulated ozone concentrations downwind of urban areas. Since different VOC, and their secondary oxidized products such as R'CHO in R3 have different reactivities in the atmosphere, several modeled VOC species are required in the SAPRC99 mechanism to correctly represent the gas-phase reaction kinetics of the atmosphere.

Chemistry of Atmospheric Aerosols

Chemistry of atmospheric secondary aerosols is more complex than ozone due to the number of chemical species, and the reactions involve compounds from all three physical phases: solid, gas, and liquid. Secondary aerosols are reaction products that have low saturation vapor pressures and exist as solid phase salts, organic conglomerates, or as aqueous phase ions in the atmosphere. The particle size is usually small, with aerodynamic diameter less than 2.5 μm. Both organic and inorganic gas reactions can contribute to the

formation of secondary aerosols. Inorganic aerosol chemistry is better understood than organic aerosol chemistry due to complexities in atmospheric organic compounds.

In the CMAQ model, atmospheric aerosols are simulated by separate aerosol modules following gas-phase chemistry. The aerosol module applies the modal approach in representing aerosol size fractions: Atkin mode (0.01 μm to 1 μm), accumulation mode (0.1 μm to 10 μm) and a coarse mode (>2.5 μm). Primary particulate matter emitted directly into the atmosphere is simulated by physical transport, accounting for losses via deposition, with no additional chemistry. Secondary aerosols are formed from reactions with precursor emissions or secondary reaction products from gas-phase chemistry. In the current version of CMAQ, the aerosol module is further divided into inorganic and organic components. The inorganic aerosol dynamic is based on the ISORROPIA algorithm of Nenes et al. (1998) and the secondary organic aerosol module is based on the SORGAM algorithm of Schell et al. (2001).

The inorganic ISORROPIA module is a thermodynamic equilibrium model that solves the equilibrium concentrations of inorganic chemical species under modeled atmospheric conditions. The module calculates aerosol concentrations from sodium-ammonium-chloride-sulfate-nitrate-water reactions. The system adjusts the equilibrium constants with modeled temperature, and accounts for aerosol solubility and aerosol water content with input relative humidity. It is an internally mixed model, such that all particles of the same size are assumed to have the same composition in the system. Through the combinations of different inorganic ions, the system solves the equilibrium concentrations of 9 solid phase species, 13 aqueous phase species, and 4 gas phase species across 15 equilibrium reactions. The algorithm is executed at every grid for every time step after the gas-phase chemistry.

The algorithm of ISORROPIA is highly efficient. By using concentration ratios of $R_{Na} = [Na^+]/[SO_4^{-2}]$ and $R_{SO4} = ([Na^+]+[NH_4^+])/[SO_4^{-2}]$ the module predetermines the presence and

physical states of many inorganic aerosol compounds, and thus reduces the need of numerical solvers and iterations for complex equilibrium calculations. The concentration ratios partition the aerosol system into sulfate rich/poor and sodium rich/poor regimes, and define the aerosol system with following properties:

Sulfate Rich (free acid)	$R_{SO4} < 1$	No cations to neutralize sulfates – cause formation of H_2SO_4 to occur in liquid phase because sulfuric acid is highly hygroscopic
Sulfate Rich (no-free acid)	$1 \leq R_{SO4} < 1$	Not enough cations to neutralize all sulfates, sulfate exits as unneutralized HSO_4^- and SO_4^{-2}
Sulfate Poor Sodium Poor	$R_{SO4} \geq 2$ $R_{Na} < 2$	Enough NH_4^+ to fully neutralize sulfate, forming $(NH_4)_2SO_{4(s)}$, but not enough Na^+ to neutralize sulfate by itself. The excess NH_4^+ can therefore react with other gas species to form salts (NH_4Cl, NH_4NO_3)
Sulfate Poor Sodium Rich	$R_{SO4} \geq 2$ $R_{Na} > 2$	Enough Na^+ to fully neutralize the sulfates, and there are excess NH_4^+ and Na^+ to react with other gas species to form salts (NH_4Cl, NH_4NO_3, NaCl, $NaNO_3$). All sulfates are neutralized with sodium as Na_2SO_4

Within each predefined regime, the module further determines the individual species concentrations via iterative equilibrium calculations with temperature adjusted equilibrium constants. The module also calculates the aerosol water content based on the ZSR method of Robinson and Stokes (1965). The method parameterizes the water content as function of both relative humidity and concentrations of individual chemical components in the system mixture.

Compared to the inorganic aerosol module, the approach of modeling secondary organic aerosol (SOA) in CMAQ is more straightforward and simple. The current SOA module in CMAQ was revised from the previous version with fixed aerosol yields of Pandis et al. (1993) to one with variable organic aerosol yields. The new version parameterizes the aerosol yields as functions of ambient temperature and the amount of absorbing materials, or absorbents, present in the air.

Atmospheric SOA are produced from low vapor pressure products of oxidized VOC. When large VOC molecules undergo oxidation by atmospheric oxidants such as O_3, OH·, or NO_3· (nitrate radicals), fractions of the reaction products form condensable organic that can partition into the aerosol phase. Most of the precursor VOC species that form condensable organic products are long-chain hydrocarbon or large aromatic molecules. In CMAQ, these are: toluene, xylene, cresol, terpenes, C-8 or higher alkanes, and internal alkenes. The reaction processes can be represented by R7, where VOC represent the precursor gases and $C_{tot,i}$ are the organic products after oxidation. The oxidation product, $C_{tot,i}$ can then partition in either gas-phase as $C_{gas,i}$ or into the aerosol phase as SOA, represented by $C_{aer,I}$ as in Equation E8:

$$VOC + [O_3, NO_3\cdot, OH\cdot] \rightarrow C_{tot,i} \qquad (R7)$$

$$C_{tot,i} = C_{aer,i} + C_{gas,i} \qquad (E2)$$

In the older version of CMAQ, the fraction that partitions into the aerosol-phase is assumed to be constant such that:

$$C_{aer,i} = Y_i \cdot C_{tot,i} \qquad (E3)$$

where Y_i is the organic aerosol yield fraction that varies only by the oxidized VOC species. However, in many chamber experiments, organic aerosol yields are variable, and are functions of both environmental conditions and the amount of total condensable organics already present in the atmosphere (Seinfeld, J. H. et al., 1998). To account for these, the SOA module in CMAQ expresses the gas-phase fractions $C_{gas,i}$ as:

$$C_{gas,i} = C_{sat,i} = C^*_{sat,i} \cdot X_{i,om} \qquad (E4)$$

where $C_{sat,i}$ [μg/m^3] is the saturation concentration of oxidized product *i*. This is further estimated as the product of saturation concentration of pure component *i*, ($C^*_{sat,i}$) [μg/m^3], and the mole fraction of secondary organic aerosol to total organic matter in the system ($X_{i,om}$). The saturation concentration of pure component $C^*_{sat,i}$ is a function of the temperature dependent saturation vapor pressure, which is parameterized with the Clausius-Clapeyron equation. The

total organic matter in the model fraction, $X_{i,om}$, represents the absorbent materials in the system, part of which is made up of the produced SOA. The mole fraction is calculated as:

$$X_{i,om} = \frac{C_{aer,i}/m_i}{\sum_{j=1}^{n}\left(C_{aer,j}/m_j\right)+\left(C_{init}/m_{init}\right)} \qquad \text{(E5)}$$

where C_{init} and m_{init} represent the concentration and molecular weight of initial absorbing material already present in the system, and m_i is the molecular weight of the secondary aerosol product *i*.

Combining the equations, the concentration of SOA after oxidation can therefore be represented as:

$$C_{aer,i} = C_{tot,i} - C^{*}_{sat,i} \cdot \frac{C_{aer,i}/m_i}{\sum_{j=1}^{n}\left(C_{aer,j}/m_j\right)+\left(C_{init}/m_{init}\right)} \qquad \text{(E6)}$$

Equation E6, one for each of the six precursor VOC emissions in CMAQ, is a set of coupled nonlinear equations. The equations are solved iteratively within the organic aerosol module for each grid and simulation time step to resolve the SOA concentrations from gas phase oxidations.

Through the above approach, the organic aerosol module takes into account temperature effects upon the organics partitioning into the aerosol phase and the amount of absorbing material already present in the air. The secondary organic aerosol yield after each VOC oxidation is therefore variable and changes with these parameters.

Although the current SOA algorithm in CMAQ greatly improved upon the earlier version in both algorithms and results (Jiang et al., 2003), it is still considered simplistic compared to more complex algorithms such as MADRID and CACM mechanisms developed recently (Zhang et al., 2004; Griffin et al., 2002). However, the complex mechanisms have draw backs, mainly,

they require much longer computational time, and are thus, not suitable for implementing in the highly time constrained forecast systems. Furthermore, recent evaluations of the algorithms suggest poorer model performance than expected from such complex algorithms (Chen et al., 2006; Pun et al., 2006). This is mostly due to the limited availability of highly detailed VOC emissions dataset required as model input to take advantage of the complex chemical mechanisms.

Reference

Benner, T. C., 2004. Brief Survey of EPA Standard-Setting and Health Assessment. Environmental Science & Technology 38(13), 3457-3464.

Brauer, M., Ebelt, S. T., Fisher, T. V., Brumm, J., Petkau, A. J., and Vedal, S., 2001. Exposure of Chronic Obstructive Pulmonary Disease Patients to Particles: Respiratory and Cardiovascular Health Effects. Journal of Exposure Analysis and Environmental Epidemiology 11(6), 490-500.

Bullock, O. R. and Brehme, K. A., 2002. Atmospheric Mercury Simulation Using the CMAQ Model: Formulation Description and Analysis of Wet Deposition Results. Atmospheric Environment 36(13), 2135-2146.

Byun, D. and Schere K. L., 2006. Review of the Governing Equations, Computational Algorithms, and Other Components of the Models-3 Community Multiscale Air Quality (CMAQ) Modeling System. Applied Mechanics Reviews 59(2), 51-77.

Byun, D. W. and Ching, J. K. S., 1999. Science Algorithms of the EPA Models-3 Community Multiscale Air Quality (CMAQ) Modeling System. U.S. Environmental Protection Agency, EPA/600/R-99/030.

Carter, W. P. L., 2000. Documentation of the SAPRC-99 Chemical Mechanism for VOC Reactivity Assessment. California Air Resources Board, Contract No. 92-329, and 95-308.

Chen, J. J., Mao, H. T., Talbot, R. W., and Griffin, R. J., 2006. Application of the CACM and MPMPO Modules Using the CMAQ Model for the Eastern United States. Journal of Geophysical Research-Atmospheres 111(D23), doi:10.1029/2006JD007603.

Choi, Yu-Jin, Hyde, Peter, and Fernando, H. J. S., 2006. Modeling of episodic particulate matter events using a 3-D air quality model with fine grid: Applications to a pair of cities in the US/Mexico border. Atmospheric Environment 40(27), 5181-5201.

Civerolo, K. L., Sistla, G., Rao, S. T., and Nowak, D. J., 2000. The Effects of Land Use in Meteorological Modeling: Implications for Assessment of Future Air Quality Scenarios. Atmospheric Environment 34(10), 1615-1621.

Davis, J. M. and Swall, J. L., 2006. An Examination of the Cmaq Simulations of the Wet Deposition of Ammonium from a Bayesian Perspective. Atmospheric Environment 40(24), 4562-4573.

Delle Monache, L., Deng, X. X., Zhou, Y. M., and Stull, R., 2006. Ozone Ensemble Forecasts: 1. A New Ensemble Design. Journal of Geophysical Research-Atmospheres 111(D5), doi:10.1029/2005JD006310.

Dentener, F., Drevet, J., Lamarque, J., Bey, I., Eickhout, B., Fiore, A., Hauglustaine, D., Horowitz, L., Krol, M., Kulshrestha, U., Lawrence, M., Galy-Lacaux, C., Rast, S., Shindell, D., Stevenson, D., Van Noije, T., Atherton, C., Bell, N., Bergman, D., Butler, T., Cofala, J., Collins, B., Doherty, R., Ellingsen, K., Galloway, J., Gauss, M., Montanaro, V., Muller, J. F., Pitari, G., Rodriguez, J., Sanderson, M., Solmon, F., Strahan, S., Schultz, M., Sudo, K., Szopa, S., and Wild, O., 2006. Nitrogen and Sulfur Deposition on Regional and Global Scales: a Multimodel Evaluation. Global Biogeochemical Cycles 20(4), doi:10.1029/2005GB002672.

Eder, B., Kang, D. W., Mathur, R., Yu, S. C., and Schere, K., 2006a. An Operational Evaluation of the

ETA-CMAQ Air Quality Forecast Model. Atmospheric Environment 40(26), 4894-4905.

Eder, B. and Yu, S. C., 2006b. A Performance Evaluation of the 2004 Release of Models-3 CMAQ. Atmospheric Environment 40(26), 4811-4824.

Elleman, R., 2007. Aerosol Size Distribution Modeling for the Pacific Northwest. PhD Dissertation, Department of Atmospheric Sciences, University of Washington.

Feddema, Johannes J., Oleson, Keith W., Bonan, Gordon B., Mearns, Linda O., Buja, Lawrence E., Meehl, Gerald A., and Washington, Warren M., 2005. The Importance of Land-Cover Change in Simulating Future Climates. Science 310(5754), 1674-1678.

Foley, J. A., DeFries, R., Asner, G. P., Barford, C., Bonan, G., Carpenter, S. R., Chapin, F. S., Coe, M. T., Daily, G. C., Gibbs, H. K., Helkowski, J. H., Holloway, T., Howard, E. A., Kucharik, C. J., Monfreda, C., Patz, J. A., Prentice, I. C., Ramankutty, N. n, and Snyder, P. K., 2005. Global Consequences of Land Use. Science 309(5734), 570-574.

Folinsbee, L. J., 1993. Human Health-Effects of Air-Pollution. Environmental Health Perspectives 10045-56.

Gbor, P. K., Wen, D. Y., Meng, F., Yang, F. Q., Zhang, B. N., and Sloan, J. J., 2006. Improved Model for Mercury Emission, Transport and Deposition. Atmospheric Environment 40(5), 973-983.

Gbor, Philip K., Wen, Deyong, Meng, Fan, Yang, Fuquan, and Sloan, James J., 2007. Modeling of mercury emission, transport and deposition in North America. Atmospheric Environment 41(6), 1135-1149.

Griffin, R. J., Dabdub, D., Kleeman, M. J., Fraser, M. P., Cass, G. R., and Seinfeld, J. H., 2002. Secondary Organic Aerosol - 3. Urban/Regional Scale Model of Size- and Composition-Resolved Aerosols. Journal of Geophysical Research-Atmospheres 107(D17), doi:10.1029/2001JD000544.

Guenther, A., Karl, T., Harley, P., Wiedinmyer, C., Palmer, P. I., and Geron, C., 2006. Estimates of Global Terrestrial Isoprene Emissions Using MEGAN (Model of Emissions of Gases and Aerosols from Nature). Atmospheric Chemistry and Physics Discussions 6107-173.

Hogrefe, C., Lynn, B., Civerolo, K., Ku, J. Y., Rosenthal, J., Rosenzweig, C., Goldberg, R., Gaffin, S., Knowlton, K., and Kinney, P. L., 2004. Simulating Changes in Regional Air Pollution Over the Eastern United States Due to Changes in Global and Regional Climate and Emissions. Journal of Geophysical Research-Atmospheres 109(D22), doi:10.1029/2004JD004690.

Horowitz, L. W., 2006. Past, Present, and Future Concentrations of Tropospheric Ozone and Aerosols: Methodology, Ozone Evaluation, and Sensitivity to Aerosol Wet Removal. Journal of Geophysical Research-Atmospheres 111(D22), doi:10.1029/2005JD006937.

Jiang, W., Giroux, E., Yin, D., and Roth, H., 2003. Comparison of Three Secondary Organic Aerosol Algorithms Implemented in CMAQ. Proceeding for the 2nd Annual CMAS Models-3 User's Conference, 2003, Research Triangle Park, NC.

Knowlton, K., Rosenthal, J. E., Hogrefe, C., Lynn, B., Gaffin, S., Goldberg, R., Rosenzweig, C., Civerolo, K., Ku, J. Y., and Kinney, P. L., 2004. Assessing Ozone-Related Health Impacts Under a Changing Climate. Environmental Health Perspectives 112(15), 1557-1563.

Lamb, B., Chen, J., O'Neill, S., Avise, J., Vaughan, J. , Larkin, S., and Solomon, S., 2007. Real-Time Numerical Foresting of Wildfire Emissions and Perturbations to Regional Air Quality. EOS, Transactions, American Geophysical Union, Submitted.

Lamb, B., Gay, D., Westberg, H., and Pierce, T., 1993. A Biogenic Hydrocarbon Emission Inventory for the USA Using a Simple Forest Canopy Model. Atmospheric Environment Part a-General Topics 27(11), 1673-1690.

Luecken, D. J., Hutzell, W. T., and Gipson, G. L., 2006. Development and Analysis of Air Quality Modeling Simulations for Hazardous Air Pollutants. Atmospheric Environment 40(26), 5087-5096.

Mckeen, S., Wilczak, J., Grell, G., Djalalova, I., Peckham, S., Hsie, E. Y., Gong, W., Bouchet, V., Menard, S., Moffet, R., Mchenry, J., Mcqueen, J., Tang, Y., Carmichael, G. R., Pagowski, M., Chan, A., Dye, T., Frost, G., Lee, P., and Mathur, R., 2005. Assessment of an Ensemble of Seven Real-Time Ozone Forecasts Over Eastern North America During the Summer of 2004. Journal of Geophysical Research-Atmospheres 110(D21), doi:10.1029/2005JD005858.

Mebust, M. R., Eder, B. K., Binkowski, F. S., and Roselle, S. J., 2003. Models-3 Community Multiscale Air Quality (CMAQ) Model Aerosol Component - 2. Model Evaluation. Journal of Geophysical Research-Atmospheres 108(D6), doi:10.1029/2001JD001410.

Nenes, A., Pandis, S. N., and Pilinis, C., 1998. ISORROPIA: a New Thermodynamic Equilibrium Model for Multiphase Multicomponent Inorganic Aerosols. Aquatic Geochemistry 4(1), 123-152.

Nenes, A., Pandis, S. N., and Pilinis, C., 1999. Continued Development and Testing of a New Thermodynamic Aerosol Module for Urban and Regional Air Quality Models. Atmospheric Environment 33(10), 1553-1560.

O'Neill, S., Lamb, B., Chen, J., Claiborn, C., Finn, D., Otterson, S., Figueroa, C., Bowman, C., Boyer, M., Wilson, R., Arnold, J., Aalbers, S., Stocum, J., Swab, C., Stoll, M., Dubois, M., and Anderson, M., 2006. Modeling Ozone and Aerosol Formation and Transport in the Pacific Northwest with the Community Multi-Scale Air Quality (CMAQ) Modeling System. Environmental Science & Technology 40(4), 1286-1299.

Otte, T. L., Pouliot, G., Pleim, J. E., Young, J. O., Schere, K. L., Wong, D. C., Lee, P. C. S., Tsidulko, M., Mcqueen, J. T., Davidson, P., Mathur, R., Chuang, H. Y., Dimego, G., and Seaman, N. L., 2005. Linking the ETA Model with the Community Multiscale Air Quality (CMAQ) Modeling System to Build a National Air Quality Forecasting System. Weather and Forecasting 20(3), 367-384.

Pandis, S. N., Wexler, A. S., and Seinfeld, J. H., 1993. Secondary Organic Aerosol Formation and Transport .2. Predicting the Ambient Secondary Organic Aerosol-Size Distribution. Atmospheric Environment Part a-General Topics 27(15), 2403-2416.

Park, S. K., Marmur, A., Kim, S. B., Tian, D., Hu, Y. T., Mcmurry, P. H., and Russell, A. G., 2006. Evaluation of Fine Particle Number Concentrations in CMAQ. Aerosol Science and Technology 40(11), 985-996.

Pleim, J. and Mathur, R., 2005. Diagnostic Evaluation, Sensitivity Analyses and New Development in the ETA/CMAQ Air Quality Forecast System. Proceeding for the 7th Conference on Atmospheric Chemistry by the American Meteorological Society, 2005, San Diego, CA.

Prather, M., Gauss, M., Berntsen, T., Isaksen, I., Sundet, J., Bey, I., Brasseur, G., Dentener, F., Derwent, R., Stevenson, D., Grenfell, L., Hauglustaine, D., Horowitz, L., Jacob, D., Mickley, L., Lawrence, M., Von Kuhlmann, R., Muller, J. F., Pitari, G., Rogers, H., Johnson, M., Pyle, J., Law, K., Van Weele, M., and Wild, O., 2003. Fresh Air in the 21st Century? Geophysical Research Letters 30(2), doi:10.1029/2002GL016285.

Pudykiewicz, J. A. and Koziol, A. S., 2001. The Application of Eulerian Models for Air Quality Prediction and the Evaluation of Emission Control Strategies in Canada. International Journal of

Environment and Pollution 16(1-6), 425-438.

Pun, B. K., Seigneur, C., Vijayaraghavan, K., Wu, S. Y., Chen, S. Y., Knipping, E. M., and Kumar, N., 2006. Modeling Regional Haze in the Bravo Study Using CMAQ-MADRID: 1. Model Evaluation. Journal of Geophysical Research-Atmospheres 111(D6), doi:10.1029/2004JD005608.

Rabl, A. and Spadaro, J. V., 1999. Damages and Costs of Air Pollution: an Analysis of Uncertainties. Environment International 25(1), 29-46.

Robinson, R. A. and R. H. Stokes, Electrolyte Solutions second edition, Dover Publications, Butterworths, London, 1965.

Roy, B., Pouliot, G. A., Gilliland, A., Pierce, T., Howard, S., Bhave, P. V., and Benjey, W., 2007. Refining Fire Emissions for Air Quality Modeling With Remotely Sensed Fire Counts: a Wildfire Case Study. Atmospheric Environment 41(3), 655-665.

Schell, B., Ackermann, I. J., Hass, H., Binkowski, F. S., and Ebel, A., 2001. Modeling the Formation of Secondary Organic Aerosol Within a Comprehensive Air Quality Model System. Journal of Geophysical Research-Atmospheres 106(D22), 28275-28293.

Seigneur, C., Tonne, C., Vijayaraghavan, K., Pai, P., and Levin, L., 2000. The Sensitivity of Pm2.5 Source-Receptor Relationships to Atmospheric Chemistry and Transport in a Three-Dimensional Air Quality Model. Journal of the Air & Waste Management Association 50(3), 428-435.

Seinfeld, J. H. and S. N. Pandis, Atmospheric Chemistry and Physics: From Air Pollution to Climate Change, John Wiley & Sons Inc., 1998.

Shindell, D. T., Faluvegi, G., Unger, N., Aguilar, E., Schmidt, G. A., Koch, D. M., Bauer, S. E., and Miller, R. L., 2006. Simulations of Preindustrial, Present-Day, and 2100 Conditions in the Nasa Giss Composition and Climate Model G-Puccini. Atmospheric Chemistry and Physics 64427-4459.

Smagorinsky, J., 1963. General Circulation Experiments with the Primitive Equations, 1: The Basic Experiment. Monthly Weather Review 9199-164.

Smyth, S. C., Jiang, W. M., Yin, D. Z., Roth, H., and Giroux, T., 2006. Evaluation of CMAQ O_3 and $PM_{2.5}$ Performance Using Pacific 2001 Measurement Data. Atmospheric Environment 40(15), 2735-2749.

Steiner, A. L., Tonse, S., Cohen, R. C., Goldstein, A. H., and Harley, R. A., 2006. Influence of Future Climate and Emissions on Regional Air Quality in California. Journal of Geophysical Research-Atmospheres 111(D18), doi:10.1029/2005JD006935.

Vaughan, J., Lamb, B., Frei, C., Wilson, R., Bowman, C., Figueroa-Kaminsky, C., Otterson, S., Boyer, M., Mass, C., Albright, M., Koenig, J., Collingwood, A., Gilroy, M., and Maykut, N., 2004. A Numerical Daily Air Quality Forecast System for the Pacific Northwest. Bulletin of the American Meteorological Society 85(4), 549-561.

Yu, S. C., Mathur, R., Kang, D. W., Schere, K., Eder, B., and Pleirn, J., 2006. Performance and Diagnostic Evaluation of Ozone Predictions by the ETA-Community Multiscale Air Quality Forecast System during the 2002 New England Air Quality Study. Journal of the Air & Waste Management Association 56(10), 1459-1471.

Zhang, M. G., Uno, I., Zhang, R. J., Han, Z. W., Wang, Z. F., and Pu, Y. F., 2006. Evaluation of the Models-3 Community Multi-Scale Air Quality (CMAQ) Modeling System with Observations Obtained During the Trace-P Experiment: Comparison of Ozone and Its Related Species.

Atmospheric Environment 40(26), 4874-4882.

Zhang, Y., Pun, B., Vijayaraghavan, K., Wu, S. Y., Seigneur, C., Pandis, S. N., Jacobson, M. Z., Nenes, A., and Seinfeld, J. H., 2004. Development and Application of the Model of Aerosol Dynamics, Reaction, Ionization, and Dissolution (MADRID). Journal of Geophysical Research-Atmospheres 109(D1), doi:10.1029/2003JD003501.

CHAPTER TWO

Enhancement and Evaluation of the AIRPACT Ozone and $PM_{2.5}$ Forecast System for the Pacific Northwest

Jack Chen, Joe Vaughan, Jeremy Avise, Brian Lamb
Washington State University, Department of Civil and Environmental Research

Susan O'Neill
United States Department of Agriculture, Natural Resources Conservation Service

Abstract

The AIRPACT-3 real-time numerical air quality forecast system operates daily in the Pacific Northwest region to predict hourly concentrations of ozone, $PM_{2.5}$ and related precursor and product species. In an update to the existing AIRPACT-2 forecast system, the MM5/SMOKE/CMAQ modeling system replaces the existing MM5/CALMET/CALGRID model framework. The new modeling domain encompasses Washington, Oregon and Idaho and bordering areas with 12 km x 12 km grid cells and 21 vertical layers. The system includes a dynamic emission processing subsystem with the real-time wildfire and prescribed fire emission, and dairy ammonia emission operations. A comprehensive evaluation was performed for the August – November 2004 period to evaluate the system performance against measurement data. Results showed that the system performed well for ground level ozone and $PM_{2.5}$ concentrations, and is accurate within current model performance limits. The system is skillful in predicting episodic ozone conditions (8-hr daily maxima) above 50 ppbv, but systematically over-predicts concentrations less than 40 ppbv. In terms of $PM_{2.5}$, the model correctly captures the concentration variations between urban and rural regions, and captures qualitatively the speciated distribution of fine PM components. $PM_{2.5}$ forecast performance is generally poor for sites within the Columbia River Gorge regions which is attributed to errors in predicting transport within the complex gorge topography.

Introduction

Air pollutants such as tropospheric ozone and particulate matter can cause adverse health effects in humans and degrade ecosystem integrity. To protect the public health and welfare the U.S. Environmental Protection Agency (EPA) established the National Ambient Air Quality Standards (NAAQS) for ozone (O_3) particulate matter (PM) with aerodynamic diameters less than 10 μm (PM_{10}) and 2.5 μm ($PM_{2.5}$). In 1997 the ozone standard was revised to a more stringent level of 80 ppbv over 8-hour average period, and in 2006 the 24-hour average $PM_{2.5}$ standard was also revised from 65 $\mu g/m^3$ to 35 $\mu g/m^3$.

There has been growing interest in many countries, including the US, to predict the onset of pollution episodes in order to provide early warnings to the general public. Recently, with advances in computation technology, regional air quality forecast systems have shifted from analysis of forecast meteorology and statistical methods to the use of sophisticated numerical models that account for meteorology, transport and chemistry simultaneously. Several such systems have been implemented around the world and in the US; examples include: the Australian AAQFS (http://www.epa.vic.gov.au/air/aaqfs/), the Canadian CHRONOS (http://www.msc-smc.ec.gc.ca/aq_smog/chronos_e.cfm; (Pudykiewicz et al., 2001), the UK NAME-III system (http://www.airquality.co.uk), and in the US, several systems for the Eastern US (Mckeen et al., 2005) and the EPA AIRNOW (http://airnow.gov) network for the conterminous US.

In the Pacific Northwest Region, as part of the Northwest International Air Quality Environment Science & Technology Consortium (NW-AIRQUEST, http://www.nwairquest.wsu.edu) , the Air Indicator Report for Public Access and Community Tracking (AIRPACT) real-time numerical air quality forecast system, has been providing hourly air pollutant predictions since May, 2001 (Vaughan et al., 2004). The system was based on the

MM5/CALMET/CALGRID modeling system (AIRPACT-1 and AIRPACT-2) and was primarily designed for prediction of ground level ozone pollution. Recently, because of the interest in $PM_{2.5}$ health and visibility effects, the AIRPACT system was upgraded as AIRPACT-3 to include aerosol chemistry and fate via the EPA Community Multi-scale Air Quality (CMAQ) modeling system (Byun et al., 1999).

In this paper, we describe AIRPACT-3 which was initiated in December, 2005 to produce daily 24 hour forecasts (http://airpact-3.wsu.edu). To assess the ability of the new system to capture the onset and evolution of air pollution events, the system was re-run in forecast mode for a 4-month evaluation period covering August – November 2004 and results compared with measurement data for ozone and fine particulate matter. This evaluation provides valuable information concerning forecast accuracy for individual pollutant species, and the CMAQ model ability to capture atmospheric chemical conditions with forecast emissions and meteorology. In the following sections, we first describe the modeling system framework followed by a description of the evaluation period setup, observational data used for the evaluation, and AIRPACT-3 forecast performance results.

Model System Description

Chemical Transport Model

The core photochemical transport model used in AIRPACT-3 is the CMAQ Chemical Transport Model (CCTM, version 4.6). The model accounts for chemical interactions for compounds in gas, aqueous and aerosol phases. The chemical mechanism applied in the model is the "saprac99_ae4_aq", with the SAPRC99 gas-phase chemical mechanism (Carter, 2000) and aerosol module (version 4) that includes the ISORROPIA secondary inorganic aerosol algorithms (Nenes et al., 1998) and the SORGAM secondary organic aerosol formulations (Schell et al., 2001). The aerosol module contains aerosol process dynamics for

nucleation, coagulation, condensation, evaporation and dry deposition (Binkowski et al., 2003). Wet deposition of both aerosol and gas-phase compounds are included in cloud processes that scavenge chemical species via aqueous chemistry and attenuate incoming shortwave radiation that is important for photolytic reactions.

CMAQ represents aerosols via the modal approach with overlapping log-normal aerosol size distributions for three modes: Aitkin mode, accumulation mode and coarse mode. To convert the long-normal distribution representation to size-resolved mass concentration, the PMx program (Jiang et al., 2006) is used to post process model output for $PM_{2.5}$ mass concentrations for individual aerosol component species.

Model Domain and Forecast Period

The domain of the AIRPACT-3 system is shown in Figure 1. The domain encompasses all of Washington, Oregon and Idaho along with portions of bordering states and Canadian provinces. The large domain allows the system to better capture pollutant transport over longer distances and lessens the influence of model boundary conditions on forecast results. The domain consists of 95 by 95 horizontal grids with 12 km x 12 km horizontal grid cells. Vertically, there are 21 layers. There are 12 layers in the lower 1,000 meters and an additional 9 layers up to the tropopause (10 km). Table 1 shows the vertical distribution of vertical layers with sigma (σ) values at layer boundaries and the corresponding approximate elevation from sea level.

Timing of model output is important for forecast products such as AIRPACT. In the configuration used for this evaluation, AIRPACT-3 provides a 24-hour air quality forecast beginning at 08-hour GMT (0-hour PST) for the next day. The system is initiated daily at midnight and is able to complete the entire simulation and post processing in less than 4 hours with graphical outputs available by 4 am local time. In January, 2007, the system was extended

to provide 64 hour forecasts, but these longer term forecasts are not considered in the evaluation presented here.

Meteorology

The forecast meteorology for AIRPACT-3 comes from the Mesoscale Meteorological model (MM5 version 3.7.3) (Grell et al., 1994) operated in forecast mode by Mass and colleagues at the University of Washington (http://www.atmos.washington.edu/mm5rt). This real-time MM5 forecast system provides hourly, 3-dimensional, gridded meteorological variables over the Pacific Northwest region at 36-, 12- and 4-km grid resolutions with 37 vertical levels for the next 48 to 72 hours. The AIRPACT-3 system uses the 12-km MM5 output initialized with the 00Z-hour data from the National Center for Environmental Prediction (NCEP) GFS model results. In the current system setup, the forecast 12-km MM5 model is run in non-hydrostatic mode with CCM2 radiation scheme, Reisner-2 moisture microphysics parameterization, Kain-Fritsch cumulus parameterization and the MRF/Hong-Pan planetary boundary layer (PBL) scheme. More information, including model configuration updates, for the forecast MM5 simulations and general model performance can be found in Mass et al. (2003) and on the MM5 website.

The AIRPACT-3 system is initiated nightly after the meteorological data from MM5 becomes available. The Meteorology-Chemistry Interface Processor (MCIP version 3.1) pre-processes the MM5 model results and collapses the vertical level from 37 sigma layers to 21 layers while retaining key parameters such as PBL heights, incoming solar radiation, and momentum and heat fluxes for CMAQ.

Emissions

A realistic emission inventory is critical to the accuracy of air quality forecast results. The AIRPACT-3 emission subsystem includes a series of emission processing steps to

generate gridded, hourly emission data that reflect the existing conditions for each hour and each grid point. The subsystem is initiated at each forecast day to process emissions from anthropogenic and biogenic sources, including ammonia emissions from dairy operations, and emissions from wild and prescribed fires. The following sections describe these processes in greater detail. Table 2 summarizes emissions by source categories and states in the domain for a typical weekday scenario.

Anthropogenic Emission

The SMOKE (Sparse Matrix Operator Kernel Emissions) processor version 2.1 (Houyoux et al., 2005) was modified to process area, on-road mobile, non-road mobile and point source emission categories for each simulation day. Area and non-road mobile emissions are based on the 2002 EPA National Emission Inventory (NEI-2002) dataset and adjusted to year 2005 with county and source specific projection factors from the EPA Economic Growth Analysis System (EGAS) software (U.S. EPA, 2004). On-road mobile emissions are generated using the EPA MOBILE-6 (US. EPA, 2003) emission factors, with 2005 mobile activity data from individual states. Point source inventory is also based on the NEI-2002 dataset. The inventory was updated to reflect 2005 operation activities for states of Washington, Idaho and Oregon by the emissions workgroup within NW-AIRQUEST, involving the Washington State Department of Ecology with inputs from the Idaho and Oregon state agencies. Anthropogenic emissions data for area, mobile and point sources over province of British Columbia, Canada were also included (GVRD, 2002). Canadian emissions were applied as-is without projections to future years.

The emission inventory datasets for anthropogenic sources are imported as annual totals by source categories. At the beginning of each forecast, the emission processor allocates the annual emissions to hourly time step based on SMOKE temporal profiles for the day and source category type. This method allows for dynamic temporal adjustments by month,

weekday/weekend/holiday and hour. In addition, on-road mobile sources are adjusted with gridded, hourly temperatures to account for evaporative loss emissions, and point source emissions are allocated vertically according to calculated plume rise using the gridded, hourly meteorological data.

Biogenic Emission

The biogenic emissions inventory system version 3 (BEIS3) model from EPA (U.S. EPA, 2002), as part of the SMOKE processor, is used to estimate daily biogenic emissions for the AIRPACT-3 system. The gridded 1-km BELD3 landuse dataset was preprocessed to the 12-km AIRPACT-3 domain and used to generate normalized biogenic emissions for summer and winter biomass distributions. For each forecast, the seasonal normalized emissions are adjusted with forecast hourly temperature and shortwave radiation to produce gridded VOC and NOx emissions for CMAQ. Emissions include soil and vegetative NOx, isoprene, terpenes and other non-specific biogenic VOC.

Ammonia Emission

Gas-phase ammonia in the atmosphere plays an important role in the formation of secondary inorganic aerosol through interactions with sulfur and nitrogen compounds. The significance of accurate ammonia emissions in modeling aerosol formation have been discussed in several recent studies (Pinder et al., 2006). Livestock facilities produce large amounts of ammonia emissions from various operational conditions and processes (Rumburg, 2006).

The AIRPACT-3 system incorporates a new dairy ammonia emission module (Rumburg et al., 2005). The module incorporates emission algorithms for three types of dairy operations: animal housing, manure storage and manure processing. The emission algorithms for each operation were developed through various measurement studies for a northwestern dairy and

compiled into a single emission processing module. For more detailed descriptions of the study and algorithm development, please refer to Rumburg (2006).

In this application of the emission module, dairy ammonia emissions are estimated using dairy locations by latitude and longitude where each dairy is treated as a point source. Additional input parameters such as dairy capacity (number of cattle), manure storage type, manure loading, and manure process method were obtained and derived from Oregon State Department of Environmental Quality and Washington Department of Ecology. The module is executed for each AIRPACT-3 forecast simulation. The emission algorithm adjusts ammonia emissions with hourly forecast temperature and wind speed. Table 2 lists typical daily ammonia emissions for Washington and Oregon states from the module. Ammonia from dairy operations represents 38% and 88% of total state-wide anthropogenic ammonia emission for Washington and Oregon states, respectively. For the current evaluation period, NH_3 emissions for Idaho and other areas were taken from the EPA NEI emission inventory.

In addition to dairy operations, ammonia emissions from sources such as fertilizer application, feedlot operations and industrial activities are included in the area and point source categories and processed as part of the anthropogenic inventory.

Wild and Prescribed Fire Emission

Large scale fires contribute significant amount of pollutants and pollutant precursors to the atmosphere. They affect formation of both ground level ozone and particulate matter over large regional areas (Miranda, 2004; Malm et al., 2004). AIRPACT-3 incorporates forecast fire emissions via an interface with the USDA-Forest Service BlueSky smoke modeling system (www.BlueSkyRains.org, Larkin et al., 2007). Each day, the BlueSky model system estimates fire emissions by location with fire event data from the National Interagency Fire Center (http://www.nifc.gov). Output from the BlueSky model contains emission estimates for CO, total

organic gas (TOG), NOx, fine and coarse particulate matter, as well as total fire area and heat flux. For each forecast simulation, AIRPACT-3 automatically retrieves these fire emission estimates and incorporates them via the SMOKE processor as part of the emissions input. There is extensive agricultural field burning within eastern Washington and northern Idaho, and these sources are currently managed using the ClearSky smoke dispersion forecast system (http://www.clearsky.wsu.edu, Jain et al., 2006). However, currently the emissions from these burns are not included in AIRPACT-3 primarily because the burn managers in the region consider a wide range of burn scenarios and it is, thus, difficult to specify an accurate acreage forecast to be burned for the next day.

Fire emissions in AIRPACT-3 are treated as individual point sources at reported locations. The emissions are allocated to vertical layers using the buoyant area source plume rise algorithm in the SMOKE processor. The input emission species are further speciated according to the CMAQ chemical kinetic mechanism. Currently, 77% of total $PM_{2.5}$ from fire is assumed to be of primary organic aerosol origin (POA), 16% as elemental carbon (PEC), 5% as primary unspecific fine PM (PMFINE) and 2% as fine sulfate aerosol (PSO4). In addition, gas phase TOG is allocated as percentage fractions to input emission following profiles in Table 3.

Initial and Boundary Conditions

Boundary conditions represent the influx of chemical species into the domain throughout the simulation period. The boundary conditions can have a significant influence on background chemical representation in the model system. Measurement studies have shown ozone and other chemical concentrations change throughout the year due to long range transport and season cycles (Weiss-Penzias et al., 2004). To better account for seasonal chemical variations, boundary conditions in AIRPACT-3 are compiled from MOZART-2 (Ozone and Related Chemical Tracers version 2, Horowitz et al., 2003) global chemical model output. Long-term

simulation outputs (1990-1999) from the MOZART-2 model were diurnally averaged by month and grid across the AIRPACT-3 domain boundary and reformatted as boundary conditions for the CMAQ model. The resulting AIRPACT-3 boundary conditions represent diurnal concentration profiles of chemical species that change monthly and spatially across all sides and layers of the model domain. Several recent studies showed improvements to regional model performance with using boundary conditions from global chemical models (Barna et al., 2006; Tong et al., 2006). Table 4 summarizes the average boundary conditions used in AIRPACT-3 by vertical layer and season for selected chemical species.

Initial conditions for each forecast period are obtained using the "daisy-chain" approach where results from the last simulation hour from the previous day forecast are used to initialize the new run. This approach maintains the continuity of chemical conditions between periods and reduces the need for model spin-up associated with using static initial conditions.

Web Presentation of Results

Following each forecast, input and output data are processed for display on the AIRPACT-3 web site. Animated maps of meteorological variables, emission rates, and species concentrations are displayed for selected parameters. On the day following the forecast, observations available from a regional real-time observational network are automatically retrieved and paired with the model predictions. The observational data are graphed on the model contour maps for web retrieval as historical simulations. The model output is also used to compile monthly maps that include monthly maxima and other accumulated air quality parameters. Finally, the paired observed and predicted concentrations are archived for further analysis and model evaluation.

Description of AIRPACT-3 Evaluation

In order to comprehensively evaluate AIRPACT-3 forecast performance, the system was re-run for a 4-month historical period (August – November 2004) in the forecast mode without any observational analysis or nudging. This period was chosen specifically to coincide with a measurement program in the Columbia River Gorge area conducted by the Southwest Clean Air Agency (SWCAA). In addition, the evaluation period covers both summer ozone and early winter PM seasons. Since this is a historical re-run, the initial conditions were generated from a 1-month model spin-up prior to the start of the actual evaluation run. All other settings and input processing were identical to the forecast system.

Wild and prescribed fire emissions were obtained from the BlueSky system output with reported fire events for the evaluation period. Table 5 shows the monthly total wild and prescribed fire emissions by state in the domain and the percentage fraction of wild fire with respect to total fire emissions. Of the four-month period, August had the highest wild fire activity with all fire emissions contributed from wildfires. The major wildfire events in August 2004 were the Porter fire in Salmon-Challis National Forest near Central Idaho, the French fire in northern California, and the Fischer fire in south central Washington. For the rest of the months, fire emissions were dominated by prescribed fires in Washington, Oregon, Idaho and Montana.

Forecast MM5 meteorological output for the evaluation period was obtained from the University of Washington MM5 data archive. To assess the MM5 model performance during this period, model outputs were compared with observational data from stations across the domain. Model performance statistics were compiled for parameters important to air quality: surface temperature, wind direction, wind speed, precipitation and relative humidity. Table 6 summarizes the statistics by month for all combined stations. In general, MM5 was reasonably accurate in terms of the mean bias associated with wind direction, surface temperature, 24-hour precipitation and relative humidity, but it slightly over-estimated wind speed with mean errors of

1.4 m/s to 1.9 m/s. MM5 performance in terms of absolute errors provides a more useful measure of model error, and shows that there can be significant forecast errors in wind direction (60° to 70°) for given locations and times. Absolute errors in wind speed were approximately 2 m/s and absolute errors in temperature were approximately 2°C. This level of model performance is commonly observed for MM5 forecast simulations for the region, and the performance statistics are generally comparable, but slightly higher than those obtained using MM5 with observational nudged simulations for the same region (Barna et al., 2000a; O'Neill et al., 2005).

Ozone and $PM_{2.5}$ measurement data during the evaluation period were collected from measurement stations in Washington, Oregon and Idaho. Ozone measurement data were collected from the EPA-AQS network (http://www.epa.gov/ttn/airs/airsaqs). $PM_{2.5}$ measurement data, including chemically speciated fine PM components: nitrate (PNO3), sulfate (PSO4), ammonium (PNH4), elemental carbon (PEC) and organic carbon (POC), were collected from the IMPROVE measurement network (http://vista.cira.colostate.edu/improve), the EPA-AQS network and the Columbia Gorge measurement program by the SWCAA (Green et al., 2006). Table 7 lists the network monitor stations, their latitude/longitude locations, and the respective species used in this evaluation. Figure 1 depicts the locations of these observation stations in the modeling domain. The IMPROVE stations were mostly in Class I wilderness areas and national parks. The EPA-AQS stations were mostly in urban and suburban areas. The measurement program by the SWCAA was limited to sites inside the Columbia River Gorge.

Evaluation Results and Discussions

Ground Level Ozone Forecast

Evaluation of AIRPACT-3 ozone forecasts emphasizes the daily maximum 8-hour averaged (daily max 8-hr) concentrations compiled from hourly measured and modeled data.

This is the measurement matrix used to determine air quality alerts and NAAQS exceedances. Since ozone is a summer time pollutant, the following analyses were limited to August and September, 2004.

General Performance

Figure 2 shows a scatter plot of modeled and measured daily max 8-hr ozone concentrations paired by site and day. Overall, there was no ozone episode exceeding the NAAQS standard, however, ozone levels greater than 70 ppbv were observed. The mean measured daily max 8-hr ozone concentration over all sites was 34 ppbv, and highest observed value was 79 ppbv at North Bend, WA downwind of Seattle. The mean modeled daily max 8-hr ozone concentration over all sites was 46 ppbv, and highest modeled value was 87 ppbv at Enumclaw WA, also downwind of Seattle. The AIRPACT-3 forecast system was able to capture the general pollutant conditions during the evaluation period with 95% of the data points within a factor of 2 of measured concentrations. Data points outside this margin were mostly from low measured concentrations (<20 ppbv), where AIRPACT-3 over-predicted surface ozone concentrations.

AIRPACT performance statistics for daily max 8-hr ozone in terms of mean bias (MB), normalized mean bias (NMB), mean error (ME), normalized mean error (NME), root mean square error (RMSE) and correlation coefficient (R) are shown in Table 8. These terms are defined in Appendix A. The statistics were calculated from paired daily maxima ozone concentrations extracted from 8-hr running means across the two month period. Times with measured ozone concentration less than 30 ppbv were excluded to emphasize high ozone events important for the forecast system. Excluding low observed data point also makes interpretation of the performance statistics more meaningful since low observed concentrations can cause normalized statistics to become large (Boylan et al., 2006).

On average the model slightly over-predicted daily max 8-hr ozone concentrations with a mean bias of 2.7 ppbv (NMB of 6%). The mean absolute error was 7.2 ppbv (NME of 17%) with RMSE of 9.1 ppbv and a correlation coefficient of 0.55. The range of model statistics was comparable, if not better, than other air quality forecast systems using CMAQ (Mckeen et al., 2005; Eder et al., 2006a). The system performed well, and is within EPA's recommendation for air quality models with bounds of ±15% for normalized mean bias and 35% for normalized mean error (U.S. EPA, 1991). Figure 3 shows the ratio of measured to modeled daily max 8-hr ozone concentrations versus the measured ozone concentration. These results show that AIRPACT-3 performed well at capturing high ozone episodes. However, it systematically over-predicted concentrations less than 40 ppbv. The over-prediction was worse with lower observed ozone levels. This systematic over-prediction at low levels is often observed in numerical air quality models. In the work of Russell et al. (2000) they attributed this to excessive turbulent mixing in modeling transport during nighttime or non-convective, stable conditions. In an evaluation of CMAQ for the eastern US, Eder et al. (2006a) found similar positive bias and attributed it to excessive downward transport of high level ozone aloft and too much photolysis under high cloud conditions.

Spatial

In terms of the spatial distribution of predicted ozone concentrations during the evaluation period, Figure 4 shows modeled and observed averaged daily max 8-hr ozone surface distribution contours for the August and September months. The observed ozone concentrations are represented by colored diamonds with the same color scale as the modeled surface contour. The ozone spatial distribution varied between the two months, with August having generally higher ozone than September. Both modeled and observed data showed higher ozone levels in the inland areas than along the costal regions.

In August, ozone levels of 30 ppbv to 42 ppbv for sites west of the Cascade Mountain were captured by the model while slightly higher levels of 45 ppbv to 55 ppbv were correctly modeled for sites east of the Cascade Mountain. Peak ozone in August occurred at WhitneyEle site in Idaho with observed average daily max 8-hr ozone of 54 ppbv. AIRPACT-3 system slightly underestimated this with predicted ozone concentration of 51 ppbv. In September, ozone concentrations were lower, and AIRPACT-3 overestimated many of the measurement values. Ozone levels for Seattle and Portland urban areas were better predicted in September compared to August. Peak ozone during the month occurred at the Craters of the Moon site in Idaho with observed daily max 8-hr ozone of 45 ppbv; AIRPACT-3 overestimated this by 5 ppbv at 50 ppbv.

Quantitatively, Figure 5 shows the NMB and NME for individual measurement sites for daily max 8-hr ozone over the two month periods. The NMB values ranged from -3% at Talent, OR to 21% at the Olympic National Park (OlympicNP) site, and of the total 30 measurement sites, 17 sites had NMB below ±10%. Most sites showed a positive bias due to over-predictions at low observed ozone levels as discussed previously. Similarly, the NME ranged from 10% at RangerStn, WA to 23% at the Mt. Rainier National Park site, and there were 22 sites with NME less than 20%.

Comparisons between urban/suburban and rural sites showed general better performance statistics for urban/suburban sites with the average NMB equal to 5% and the NME equal to 17%. CMAQ had better skill in capturing episodic ozone conditions but over-estimated rural ozone conditions. At rural sites, the observed daily max 8-hr ozone was 59 ppbv, and there was a higher bias (NMB of 10%), but similar error (NME of 17%) compared to urban/suburan sites.

Temporal

Figure 6 shows the time series of modeled and measured daily max 8-hr ozone concentrations and the resulting model statistics (ME, MB, R) during the two-month evaluation period. Overall, the model performed well with averaged modeled concentration tracking closely to the measured values. The period of high measured ozone concentration during the second week of August was correctly captured by the system with a slight positive bias of 5 to 10 ppbv. The ME ranged from 0 to 10 ppbv and MB from -10 to +15 ppbv. It is evident that MB was generally positive after August 20 when average observed ozone concentrations were relatively low (< 50 ppbv). The daily correlation coefficient for the period ranged from 0.9 to -0.3. The correlation was worse for the period between September 24 and October 1 when the averaged correlation coefficient was only 0.05 compared to the overall average of 0.53. A closer look at the period showed a general over-prediction across all measurement sites. The average maximum predicted 8-hr ozone across all sites was 56 ppbv whereas the measured concentration was 48 ppbv. During this period the model predicted a possible onset of pollution event with calm winds, high daytime temperature and relatively stable conditions across the region. However, this ozone conducive condition did not take place, instead, the observed meteorological condition across the region had lower temperature with periods of precipitation. The MM5 model performance for this period showed a mean bias across the region for ground temperature, and 24-hour precipitation of +1.7 ^{0}C and -0.1 mm respectively.

In terms of predicting hourly onsets of maximum ozone concentration within the day, Figure 7 shows the distribution of hourly differences between modeled daily peak time and observed daily peak time over the two month period for all sites. There were 1823 data points across 30 measurement sites; of this, 20% of the time the model was accurate in predicting the hourly onset of maximum daily peak ozone, and 75% of the time the model was accurate within 3 hours of the observed peak hour.

Site Specific Ozone Performance

This section takes a closer look at AIRPACT-3 predictions for sites with high observed ozone concentrations. Figure 8 shows the quantile-quantile plot of modeled and observed daily max 8-hr ozone concentrations at the NorthBend, WA, Enumclaw, WA, Talent, OR, Carus, OR, and WhitneyEle, ID sites. These sites had high observed 8-hr ozone concentrations exceeding 75 ppbv. NorthBend, Enumclaw and Carus are urban sites. NorthBend and Enumclaw are downwind of Seattle, while Carus is downwind Portland. AIRPACT-3 over-estimated both high and low observed ozone levels in these areas with Enumclaw showing constant over-prediction across most concentration levels. The mean bias for Enumclaw was 5.7 ppbv. On the other hand Talent and WhitneyEle are more rural sites in southwest Oregon and south central Idaho respectively. AIRPACT-3 generally under-predicted the highs and over-predicted the lows at these locations. The under-prediction was most severe at Talent. The period maximum observed 8-hr ozone was 75 ppbv and AIRPACT-3 predicted 58 ppbv. The period MB at Talent was also the lowest of all measurement sites at -1.4 ppbv.

Figure 9 shows the modeled and measured averaged diurnal ozone concentrations for the five sites. The solid lines indicate mean daily 8-hr ozone for the hour and the error bars represent 75 and 25 percentile values. Both observed and modeled concentrations displayed clear diurnal profiles with peak daily concentration during midday. The peak time was better captured at Enumclaw and NorthBend at 11 am local time. However, AIRPACT-3 overestimated the magnitude of ozone for all hours at both locations. At Carus, Talent and WhitneyEle the magnitudes of daily maximum ozone concentrations were better predicted, however, the predicted peak was earlier by 1 to 3 hours than the observed. The graph also shows that AIRPACT-3 over-estimated night time ozone across all 5 sites. The observed mean nighttime low concentration ranged from 9 ppbv at NorthBend to 24 ppbv at Talent. AIRPACT-3 overestimated this with the modeled mean night time low ranged from 21 at Carus to 29 ppbv at

Enumclaw. This inaccuracy in predicting nighttime low ozone is commonly observed in model studies using CMAQ (Smyth et al., 2006; O'Neill et al., 2006). This is typically attributed to underestimation of NOx emissions at night and incorrect treatment of turbulent mixing during stable nighttime conditions.

Surface $PM_{2.5}$ Mass Concentration Forecast

EPA's NAAQS exceedances criterion for $PM_{2.5}$ is based on mass concentration loading over a daily (24-hour) period. Measurement data collected for this evaluation were also based on 24-hour accumulated concentrations. The hourly AIRPACT-3 forecast results were averaged over the same period for comparison by site and measurement timeframe.

Predicting PM concentrations is considerably more difficult than that of gas-phase ozone (Seigneur, 2001). Simulating PM formation involves tracking the transport and interactions of both primary and secondary pollutants across gas, solid and aqueous phase chemical interactions. Furthermore, measurements of particulate matter for model validations are less abundant compared to ozone measurements and contain much higher uncertainties due to complications in PM chemistry and less mature measurement techniques. For example, Soloment et al. (2004) found 15% to 30% differences in PM measurements from co-located monitoring sites between two network instruments. Since measurement methods, uncertainty and error associated from monitoring networks differ, the evaluation results in this section are separated by measurement networks. This also provides a general performance comparison between urban and rural regions as most EPA-AQS network sites are in urban areas while the IMPROVE sites and the SWCAA sites are in rural locations.

General Performance

Figure 10 shows the scatter plot of measured and modeled $PM_{2.5}$ concentrations for the 4-month evaluation period. Table 9 shows the performance statistics for the same period. The

IMPROVE network monitors located in rural regions had lower mean observed concentration of 6 $\mu g/m^3$ compared to the EPA-AQS network sites of 11 $\mu g/m^3$. AIRPACT-3 captured this overall difference, albeit with a slight over-prediction, with average predicted concentrations of 8.2 $\mu g/m^3$ and 13 $\mu g/m^3$ respectively.

For both IMPROVE and EPA-AQS sites, AIRPACT-3 results had RMSE of around 10 and R of 0.5. The MB and NMB were 2.2 $\mu g/m^3$ and 37% for IMPROVE, and 2.0 $\mu g/m^3$ and 17% for EPA-AQS sites respectively. The ME and NME were 5.5 $\mu g/m^3$ and 85% for IMPROVE, and 8.0 $\mu g/m^3$ and 70% for EPA-AQS sites respectively. In contrast to the ozone performance, there was no clear observed concentration range where AIRPACT-3 performed significantly better or worse. Of all the data points, 61% fall within a factor of 2 of measurement values.

Additional performance measures specifically for PM evaluation are fractional bias (FB) and fractional error (FE) as proposed by Boylan et al. (2006). These statistics allow for less stringent performance evaluations for lower observed concentration data to account for higher uncertainties associated with lower measurement concentrations. The FB ranges from -200% to +200% and the FE ranges from 0% to +200%. Boylan et al. (2006) recommended current air quality models should have a performance goal for FB within ±30% and FE less than 50%, and performance criteria for FB within ±75% and FE of less than 60%. For the evaluation, AIRPACT-3 achieved an overall FB of 3% and FE of 58%. The low FB was within the performance goal, but the large FE exceeded the goal but was within the performance criteria limit.

Figure 11 shows the $PM_{2.5}$ FE and FB versus averaged measured concentrations by site for the 4 month period. AIRPACT-3 performed well in capturing the monthly $PM_{2.5}$ concentrations with most points within the model performance criteria limit (dotted line). Of all the measurement comparisons, IMPROVE sites had 82% and 77% of data points within the

performance criteria limit for FE and FB, respectively. Similarly, for the EPA-AQS sites, 68% and 61% of all data points were within the performance criteria for FE and FB.

The FE and FB plots also showed higher $PM_{2.5}$ concentrations and more scatter for the EPA-AQS sites compared to IMPROVE sites. The EPA-AQS monitors in urban areas receive large anthropogenic influence of primary PM and PM precursor emissions such as NOx, SO_2 and VOC. $PM_{2.5}$ concentration and concentration variability at EPA-AQS sites are thus, higher, and AIRPACT-3 performed slightly worse due to the model's inability to capture such changes.

Spatial

The spatial distribution of $PM_{2.5}$ concentrations vary due to occurrences of wild fires and anthropogenic influences in urban areas. Figure 12 shows the predicted monthly average $PM_{2.5}$ concentrations. General modeled $PM_{2.5}$ background concentrations were between 0 $\mu g/m^3$ to 5 $\mu g/m^3$. August had the highest predicted domain-wide concentrations because of numerous wild-fires during this month. The Porter Fire in central Idaho was the largest wild fire that burned throughout August. It resulted in a large regional impact with peak 24-hr $PM_{2.5}$ reaching 40 $\mu g/m^3$ predicted by AIRPACT-3. Smaller fires in central Washington, southern Oregon, British Columbia and northern California were also captured and resulted in hot-spots of elevated $PM_{2.5}$ concentrations between 25 $\mu g/m^3$ and 35 $\mu g/m^3$. Wild-fire activity decreased for the other months, and the predicted monthly $PM_{2.5}$ spatial distributions were more similar, with elevated concentrations in urban areas: Seattle, Portland, Spokane, Boise, and areas along the Interstate-5 (I-5) highway.

Figure 12 shows the corresponding error maps by monthly FB and FE for monitoring sites in the domain. Forecast accuracy varied by sites and months. In general, AIRPACT-3 performed slightly better for sites along the coastal regions than inland, and August had the worst overall $PM_{2.5}$ forecast compared to the rest of the months. Throughout the four months,

FB ranged between minimum of -119% at the NezPerceNP site in August to +157% at the CRMO site, also in August. The FE ranged from 6% at the PASA site in September to 157% at the CRMO site in August. In August, 47% of all sites exceeded the model criteria limit for FB and 30% exceeded the criteria limit for FE. However, for the rest of the months, AIRPACT-3 performed well with more than 75% of all observational sites within the criteria limit for both FE and FB.

The poor performance in August can be attributed to significant over-predictions for sites in central Idaho and under-predictions for sites east of Washington and south of Oregon. The over-prediction errors were possibly due to inaccuracy in wild-fire emission estimates and CMAQ model formulation. Since the Porter fire burned during most of August, over prediction in fire emissions could lead to a large bias in the AIRPACT-3 $PM_{2.5}$ forecast. In addition, CMAQ has been found to under-predict aerosol deposition rates (Dong, 2004). This can cause PM to be transported further and impact a larger area. In this case, PM emissions from the Porter Fire were transported 200 km to 300 km south, and caused over-predictions at the CRMO and SAWT sites. The August observed $PM_{2.5}$ at CRMO and SAWT sites were 4 $\mu g/m^3$ and 7 $\mu g/m^3$; AIRPACT-3 over-estimated this with 13 $\mu g/m^3$ and 36 $\mu g/m^3$, respectively.

Temporal

In terms of the $PM_{2.5}$ forecast over time, Figure 13 shows the time series of modeled and measured daily $PM_{2.5}$ concentrations, and the performance statistics (FE, FB and R) averaged over the IMPROVE and EPA-AQS network stations. AIRPACT-3 captured the concentration differences between the two networks, with EPA-AQS sites having consistently higher concentrations than the IMPROVE sites. For the EPA-AQS stations, the observed $PM_{2.5}$ concentrations ranged from 2.5 $\mu g/m^3$ to 28 $\mu g/m^3$, and the modeled concentrations ranged from 4.3 $\mu g/m^3$ to 24 $\mu g/m^3$. The concentration range was smaller at the IMPROVE stations, with observed concentrations from 2.7 $\mu g/m^3$ to 8.5 $\mu g/m^3$, and modeled concentrations from 3.5

$\mu g/m^3$ to 15 $\mu g/m^3$. The larger concentration range for the EPA-AQS stations resulted in larger FE of 8% to 137% compared with the IMPROVE stations of 13% to 96%. The model correlation coefficient (R) also changed more rapidly with time for the EPA-AQS stations from -1 to 0.99 compared to -0.4 to 0.9 for the IMPROVE stations.

Throughout the 4-month period, large concentration fluctuations were observed for the IMPROVE stations in August when wild-fire activities were high. During this period AIRPACT-3 over-predicted the fire impacts with FB reaching +68%. For October and November, $PM_{2.5}$ concentrations stayed low and the FB ranged from -24% to 41%, while FE ranged from 13% to 90%. At the urban sites, represented by the EPA-AQS stations, large concentration fluctuations were observed during October and November when stagnant atmospheric conditions are more frequent. During these two months AIRPACT-3 performed well in predicting the concentration changes. The system over-predicted the elevated concentrations in early October with FB ranging 4% to 74% and slightly under predicted the period peak concentration in early November with FB ranging from 0% to -33%.

Speciated $PM_{2.5}$ Component Forecast

CMAQ simulates the transport and chemical formations of individual inorganic and organic aerosol species to produce total $PM_{2.5}$ mass concentration. The accuracy of the $PM_{2.5}$ forecast, therefore, depends on the correct representation of speciated aerosol composition. In this section we look at AIRPACT-3 performance in predicting the speciated $PM_{2.5}$: PNO3, PSO4, PNH4, PEC and POC.

Measurement data for speciated aerosol during the evaluation period were available from 18 IMPROVE sites, 8 EPA-AQS sites and 3 SWCAA sites. Figure 14 shows monthly aerosol component concentrations comparing AIRPACT-3 predicted output with measured values averaged across the three network sites. Figure 15 shows comparisons by quantile-

quantile plots with data unpaired, and sorted in time, and paired by measurement networks. Table 10 summarizes the model performance statistics for each species over the evaluation period. The total aerosol components concentrations were similar to the $PM_{2.5}$ levels discussed earlier, with EPA-AQS sites generally higher than the IMPROVE sites. The forecast performance varied by species and measurement networks. In general, AIRPACT-3 performed well in predicting the aerosol compositions for urban and rural sites represented by EPA-AQS and IMPROVE network monitors, respectively. However, it underestimated several major PM species in the Columbia River Gorge, represented by the SWCAA sites. Quantitatively, AIRPACT-3 over-predicted POC and PEC at most sites across the domain, and significantly under-predicted PSO4. Forecast performances were better for PNH4 and PNO3 for stations in the EPA-AQS measurement network.

AIRPACT-3 performed well in predicting the monthly fine aerosol component concentrations and their percent $PM_{2.5}$ concentration fractions during the evaluation period (Figure 14). The system correctly simulated POC as the major aerosol component for all months. The average observed POC concentrations were 5.2 $\mu g/m^3$ and 2.3 $\mu g/m^3$ for EPA-AQS and IMPROVE sites, respectively; AIRPACT-3 simulated this with 5.5 $\mu g/m^3$ and 1.9 $\mu g/m^3$. The MB and ME were 0.34 $\mu g/m^3$ and 3.7 $\mu g/m^3$ for the EPA-AQS sites and -0.45 $\mu g/m^3$ and 2.0 $\mu g/m^3$ for IMPROVE sites. The correlation coefficients were poor at 0.4 for both networks. The quantile-quantile plot showed large over-predictions of POC above 8 $\mu g/m^3$ for sites in all three monitor networks. These are mostly due to the wild fire events in August. Since 77% of all $PM_{2.5}$ from fire are allocated to organic aerosol (POA), over-predicting fire emissions will cause POC to dominate the PM fraction. In addition, POC is difficult to model due to uncertainties in biogenic and anthropogenic VOC emission inventories, and the complex chemistry involved in simulating secondary organic aerosol formations.

PEC and PSO4 were the second major aerosol components at the EPA-AQS and IMPROVE sites. AIRPACT-3 generally over-predicted PEC, and under-predicted PSO4 at both network sites. For PEC, AIRPACT-3 performed slightly better at the EPA-AQS sites with R of 0.5, compared to IMPROVE sites with R of 0.4. The MB and ME were 0.52 $\mu g/m^3$ and 0.8 $\mu g/m^3$ for the EPA-AQS sites, and 0.44 $\mu g/m^3$ and 0.72 $\mu g/m^3$ for the IMPROVE sites. AIRPACT-3 over-predicted PEC for observed concentrations above 1 $\mu g/m^3$. This is again likely due to over-predicting aerosol contributions from fire. In the current aerosol species allocation, 16% of all $PM_{2.5}$ from fires are treated as PEC. For PSO4, the overall system performance was better at the IMPROVE sites. The MB and ME were -0.82 $\mu g/m^3$ and 0.83 $\mu g/m^3$ for the EPA-AQS sites, and -0.51 $\mu g/m^3$ and 0.57 $\mu g/m^3$ for the IMPROVE sites. The performance of PSO4 is considered to be poor compare with other model studies using CMAQ for the region (O'Neill et al., 2006; Smyth et al., 2006). Model performance for PSO4 was expected to be better given that sulfate science algorithms were derived from the early Regional Acid Deposition Model (Stockwell et al., 1990) to address acid deposition problem.

PNO3 was under-predicted for all months and all sites, except October. The MB and ME were -0.31 $\mu g/m^3$ and 1.2 $\mu g/m^3$ for the EPA-AQS sites, and -0.51 $\mu g/m^3$ and 0.57 $\mu g/m^3$ for the IMPROVE sites. The measured concentrations at the two sites were similar with EPA-AQS at 1.2 $\mu g/m^3$ and IMPROVE sites at 0.8 $\mu g/m^3$. AIRPACT-3 slightly under-estimated these averages with 0.9 $\mu g/m^3$ and 0.6 $\mu g/m^3$, respectively. Overall, predictions for PNO3 is considered to be very good, compared with many air quality model studies in the literature. It is widely known that current air quality models perform poorly in predicting PNO3 concentrations with very large bias and errors (Eder et al., 2006b; Makar et al., 2003). The good performance in this evaluation may reflect better representation of regional NH_3 and NOx emissions, and the updated scientific algorithms in the current inorganic aerosol module.

In terms of PNH4, observations were available form the EPA-AQS sites and two SWCAA measurements sites in the Columbia River Gorge (COGO, CORI). The two SWCAA monitors were co-located with the IMPROVE network sites. The COGO site and the CORI sites were 20 km and 100 km east of Portland, OR, respectively. For all four months, AIRPACT-3 under-predicted PNH4 at both EPA-AQS and SWCAA networks. The under-prediction was worse for the SWCAA sites with MB and ME of -0.40 $\mu g/m^3$ and 0.43 $\mu g/m^3$, compared to EPA-AQS sites with MB and ME of -0.19 $\mu g/m^3$ and 0.39 $\mu g/m^3$. Despite the under predictions, the overall AIPRACT performance for PNH4 is considered to be good for the region. The model system had R of 0.5 and RMSE less than 1.0 $\mu g/m^3$ at both network sites. In other areas, PNH4 has been very difficult to model correctly due to high uncertainties in regional ammonia emission estimates. The improvements in AIRPACT-3 could result from the addition of the dynamic dairy ammonia emissions module, which provided better ammonia emission characterizations, both quantitatively and spatially, in the region.

Among the three network evaluations, the predictions for the Columbia River Gorge were generally poor with overall under-predictions for most species, particularly the PSO4 component. For all months, PSO4 was the dominant species in the Gorge area. The average observed PSO4 concentration was 2.0 $\mu g/m^3$. AIRPACT-3 significantly under-predicted PSO4 with 0.2 $\mu g/m^3$. The ME and MB were 1.8 $\mu g/m^3$ and -1.8 $\mu g/m^3$ respectively. High PSO4 concentrations in the Gorge area are commonly observed, since the largest regional source of sulfur dioxide, the Boardman coal-fired power plant, is located just east of the Gorge entrance and 250 km east of Portland.

In addition to PSO4, model performance for other aerosol components was also poor for the SWCAA sites. The model correlation coefficients for all aerosol components were less than 0.2, and the NMB and NME were large. The poor model performance was not surprising due to the complexity of terrain within the Gorge. The model resolution of 12-km is insufficient to

properly resolve the complex transport within the Gorge topography. The Columbia River Gorge is approximately 1000 m deep and 5 km wide. Second, a much higher measurement frequency of hourly data was used to evaluate AIRPACT-3 performance from the SWACC monitors. Unlike gas-phase pollutants, simulating aerosol concentration variations at short temporal timescales is much more difficult. This is primarily due to incomplete scientific understandings of aerosol chemistry and physics, and higher uncertainties in regional emissions of both primary PM, and PM precursor gas pollutants from anthropogenic and natural sources.

Site Specific PM Performance

In this section, we investigate a stagnant atmospheric event that happened in early November for sites with high observed $PM_{2.5}$ concentrations. In addition, we look at hourly AIRPACT-3 performance in predicting PM component concentrations at the Columbia River Gorge with available measurement data from the SWCAA network.

November Stagnant Period

A stagnant atmospheric condition was observed for a two-week period beginning November 3. During this time, low ventilation across the region trapped pollutants near the ground and caused elevated $PM_{2.5}$ concentrations exceeding the EPA NAAQS. Figure 16 shows the averaged daily maximum $PM_{2.5}$ concentrations during this time. Elevated concentrations were predicted along the west coast, in eastern Washington and in the Idaho Treasure Valley. Conditions were worse for urban areas with high anthropogenic emissions. Monitor sites in Seattle, WA (Jefferson Park); Portland OR (Mt. Tabor Park); and Boise, ID (Mt. View Park) had high observed concentrations. Figure 17 shows the time series of predicted and measured daily $PM_{2.5}$ concentrations for the three urban locations. All sites had observed daily $PM_{2.5}$ greater than the 35 $\mu g/m^3$ NAQQS. In Seattle and Portland, observed $PM_{2.5}$ concentrations were high for the first 3 measurement periods, and decreased slightly at the end

of the event. In Boise, the concentrations were generally lower, but peaked on November 8, when concentrations reached 44 μg/m^3. AIRPACT-3 captured the overall concentration trends but over-predicted at Seattle and Portland sites. Predictions were better at the Boise site, but AIRPACT-3 missed the period maximum with a modeled $PM_{2.5}$ concentration of 36 μg/m^3.

Figure 18a and 18b show the aerosol component concentrations and their percentage fraction with respect to total $PM_{2.5}$ measured and modeled at the three urban sites. A closer look shows, even though the total $PM_{2.5}$ was well predicted at Boise, the component concentrations were inaccurately represented. AIRPACT-3 under predicted all aerosol components at Boise, especially PNO3 and POC, which were dominating species at the site. In terms of percentage fraction, the speciated PM components represented much higher total $PM_{2.5}$ in measured data, than the modeled values in AIRPACT. The major predicted component in Boise was other unspecified $PM_{2.5}$. This suggests that during this period, the model under-predicted $PM_{2.5}$ contributions from secondary speciated PM components, but over-predicted contributions from primary emission such as fine soil.

AIRPACT performed slightly better at predicting the PM components at Seattle and Portland sites. It correctly predicted the dominant POC component, and concentrations of PNH4 and PNO3. The total $PM_{2.5}$ concentration fractions were better captured, however, the model still under represented the total $PM_{2.5}$ contributions from the speciated aerosol species.

Hourly PM Forecast at the Columbia River Gorge

Figures 19 and 20 show the hourly time series of predicted and measured aerosol component concentrations at the Bonneville Dam and Mt. Zion sites, respectively, for the month of November. Both sites were part of SWCAA network in the Columbia River Gorge. As discussed earlier, AIRPACT-3 performed poorly in the Columbia River Gorge due to coarse model resolution. These graphs showed that the model failed to simulate the observed

concentration variations at both sites. Throughout the month, AIRPACT-3 significantly under predicted PSO4, with modeled concentrations less than 1μg/m^3 and observed concentrations ranging from 1 μg/m^3 to 10 μg/m^3. This gross under-prediction may be attributed to incorrect SO_2 emission representations in the region. Since sulfate aerosol is hygroscopic and produced from oxidizing gas-phase SO_2, under representing SO_2 emission can result in overall low predicted concentrations in sulfate aerosol.

The forecast was slightly better for PNO3. AIRPACT-3 captured the general PNO3 concentration background of less than 1 μg/m^3, however the system failed to simulate the episodic conditions observed during November 6 – 16.

The predictions were much better for POC and PEC. The model forecast captured the general concentration changes over time including the episodic conditions between November 6 – 13, and November 22 – 24. However the occasional spikes of high predicted concentrations were incorrectly simulated especially for at Mt. Zion. These spikes may due to shifting of emission plumes impacting the monitor sites from source such as prescribed-fire. The errors were most likely result of insufficient spatial resolution such that the model incorrectly simulated the pollutant transport within the gorge.

Conclusion

In this paper, we have presented an implementation of a new numerical model framework to an existing regional air quality forecast system, and demonstrated its ability to accurately forecast ground level ozone and $PM_{2.5}$ concentrations within current model performance limits.

The new AIRPACT-CMAQ modeling system uses forecast MM5 meteorology, and the coupled SMOKE emission processor and CMAQ model to simulate hourly concentrations of air

pollutants including ground level ozone (O_3) and fine particulate matter ($PM_{2.5}$). The 24-hour forecast covers all of Washington, Oregon and Idaho, and bordering areas. The system uses 12-km by 12-km horizontal grid cells with 21 vertical layers. The system represents the latest state-of-science knowledge in atmospheric processes, with updated scientific algorithms for gas phase mechanisms, and organic and inorganic aerosol modules. The dynamic emission processor in AIRPACT-3 explicitly accounts for hourly changes in emissions due to anthropogenic activity patterns and meteorology, and includes a special diary NH_3 emissions module, and the incorporations of real-time wildfire emissions.

The emission inventory includes anthropogenic and natural sources. Anthropogenic emissions were based on EPA NEI-2002 inventory with projection factors to 2005. Biogenic emissions were generated daily from the BEIS3 model with hourly predicted temperature and solar radiation. Two significant additions to the emission processor were the real-time wild- and prescribe-fire emissions and the dynamic ammonia emissions from dairy operations. By interfacing with the BlueSky system at USDA Forest Service, AIRPACT-3 retrieves realistic fire emissions for individual fire event and location reported by forest managers in the region. The ammonia emissions module generates hourly ammonia emissions by dairy operations. The emission algorithms correct the predicted ammonia emission by dairy with forecast meteorology to better characterize emission input to the system.

Ancillary model input in AIRPACT, such as initial conditions and boundary conditions, were also dynamic. Since each forecast simulation is ‘dairy-chained’, the initial conditions were extracted from last hour of previous-day simulation to maintain simulation continuity and eliminate model spin-up requirement. Boundary conditions were compiled from long-term averages of global chemical model output. The boundary conditions vary diurnally with hour, seasonally by month and spatially by input locations.

The forecast system was re-run for August – November 2004, in forecast mode, and results compared with available measurement data from three monitor networks: EPA-AQS, IMPROVE and SWCAA. Preliminary results showed the system performed well for both ground level ozone and $PM_{2.5}$ predictions. The performance statistics were comparable, and sometimes, better than other model studies reported in the literature.

In terms of daily maximum 8-hr ozone, concentrations greater than 70 ppbv were observed and captured by the system. In general, the forecast skills were good with 95% of all data points within a factor of two of the observed concentrations. Most data points outside this margin were from low measured concentrations less than 20 ppbv. The system slightly over-predicted with NMB of +6% and NME of 17%. The MB and ME were 2.7 ppbv and 7.2 ppbv, respectively. The correlation coefficient ranged from 0.85 to -0.3 for the August – September period, with site average R at 0.5. The system was more skillful in predicting episodic ozone conditions above 50 ppbv, but systematically over-predicted concentrations less than 40 ppbv. The system was also accurate in predicting the time of day of the daily peak ozone concentration. Among all the comparisons by site and day, the model was accurate 75% of the time in predicting daily peak within 3 hours of observed daily maximum.

Forecast performances for $PM_{2.5}$ were worse than for ground level ozone due to immature scientific understandings of complex aerosol chemistry and physics, and general higher uncertainties in PM emissions and measurements. Predicted $PM_{2.5}$ mass concentrations were evaluated against measurements from rural sites and urban sites, represented by IMPROVE and EPA-AQS networks, respectively. The system accurately captured the overall concentration difference between the two networks. The averaged observed concentrations for the IMPROVE and EPA-AQS sites were 11 $\mu g/m^3$ and 6 $\mu g/m^3$, respectively; AIRPACT-3 predicted at 13 $\mu g/m^3$ and 8 $\mu g/m^3$, respectively. Overall, the forecast performance for the IMPROVE sites were slightly better than the EPA-AQS sites. At the IMPROVE sites, the ME

and MB were 5.5 μg/m^3 and 2.2 μg/m^3, respectively, and the NME was 37% and NMB was 85%. At the EPA-AQS sites, the ME and MB were 8 μg/m^3 and 2 μg/m^3, respectively, and the NME was 85% and NMB was 37%. In terms of FE and FB with respect to current aerosol model performance criteria, the IMPROVE sites had 82% of all data point fall within the limit for FE and 77% for FB, similarly the EPA-AQS sites had 68% and 61% of all data points within the FE and FB model performance criteria limit.

Fine aerosol component concentrations for PSO4, PNO3, PNH4, POC and PEC were also evaluated from available observation sites. Over the 4-month period, AIRPACT-3 component concentrations were captured relatively well for the EPA-AQS and IMPROVE monitor sites. Both locations had POC as major component species follow by PEC and PSO4. AIRPACT-3 slightly over-predicted PEC and significant under-predicted PSO4. Forecast performance for PNO3 and PNH4 were good compared to other model study for the region.

AIRPACT performances were generally poor for sites in the Columbia River Gorge, represented by the SWCAA network monitors. The system under predicted concentrations of most aerosol species, particularly, the dominant PSO4 aerosol. Hourly time series comparison showed, AIRPACT-3 captured the general concentration trends for POC, PEC and PNO3, however, detailed concentration structures were incorrectly represented in the model. The errors were most likely due to insufficient spatial resolution such that the model incorrectly simulated the pollutant transport within the complex gorge topography.

References

Barna, M. and Lamb, B., 2000a. Improving Ozone Modeling in Regions of Complex Terrain Using Observational Nudging in a Prognostic Meteorological Model. Atmospheric Environment 34(28), 4889-4906.

Barna, M., Lamb, B., O'Neill, S., Westberg, H., Figueroa-Kaminsky, C., Otterson, S., Bowman, C., and Demay, J., 2000b. Modeling Ozone Formation and Transport in the Cascadia Region of the Pacific Northwest. Journal of Applied Meteorology 39(3), 349-366.

Barna, M. G. and Knipping, E. M., 2006. Insights From the Bravo Study on Nesting Global Models to Specify Boundary Conditions in Regional Air Quality Modeling Simulations. Atmospheric Environment 40, S574-S582.

Binkowski, F. S. and Roselle, S. J., 2003. Models-3 Community Multiscale Air Quality (CMAQ) Model Aerosol Component - 1. Model Description. Journal of Geophysical Research-Atmospheres 108(D6), ISI:000182818000003.

Boylan, J. W. and Russell, A. G., 2006. PM and Light Extinction Model Performance Metrics, Goals, and Criteria for Three-Dimensional Air Quality Models. Atmospheric Environment 40(26), 4946-4959.

Byun, D. W. and Ching, J. K. S., 1999. Science Algorithms of the EPA Models-3 Community Multiscale Air Quality (CMAQ) Modeling System. U.S. Environmental Protection Agency, EPA/600/R-99/030.

Carter, W. P. L., 2000. Documentation of the SAPRC-99 Chemical Mechanism for VOC Reactivity Assessment. California Air Resources Board, Contract No. 92-329, and 95-308.

Chen, J., Lamb, B. K., O'Neill, M. S., 2007. A Model Study on Combined Effects of Emission Changes on $PM_{2.5}$ and Ozone Concentrations in the Pacific Northwest. Submitted to Atmospheric Environment.

Eder, B., Kang, D. W., Mathur, R., Yu, S. C., and Schere, K., 2006a. An Operational Evaluation of the Eta-Cmaq Air Quality Forecast Model. Atmospheric Environment 40(26), 4894-4905.

Eder, B. and Yu, S. C., 2006b. A Performance Evaluation of the 2004 Release of Models-3 CMAQ. Atmospheric Environment 40(26), 4811-4824.

Green, M., Adhikari, J. X., and Nikolich, G., 2006. Columbia River Gorge Haze Gradient Study. Southwest Clean Air Agency, Vancouver, WA, [online] http://www.swcleanair.org/reports.html.

Grell, A. G., Dudhia, J., and Stauffer, D. R., 1994. A description of the fifth-generation Penn State/NCAR Mesoscale Model (MM5). National Center for Atmospheric Research, NCAR Technical Note NCAR/TN-398+STR.

GVRD, FVRD Canada, 2002. 2000 Emission Inventory for the Lower Fraser Valley Airshed. Greater Vancouver Regional District, Fraser Valley Regional District, [online] http://www.gvrd.bc.ca/air/pdfs/2000EmissionInventory.pdf.

Horowitz, L. W., Walters, S., Mauzerall, D. L., Emmons, L. K., Rasch, P. J., Granier, C., Tie, X. X., Lamarque, J. F., Schultz, M. G., Tyndall, G. S., Orlando, J. J., and Brasseur, G. P., 2003. A Global Simulation of Tropospheric Ozone and Related Tracers: Description and Evaluation of Mozart, Version 2. Journal of Geophysical Research-Atmospheres 108(D24), doi:10.1029/2002JD002853.

Houyoux, Marc, Vukovich, Jeff, and Brandmeyer, J. E., 2005. Sparse Matrix Operator Kernel Emissions Modeling System User Manual. [online] http://cf.unc.edu/cep/empd/products/smoke.

Jang, J. C. C., Jeffries, H. E., Byun, D., and Pleim, J. E., 1995. Sensitivity of Ozone to Model Grid Resolution .1. Application of High-Resolution Regional Acid Deposition Model. Atmospheric Environment 29(21), 3085-3100.

Jain, R., Vaughan, J., Heitkamp, K., Ramos, C., Claiborn, C., Lamb, B., 2007, Development of the ClearSky Smoke Dispersion Forecast System for Agricultural Field Burning in the Pacific Northwest. Submitted to Atmospheric Environment.

Jiang, W. M., Smyth, S., Giroux, E., Roth, H., and Yin, D. Z., 2006. Differences between CMAQ Fine Mode Particle and $PM_{2.5}$ Concentrations and Their Impact on Model Performance Evaluation in the Lower Fraser Valley. Atmospheric Environment 40(26), 4973-4985.

Larkin, N. K., O'Neill, S. M., Solomon, R., Krull, C., Raffuse, S., Rorig, M., Peterson, J., and Ferguson, S. A., 2007. The BlueSky Smoke Modeling Framework. Atmospheric Environment, In Press.

Makar, P. A., Moran, M. D., Scholtz, M. T., and Taylor, A., 2003. Speciation of Volatile Organic Compound Emissions for Regional Air Quality Modeling of Particulate Matter and Ozone. Journal of Geophysical Research-Atmospheres 108(D2), doi:10.1029/2001JD000797.

Malm, W. C., Schichtel, B. A., Pitchford, M. L., Ashbaugh, L. L., and Eldred, R. A., 2004. Spatial and Monthly Trends in Speciated Fine Particle Concentration in the United States. Journal of Geophysical Research-Atmospheres 109(D3), doi:10.1029/2003JD003739.

Mass, C. F., Albright, M., Ovens, D., Steed, R., Maciver, M. , Grimit, E., Eckel, T., Lamb, B., Vaughan, J., Westrick, K., Storck, P., Colman, B., Hill, C., Maykut, N., Gilroy, M., Ferguson, S. A., Yetter, J., Sierchio, J. M., Bowman, C., Stender, R., Wilson, R., and Brown, W., 2003. Regional Environmental Prediction Over the Pacific Northwest. Bulletin of the American Meteorological Society 84(10), 1353-1366.

Mckeen, S., Wilczak, J., Grell, G., Djalalova, I., Peckham, S., Hsie, E. Y., Gong, W., Bouchet, V., Menard, S., Moffet, R., Mchenry, J., Mcqueen, J., Tang, Y., Carmichael, G. R., Pagowski, M., Chan, A., Dye, T., Frost, G., Lee, P., and Mathur, R., 2005. Assessment of an Ensemble of Seven Real-Time Ozone Forecasts Over Eastern North America During the Summer of 2004. Journal of Geophysical Research-Atmospheres 110(D21), doi:10.1029/2005JD005858.

Mcqueen, J. T., Draxler, R. R., and Rolph, G. D., 1995. Influence of Grid Size and Terrain Resolution on Wind-Field Predictions From an Operational Mesoscale Model. Journal of Applied Meteorology 34(10), 2166-2181.

Miranda, A. I., 2004. An Integrated Numerical System to Estimate Air Quality Effects of Forest Fires. International Journal of Wildland Fire 13(2), 217-226.

Nenes, A., Pandis, S. N., and Pilinis, C., 1998. Isorropia: a New Thermodynamic Equilibrium Model for Multiphase Multicomponent Inorganic Aerosols. Aquatic Geochemistry 4(1), 123-152.

O'Neill, S. M. and Lamb, B. K., 2005. Intercomparison of the Community Multiscale Air Quality Model and Calgrid Using Process Analysis. Environmental Science & Technology 39(15), 5742-5753.

O'Neill, S. M., Lamb, B. K., Chen, J., Claiborn, C., Finn, D. , Otterson, S., Figueroa, C., Bowman, C., Boyer, M., Wilson, R., Arnold, J., Aalbers, S., Stocum, J., Swab, C., Stoll, M., Dubois, M., and Anderson, M., 2006. Modeling Ozone and Aerosol Formation and Transport in the Pacific Northwest With the Community Multi-Scale Air Quality (CMAQ) Modeling System. Environmental

Science & Technology 40(4), 1286-1299.

Pinder, R. W., Adams, P. J., Pandis, S. N., and Gilliland, A. B., 2006. Temporally Resolved Ammonia Emission Inventories: Current Estimates, Evaluation Tools, and Measurement Needs. Journal of Geophysical Research-Atmospheres 111(D16), ISI:000240100400001.

Pudykiewicz, J. A. and Koziol, A. S., 2001. The Application of Eulerian Models for Air Quality Prediction and the Evaluation of Emission Control Strategies in Canada. International Journal of Environment and Pollution 16(1-6), 425-438.

Rumburg, B., Chen, J., Mount, G. H., and Lamb, B., 2005. Final Report for the Washington State Dairy Ammonia Emissions Model. Washington State Department of Ecology,

Rumburg, B. P., Differential Optical Absorption Spectroscopy (DOAS) Measurements of Atmospheric Ammonia in the Mid-Ultraviolet From a Dairy: Concentrations, Emissions, and Modeling, PhD Dissertation, Washington State University, Department of Civil & Environmental Engineering, Pullman, WA, 2006.

Schell, B., Ackermann, I. J., Hass, H., Binkowski, F. S., and Ebel, A., 2001. Modeling the Formation of Secondary Organic Aerosol Within a Comprehensive Air Quality Model System. Journal of Geophysical Research-Atmospheres 106(D22), 28275-28293.

Seigneur, C., 2001. Current Status of Air Quality Models for Particulate Matter. Journal of the Air & Waste Management Association 51(11), 1508-1521.

Smyth, S. C., Jiang, W. M., Yin, D. Z., Roth, H., and Giroux, T., 2006. Evaluation of CMAQ O3 and PM2.5 Performance Using Pacific 2001 Measurement Data. Atmospheric Environment 40(15), 2735-2749.

Solomon, P., Klamser-Williams, T., Egeghy, P., Crumpler, D., Rice, J., 2004. STN/IMPROVE comparison study – preliminary results. Presented at PM Model Performance Workshop, Chapel Hill, NC. 10 February 2004. [online] http://www.cleanairinfo.com/PMModelPerformanceWorkshop2004/presentations/RiceSTNImprove.ppt

Stockwell, W. R., Middleton, P., Chang, J. S., and Tang, X. Y., 1990. The 2nd Generation Regional Acid Deposition Model Chemical Mechanism for Regional Air-Quality Modeling. Journal of Geophysical Research-Atmospheres 95 (D10), 16343-16367.

Tong, D. Q. and Mauzerall, D. L., 2006. Spatial Variability of Summertime Tropospheric Ozone over the Continental United States: Implications of an Evaluation of the CMAQ Model. Atmospheric Environment 40(17), 3041-3056.

U.S. EPA, 1991. Guidance for Regulatory Application of the Urban Airshed Model. U.S. Environmental Protection Agency, [online] http://www.epa.gov/scram001/guidance/guide/uamreg.pdf

U.S. EPA, 2002. Biogenic Emissions Inventory System (BEIS) Model, Accessed: January, 2006, URL: [online] http://www.epa.gov/asmdnerl/biogen.html

U.S. EPA, 2004. Economic Growth Analysis System (EGAS) version 5.0 User Manual. U.S. Environmental Protection Agency, [online] http://www.epa.gov/ttn/ecas/egas5.htm

US. EPA, 2003. MOBILE6 Vehicle Emission Modeling Software User Guide. U.S. Environmental Protection Agency, EPA420-R-03-010.

Vaughan, J., Lamb, B., Frei, C., Wilson, R., Bowman, C., Figueroa-Kaminsky, C., Otterson, S., Boyer, M., Mass, C., Albright, M., Koenig, J., Collingwood, A., Gilroy, M. , and Maykut, N., 2004. A Numerical Daily Air Quality Forecast System for the Pacific Northwest. Bulletin of the American Meteorological Society 85(4), 549-561.

Weiss-Penzias, P., Jaffe, D. A., Jaegle, L., and Liang, Q., 2004. Influence of Long-Range-Transported Pollution on the Annual and Diurnal Cycles of Carbon Monoxide and Ozone at Cheeka Peak Observatory. Journal of Geophysical Research-Atmospheres 109(D23), doi:10.1029/2004JD004505.

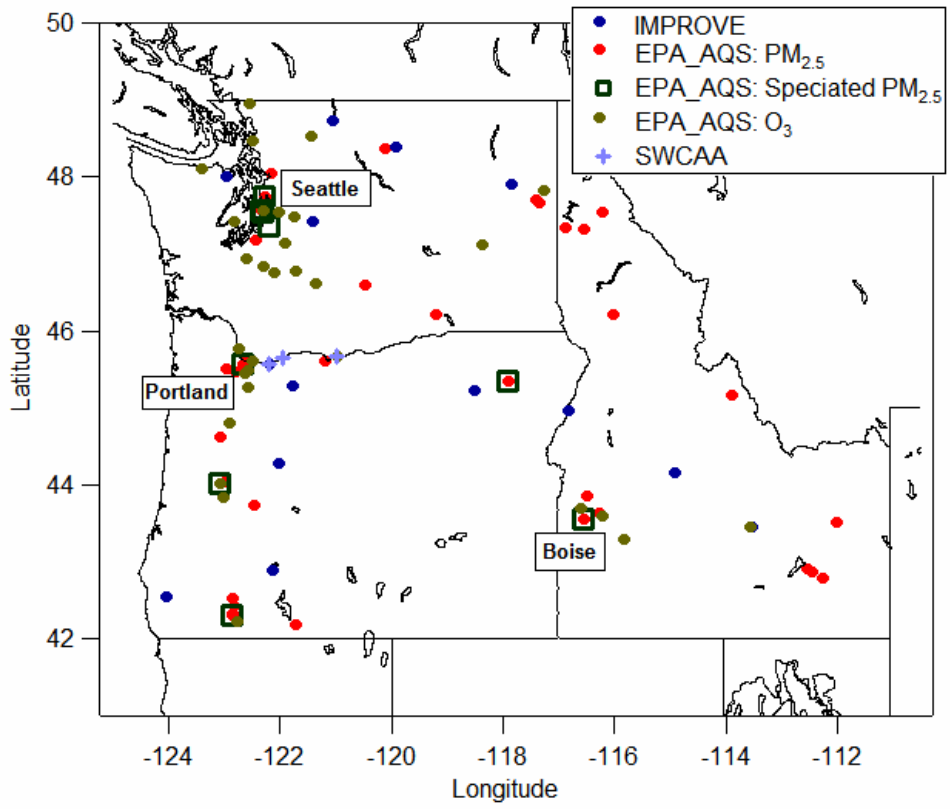

Figure 1. AIRPACT-3 model domain and the location of measurement sites where data were used in the evaluation.

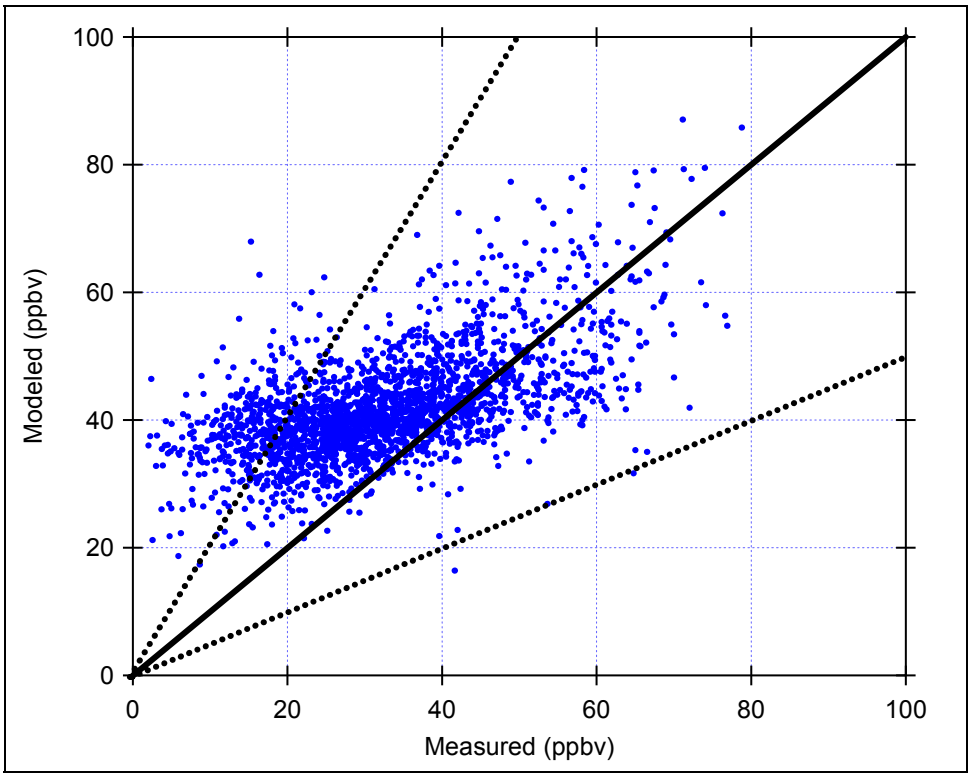

Figure 2. Scatter plot of modeled and measured daily maximum 8-hr ozone concentration with 1:1 (solid) and 1:2 (dotted) reference lines.

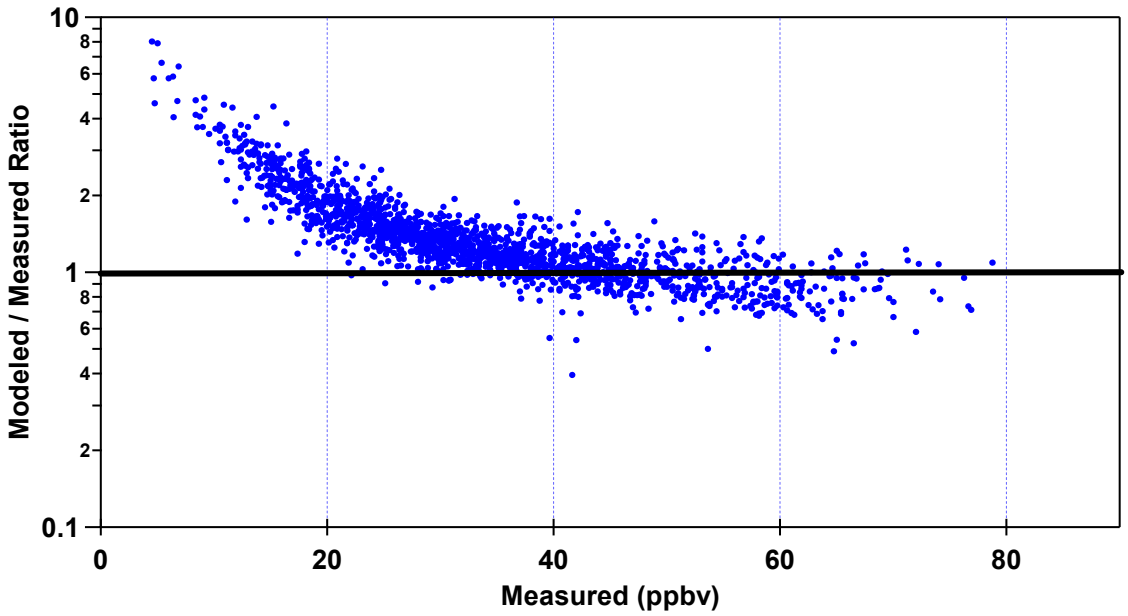

Figure 3. Ratio of modeled to measured daily maximum 8-hr ozone concentration versus measured daily maximum 8-hr ozone concentration for all sites during the August and September 2004 evaluation period.

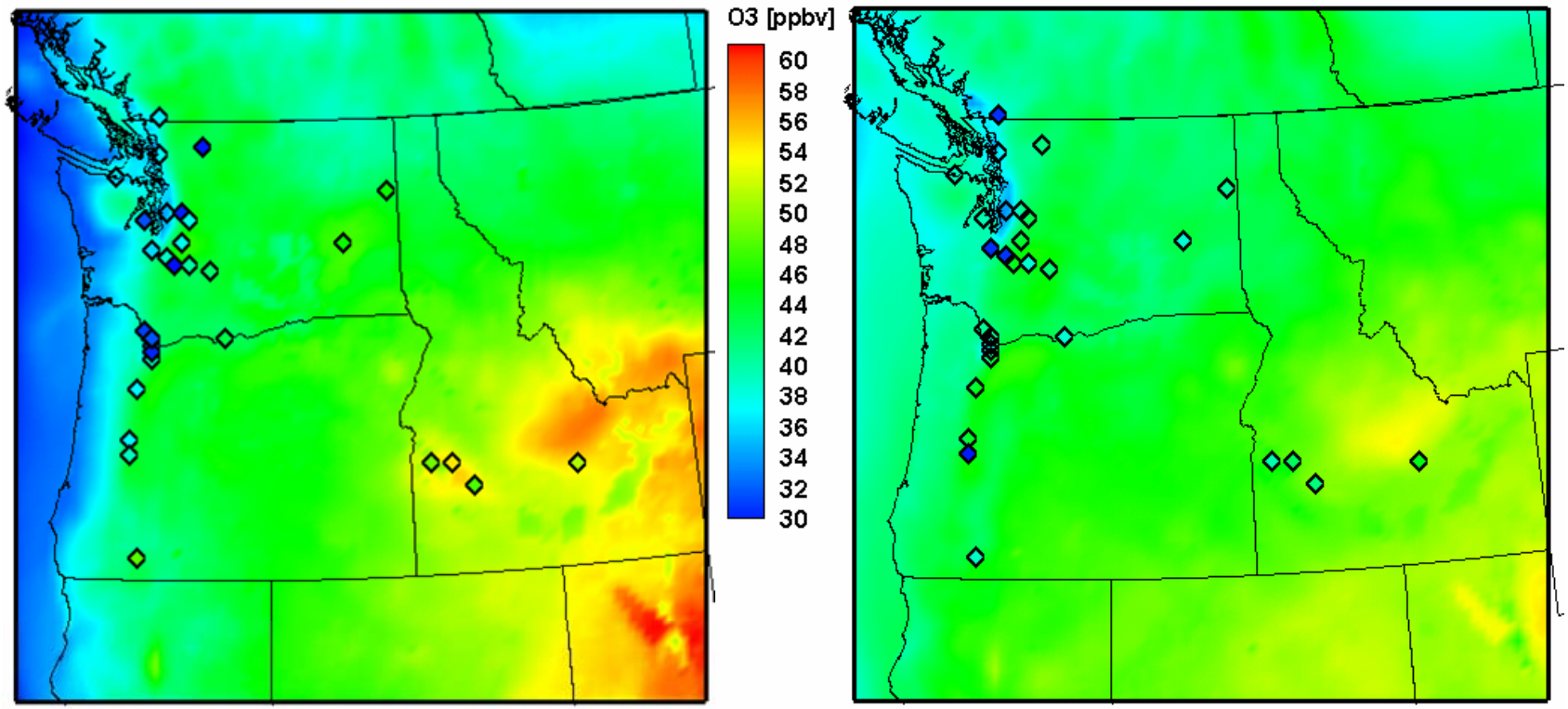

Figure 4. Average daily maximum 8-hr ozone concentration for modeled (color surface contour) and measured (diamond) for August (left) and September 2004 (right).

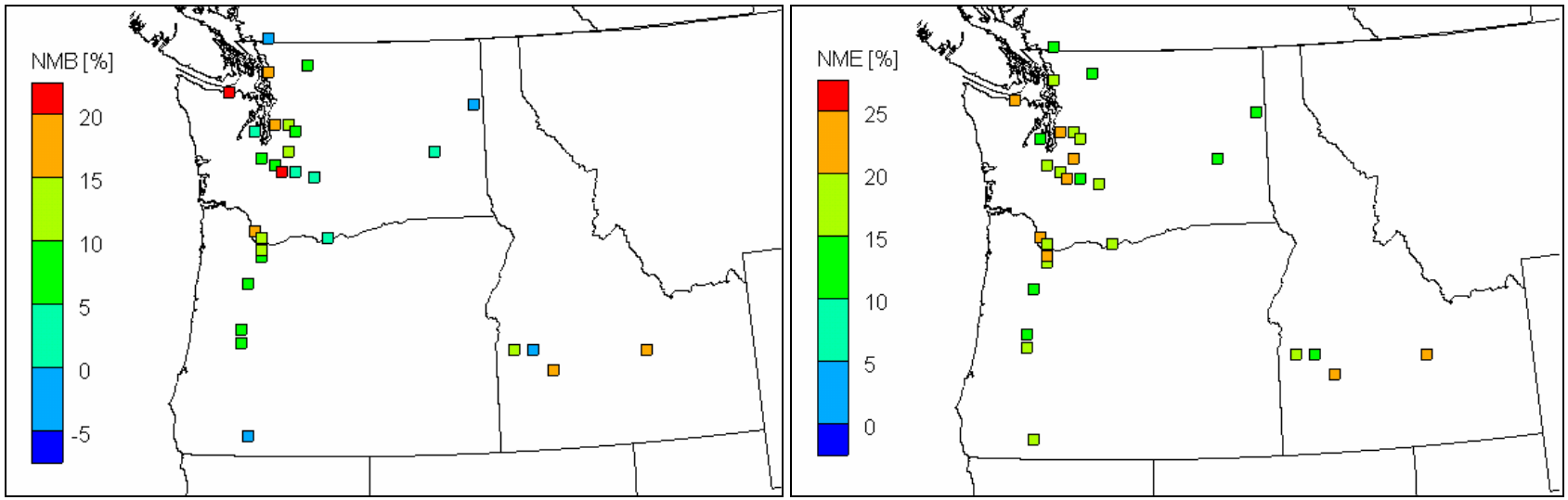

Figure 5. Spatial distribution of normalized mean bias (left) and normalized mean error (right) by measurement sites associated with the daily maximum 8-hr ozone concentration during the August and September 2004 evaluation period.

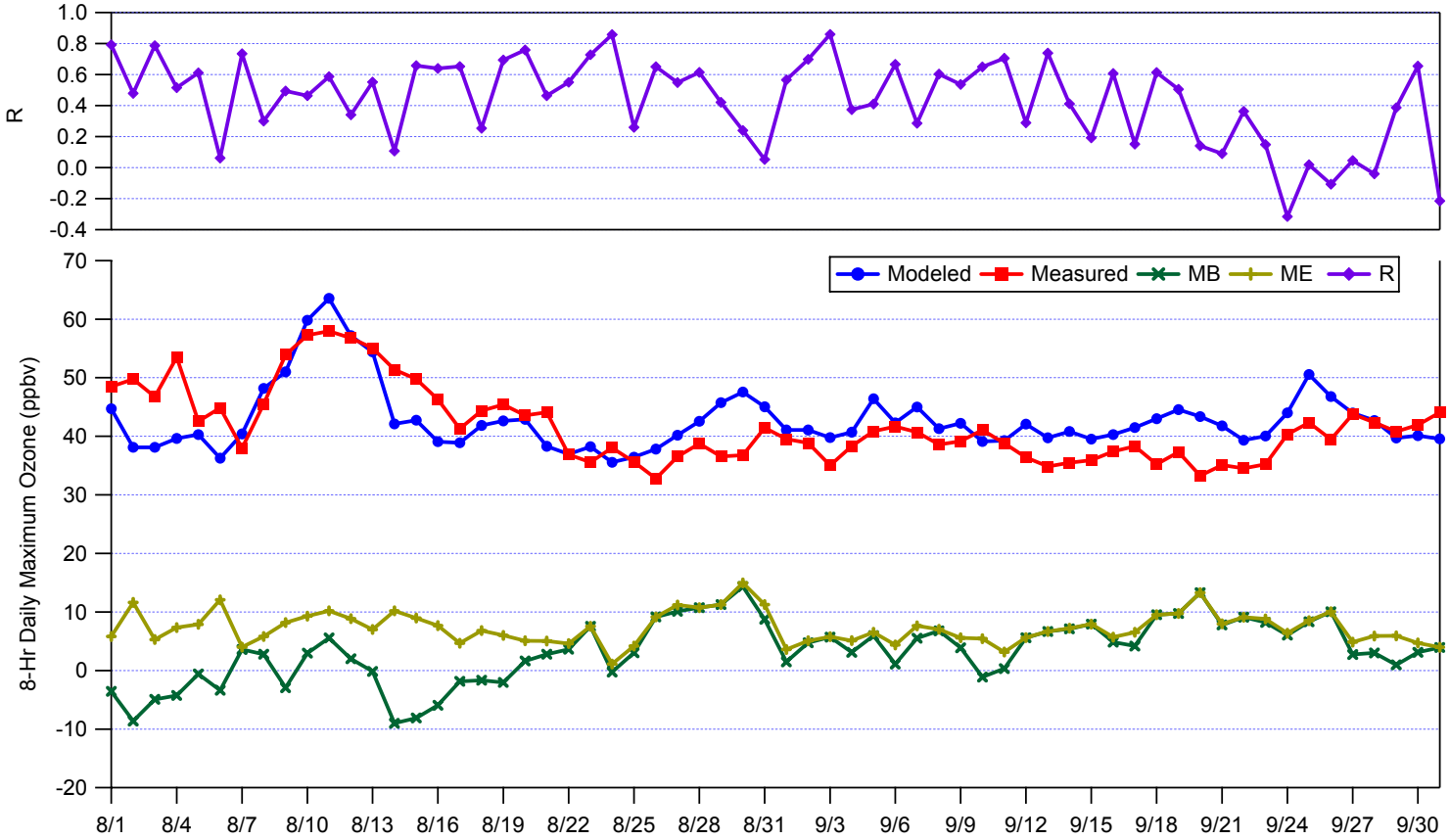

Figure 6. Time series of the modeled and measured average daily maximum 8-hr ozone concentrations, and the resulting model statistics for mean bias (MB), mean error (ME) and correlation coefficient (R).

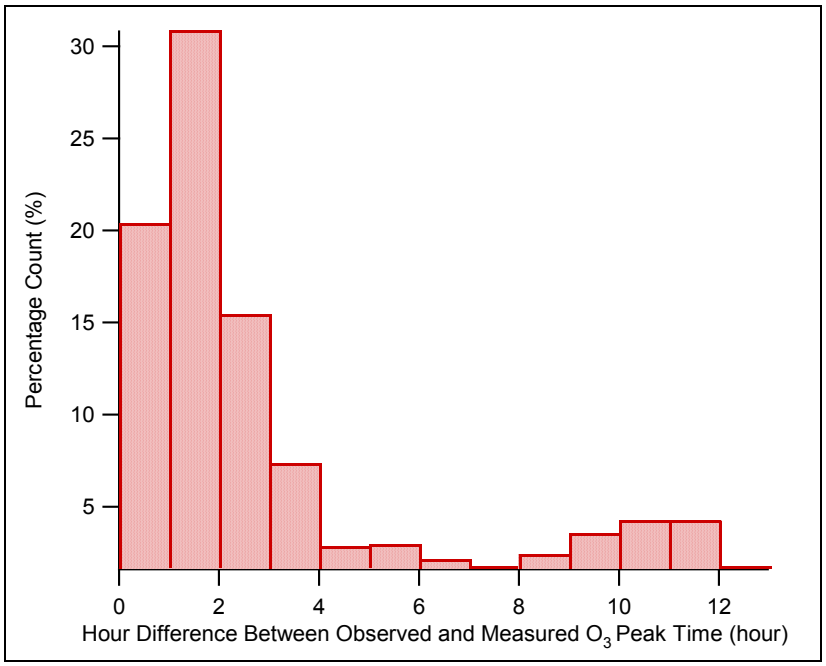

Figure 7. Percent distribution of hourly difference between modeled 8-hr ozone daily peak time and measured 8-hr ozone daily peak over the August and September 2004 evaluation period

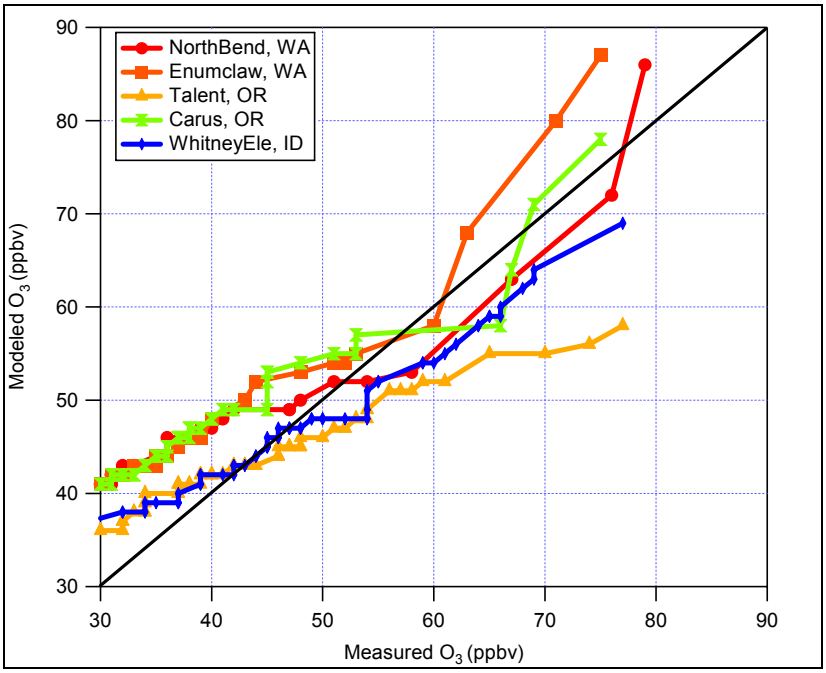

Figure 8. Quantile-quantile plot of ranked modeled and measured daily maximum 8-hr ozone concentrations at measurement sites with high concentrations during the August – September 2004 period.

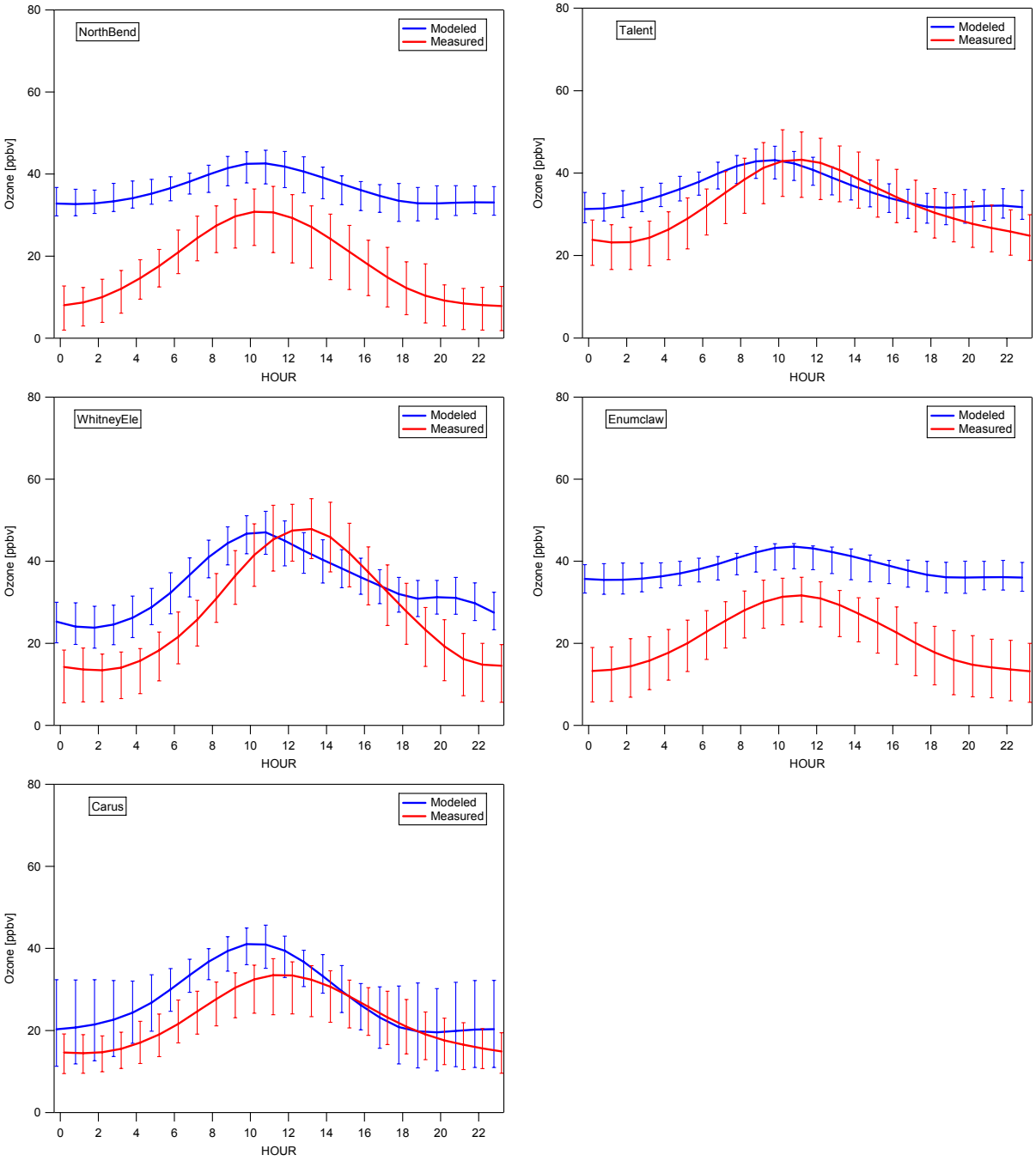

Figure 9. Modeled (blue) and measured (red) diurnal 8-hr ozone concentration profile averaged across the August and September 2004 evaluation period. The solid lines indicate mean ozone concentrations and the error bars represent 25th and 75th percentile values.

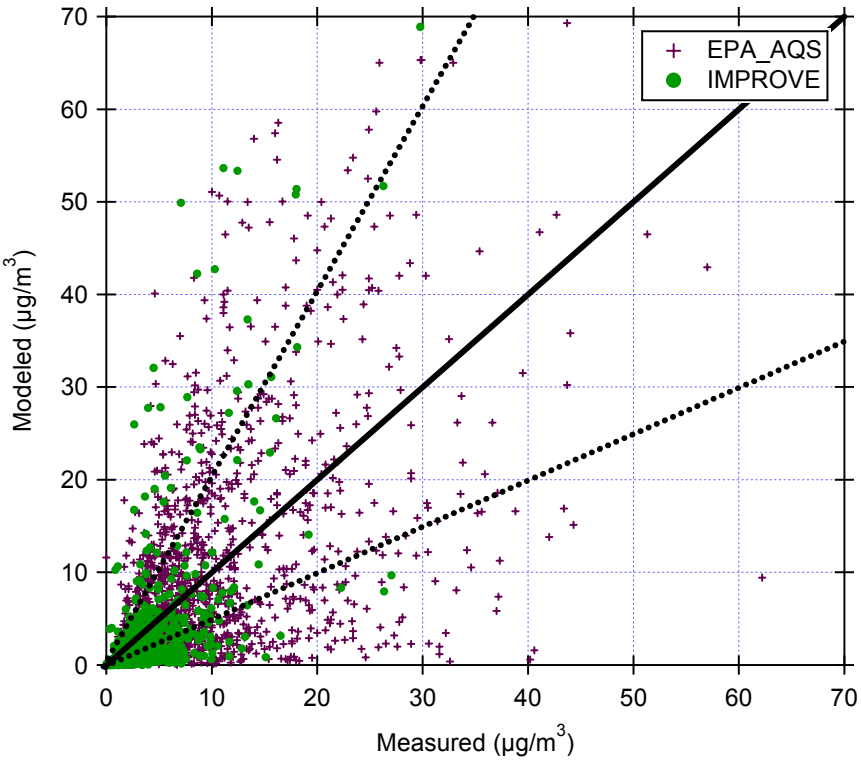

Figure 10. Scattered plot of modeled and measured daily mean $PM_{2.5}$ concentration for EPA-AQS (cross) and IMPROVE (dot) measurement sites, with 1:1 (solid) and 1:2 (dotted) reference lines.

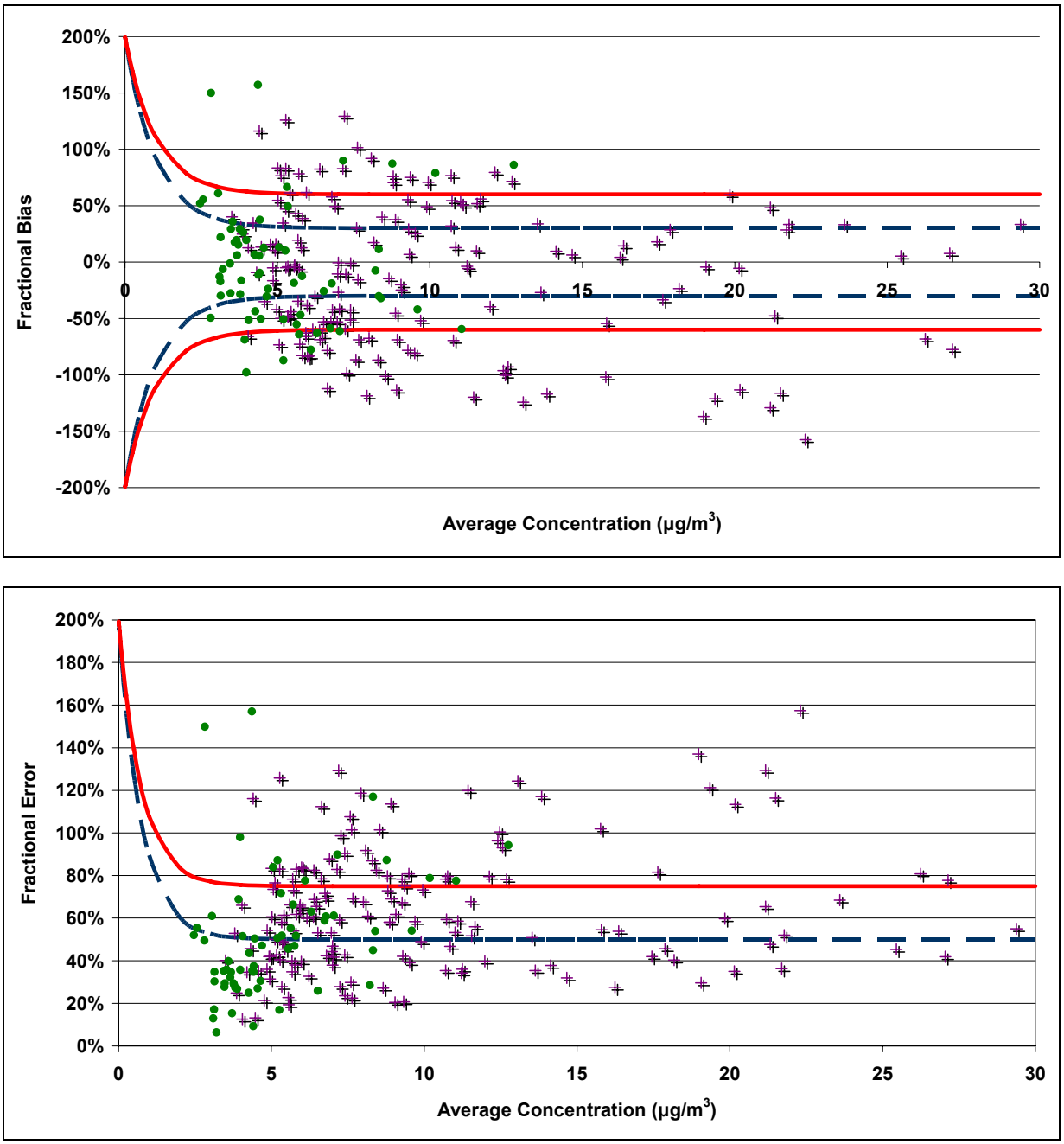

Figure 11. Fractional bias (top) and fractional error (bottom) of AIRPACT-3 $PM_{2.5}$ prediction versus average measured $PM_{2.5}$ concentrations for EPA-AQS (cross) and IMPROVE (dot) measurement sites. Model performance goal and criteria ranges are represented by solid and dotted lines respectively.

(a) August 2004

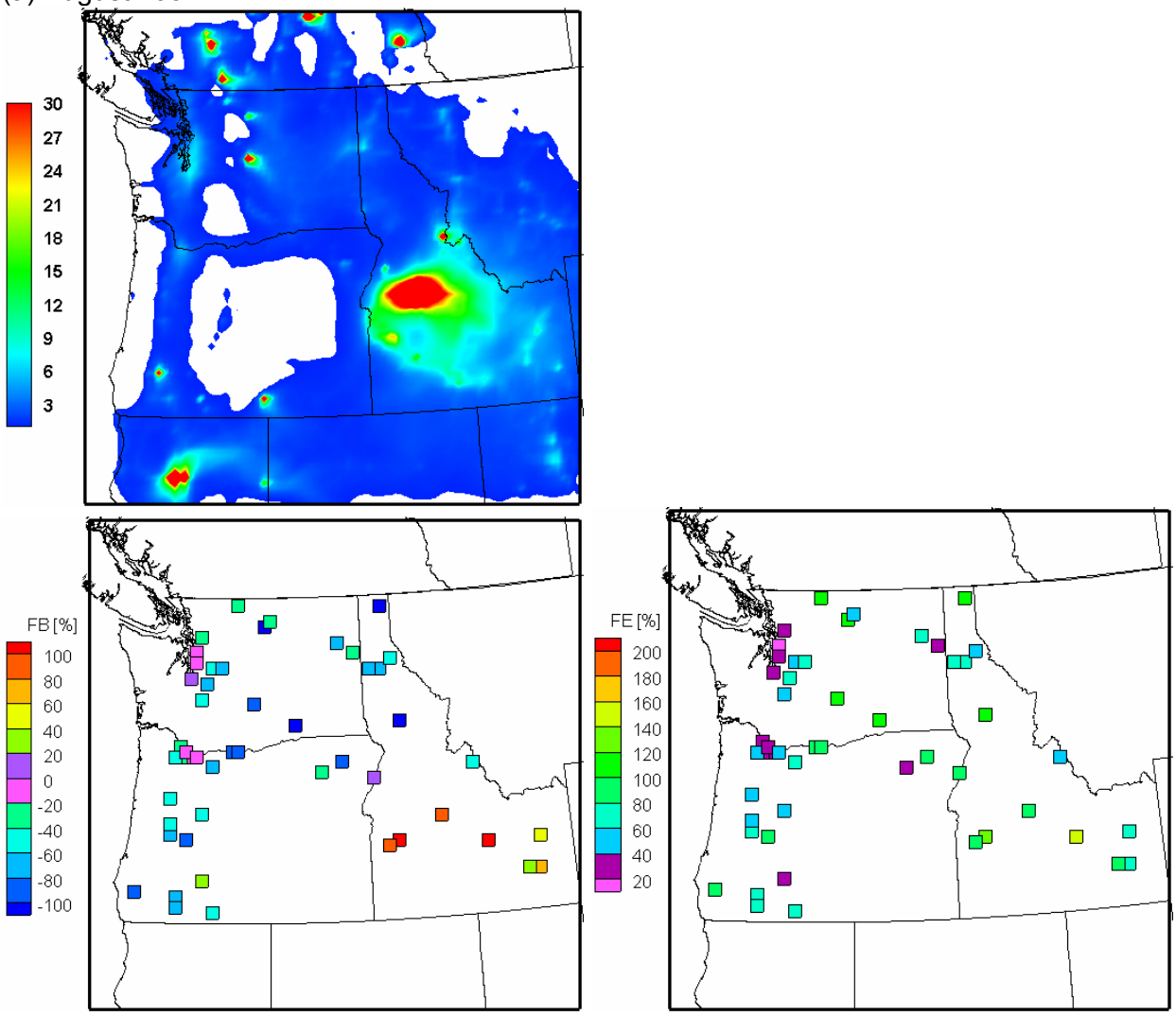

Figure 12a. Predicted monthly averaged $PM_{2.5}$ concentrations ($\mu g/m^3$) and the corresponding fractional bias (%) and fractional error (%) by measurement sites for August 2007.

(b) September 2004

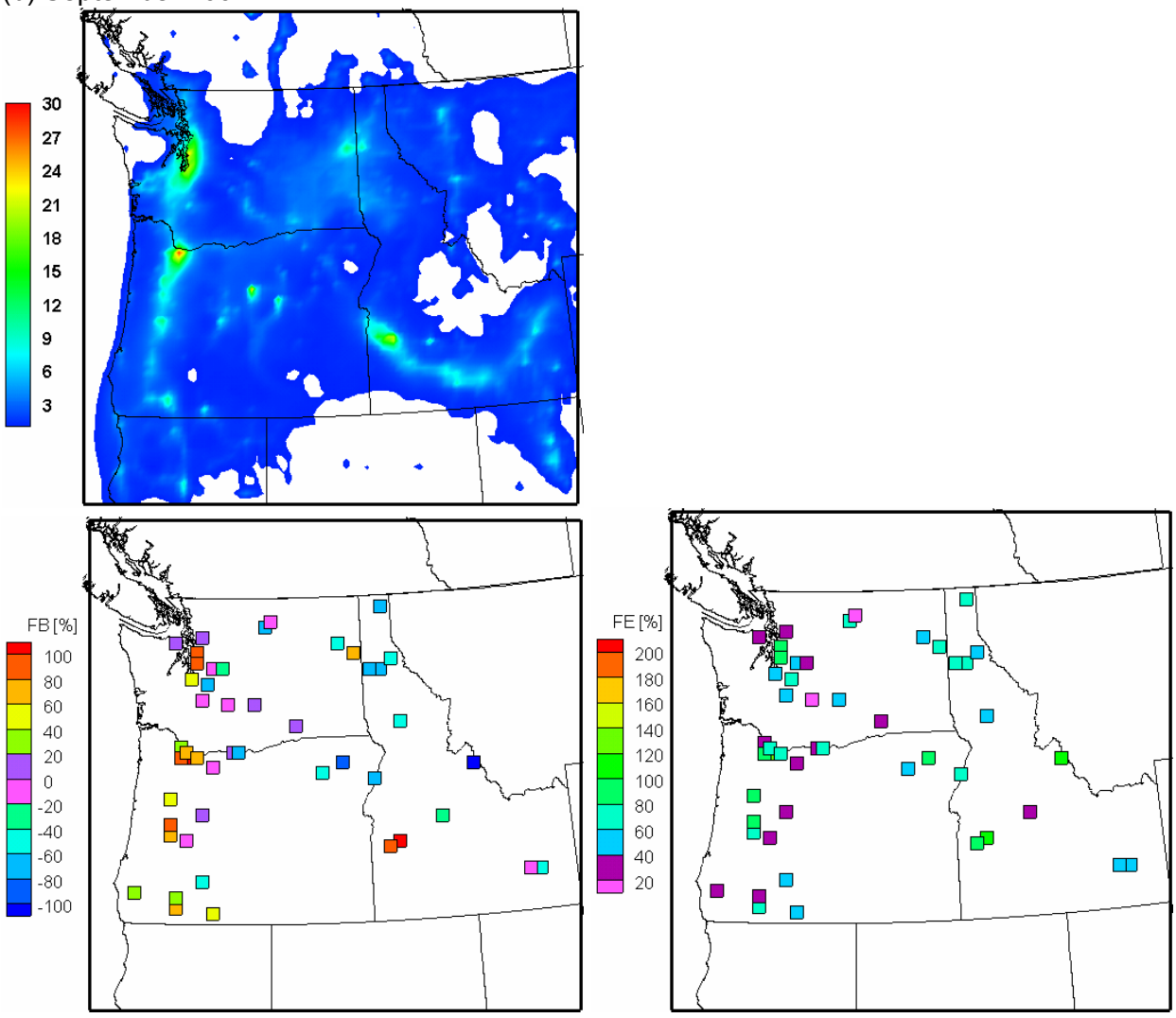

Figure 12b. Predicted monthly averaged $PM_{2.5}$ concentrations ($\mu g/m^3$) and the corresponding fractional bias (%) and fractional error (%) by measurement sites for September 2007.

(c) October 2004

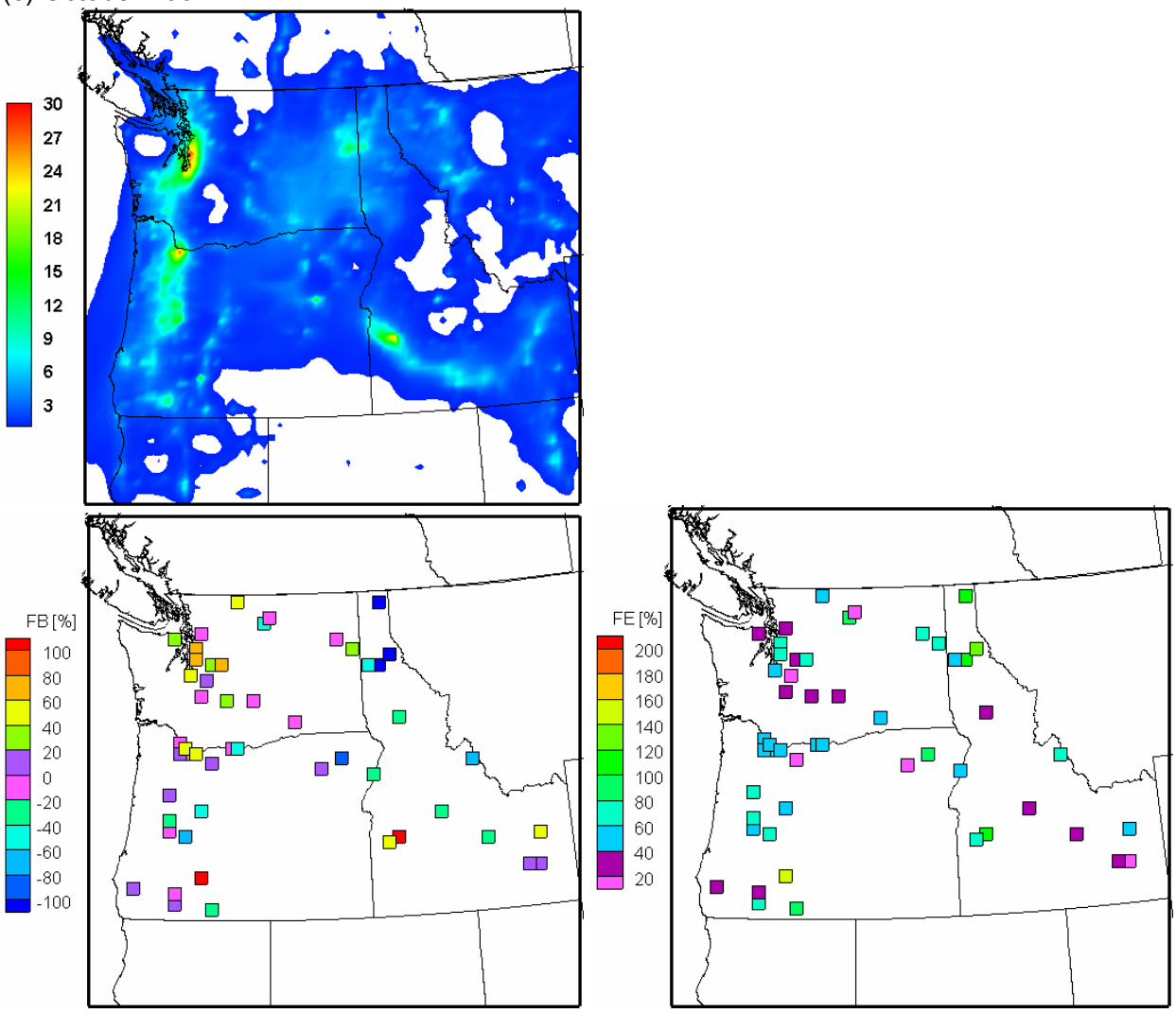

Figure 12c. Predicted monthly averaged $PM_{2.5}$ concentrations ($\mu g/m^3$) and the corresponding fractional bias (%) and fractional error (%) by measurement sites for October 2007.

(d) November 2004

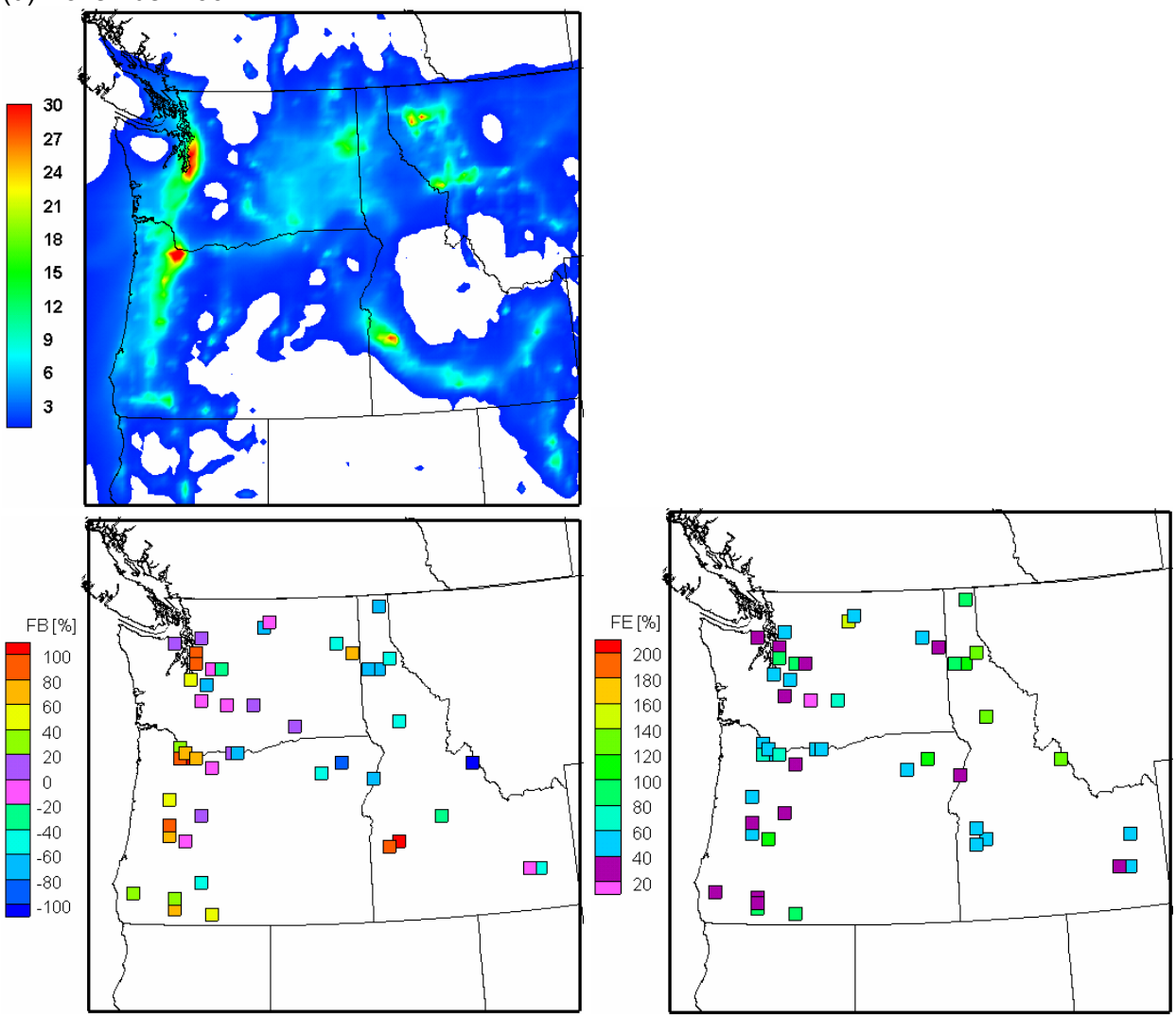

Figure 12d. Predicted monthly averaged $PM_{2.5}$ concentrations ($\mu g/m^3$) and the corresponding fractional bias (%) and fractional error (%) by measurement sites for November 2007.

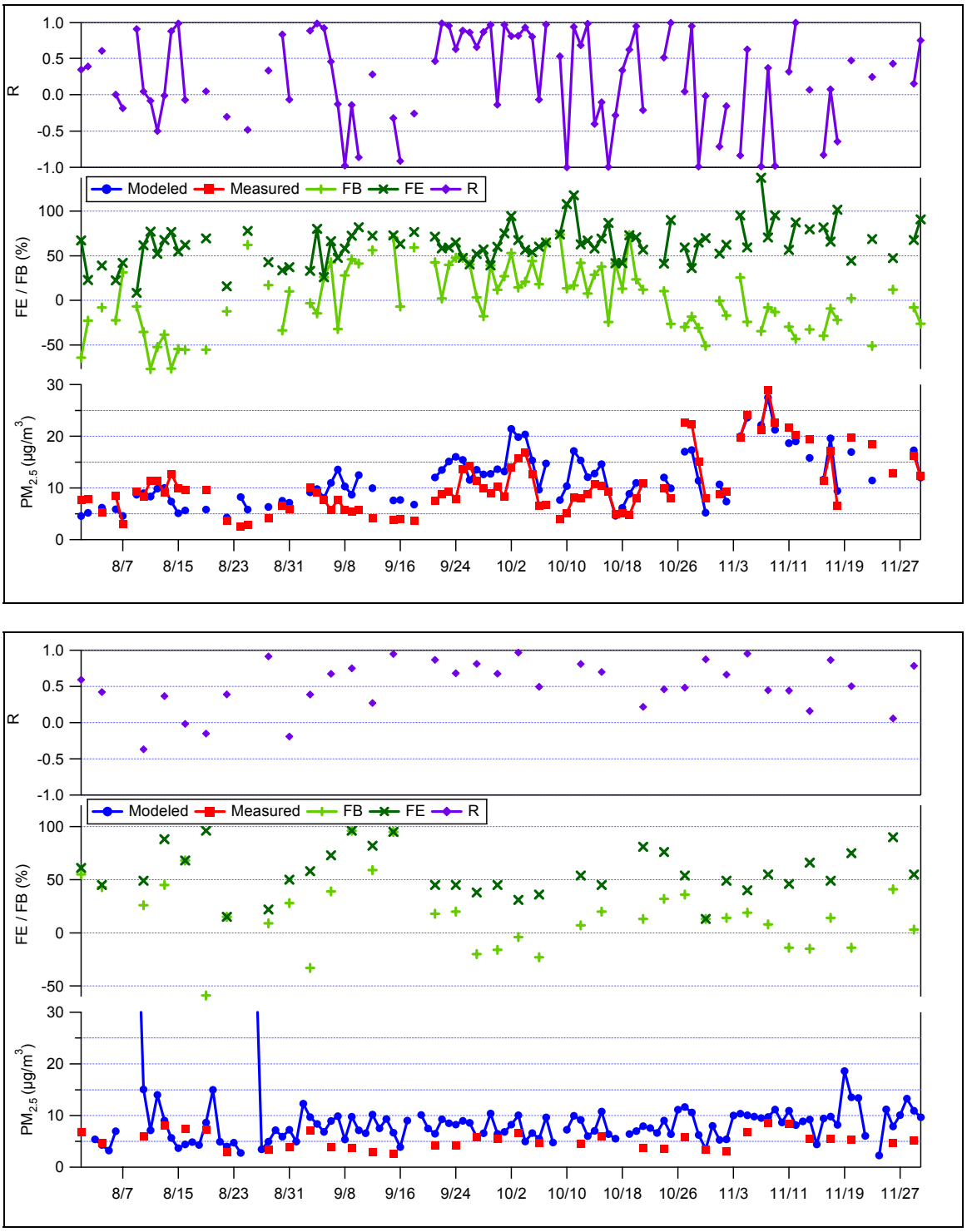

Figure 13. Time series of modeled and measured 24-hr $PM_{2.5}$ concentrations and the corresponding model statistics (FE, FB and R) average across the EPA-AQS measurement sites (top) and the IMPROVE measurement sites (bottom).

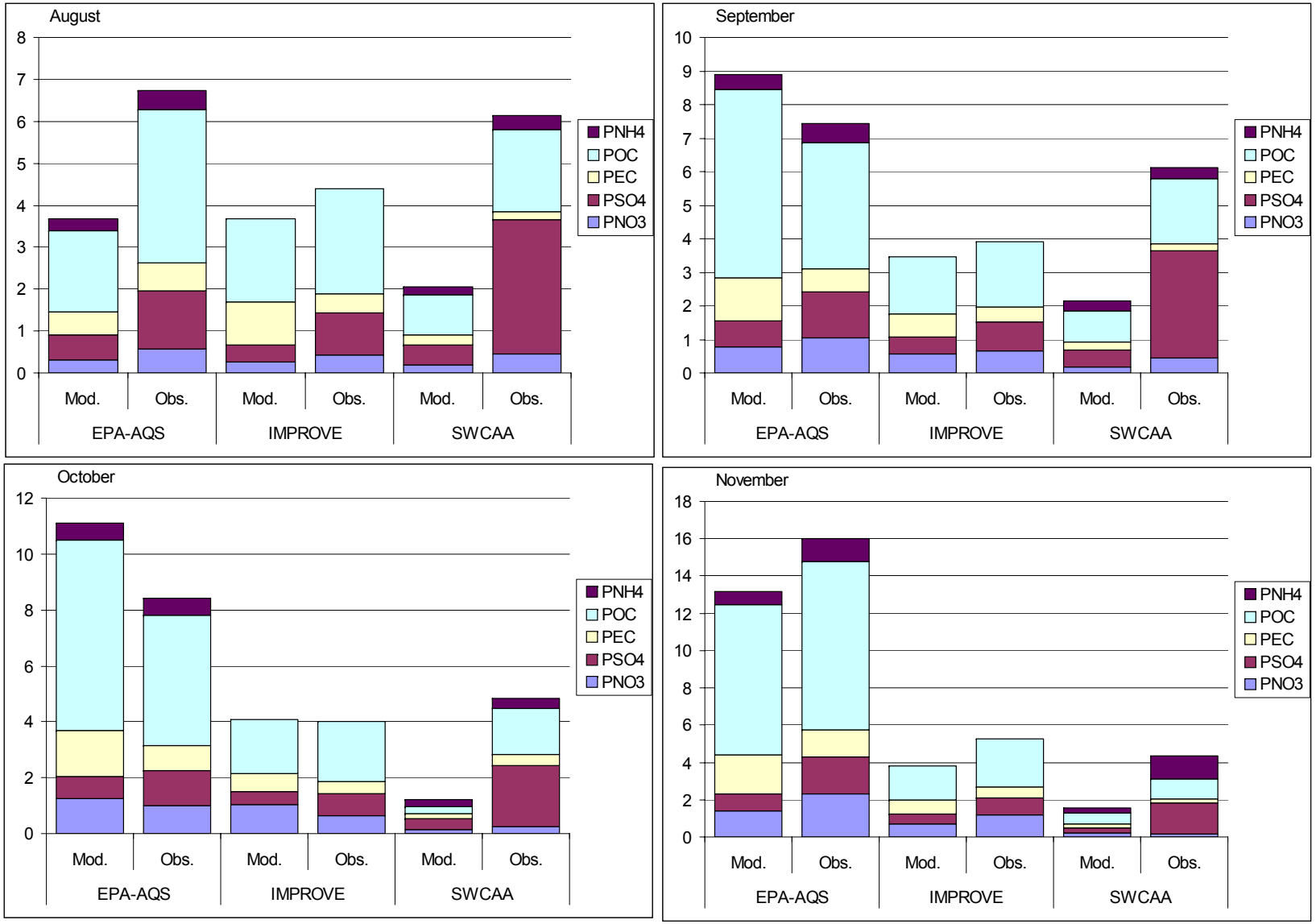

Figure 14. Measured (right) and modeled (left) aerosol component concentrations averaged by month and measurement network.

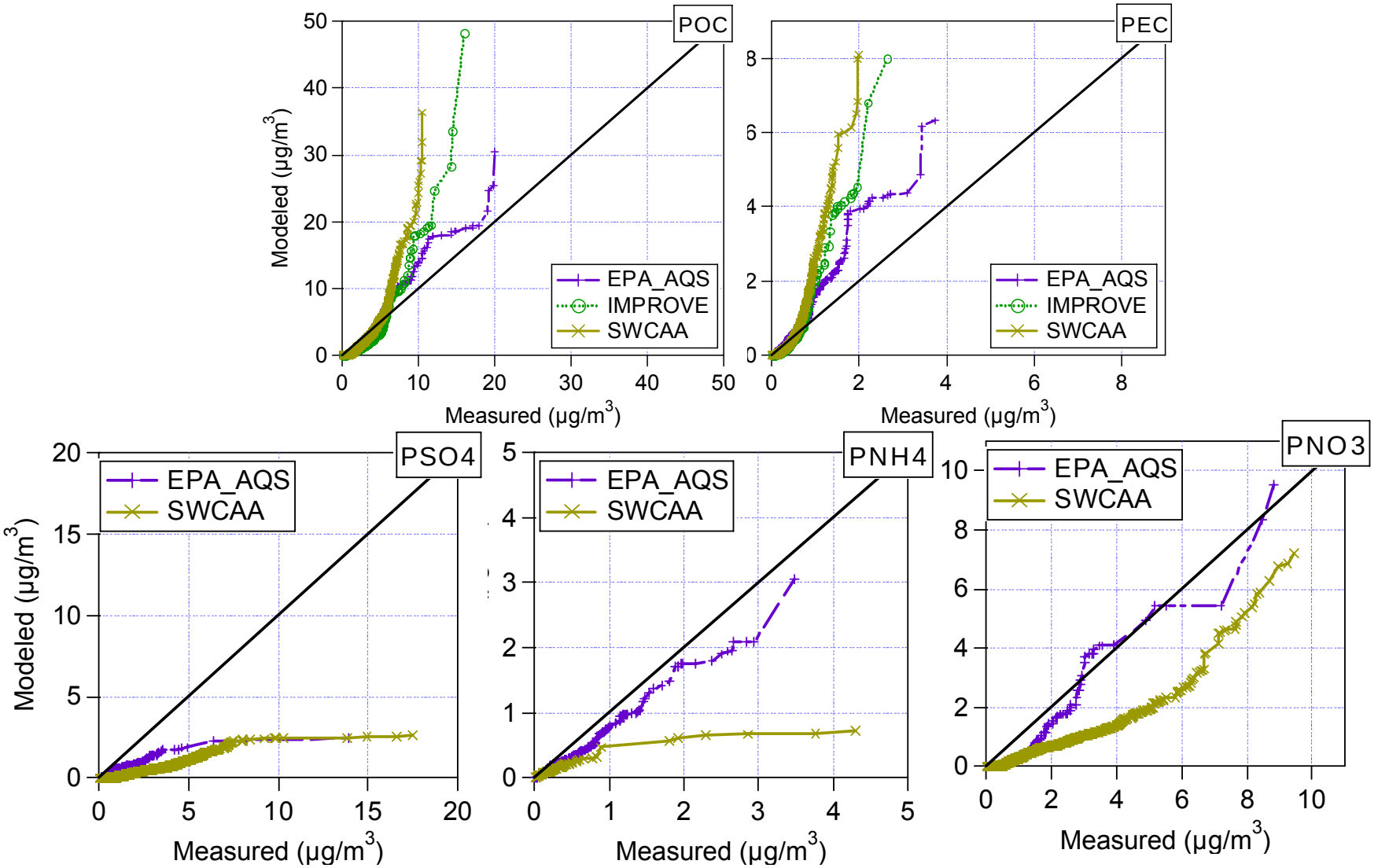

Figure 15. Quantile-quantile plots of $PM_{2.5}$ component species by measurement networks. Data points are unpaired in time and space, but paired by measurement networks.

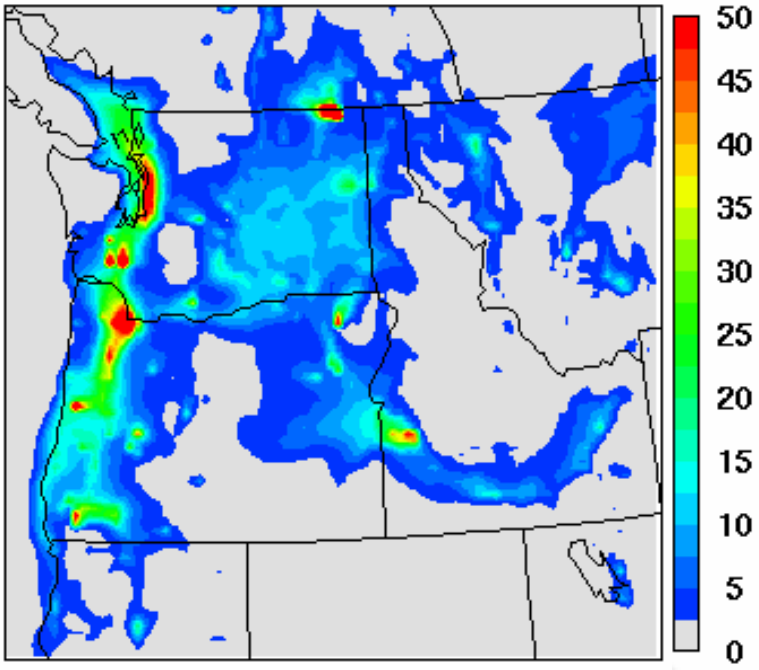

Figure 16. Predicted average daily maximum $PM_{2.5}$ concentrations ($\mu g/m^3$) during the November 3 – 18 2004 stagnation period.

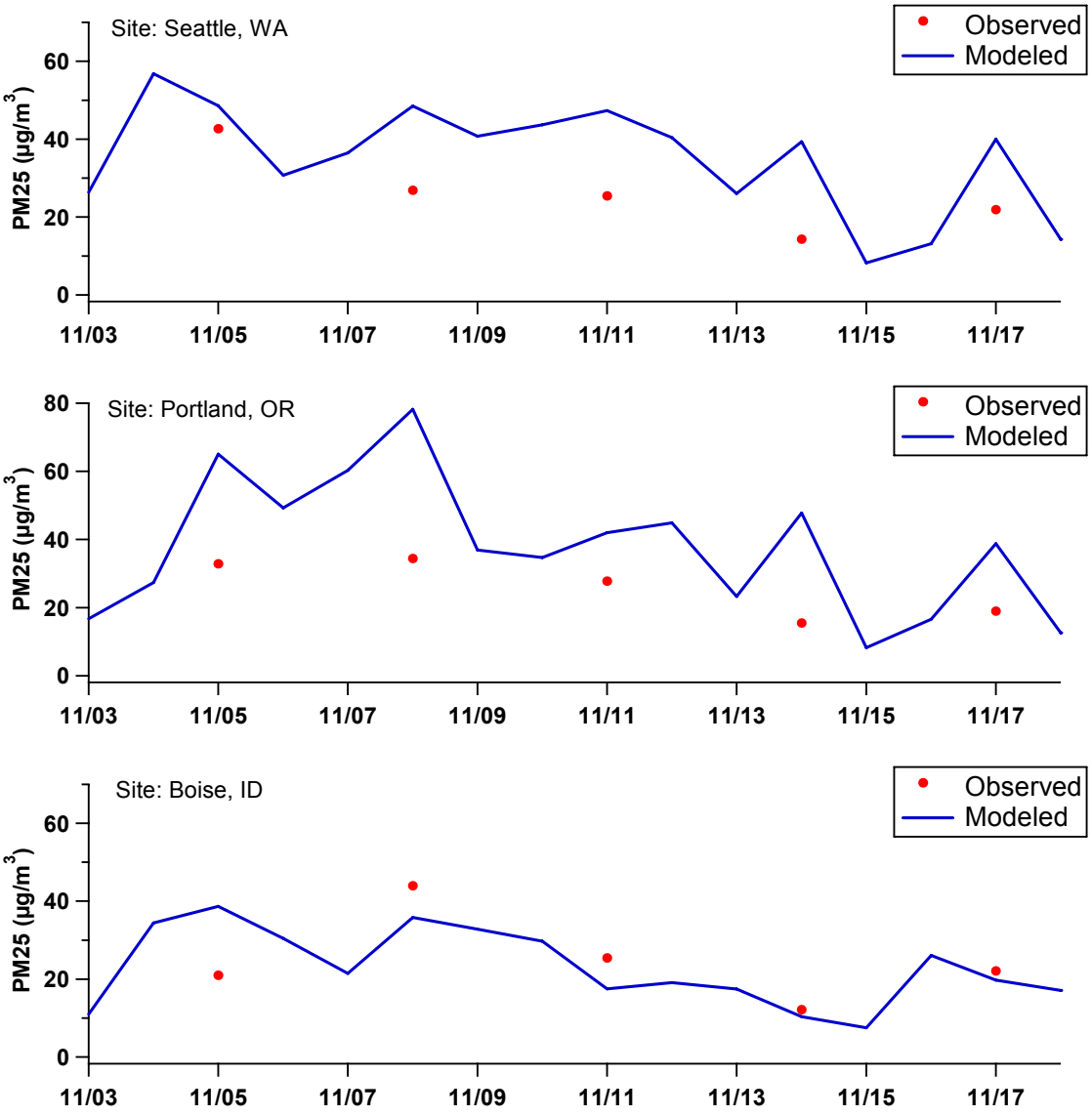

Figure 17. Measured (dot) and modeled (solid line) time series of daily $PM_{2.5}$ concentrations for Seattle, Portland and Boise measurement sites during the November 3 – 18 2004 stagnation period.

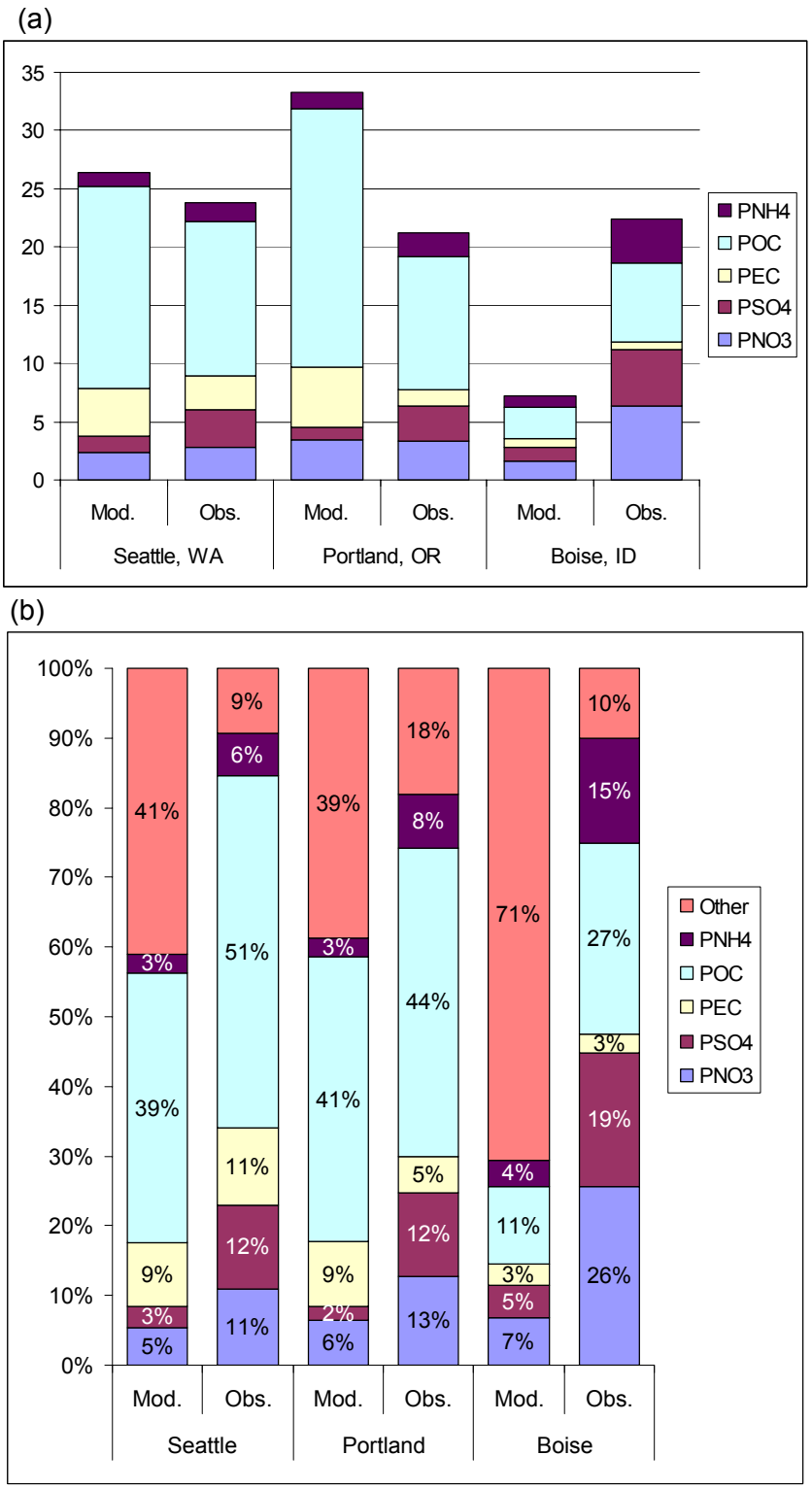

Figure 18. (a) Measured (right) and modeled (left) aerosol component concentrations averaged by site during the November 3 – 18 2004 stagnation period. (b) Percentage fraction of aerosol components with respect to total measured $PM_{2.5}$ for the same period. The other unspecified $PM_{2.5}$ was calculated from subtracting total $PM_{2.5}$ from the sum of component concentrations.

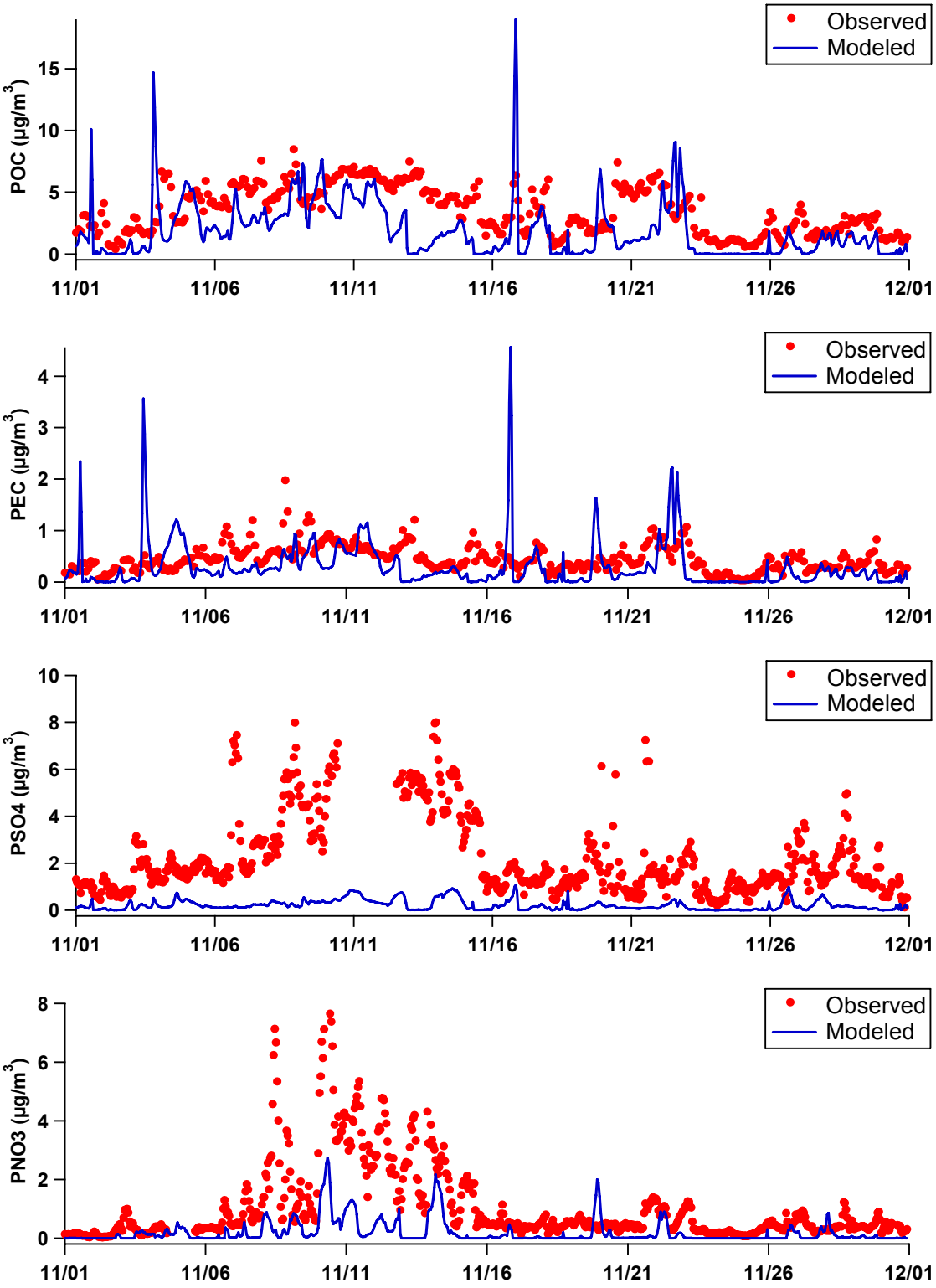

Figure 19. November 2004 hourly time series of measured (dot) and modeled (solid line) $PM_{2.5}$ component concentrations for PEC, POC, PSO4 and PNO3 at the Bonneville Dam site from the SWCAA measurement network in the Columbia River Gorge.

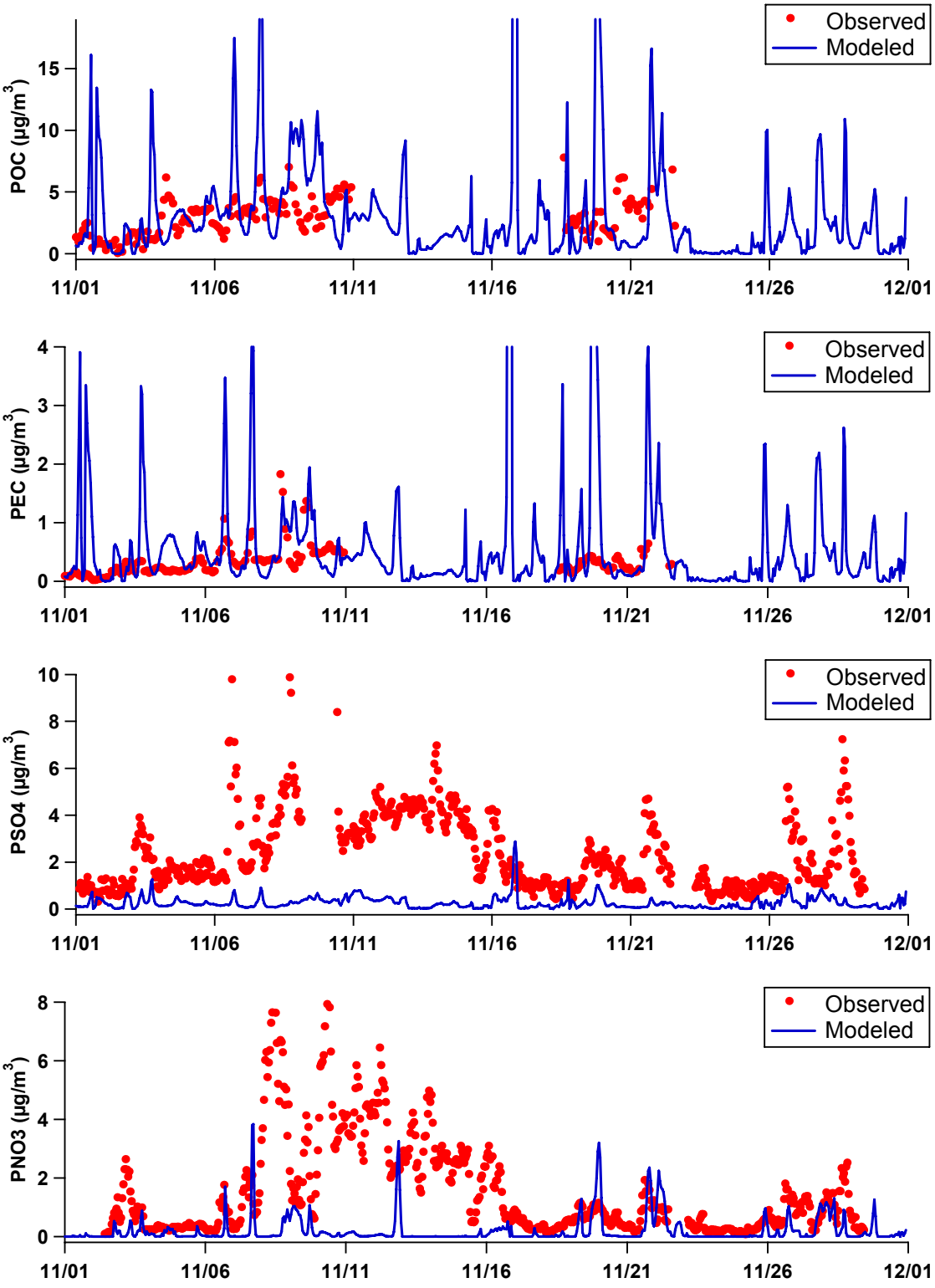

Figure 20. November 2004 hourly time series of measured (dot) and modeled (solid line) $PM_{2.5}$ component concentrations for PEC, POC, PSO4 and PNO3 at the Mt. Zion site from the SWCAA measurement network in the Columbia River Gorge.

Table 1. Vertical grid structure by sigma layer and the approximate elevation from surface for the AIRPACT-3 and MM5 modeling systems.

Layer Index	MM5 37 σ Layers	AIRPACT-3 21 σ Layers	Approximate Elevation (m)
38	0.000	0.000	11471
37	0.040		10484
36	0.080		9616
35	0.120	0.120	8840
34	0.160		8135
33	0.200		7490
32	0.240	0.240	6894
31	0.280		6339
30	0.320		5819
29	0.360	0.360	5331
28	0.400		4869
27	0.440		4432
26	0.480	0.480	4015
25	0.520		3618
24	0.560		3239
23	0.600	0.600	2875
22	0.640		2526
21	0.680		2231
20	0.710	0.710	1985
19	0.740		1747
18	0.770	0.770	1514
17	0.800		1287
16	0.830	0.830	1066
15	0.860	0.860	885
14	0.880	0.880	744
13	0.900	0.900	639
12	0.910	0.910	569
11	0.920	0.920	500
10	0.930	0.930	432
9	0.940		364
8	0.950	0.950	297
7	0.960	0.960	230
6	0.970	0.970	164
5	0.980	0.980	114
4	0.985		82
3	0.990	0.990	49
2	0.995	0.995	16
1	1.000	1.000	0

Table 2. Summary of typical week-day emission inventory by source category within the AIRPACT-3 modeling domain.

Area Source [tons/day]

	CO	NOx	VOC	NH_3	SO_2	PM_{10}	$PM_{2.5}$
California	115	5	36	7	1	119	39
Idaho	98	90	365	161	3	255	250
Montana	77	9	49	72	6	552	103
Nevada	3	0	4	2	1	49	8
Oregon	940	56	641	36	14	125	120
Utah	63	38	133	28	58	148	36
Washington	931	54	626	122	22	741	245
British Columbia	162	35	164	73	77	195	53

Dairy Operations [tons/day]

	NH_3
Oregon	40
Washington	39

Point Source [tons/day]

	CO	NOx	VOC	NH_3	SO_2	PM_{10}	$PM_{2.5}$
California	37	13	2	752	1	0	0
Idaho	66	31	6	3	48	12	10
Montana	64	23	7	1	7	10	10
Nevada	17	50	1	0	39	2	2
Oregon	96	67	39	0	48	27	22
Utah	24	28	12	1	20	17	10
Washington	112	112	35	2	120	20	15
British Columbia	226	52	27	3	41	38	22

On-road Mobile Source [tons/day]

	CO	NOx	VOC	NH_3	SO_2	PM_{10}	$PM_{2.5}$
California	300	38	36	1	1	1	1
Idaho	732	95	82	4	3	3	2
Montana	368	50	41	2	2	1	1
Nevada	71	10	8	0	0	0	0
Oregon	1786	242	214	10	5	6	4
Utah	998	136	110	6	5	4	3
Washington	2987	402	382	15	8	10	7
British Columbia	798	112	113	5	1	3	2

Non-road Mobile Source [tons/day]

	CO	NOx	VOC	NH_3	SO_2	PM_{10}	$PM_{2.5}$
California	141	18	1	0	1	2	2
Idaho	490	80	1	0	19	9	8
Montana	168	86	3	0	6	5	4
Nevada	8	11	0	0	1	0	0
Oregon	944	142	97	0	17	11	10
Utah	422	75	1	0	8	7	6
Washington	1600	304	7	1	47	21	20

Biogenic Source [tons/day]
(OVOC excludes isoprene and terpene emissions)

	NO	OVOC	Isoprene	Terpenes
California	8	1360	435	582
Idaho	32	1726	285	1006
Montana	28	1568	118	787
Nevada	8	291	89	183
Oregen	29	3171	237	1429
Utah	7	137	87	90
Washington	36	1472	97	922
British Columbia	6	653	734	683
Total	152	10378	2082	5682

Total Anthropogenic [tons/day]

	CO	NOx	VOC	NH_3	SO_2	PM_{10}	$PM_{2.5}$
Califonia	593	75	74	760	4	122	41
Idaho	1387	296	454	168	73	279	270
Montana	677	168	99	75	21	568	118
Nevada	98	70	13	3	41	51	10
Oregon	3766	507	991	45	84	169	156
Utah	1508	277	256	35	91	175	54
Washington	5630	872	1050	140	197	792	287
British Columbia	1186	199	304	81	120	236	78
Total	14846	2465	3241	1306	631	2393	1014

Table 3. Volatile organic gas chemical allocation profile for wild and prescribed fire emissions by CMAQ SAPRC99 mechanism species.

CMAQ Mechanism Species	Species Descriptions	Percentage Fraction
ALK1	Alkanes with OH reacitivity as ethane	10%
ALK2	Alkanes with OH reacitivity as propane, acetylene	9%
ALK4	Alkanes and non-aeromatic compounds	1%
CH4	Methane	10%
ETHENE	Ethene	19%
OLE1	Alkenes with kOH < 7E4 ppm-1 min-1	5%
OLE2	Alkenes with kOH > 7E4 ppm-1 min-1	1%
NR	Non-reactive species	45%

Table 4. Seasonal averages of AIRPACT-3 chemical boundary conditions by vertical layers compiled from the MOZART global chemical model. VOC is comprised of SAPRC99 species for HCHO, PROD2, ACET, PHEN, RCHO, MGLY, BALD, ISOPROD.

	O_3 (ppbv)				NOx (pptv)				VOC (ppbvC)			
	DJF	MAM	JJA	SON	DJF	MAM	JJA	SON	DJF	MAM	JJA	SON
Layer21	684	768	436	387	228	383	482	365	1	1	1	1
Layer20	268	299	157	136	165	235	224	183	1	1	1	1
Layer19	94	115	95	81	69	80	63	65	3	2	1	2
Layer18	45	57	57	51	27	29	32	31	5	4	1	3
Layer17	42	52	54	50	17	21	27	24	7	5	1	3
Layer16	40	49	50	47	17	22	31	24	9	6	2	4
Layer15	38	46	47	45	22	27	37	29	11	7	3	5
Layer14	38	45	45	44	31	34	44	37	12	8	3	6
Layer13	37	45	43	43	43	42	50	45	13	8	4	6
Layer12	37	44	42	43	52	48	55	51	14	9	4	7
Layer11	37	44	42	43	62	53	60	58	15	9	5	7
Layer10	36	44	41	42	71	58	64	64	15	10	5	8
Layer9	36	44	41	42	78	61	67	68	16	10	5	8
Layer8	36	44	41	42	86	65	71	73	16	10	5	8
Layer7	35	42	38	40	98	72	77	81	17	11	6	9
Layer6	33	40	36	38	113	79	86	91	18	11	6	9
Layer5	33	40	36	38	124	85	93	99	18	11	7	10
Layer4	33	40	36	38	136	92	102	108	19	12	7	10
Layer3	31	38	34	36	149	101	116	118	20	12	7	10
Layer2	30	36	33	34	160	109	131	127	20	12	8	11
Layer1	30	36	32	34	167	114	141	133	20	13	8	11

	CO (ppbv)				ASO4 (pg/m^3)				ANO3 (pg/m^3)			
	DJF	MAM	JJA	SON	DJF	MAM	JJA	SON	DJF	MAM	JJA	SON
Layer21	35	31	33	37	23	22	33	35	0	0	0	0
Layer20	52	52	54	54	39	65	58	49	0	0	0	0
Layer19	72	76	65	67	45	89	52	44	0	0	2	1
Layer18	87	89	67	74	43	93	47	41	0	0	2	1
Layer17	97	96	67	78	43	91	52	45	0	1	4	1
Layer16	105	101	69	82	51	98	70	61	0	2	17	3
Layer15	110	105	72	86	70	117	94	87	1	4	23	6
Layer14	113	108	74	89	98	141	113	119	6	6	12	7
Layer13	116	111	76	92	135	168	127	153	15	8	6	8
Layer12	118	112	77	93	161	185	136	176	24	10	4	9
Layer11	119	114	77	95	186	202	146	200	35	11	3	11
Layer10	120	114	78	96	211	216	155	221	47	13	2	12
Layer9	121	115	79	96	229	226	162	236	56	14	1	14
Layer8	122	116	79	97	248	237	169	252	65	15	1	15
Layer7	123	117	80	98	278	253	181	278	81	17	1	19
Layer6	124	117	81	99	310	271	194	307	99	20	1	24
Layer5	125	118	81	100	329	283	204	327	111	22	1	28
Layer4	126	118	81	100	347	296	215	347	124	24	1	32
Layer3	126	119	82	101	365	309	227	368	138	26	2	37
Layer2	127	119	82	102	379	319	236	384	149	28	3	40
Layer1	127	120	83	102	388	327	242	394	156	29	4	42

Table 5. Wild and prescribed fire emissions by months during the August – November 2004 evaluation period.

	August [tons/month]					September [tons/month]			
	CO	TOG	$PM_{2.5}$	PMC		CO	TOG	$PM_{2.5}$	PMC
California	213434	17733	25336	2132		632	53	75	6
Idaho	1203187	100098	142903	11920		12672	967	1357	115
Montana	1193	98	140	13		6207	450	623	53
Nevada	15	1	2	0		48	4	5	1
Oregon	55435	4521	6520	619		13068	1096	1475	157
Utah	578	47	68	7		14	1	1	0
Washington	114036	6833	8976	721		37917	4017	3817	365
British Columbia	128022	10752	15279	1190		241	20	29	2
% total from Wild Fire	100%	100%	100%	100%		2%	1%	2%	2%

	October [tons/month]					November [tons/month]			
	CO	TOG	$PM_{2.5}$	PMC		CO	TOG	$PM_{2.5}$	PMC
California	2269	189	270	22		38	3	5	0
Idaho	33393	2430	3369	287		10427	734	1005	84
Montana	48393	3534	4910	426		78141	5747	8001	695
Nevada	0	0	0	0		0	0	0	0
Oregon	173964	11701	14144	1307		80724	5575	6502	587
Utah	36	2	2	0		312	17	21	2
Washington	51369	5053	5263	509		33077	3084	3264	312
British Columbia	0	0	0	0		0	0	0	0
% total from Wild Fire	1%	1%	1%	1%		1%	1%	1%	1%

Table 6. Monthly MM5 model performance statistics over the evaluation August-November 2004 period.

	August					September				
	Surface Temperature (^{o}C)	Wind Direction (deg)	Wind Speed (m/s)	24-hr Precipitation (mm)	Relative Humidity (%)	Surface Temperature (^{o}C)	Wind Direction (deg)	Wind Speed (m/s)	24-hr Precipitation (mm)	Relative Humidity (%)
Mean Error	-0.3	5	1.6	0.0	4	0.7	7	1.4	-0.8	-3
Mean Absolute Error	2.4	64	2.3	1.7	13	2.1	62	2.2	1.8	12
Root Mean Square Error	3.2	81	2.8	6.7	17	2.7	79	2.7	13.9	16
Standard Deviation	3.1	81	2.2	6.7	17	2.6	79	2.2	13.9	16
Number of data points	32569	24892	25476	12378	23466	20012	12544	12929	3099	11106

	October					November				
	Surface Temperature (^{o}C)	Wind Direction (deg)	Wind Speed (m/s)	24-hr Precipitation (mm)	Relative Humidity (%)	Surface Temperature (^{o}C)	Wind Direction (deg)	Wind Speed (m/s)	24-hr Precipitation (mm)	Relative Humidity (%)
Mean Error	0.6	6	1.9	-0.4	1	0.3	8	1.8	-0.4	3
Mean Absolute Error	2.1	65	2.5	2.8	13	2.2	70	2.4	2.1	14
Root Mean Square Error	2.9	83	3.1	13.2	17	3.0	87	3.1	15.3	19
Standard Deviation	2.8	82	2.5	13.2	17	3.0	87	2.4	15.3	18
Number of data points	29285	20827	21201	11024	19027	32956	24416	24978	10887	22931

Table 7. Measurement stations by monitor networks and measured pollutant species used in the August-November 2004 evaluation period.

EPA-AQS (Hourly Ozone)

Site Name	Latitude	Longitude
Ritzville	47.129	-118.382
Yelm	46.936	-122.611
Wishram	45.664	-121.000
Belfair	47.419	-122.850
Custer	48.954	-122.565
HWY12	46.624	-121.387
LakeSammaish	47.552	-122.044
MtViewSchool	45.617	-122.517
OlymPark	48.098	-123.426
MtRainierJackson	46.785	-121.733
RangerStn	48.539	-121.447
NorthBend	47.490	-121.773
NorthEnd	48.460	-122.519
Enumclaw	47.141	-121.933
GreenBluff	47.827	-117.275
BeaconHill	47.570	-122.313
PackForest	46.843	-122.318
MtRainierNP	46.761	-122.122
Carus	45.260	-122.588
Sauviels	45.768	-122.772
CascdJrH	44.809	-122.914
AmazonPk	44.026	-123.084
Lafayette	45.497	-122.602
Talent	42.229	-122.788
Saginaw	43.834	-123.035
Milwaukie	45.443	-122.638
S3rdAveW	43.706	-116.623
TilliRd	43.287	-115.853
WhitneyEle	43.589	-116.223
CrMoon	43.461	-113.562

EPA-AQS (Twice Weekly $PM_{2.5}$)

Site Name	Latitude	Longitude
Boise	43.636	-116.270
Pocatello	42.877	-112.460
Inkom	42.796	-112.258
StMaries	47.317	-116.570
Plummer	47.339	-116.885
IdahoFall	43.518	-112.021
BonnersFerry	48.706	-116.369
Nampa	43.562	-116.563
Emmett	43.856	-116.515
NezPerceNP	46.209	-116.028
Salmon	45.171	-113.892
Pinehurst	47.536	-116.237
Ridgefield	45.768	-122.772
Medford	42.314	-122.879
EaglePoint	42.536	-122.875
WhiteCity	42.426	-122.851
KlamathFalls	42.189	-121.723
Eugene	44.026	-123.084
CottegeGrove	43.834	-123.035
Oakridge	43.744	-122.481
Albany	44.616	-123.092
Portland	45.497	-122.602
LaGrande	45.339	-117.905
TheDalles	45.602	-121.203
Beaverton	45.470	-122.816
Hillsboro	45.518	-122.967
Kennewick	46.219	-119.206
Vancouver	45.648	-122.587
NorthBend	47.490	-121.773
Enumclaw	47.141	-121.933
LkForestPk	47.753	-122.277
Seattle	47.563	-122.338
Twisp	48.364	-120.121
Tacoma	47.188	-122.450
Marysville	48.056	-122.173
Spokane	47.661	-117.357
Yakima	46.598	-120.499

IMPROVE ($PM_{2.5}$, PSO4, PNO3, POC, PEC)

Site Name	Latitude	Longitude
CRMO	43.461	-113.555
SAWT	44.171	-114.927
MOHO	45.289	-121.784
KALM	42.552	-124.059
CRLA	42.896	-122.136
THSI	44.291	-122.043
STAR	45.225	-118.513
HECA	44.970	-116.844
OLYM	48.007	-122.973
PUSO	47.570	-122.312
SNPA	47.422	-121.426
CORI	45.664	-121.001
COGO	45.569	-122.210
WHPA	46.624	-121.388
PASA	48.388	-119.928
MORA	46.758	-122.124
SPOK	47.905	-117.861
NOCA	48.732	-121.065

EPA-AQS (PSO4, PNO4, PNH4, POC, PEC)

Site Name	Latitude	Longitude
Boise	43.562	-116.563
Medford	42.314	-122.879
Eugene	44.026	-123.084
Portland	45.561	-122.679
LaGrande	45.339	-117.905
LkForestPk	47.546	-122.322
Kent	47.370	-122.198
Seattle	47.563	-122.338

SWCAA (Hourly PSO4, PNO4, POC, PEC)

Site_Name	Latitude	Longitude
Bonneville Dam	45.646	-121.943
Mt Zion	45.568	-122.212
CORI (PNH4)	45.664	-121.001
COGO (PNH4)	45.569	-122.210

Table 8. AIRPACT-3 performance statistics for daily maximum 8-hr ozone concentrations.

O_3	
Number of Points	1033
MB (ppbv)	2.7
ME (ppbv)	7.2
NMB	6%
NME	17%
RMSE	9.1
R	0.55
Mod. Avg. (ppbv)	46
Obs. Avg. (ppbv)	43

Table 9. AIRPACT-3 performance statistics for 24-hr $PM_{2.5}$ concentrations by the EPA-AQS, IMPROVE measurement networks, and over all measurement sites.

$PM_{2.5}$	EPA-AQS	IMPROVE	All Sites
Number of Points	1008	233	1241
MB (μg/m^3)	2.0	2.2	2.1
ME (μg/m^3)	8.0	5.5	7.5
NMB	17%	37%	19%
NME	70%	85%	71%
FB	3%	3%	3%
FE	59%	53%	58%
RMSE	11.4	9.7	11
R	0.46	0.53	0.49
Mod. Avg. (μg/m^3)	13	8.2	11
Obs. Avg. (μg/m^3)	11	6.0	9.0

Table 10. Summary of AIRPACT-3 performance statistics for component $PM_{2.5}$ by EPA-AQS, IMPROVE and SWCAA measurement networks.

	POC			PEC		
	EPA-AQS	**IMPROVE**	**SWCAA**	**EPA-AQS**	**IMPROVE**	**SWCAA**
Number of Point	254	502	1872	189	129	874
MB	0.3	-0.4	0.0	0.5	0.4	0.3
ME	3.7	2.0	2.1	0.8	0.7	0.6
NMB	7%	-17%	1%	54%	63%	62%
NME	71%	76%	78%	83%	104%	110%
FB	-18%	-52%	-28%	26%	15%	15%
FE	72%	80%	73%	58%	63%	61%
RMSE	5.1	3.9	3.6	1.2	1.3	1.1
R	0.4	0.4	0.2	0.5	0.4	0.0
Mod. Avg.	5.5	1.9	2.4	1.4	0.9	0.7
Obs. Avg.	5.2	2.3	2.4	0.9	0.5	0.4

	PNO3			PSO4			PNH4	
	EPA-AQS	**IMPROVE**	**SWCAA**	**EPA-AQS**	**IMPROVE**	**SWCAA**	**EPA-AQS**	**SWCAA**
Number of Point	111	54	725	214	209	2686	196	46
MB	-0.3	-0.2	-0.3	-0.8	-0.5	-1.8	-0.2	-0.4
ME	1.2	0.9	0.9	0.9	0.6	1.8	0.4	0.4
NMB	-17%	-14%	-30%	-53%	-52%	-77%	-26%	-61%
NME	67%	63%	78%	57%	58%	78%	53%	66%
FB	-39%	-24%	-23%	-57%	-62%	-118%	-25%	-55%
FE	74%	63%	70%	66%	71%	119%	56%	66%
RMSE	1.8	1.4	1.6	1.5	0.8	2.3	0.8	0.9
R	0.4	0.5	0.1	0.4	0.5	0.2	0.5	0.5
Mod. Avg.	0.9	0.6	0.9	0.6	0.2	0.2	0.5	0.2
Obs. Avg.	1.2	0.8	1.2	1.4	0.7	2.0	0.7	0.6

CHAPTER THREE

Global Change Impacts on Future Regional Air Quality in the United States

Jack Chen, Jeremy Avise, Brian Lamb
Washington State University, Department of Civil and Environmental Research

Clifford Mass, Eric Salathé
University of Washington

Alex Guenther, Christine Wiedinmyer
National Center for Atmospheric Research

Donald McKenzie, Narasimhan Larkin
United States Department of Agriculture, Forest Service

Susan O'Neill
United States Department of Agriculture, Natural Resources Conservation Service

Abstract

A comprehensive numerical modeling framework has been developed to estimate impacts of global change upon regional air pollution, specifically ground level ozone, while accounting for regional anthropogenic, biogenic and wild-fire emission variations. The system was applied to simulate two 10-year periods: 1990-1999 as the base-case and 2045-2054 as a future case. The Intergovernmental Panel on Climate Change (IPCC) SRES A2 scenario was applied for the future case with the 'business as usual' greenhouse gas and ozone precursor projections. The model system coupled global climate and chemistry model, PCM and MOZART2, with the regional modeling framework, MM5 and CMAQ, over the continental US domain. The base-case results were assessed with long-term ozone measurements throughout the US. The system correctly captured episodic ozone conditions and spatial pollution distributions across the continent, however, lower averaged ozone concentrations were over-estimated. When compared with the future simulations, results showed 8-hr daily maxima concentrations increased by 5 ppbv for episodic events, and by 5-10 ppbv during non-episodic events. Spatially, the model predicted larger urban air pollution footprints due to the effects of climate change, higher predicted regional emissions and higher global pollutant background concentrations. For selected sites downwind of major urban areas, there were more pollution events per month, with episodic ozone occurrences starting earlier and ending later in the year. Furthermore, air pollution events were predicted to last longer with more consecutive days the 8-hr daily maxima ozone concentration exceed the US EPA 80 ppbv standard.

Introduction

Eularian photochemical transport models have been widely used to study complex air quality problems for historical pollution events (Russell et al., 2000). They are also valuable tools in predicting the onset of air pollution episodes for short-term, 24- to 48-hour, periods (Vaughan et al., 2004; Mckeen et al., 2005; U.S. EPA, 2003). In recent years, with the increasing awareness of global change taking place (Climate Change Science Program, 2005), there have been growing interest in using the computational grid models to assess long-term air quality impacts and the effects on human health (Knowlton et al., 2004). Global changes such as climate variability, land cover alteration, population growth and the associated emissions differences are interrelated factors that can cause significant changes to air quality in the future.

In order to account for these large scale changes collectively, comprehensive air quality model experiments are effective methods to provide insight into future air quality conditions. These models allow systematic treatment of processes affecting regional atmospheric chemistry, and provide quantitative estimates on the spatiotemporal extent of pollution changes. Recently, several such applications have been published in the literature. In predicting future climate conditions, Leung et al., (2005) suggested possible increases in air pollution events due to higher summer temperatures, higher solar radiation, lower precipitation frequency and increased stagnation events in the western US. Globally, Horowitz (2006) estimated significant changes in ozone burden from +40% to -6% between years 2000 and 2100, depending on future emission scenarios. The increases varied spatially with greater changes in the Northern Hemisphere and the tropical Atlantic Ocean. Regionally within the US, model studies by Hogrefe et al., (2004) and Jacob et al., (1999) showed future summertime ozone concentrations could increase by 2.0 to 5.0 ppbv from increases in global background and long-range transport of pollutants from Europe and Asia. With background pollutant concentrations held unchanged,

Hogrefe et al. (2004) also attributed half of the future increases to regional biogenic emissions. As for the frequency and duration of future air pollution events in the US, Murazaki et al., (2006) and Mickley et al., (2004) forecasted more severe air pollution episodes in major urban areas, with each episode lasting longer than present-day conditions.

The complex, nonlinear ozone chemistry, and the large spatial variations in emissions and meteorology can influence ozone formation differently in different regions. In this study, we estimate the regional air quality impacts 50 years in the future from predicted global change and regional emission changes in the US. The approach employs a comprehensive modeling framework that couples global and regional scale meteorology and chemical models. The model system is able to account for large scale forcings predicted by global models, as well as, capturing regional scale temporal and spatial variability that cannot be achieved by global scale simulations alone.

To assess the model system, we performed a 10-year simulation with current decade climatology for 1990-1999, and compared the results with long-term observed ozone concentrations across the US. For a future scenario, we applied the system for the period 2045-2054, and compared the future case simulation results with the current, base-case model outputs. In the following sections, we first describe the model system framework, followed by evaluation of the model results for current period simulations. Next, we assess the regional air quality impacts by spatial changes in ground level ozone concentrations, and variability of extreme ozone episodes at selected locations across the continental US.

Model System Description

The model system consists of global scale and regional scale grid models. The coupling is done through one-way nesting, where time and spatial varying outputs from global models are

extracted and used as boundary conditions for the regional models. In this paradigm, the global scale models account for effects of global change and long-range pollutant transport between continents, and the regional scale models refine the predicted results, while accounting for regional influences on local air quality. The global climate and chemistry models were PCM (Parallel Climate Model, (Washington et al., 2000), and MOZART2 (Ozone and Related Chemical Tracers version 2, (Horowitz et al., 2003), respectively; the regional scale models were the MM5 mesoscale meteorological model (Grell et al., 1994) and the CMAQ (Community Multi-scale Air Quality, (Byun et al., 1999) modeling system. The hourly predicted regional meteorological outputs from MM5 were used to generate regional emissions in the SMOKE (Sparse Matrix Operating Kernel Emissions, (Houyoux et al., 2005) processing system and to drive the CMAQ model. Figure 1 depicts the general system schematic and data flow.

Simulation Period

Simulations were carried out for two 10-year periods. The current period, 1990-1999, was the base-case, and represented contemporary air quality conditions. Results from this were compared with measurement data for model validation, and evaluated against future year simulations in 2045-2054 for changes in ozone concentrations. Global models were simulated first and processed for the subsequent regional model simulations. Both the global and regional model simulations were performed as two continuous runs across the two decades. Regional simulations were done in monthly batches with initial conditions from the last hour of the previous run. These long term simulations were necessary in order to capture large-scale signals from global change and to minimize normal inter-annual variability. The two 10-year simulations provided 10 slightly different ozone seasons per decade at the regional scale. This represented a large array of environmental conditions for pollution events due to differences in meteorology and emissions scenarios driven by global change.

Global Scale Simulations

In the global scale simulations, the PCM model provided global meteorological fields for the MOZART chemistry simulations. The model couples atmospheric, land surface, ocean, and sea-ice modules to form an earth system model for current and future climate scenarios. PCM has been widely used in climatic studies, and is part of the model family in the Intergovernmental Panel on Climate Change (IPCC) assessments (Washington et al., 2005). In this application of PCM, the model domain covered the entire globe with horizontal grid resolution at 2.8° latitude by 2.8° longitude (approximately 300 km), and vertically with 19 layers. The vertical layer structures and the approximate layer height from sea-level are summarized in Table 1. The layers were distributed unevenly with the top model layer reaching 30 km above sea level. Higher vertical layers were necessary to capture large-scale atmospheric processes and stratospheric intrusions that can affect ozone concentrations in the lower troposphere (Lamarque et al., 1996). The model produced simulation results with 6-hour output throughout the two decade simulations.

For the future climatic conditions in 2045-2054, the PCM model was applied with the IPCC SRES A2 – 'business as usual' greenhouse gas emission scenario. The A2 scenario represents the most pessimistic projected global environment among all the IPCC scenario families. It is characterized as "a very heterogeneous world with emphasis on regional self-reliance and preservation of local identities. While some attention is given to environmental issues on a regional basis, the overall global environmental concerns are weak among countries in the world" (Nakiæenoviæ, N. et al., 2000). Figure 2 from the 2001 IPCC assessment, depicts the projected changes in global population and global anthropogenic greenhouse emissions for A2 and other scenarios. The A2 scenario has a large global population of 11 billion by 2050, and high atmospheric loading, with a steady rate of increase, of greenhouse gases.

The MOZART2 global chemistry model was applied with meteorological data from the PCM model for global chemical conditions with respect to climate. Global emissions for MOZART2 was based on the EDGAR (Emissions Database for Global Atmospheric Research version 3.2; (Olivier et al., 2000) and the GEIA datasets (Global Emissions Inventory Activity – http://geiacenter.org). The inventory included sources from fossil fuel combustion, industrial activities, agriculture waste, biomass burning, lightening, aircraft, soil and oceanic volatile organic compounds (VOC). Global biogenic emissions were generated dynamically using algorithms from Guenther et al. (1995) and predicted global vegetation cover from the Community Land Model (Bonan et al., 2002). Emissions were temporally allocated to account for seasonal variability. For future simulations, the global emissions were projected to 2050 with source specific emission factors consistent with the IPCC A2 scenario. Figure 3 shows the projected NOx and VOC emissions by IPCC scenario family. Under the A2 scenario, global NOx emissions were predicted to almost double in 2050 to 70 MtN/year, while global VOC emissions were predicted to increase by approximately 80% to 275 Mt/year. The MOZART2 model adopted the same horizontal and vertical grid configurations as PCM, and produced results once every 3 hours. The model has been used in many studies, and has demonstrated good ability in capturing current global distributions of ozone and other chemical components when compared with measurement data from various parts of the world (Horowitz et al., 2003; Saraf et al., 2003).

Regional Scale Simulations

The MM5 and CMAQ regional models were used to downscale the time stepping PCM and MOZART outputs, respectively. Results from the regional models have much higher temporal and spatial resolutions. Figure 4 shows the regional model domain coverage, and Table 1 shows their vertical layer structures by sigma layer at mid-point and the approximate elevation from sea level.

MM5 Meteorological Model

The MM5 meteorological model (version 3) was applied to generate hourly meteorological conditions for CMAQ. The MM5 simulations were performed with nested configuration, at 108-km and 36-km grid resolutions. The larger outer domain covered much of Northeast Pacific and North America to capture large scale climatic processes. The inner domain, at 36-km resolution, was centered over the continental US. There were 28 vertical layers reaching the tropopause, with the bottom layer at 32 m.

The PCM to MM5 downscale was conducted at the 108-km outer domain. MM5 simulations were nudged towards the PCM results at every 6-hour simulation time step. This maintained numerical stability, and constrained MM5 results with the global model for a smooth transition between global and regional simulations. The model runs were conducted in non-hydrostatic mode with the MRF (Hong-Pan) planetary boundary layer scheme, simple-ice cloud microphysics, Kain-Fritsch cumulus parameterization, CCM2 radiation scheme, and the simple 5-layer soil model. The configuration was chosen to capture large scale meteorological processes at 36-km grid scale, as well as to optimize computational speed for long term simulations. The inner 36-km simulations were performed with one-way nesting approach from the 108-km simulation results within the MM5 model.

Model configurations for the future case simulation were identical to the present case, except for landuse input to MM5. Landuse and land cover variations are known to significantly influence regional meteorology and air quality through energy flux perturbations from the ground (Civerolo et al., 2000). For the present case simulations, landuse dataset were based on the 1-km USGS dataset with 24 land cover categories. Landuse for the future simulations were updated with model data from the Community Land Model (Bonan et al., 2002) and the Spatially Explicit Regional Growth Model (SERGOM, (Theobald, 2005). The Community Land Model provided changes in vegetation distribution by plant functional types for 2050, and the SERGOM

model provided urban and suburban population density distributions out to year 2030. Figure 5 depicts the MM5 landuse inputs for the current and future cases. Table 2 shows the quantitative comparison between the category changes by area coverage. Estimated climate change and population perturbation have significant influence on projected future landuse compared to the current case. The most striking changes are the abundances of shrub and grasslands, and dry land crop predicted in the future. Significant portions of the central US changed from grass and crop lands to pasture or dry land crop. For southwest states such as Nevada, Utah, Arizona and New Mexico, land cover changed from mostly shrub lands to sparsely vegetated coverage and grassland. In the Pacific Northwest, regions of evergreen forests were transformed to grassland and irrigated crops. Similar conditions were predicted for the southeastern states where evergreen and deciduous vegetation were converted to dry land crops and sparsely wooded wetlands.

Chemical Transport Model

Regional air quality simulations were conducted using the CMAQ model (version 4.4). The model has undergone extensive community development, and has demonstrated good performance for several regional air quality studies across the US (Tong et al., 2006; Eder et al., 2006). In this application of CMAQ, the gas-phase chemistry was represented using the SAPRC99 mechanism (Carter, 2000). The simulation domain, at 36-km grid resolution, was 10 grids smaller from each side of the inner MM5 domain to reduce effects of boundary conditions from MM5. There were 18 vertical layers distributed unevenly, with more layers at the bottom troposphere to better capture planetary boundary layer (PBL) dynamics (Table 1). The Meteorology-Chemistry Interface Processor (MCIP version 3.0) was used to process the MM5 model results and collapse the MM5 vertical levels from 28 sigma layers to 18 layers while retaining key parameters such as PBL heights, incoming solar radiation, and momentum and heat fluxes for CMAQ.

CMAQ Boundary Conditions

The time stepping boundary conditions for the CMAQ model were extracted from the MOZART global model for grids around the regional domain. The MOZART chemical species were mapped to the SAPRC99 species, and the vertical concentration profiles were interpolated into the CMAQ sigma layers. Figure 6 and Table 3 show a summary of CMAQ boundary conditions for the east and west sides of the regional domain and compare current and future periods. Concentration profiles for ozone, NOx, NOy and VOC show different vertical structures, and much higher concentrations for the east than the west sides. This is because the predominant westerly wind across the US continents brings cleaner Pacific air for the west, while air mass at the eastern boundary contains higher anthropogenic pollutions from within the US continent. The averaged ozone concentrations below 500 mb were 38 ppbv and 46 ppbv, respectively, for the western and eastern boundaries. Large concentration differences were also modeled between the two sides for NOx, NOy and VOC. Higher pollutant concentrations were predicted for the future at both sides. The changes were slightly larger for the west than the east, and the degree of increase varied with vertical layers. For the western side, averaged ozone concentrations below 500 mb increased approximately 12 ppbv in the future, while VOC concentrations almost doubled from 1.1 to 2.1 ppbv. For the eastern side, ozone concentrations were predicted to increase by 30%, and NOx, NOy and VOC concentrations were predicted to increase by approximately 50% in the future. Vertically, VOC concentrations increased constantly with height, whereas NOx, NOy and ozone concentration changes were more significant below 400 mb. These comparisons demonstrate the movement of generally more polluted air into and out of the US in the future.

Regional Emissions

Regional emissions for the CMAQ model included both anthropogenic and natural sources. The anthropogenic emission inventory was based on the 1999 EPA National Emission

Inventory (NEI-1999, http://www.epa.gov/ttn/chief/net/1999inventory.html) and processed with the SMOKE processor. The inventory included categories from area, on-road mobile, non-road mobile and point sources. The area and mobile emissions were imported as county-wide, annual totals, without temperature adjustments. Plume rise for each point source was calculated in SMOKE using MM5 meteorology and the Briggs plume rise algorithm.

The future case anthropogenic emissions were projected to year 2050 using factors from the EPA Economic Growth Analysis System (EGAS, (U.S. EPA, 2004). The EGAS system contains emission factors for each emission category by county. The EGAS module consider factors such as future changes in real personal income, real disposable income, population, employment and estimated future energy consumptions by sectors. The projections from EGAS were applied to area and mobile source categories. Point source emissions were unchanged from NEI-1999, assuming current industrial emissions are at their maximum allowable limits, set by the government. Spatial distribution of future anthropogenic emissions was updated with 2030 population and housing density estimates from the SERGOM model to account for urban area expansion in the future. Comparison between future and current case anthropogenic emission inventory showed significant changes in the future decade. Table 4 summarizes domain-wide emissions by ratios between future and current periods for each category. The biggest change was in the area source category with a predicted increase of at least 30% for all species. Emissions from on-road mobile sources were predicted to stay relatively unchanged with a small 2% increase for CO, NOx and VOC species. Non-road mobile emissions, on the other hand, were predicted to increase by 9% to 30% depending on the chemical species.

In addition to anthropogenic emissions, biogenic and fire emissions were included in the simulations. Biogenic emissions were generated dynamically with the MEGAN (Model of Emissions of Gases and Aerosols from Nature) model (Guenther et al., 2006). The model estimates hourly VOC, isoprene and monoterpene emissions from plants with a seasonal

varying vegetation dataset, and predicted hourly temperature and ground level shortwave radiation from MM5. For the base-case simulations, the seasonal vegetation dataset was derived from satellite observations with 1-km grid resolution. The data were up-sampled to match the 36-km regional domain. For the future decade, the vegetation data were updated with results from the Community Land Model to incorporate predicted changes in plant functional types due to simulated future climate change. Similar sets of land cover data were used in the MM5 simulations discussed earlier for consistency. There were significant differences between current and future biogenic emissions due to projected vegetation distributions. Figure 7 shows July isoprene emission capacity at 30°C for the two periods. Significant reduction was estimated in future isoprene emission capacity due to projected expansion of agriculture and urban areas. In the future, isoprene emitting vegetation is reduced in the southeast and north central states, and replaced with agricultural crops of lower isoprene emission capacity. The reduction is significant such that actual isoprene emissions decrease even when future temperatures were predicted to be higher. Table 4 shows overall biogenic emission magnitude for July, when the emission activity is the highest. Across the domain, total daily biogenic VOC emissions were predicted to decrease in 2050 by -37% from the present case.

Wild fire emissions play important roles in changing current and future regional air quality conditions. Large fires contribute significant amount of pollutants and pollutant precursors to the atmosphere which, in turn, affect formation of ground level ozone (Miranda, 2004; Malm et al., 2004). To account for the impact of wild-fires in regional simulations, we applied the Bluesky model (Larkin et al., 2007) with a fire occurrence dataset to generate fire emissions at each fire event by location. The coupling of the Bluesky fire emissions model with the CMAQ model has been demonstrated and shown to provide a good representation of regional fire emissions and their impacts on air quality in the Pacific Northwest (Lamb et al.,

2007). The same system was implemented here for current and future year fire emissions across the US continent. Fire events data from 1990 to 1999 were obtained from the Bureau of Land Management. The dataset contains records of fire location and fire size on federal lands necessary for the Bluesky system. For the future scenario, fire events were generated using the Fire Scenario Builder (FSB) stochastic model, developed by the USDA Forest Service (Mckenzie et al., 2006). The model translates future meteorology from MM5 into probabilistic fields of fire ignitions, fire sizes and fuel consumptions. The results were then used in the Bluesky model to estimate future emissions from predicted fire events. This stochastic method represents the best approach in modeling the highly unpredictable wild-fire occurrences for the future environments. Table 4 compares current and predicted future fire emission estimates across the domain. There were approximately 25% increases in VOC and CO emissions in the future. Given the large uncertainties in future climate, the estimated fire emission changes are not unrealistic.

Results and Discussion

In the following sections, we first discuss comparisons between current period (1990-1999) model predicted ground level ozone concentrations with observations for monitoring sites throughout the US. Next, we focus on changes in future pollution conditions by comparing current decade ozone concentrations with that of the future simulation results (2045-2054).

Regional Ozone Evaluation

Our evaluation of the base-case simulation is focused on the system's ability to capture the range and patterns of ozone concentrations under present climate and emission conditions. This is achieve by comparing 1990-1999 model output with measured surface ozone concentrations from monitor stations across the continental US during the summer month (June,

July and August), for years 1994-2003. Since the regional models were performed without observational or analysis nudging, the model output represents a realization of current ozone conditions, but does not represent ozone concentrations corresponding to specific weather events, times or locations. As a result, the evaluation must be based upon comparison of the frequency and spatial distributions of measured and predicted ozone concentrations. The comparisons are, therefore, independent of year, and data are paired only by site.

Long-term ozone measurement data were obtained from the EPA Air Quality System database (AQS http://www.epa.gov/ttn/airs/airsaqs). The 1994-2003 measurements are the earliest 10-year period available for the entire continental US. The measurement data were collected by state, local, and tribal air pollution control agencies and covers sites in urban, suburban and rural regions. Measurement data from all 1547 sites were processed, but only sites with at least 4 summers of observations were used to ensure good representation of local ozone environments. There are 1022 sites across the domain in total with more sites in the east and along coastal regions. Figure 8 depicts the locations of these sites. Stations were grouped by geographic locations in the ten EPA regions. Stations in Regions 1, 2 and 3 were grouped together to represent states in the northeast.

The comparisons are based on summer time daily maximum 8-hour (daily max 8-hr) ozone concentrations. This is the same measurement criteria that US EPA used to determine National Ambient Air Quality Standard (NAAQS) exceedances for ozone. The current NAAQS for ground level ozone is 80 ppbv over 8-hour averaged concentrations.

General Performance

A general comparison for this large dataset can be done by looking at period averaged, 98th percentile, and 20th percentile concentrations of daily max 8-hr ozone by sites across the 10 summer periods. The average concentrations represent overall ozone pollution conditions by

location for the present-day climate condition, and the 98th, and 20th percentile values indicate episodic and non-episodic conditions, respectively. Figure 9 shows these comparisons by scatter plot and Table 5 summarizes the comparisons with standard model performance statistics using mean bias (MB), normalized mean bias (NMB), mean error (ME), normalized mean error (NME), and correlation coefficient (R). These terms are defined in the Appendix C.

Overall, the model performed well in reproducing the average daily max 8-hr ozone with a correlation coefficient (R) equal to 0.62 (Figure 9, Plate a). All modeled values fall within factor of ±2, and 85% of data points are within factor of ±1.25 (75%) of the observed values. However, it is apparent that the model over-predicted the average at several regions and under-predicted higher concentrations in Region 9 above 70 ppbv. When comparing with long-term measured ozone by site, the ME and MB are 7.8 ppbv and 6.3 ppbv, respectively, with NME and NMB of 14% and 11%, respectively. Across all sites, the average observed daily max 8-hr ozone is 57 ppbv and the model over-predicted this with 63 ppbv. The system captured the spatial concentration variability across the different sites with both modeled and measured standard deviation at 8 ppbv.

Although the model system over-predicted the average concentrations at many sites, the system captured high ozone conditions accurately (Figure 9, Plate b). This is good since elevated ozone conditions have much higher impact on the environment, and it is such conditions that we want to capture for the future scenario. For the 98th percentile, model performance improved with ME of 8.5 ppbv (NME = 9%), and MB of 3.3 ppbv (NMB = 4%). The mean 98th percentile observed concentration is 90 ppbv, and the model slightly over-predicted this with 93 ppbv. Concentration variation is much higher with observed and measured standard deviation at 13 ppbv. It is common to see regional air quality models perform better at higher episodic ozone conditions than general lower ozone level. Many such cases are found in

literature for short-term episodic modeling studies and real-time ozone forecast results (Eder et al., 2006; Yu et al., 2006; Chen et al., 2007).

At the low end of the ozone concentration spectrum (Figure 9 Plate c), the associated statistics demonstrated poorer model performance in capturing the 20th percentile concentration level. In this case, the model over-predicted almost all sites with ME of 8.6 ppbv (NME = 18%), and MB of 7.3 ppbv (NMB = 15%). The model correlation was also weaker with R of 0.55. The over-prediction was the worst in Region 4 with many more data points located outside the 85% line. The average 20th percentile observed ozone concentration is 44 ppbv and the model over-predicted with 50 ppbv.

Model and measured averaged ozone concentration differences for Region 9 has noticeably more under-predictions. These under-predictions are consistent for the same sites with different levels of model/measured comparisons (overall period average, 98th percentile and 20th percentile). These suggest possible systematic errors in model inputs, such as under-estimated regional emissions across the entire simulation periods, or consistent errors in modeling PBL height due to inaccurate terrain interpretation in MM5 for the region.

Spatial Distribution

Model performances by ozone concentration spatial distributions are evaluated by comparing modeled and measured concentration contour maps as shown in Figure 10. These maps are constructed using average daily max 8-hr ozone concentrations across the 10 summer periods at each measurement site. For consistency in spatial interpolation, the modeled contour map was constructed only with concentration data from grid cells representing the measurement locations.

The system captured the overall ozone concentration structure across the US continents. The model correctly simulated higher ozone conditions in the eastern US, coastal California,

and northern Texas, as well as the cleaner conditions for the Pacific Northwest and the north central states. However, the figures also show locations where the model performed poorly by over-predicting the average ozone conditions. The over-predictions were higher in eastern large urban areas, where model predicted hot spots of 70 ppbv while the observed concentrations were lower at 55 ppbv to 60 ppbv. More specifically, over-predictions occur in the New York, Philadelphia and Washington DC urban corridor, the regions along the Ohio River Valley and city centers at Atlanta, GA and Jacksonville FL. For the west, the model captured the high ozone in Los Angeles, CA, San Diego, CA areas but failed to capture the higher observed ozone along the Interstate-5 (I-5) highway from Los Angeles, CA up to San Francisco, CA.

The spatial difference is better captured for high episodic ozone conditions. Figure 11 shows the modeled and measured 98th percentile ozone concentrations contour maps. The model successfully captured high ozone levels in most urban areas. For example, the hot spots reaching 95-105 ppbv were correctly reproduced along the New York, Philadelphia and Washington DC urban corridor; the Chicago, Lake Michigan regions; and in the west, the San Francisco, Los Angeles, and Phoenix urban areas. However, there are regions that the model missed. For example, large areas of over-predictions in south eastern cities, specifically, Tampa, FL, Jacksonville, FL and New Orleans, LA where the model predicted concentrations between 95 ppbv and 110 ppbv and the observed were between 80 ppbv to 90 ppbv. In addition, the model tended to over-predict regions downwind of urban cities. For example the model captured the high ozone levels at Houston, TX and Dallas, TX city centers but over-predicted the surrounding rural areas by roughly 5 ppbv. For the central states, the model captured the high concentrations in Denver, CO but under-predicted in Salt Lake City, UT by about 10 ppbv.

Spatial and Temporal Variability

Figure 12 shows the daily max 8-hr ozone concentration ranges for modeled and measured values across the 10 summer months. The overall ozone concentrations and model performance vary by region. As depicted in the spatial plots, the system captured the 98th percentile ozone concentrations very well. The 98th percentile concentrations ranged from the low 75 ppbv in the Pacific Northwest (Region 10) to the high of 105 ppbv in the southwest (Region 9). The period average concentrations, represented by the bar in the box plot, were better captured at Regions 8, 9 and 10 but under-predicted by 5 ppbv to 10 ppbv for the eastern states at Regions 1 to 7. In terms of concentration variability, represented by concentration ranges between 20th and 80th percentile, and 2nd and 98th percentile values, the model captured the concentration spread at most regions, with larger variability in Region 1-3 and 9, and smaller variability in Regions 7, 8 and 10. However, the model over-predicted the 80th percentile concentration magnitudes, and, except for Region 8, it over-predicted the low observed 20th percentile concentrations. The system also over-predicted the low 2nd percentile values, with Regions 4 and 6 having the worse performance with close to 20 ppbv difference.

One of the system performance goals is to capture the general year-to-year variability of the observed ozone concentrations. Figure 13 shows the cumulative distribution functions (CDF) of modeled and measured daily max 8-hr ozone concentrations for each summer across all the monitoring stations in the domain. Table 6 summarizes the parameters depicted in CFD. The system over-predicted the ozone concentration occurrence frequency below 70 ppbv, and the performance is worse at lower levels. The 10-year measured median ozone concentration range is 54 - 58 ppbv; the system over-predicted with median ozone concentration range of 60 - 64 ppbv. Frequency distribution was better captured for concentrations 80 ppbv and above. The 10-year measured 98th percentile ozone concentration range is 91 - 101 ppbv, and the model captured this with concentration range of 95 - 104 ppbv.

The observed year-to-year concentration variability, measured by the variance, was well represented by the model system. The observed 10-year concentration variance range between 361 $ppbv^2$ - 289 $ppbv^2$, and the modeled variance range between 324 $ppbv^2$ – 256 $ppbv^2$. The modeled variance is smaller as expected because the model ozone concentrations represent spatial averages over the 36 km by 36 km grid area, whereas the measurement values are for point locations in space.

In the year-to-year comparisons, it was evident that for some sites, modeled concentrations match slightly better with measurement data for the latter 5 years compared to the entire 10-summer period. An example of this is presented in Figure 14, showing the 10 summers of modeled and measured daily max 8-hr ozone concentration time series for Crestline, CA. This monitor site is located about 20 km north of San Bernardino, CA. The site has a history of very high ozone concentrations from the influence of anthropogenic pollutions upwind. Figure 14 shows that model captured the overall ozone concentrations better for the last five summers (modeled: 1995-1999, measured: 1999-2003) compared to the entire simulation period. The model tended to under-predict high ozone conditions during earlier periods (modeled: 1990-1994, measured: 1994-1998). This is most likely due to the static, year invariant, emission inventory used in the CMAQ model. The 1999 emissions inventory better represents the regional pollutant conditions for the second half of the decade, and does not reflect inventory with lesser control strategies in the earlier years. The result of lower ozone formation with emission controls is therefore not reflected in this long-term simulation. This demonstrates the sensitivity of regional air quality models towards changes in the input emission inventory.

Future Changes in US Air Quality Conditions

In the following sections, we focus on how ground level ozone changes in the future from the combined effects of large scale global changes, as well as the projected regional emission changes. Analyses compare future modeled results with the base-case simulations. We first focus on the overall changes across the US, then shift attention to selected cities with high observed ozone concentrations in the current decade.

General Changes

Similar comparisons used previously are applied here for future modeled and current modeled results. Figure 15 Plate (a) shows scatter plot comparing current and future average daily max 8-hr ozone concentrations by site across the 10 summers. Concentrations are extracted from modeled grids representing measurement sites depicted in Figure 8. The results show overall higher average daily max 8-hr ozone concentrations in all regions, except for a few sites in Regions 1-3, 4, and 9, where lower concentrations are predicted in the future compare to the current base-case. For sites that have higher future ozone, the changes ranged from 0 ppbv to 25 ppbv, with an overall average increase around 8 ppbv. For the sites that showed lower ozone concentrations in the future, the changes were smaller, in the 1 ppbv to 10 ppbv range. Several sites with the lower future ozone are located inside urban areas, along the east coast, such as, Boston, MA and New York, NY. The decreases are likely due to local increases in predicted NOx emissions, which remove ozone by NO titration, and inhibit ozone chemical production. Similar occurrences were observed in a model study for the New York metropolitan area (Civerolo et al., 2007).

The overall increase of 8 ppbv in the US over the next 50 years is comparable with other studies using global chemistry models, but slightly higher than studies using regional scale simulations. In a study analyzing 10 ensemble global chemistry models, Prather et al. (2003) found 5 ppbv to 25 ppbv increase in overall US continental ozone from year 2000 to 2100. In a

climate driven regional air quality model study, Hogrefe et al. (2004) found an overall 4.2 ppbv and 5.0 ppbv increase for the eastern US in years 2050 and 2080, respectively. Considering that the global climate scenario in this study is based on the more pessimistic future projections, and that regional emissions do not include future control strategies, this 8 ppbv future ozone increase is reasonable.

Figure 15 Plate (b) shows the 98th percentile daily max 8-hr concentration comparisons for future and current case simulations. At this higher level, upward trends in future concentrations are predicted for most sites, however, the increases are slightly less, between 0 ppbv and 15 ppbv, when compared with base-case average ozone concentrations. The average episodic ozone increase across all sites is approximately 5 ppbv. There are also more sites showing lower future ozone concentrations than the current base. The decreases in future 98th percentile ozone concentrations ranged from 20 ppbv to 40 ppbv with sites in Regions 1-3 and 4 having the most reductions. These results indicate possible extreme episodic ozone conditions in the future, however, the changes vary spatially, for some sites in Regions 1-3 and 4, there are predicted decreases in peak ozone levels throughout the summer months.

At the lower end of the ozone concentration range, Figure 15 Plate (c) shows the non-episodic, 20th percentile daily max 8-hr concentration values. The graph shows a lot more scatter with increases from 1 ppbv to 30 ppbv. Most sites in Region 6 were predicted to have higher future ozone conditions. Overall, the average increase is approximately 10 ppbv. The larger increase in low level ozone conditions may be attributed to overall higher future pollutant background into the continent. As illustrated previously, the predicted future ozone boundary conditions from the global model showed 30% to 35% increases in the summer. These large scale changes can contribute to the overall increases in the lower, non-episodic ozone conditions.

Spatial Differences

Spatial impacts of current and future predicted air quality conditions for daily max 8-hr ozone concentrations are depicted in Figure 16. Plate (c) depicts the concentration difference between the two cases. The contour maps have much more structure and spatial detail than Figure 10 because they were constructed with modeled 36-km gridded output instead of spatially interpolated data across measurement sites. Significant differences are predicted in the future with ozone pollution impacting much larger areas in the east, south and the south west. The usually clean regions in the Pacific Northwest and the inland northwest are also predicted to have higher summertime ozone in the future with close to 10 ppbv higher concentrations than the base-case.

One significant change is the higher future ozone concentrations in rural areas. Model outputs for the current base-case show areas of high ozone concentration generally confined in urban centers with minor impacts to the surrounding regional areas. In the modeled future scenario however, the high ozone conditions in urban areas reached considerably higher levels, and large rural regions surrounding them are greatly impacted with average ozone concentrations reaching 60 ppbv. The differences are greater in the east, and the southwest.

In the east, high ozone concentrations along the Ohio River Valley, and around New York, Washington DC, Greensboro, NC and Atlanta, GA urban centers create large regions of poor air quality across the entire eastern continent, with mean predicted summer time concentrations between 70 ppbv to 90 ppbv. Areas along the east coast and Gulf of Mexico also have higher predicted concentrations, of 45 – 70 ppbv from the influence of large city centers such as Orlando FL, New Orleans, LA and Houston TX. The combined effects of local emission increases, expansion of urban areas, and regional climate change caused much of the rural areas to have higher ozone from 55 – 60 ppbv to 65 – 70 ppbv. Poorer air quality conditions are also simulated for regions in the south and southeastern US, especially around

major cities such as Dallas, and San Antonio, TX. Average daily max 8-hr ozone concentrations in these areas are predicted to increase by 12 – 18 ppbv, reaching 75 – 80 ppbv. The surrounding rural regions in the south are also predicted to have slightly higher ozone with 5 ppbv to 10 ppbv increase from the current base-case.

On the west coast, the most drastic change in the future air quality centered on southern California, Nevada and Arizona regions. Average daily max 8-hr ozone concentrations increase by 10 – 15 ppbv in urban centers such as Los Angeles, CA, Las Vegas, NV and Phoenix, AZ. Areas along the I-5 highway between San Francisco, CA and Los Angeles, CA are predicted to have 5 – 10 ppbv ozone increases. Rural regions inland are significantly influenced by the higher ozone concentrations from large urban centers. Areas in southern Utah, Nevada and western New Mexico, are predicted to have higher ozone concentrations reaching 70 – 75 ppbv. The impacts are especially significant for nearby national parks such as the Mojave National Reserve, Death Valley National Park and Grand Canyon National Park, where the model predicted approximately 14 ppbv higher ozone conditions from the base-case.

Figure 17 presents the same spatial comparisons but for 98th percentile daily max 8-hr ozone concentrations over the simulation periods. Spatial changes for the episodic ozone events are similar with the average daily max 8-hr ozone, with larger differences in the east, south and southwest. Quantitatively, ozone concentrations in the future reached 5 ppbv to 15 ppbv higher with episodic 8-hr ozone concentrations reaching as high as 110 – 120 ppbv at large urban centers in the east. For the Pacific Northwest, the model predicted higher episodic ozone concentrations with approximately 10 ppbv increase from the base-case.

One additional indicator of future air pollution changes is the number of 36-km by 36-km computational grids that exceed the EPA 80 ppbv ozone standard. This represents the spatial extent of air quality differences between the two simulation cases. Using this matrix for the 98th

percentile episodic ozone in Figure 17, there are 4029 grids in the predicted future decade that exceed the 80 ppbv standard compared to just 2525 grids for the base-case simulation. This indicates an approximately 60% increase in the area predicted to exceed the EPA ozone standard due to the combined effects of global climate change, increases in global background concentrations, and predicted increases in regional anthropogenic emissions.

The large spatial changes in the predicted future ozone conditions correlate well with the predicted changes in ambient temperature. Temperature and solar radiation are important factors for the formation of secondary ozone. Figure 18 shows the current and future predicted average daily maximum 2-meter temperature over the 10-summer months. Predicted temperature change varies significantly by region. Large future temperature increases are predicted for areas in the east and southwest. Temperatures in the east are predicted to increase by 1°C to 4°C, with higher increases along the coastal region. Temperatures in the southwest are predicted to increase by up to 5°C with larger increases in southern California, Nevada, Utah and Arizona states. These spatial variations match that of predicted future ozone increases, and imply that changes in future temperature are important factors contributing to the future regional air quality.

Concentration Spatial and Temporal Variability

Figure 19 shows the range of predicted ozone concentrations by the overall average and the 98^{th}, 80^{th}, 20^{th} and 2^{nd} percentile values across the 10-summer period. Model results are extracted from same measurement sites shown in Figure 8 and grouped by EPA regions. It is clear that model predicts higher average ozone concentrations in the future across all regions. The increases ranged approximately 6 – 13 ppbv from the base-case. The south central US (Region 6) has the largest change, with average daily max 8-hr ozone concentrations increase from 59 ppbv in the current decade to 72 ppbv in the future; on the other hand, Pacific

Northwest (Region 10) has the least amount of change, with 6 ppbv increase from the 41 ppbv in the base-case.

The model predicted higher future episodic ozone conditions in each EPA regions. The modeled 98th percentile ozone concentrations increased by 8 – 17 ppbv from the base-case to 104 - 116 ppbv in the future. For Regions 8 and 9, the episodic ozone concentration increases are less at 3 ppbv and 1 ppbv, respectively, and Region 10 has a slightly lower future 98th percentile ozone concentration than the present, base-case. For Region 10, it appears differences in meteorological conditions may be responsible for the reduction in the 98th percentile ozone concentration. The model also predicted worse air quality condition for the lower 2nd and 20th percentile ozone concentrations. Region 6 has the largest increase of 15 ppbv for both 2nd and 20th percentile ozone, and Region 10 has the least increase with 5 ppbv difference. The changes in lower ozone levels are mostly due to increases in general pollution concentration background discussed earlier.

One significant difference between the current and future cases is the concentration variability of non-episodic pollution events, marked by the 80th percentile and 20th percentile concentration ranges. For all regions, the non-episodic concentration variability in the future is much smaller when compared to the base-case. In the present-day simulation, the average concentration spread between 20th and 80th percentile is about 35 ppbv, whereas, in the future case, the spread is narrower, at about 25 ppbv. This is significantly different from the concentration variability between episodic and background levels, marked by 98th and 2nd percentile concentration range, where in both bases, the ranges are at about 57 ppbv.

The differences in the non-episodic ozone concentration range imply that, within each region, the model estimates an overall smaller spatial concentration variation in the future compare to the base-case. Simulation showed elevated ozone levels in urban areas cause

surrounding rural regions to experience higher ozone pollutions, and more frequently in the future decade. This resulted in higher overall ozone environment in rural sites during non-episodic periods, and decrease concentration spatial variability between the two areas. The narrower future ozone concentration ranges are thus, due to the similar 80th percentile ozone concentrations as the present-day base-case, and the much higher 20th percentile ozone level in the future conditions.

The year-to-year temporal ozone concentration variability of the two cases are depicted in Figure 20 with the CDF of daily max 8-hr ozone occurrences frequency. Table 7 summarizes the parameters of the CDF distributions. The future modeled ozone concentrations increase at almost all occurrences by roughly 5 ppbv to 8 ppbv. The changes are larger in the 20th and 50th percentile ozone levels and are slightly smaller at the 80th and 98th percentile range. The average concentration across all sites ranged from 61 - 64 ppbv in the current decade to 70 - 73 ppbv in the future case. The year-to-year concentration variability, represented by the variance, is similar for both the base-case and future case simulations. The similarity is expected since both are model simulated results.

Changes in Ozone Season and Episode Duration

For a more in depth look at future changes in regional air quality, this section describes the impacts by site-specific ozone season and episodic duration. Eight sites are picked for this analysis (one from each of the EPA regions). The sites are selected for their high observed ozone concentrations during the 1994-2003 analysis periods. All sites are downwind of large urban areas with episodic ozone concentrations higher than the 80 ppbv EPA NAAQS. Figure 21 depicts the locations of these sites, and Table 8 lists the average and 98th percentile observed daily max 8-hr ozone concentrations during the analysis periods.

EPA defines the ozone season as the months when ozone pollution is likely to occur due to high seasonal temperatures. The ozone season varies geographically. Most regions have ozone seasons from March or April to October, when temperatures are favorable for ozone formation. For temperate states such as California and Texas, the ozone seasons are longer. Accompanying the predicted increase in future temperature, the ozone seasons are likely to lengthen within a year. The analyses compare ozone season by occurrence of episodic ozone events between the base-case and the future case. Figure 22 shows average number of days per month daily max 8-hr ozone concentration exceeds 80 ppbv, as well as the average number of days per month 2-meter daily maximum temperature exceeds 30°C for the two simulations. In the current base-case, ozone exceedances usually occur within the ozone seasons defined by EPA, between May and September. Of the 8 sites in the current period, Winslow, GtSmokyMt, Wilmington, Alton and Crestline have the longest ozone seasons from April to September. Denton, TX has the most number of days exceed 30°C and has an ozone season from May to September. The two sites with least number of days exceed 30°C, ChatfieldLake and Canby, have the shortest ozone season from May to July, and June to August, respectively.

Comparing the timescale of episodic ozone occurrence frequency shows that not only does the number of high ozone days increase significantly, but the ozone season also lengthens. Across all sites, the number of ozone days exceeding 80 ppbv increases for all months, with most increases in the spring and autumn months. The changes are larger for cities in the east and California. The increases in episodic ozone days correlated with the increases in frequency of high temperature days in the future. In future case, most sites have episodic ozone conditions starting earlier, and ending later in the year. The three sites in the east, Winslow, GtSmokyMt and Wilmington are predicted to have ozone exceeding the NAAQS as early as March. For the rest of the sites, high ozone conditions are predicted to occur as early as April and continue to September. Crestline has the longest predicted episodic ozone season with an

average of 0.7 ozone episodic days in as late as October. The correlation between ozone episodic days, and high temperature days, indicates the significance of temperature for regional air pollution, both in the episodic frequencies within the month, as well as the occurrence of pollution events throughout the year.

In addition to the longer and earlier onset of ozone pollution, the model also predicted higher frequency of longer pollution episodes in the future. Figure 23 shows the percentage of ozone exceedances by number of consecutive days that the daily max 8-hr ozone concentration exceeds 80 ppbv for the 8 sites. In the current period, most sites have ozone episode lengths of less than 5 days, with 90% of all episodes shorter than 4 consecutive days. The ChatfieldLake site in Colorado has 58% of all episodes within one day, and the Canby site in Oregon has only one-day ozone episodes. The Crestline site in California has prolonged ozone episodes lasting more than a week and only 30% one-day episodes in the current decade. The rest of the sites, the model predicted episodes between 5 to 8 consecutive days with 34% to 44% of all episodic ozone events not longer than one-day.

In the future decade, significant changes are simulated with longer pollution days per ozone episode. All 8 sites have decreases in the frequency of one-day episode in exchange for more consecutive days when ozone exceeds 80 ppbv. The Canby site is predicted to have 15% of ozone pollution events lasting 2 consecutive days. Similarly, at ChatfieldLake, CO, the model predicted a 10% decrease in one-day episodic events with the accompanied increases of longer pollution episodes up to 5 consecutive days. For the rest of the sites, longer ozone episodes are predicted with up to 10 consecutive days when daily max 8-hr ozone concentrations exceed 80 ppbv. The longer ozone pollution conditions for the future will likely prolonged human exposure to elevated ozone conditions and adversely impact the overall public health in the US.

Summary and Conclusions

With the predicted changes in global climate, there are significant consequences for regional environments. These large scale forcings and the associated changes in regional emissions can have significant impacts on air quality conditions in the future. In this study, we developed a comprehensive numerical modeling system to quantify regional tropospheric ozone pollution 50 years in the future due to the combined effects of global changes and predicted emission changes within the US.

The model system was based upon coupled global and regional scale models, where the global models provide time-stepping, spatial varying boundary conditions for the regional scale models. This one-way nested modeling approach allows the large scale models to capture future global changes, and long range pollutant transport, while the regional scale models refine these signals and, simultaneously account for local factors influencing regional air quality. The PCM global climate model provided the current and future climatology for the MOZART2 global chemistry model. Regionally, the MM5 meteorological model and the CMAQ photochemical model downscale the global outputs, and simulate the regional meteorology and air quality conditions over the US at a much finer spatial and temporal resolution.

This modeling framework was applied to simulate air quality conditions for two 10-year periods. The 1990-1999 is the base-case for comparison to a future case in 2045-2054. For the future climatic condition, we adopted the IPCC-A2, “business as usual” scenario. The A2 scenario has a pessimistic projection of the global environment, with a large global population increase, and high anthropogenic emissions of both greenhouse gases and ozone precursor pollutants.

Regional emissions include sources from anthropogenic, biogenic and wild-fire. The largest projected change in the future is the anthropogenic area source, with 30% to 100%

increase from the base-case. Biogenic VOC emissions were estimated to decrease by 37% in the future due to the predicted changes in vegetation distributions. Future landuse, estimated by the Community Land Model with future climate condition, showed significant decreases in isoprene emitting vegetations for regions in the southeast and north central states. Biomass fire emissions were also included in the regional simulations. Current decade fire emissions were generated using a historical fire events dataset. Future decade fire emissions were estimated using the Fire Scenario Builder stochastic model with future meteorological conditions. Emissions from wild-fire are estimated to be higher in the future with 25% increase in both VOC and CO emissions.

The MOZART2 global model predicted higher future pollution background concentrations across all layers for both ozone and ozone precursor gases. Along the cleaner western domain, average ozone concentration increased by 12 ppbv to 50 ppbv, while VOC concentration almost doubled to 2.1 ppbv. Along the east coast, ozone increased by 30%, to 59 ppbv, while VOC and NOx increased by approximately 50%.

Comparing the daily maximum 8-hr ozone concentrations between base-case simulations with long-term ozone measurements, the system performance varied. The system captured the episodic ozone conditions very well, but over-predicted average ozone concentrations and non-episodic conditions. The mean daily max 8-hr ozone concentration was 58 ppbv and model over-predicted by 5 ppbv. The model captured the episodic ozone conditions, represented by 98^{th} percentile concentration values. The average episodic ozone concentration across all sites was 90 ppbv, and the model predicted 93 ppbv. Spatially, the system captured the observed ozone conditions with correct representations of higher concentrations in the east, coastal California and northern Texas, as well as lower concentrations for the Pacific Northwest and the north central states.

The system also captured the ozone spatial concentration variability represented by the concentration range between 2nd and 98th percentile values, but failed to simulate the magnitude of ozone concentrations at lower ranges. Similar performances were observed in year-to-year comparisons, where the model captured the inter-annual variability across the domain, but over-predicted frequency distributions for concentrations below 70 ppbv.

Significant changes in regional air quality conditions were predicted for 2045-2054 with respect to the current case simulation. Regional ozone pollution worsened from the combination of warmer climate, higher regional emissions and higher global pollution background concentrations. The mean daily max 8-hr ozone concentrations increased by 8 ppbv across the continent, and the 98th percentile of the daily max 8-hr ozone concentration increased by approximately 5 ppbv. Large increases were also predicted for non-episodic ozone, where 20th percentile ozone concentration increased by up to 15 ppbv when compared with the base-case simulations. These suggest not only poorer air quality conditions in non-episodic pollution events, but also possible extreme ozone with each episode having 5 ppbv to 15 ppbv higher ozone concentrations than the current period.

Spatially, changes in ozone pollution in the future vary across the continent. Results show larger ozone concentration differences in the east, south and southwest, as well as smaller increases in the Pacific Northwest and inland northwest. The spatial ozone differences correspond well with simulated changes in regional surface temperature with predicted 1°C to 5°C increase in the future. Elevated ozone downwind of urban centers was predicted to impact larger surrounding areas due to simulated expansions in urban landuse and higher projected anthropogenic emissions in the future. The transport of polluted air further downwind of urban areas results in higher non-episodic ozone concentrations in surrounding rural regions. Spatial ozone impacts across the US continent are predicted to increase by 60% in the future in terms

of areas exceeding the EPA 80 ppbv NAAQS. This demonstrates larger urban air pollution footprints on surrounding environments due to predicted future impacts on regional air quality.

Further analyses for eight urban sites showed air pollution events to occur more frequently, with ozone episodes lasting longer throughout the year. There were more days when daily max 8-hr ozone concentration exceed the 80 ppbv standard in the future simulation. The increase in ozone episode frequency not only occurred during summer season, as in the base-case, but also in the spring and autumn months. The results also showed higher frequency of longer ozone pollution episodes in the future with more consecutive days daily max 8-hr ozone concentrations exceed the EPA 80 ppbv standard. The increase in frequency corresponded with simulated changes in surface temperature, thus suggested influence of future climate change on regional air pollution.

It is important to note that simulations based upon other scenarios for the global and other treatments of US emissions which assume stronger controls will produce a different range of results compared to those from this study. Further work is needed to examine the uncertainties in regional air quality due to the uncertainties in future projected global and local emissions.

References

Bonan, G. B., Oleson, K. W., Vertenstein, M., Levis, S., Zeng, X. B., Dai, Y. J., Dickinson, R. E., and Yang, Z. L., 2002. The Land Surface Climatology of the Community Land Model Coupled to the NCAR Community Climate Model. Journal of Climate 15(22), 3123-3149.

Byun, D. W. and Ching, J. K. S., 1999. Science Algorithms of the EPA Models-3 Community Multiscale Air Quality (CMAQ) Modeling System. U.S. Environmental Protection Agency, EPA/600/R-99/030.

Carter, W. P. L., 2000. Documentation of the SAPRC-99 Chemical Mechanism for VOC Reactivity Assessment. California Air Resources Board, Contract No. 92-329, and 95-308.

Chen, J., Vaughan, J., Avise, J., O'Neill, S., and Lamb, B., 2007. Development and Evaluation of a New Numerical Air Quality Forecast System for the Pacific Northwest, manuscript in preparation.

Civerolo, K. L., Sistla, G., Rao, S. T., and Nowak, D. J., 2000. The Effects of Land Use in Meteorological Modeling: Implications for Assessment of Future Air Quality Scenarios. Atmospheric Environment 34(10), 1615-1621.

Civerolo, Kevin, Hogrefe, Christian, Lynn, Barry, Rosenthal, Joyce, Ku, Jia-Yeong, Solecki, William, Cox, Jennifer, Small, Christopher, Rosenzweig, Cynthia, Goldberg, Richard, Knowlton, Kim, and Kinney, Patrick, 2007. Estimating the effects of increased urbanization on surface meteorology and ozone concentrations in the New York City metropolitan region. Atmospheric Environment 41(9), 1803-1818.

Climate Change Science Program, 2005. Our Changing Planet - The U.S. Climate Change Science Program FY2006 - A Supplement to the President's Budget. Climate Change Science Program Office Washington D.C.,

Constable, J. V. H., Guenther, A. B., Schimel, D. S., and Monson, R. K., 1999. Modelling Changes in Voc Emission in Response to Climate Change in the Continental United States. Global Change Biology 5(7), 791-806.

Eder, B. and Yu, S. C., 2006. A Performance Evaluation of the 2004 Release of Models-3 CMAQ. Atmospheric Environment 40(26), 4811-4824.

Fiore, A., Jacob, D. J., Liu, H., Yantosca, R. M., Fairlie, T. D., and Li, Q., 2003. Variability in Surface Ozone Background Over the United States: Implications for Air Quality Policy. Journal of Geophysical Research-Atmospheres 108(D24), doi:10.1029/2003JD003855.

Grell, A. G., Dudhia, J., and Stauffer, D. R., 1994. A description of the fifth-generation Penn State/NCAR Mesoscale Model (MM5). National Center for Atmospheric Research, NCAR Technical Note NCAR/TN-398+STR.

Guenther, A., Hewitt, C. N., Erickson, D., Fall, R., Geron, C., Graedel, T., Harley, P., Klinger, L., Lerdau, M., Mckay, W. A., Pierce, T., Scholes, B., Steinbrecher, R., Tallamraju, R., Taylor, J., and Zimmerman, P., 1995. A Global-Model of Natural Volatile Organic-Compound Emissions. Journal of Geophysical Research-Atmospheres 100(D5), 8873-8892.

Guenther, A., Karl, T., Harley, P., Wiedinmyer, C., Palmer, P. I., and Geron, C., 2006. Estimates of global terrestrial isoprene emissions using MEGAN (Model of Emissions of Gases and Aerosols from Nature). Atmospheric Chemistry and Physics Discussions 6107-173.

Hogrefe, C., Lynn, B., Civerolo, K., Ku, J. Y., Rosenthal, J., Rosenzweig, C., Goldberg, R., Gaffin, S., Knowlton, K., and Kinney, P. L., 2004. Simulating Changes in Regional Air Pollution Over the Eastern United States Due to Changes in Global and Regional Climate and Emissions. Journal of Geophysical Research-Atmospheres 109(D22), doi:10.1029/2004JD004690.

Horowitz, L. W., 2006. Past, Present, and Future Concentrations of Tropospheric Ozone and Aerosols: Methodology, Ozone Evaluation, and Sensitivity to Aerosol Wet Removal. Journal of Geophysical Research-Atmospheres 111 (D22),

Horowitz, L. W., Walters, S., Mauzerall, D. L., Emmons, L. K., Rasch, P. J., Granier, C., Tie, X. X., Lamarque, J. F., Schultz, M. G., Tyndall, G. S., Orlando, J. J., and Brasseur, G. P., 2003. A Global Simulation of Tropospheric Ozone and Related Tracers: Description and Evaluation of MOZART, Version 2. Journal of Geophysical Research-Atmospheres 108(D24), doi:10.1029/2002JD002853.

Houyoux, Marc, Vukovich, Jeff, and Brandmeyer, J. E., 2005. Sparse Matrix Operator Kernel Emissions Modeling System User Manual. [online] http://cf.unc.edu/cep/empd/products/smoke.

Jacob, D. J., Logan, J. A., and Murti, P. P., 1999. Effect of Rising Asian Emissions on Surface Ozone in the United States. Geophysical Research Letters 26(14), 2175-2178.

Knowlton, K., Rosenthal, J. E., Hogrefe, C., Lynn, B., Gaffin, S., Goldberg, R., Rosenzweig, C., Civerolo, K., Ku, J. Y., and Kinney, P. L., 2004. Assessing Ozone-Related Health Impacts Under a Changing Climate. Environmental Health Perspectives 112(15), 1557-1563.

Lamarque, J. F., Langford, A. O., and Proffitt, M. H., 1996. Cross-Tropopause Mixing of Ozone Through Gravity Wave Breaking: Observation and Modeling. Journal of Geophysical Research-Atmospheres 101(D17), 22969-22976.

Lamb, B., Chen, J., O'Neill, S., Avise, J., Vaughan, J., Larkin, S., and Solomon, S., 2007. Real-Time Numerical Foresting of Wildfire Emissions and Perturbations to Regional Air Quality. EOS, Transactions, American Geophysical Union, Submitted.

Larkin, N. K., O'Neill, S. M., Solomon, R., Krull, C., Raffuse, S., Rorig, M., Peterson, J., and Ferguson, S. A., 2007. The BlueSky Smoke Modeling Framework. Atmospheric Environment, In Press.

Leung, L. R. and Gustafson, W. I., 2005. Potential Regional Climate Change and Implications to Us Air Quality. Geophysical Research Letters 32(16), doi:10.1029/2005GL022911.

Malm, W. C., Schichtel, B. A., Pitchford, M. L., Ashbaugh, L. L., and Eldred, R. A., 2004. Spatial and Monthly Trends in Speciated Fine Particle Concentration in the United States. Journal of Geophysical Research-Atmospheres 109(D3), doi:10.1029/2003JD003739.

Mass, C. F., Albright, M., Ovens, D., Steed, R., Maciver, M. , Grimit, E., Eckel, T., Lamb, B., Vaughan, J., Westrick, K., Storck, P., Colman, B., Hill, C., Maykut, N., Gilroy, M., Ferguson, S. A., Yetter, J., Sierchio, J. M., Bowman, C., Stender, R., Wilson, R., and Brown, W., 2003. Regional Environmental Prediction Over the Pacific Northwest. Bulletin of the American Meteorological Society 84(10), 1353-1366.

Mckeen, S., Wilczak, J., Grell, G., Djalalova, I., Peckham, S., Hsie, E. Y., Gong, W., Bouchet, V., Menard, S., Moffet, R., Mchenry, J., Mcqueen, J., Tang, Y., Carmichael, G. R., Pagowski, M., Chan, A., Dye, T., Frost, G., Lee, P., and Mathur, R., 2005. Assessment of an Ensemble of Seven Real-Time Ozone Forecasts Over Eastern North America During the Summer of 2004. Journal of Geophysical Research-Atmospheres 110(D21), doi:10.1029/2005JD005858.

Mckenzie, D., O'neill, S. M., Larkin, N. K., and Norheim, R. A., 2006. Integrating Models to Predict Regional Haze From Wildland Fire. Ecological Modelling 199(3), 278-288.

Mickley, L. J., Jacob, D. J., Field, B. D., and Rind, D., 2004. Effects of Future Climate Change on Regional Air Pollution Episodes in the United States. Geophysical Research Letters 31(24), doi:10.1029/2004GL021216.

Miranda, A. I., 2004. An Integrated Numerical System to Estimate Air Quality Effects of Forest Fires. International Journal of Wildland Fire 13(2), 217-226.

Murazaki, K. and Hess, P., 2006. How does climate change contribute to surface ozone change over the United States? Journal of Geophysical Research-Atmospheres 111(D05301), doi:10.1029/2005JD005873.

Nakićenović, N., J. Alcamo, G. Davis, B. de Vries, B. _Fenhann, S. Gaffin, Gregory K., A. Grübler, T. Y. Jung, T. Kram, E. L. La Rovere, E. L. Michaelis, S. Mori, T. Morita, W. Pepper, H. Pitcher, L. Price, K. Raihi, A. Roehrl, H.-H. Rogner, A. Sankovski, M. Schlesinger, P. Shukla, S. Smith, R. Swart, S. van Rooijen, N. Victor, and Z. Dadi, IPCC Special Report on Emissions Scenarios, Cambridge University Press, Cambridge, United Kingdom and New York, NY, USA, 2000.

Olivier, J. G. J., Berdowski, J. J. M., Peters, J. A. H. W., Bakker, J., Visschedijk, A. J. H., and Bloos, J. P. J., 2000. Applications of EDGAR. Including a Description of EDGAR V3.0: Reference Database with Trend Data for 1970-1995. RIVM, Bilthoven, The Netherlands, NRP report no. 410200 051 / RIVM report no. 773301 001.

Prather, M., Gauss, M., Berntsen, T., Isaksen, I., Sundet, J., Bey, I., Brasseur, G., Dentener, F., Derwent, R., Stevenson, D., Grenfell, L., Hauglustaine, D., Horowitz, L., Jacob, D., Mickley, L., Lawrence, M., Von Kuhlmann, R., Muller, J. F., Pitari, G., Rogers, H., Johnson, M., Pyle, J., Law, K., Van Weele, M., and Wild, O., 2003. Fresh Air in the 21st Century? Geophysical Research Letters 30(2),

Russell, A. and Dennis, R., 2000. Narsto Critical Review of Photochemical Models and Modeling. Atmospheric Environment 34(12-14), 2283-2324.

Saraf, N., Beig, G., and Schultz, M., 2003. Tropospheric Distribution of Ozone and Its Precursors Over the Tropical Indian Ocean. Journal of Geophysical Research-Atmospheres 108(D20),

Theobald, D. M., 2005. Landscape Patterns of Exurban Growth in the Usa From 1980 to 2020. Ecology and Society 10(1), [online] http://www.ecologyandsociety.org/vol10/iss1/art32/.

Tong, D. Q. and Mauzerall, D. L., 2006. Spatial Variability of Summertime Tropospheric Ozone over the Continental United States: Implications of an Evaluation of the CMAQ Model. Atmospheric Environment 40(17), 3041-3056.

U.S. EPA, 2003. Guidelines for Developing Air Quality (Ozone and $PM_{2.5}$) Forecasting Program. U.S. Environmental Protection Agency, EPA-456/R-03-002.

U.S. EPA, 2004. Economic Growth Analysis System (EGAS) version 5.0 User Manual. U.S. Environmental Protection Agency, [online] http://www.epa.gov/ttn/ecas/egas5.htm.

Vaughan, J., Lamb, B., Frei, C., Wilson, R., Bowman, C., Figueroa-Kaminsky, C., Otterson, S., Boyer, M., Mass, C., Albright, M., Koenig, J., Collingwood, A., Gilroy, M., and Maykut, N., 2004. A Numerical Daily Air Quality Forecast System for the Pacific Northwest. Bulletin of the American Meteorological Society 85(4), 549-561.

Washington, W. M. and Parkinson, C. L., An Introduction to Three-Dimensional Climate Modeling, University Science Books, USA, 2005.

Washington, W. M., Weatherly, J. W., Meehl, G. A., Semtner, A. J., Bettge, T. W., Craig, A. P., Strand, W. G., Arblaster, J., Wayland, V. B., James, R., and Zhang, Y., 2000. Parallel Climate Model (PCM) Control and Transient Simulations. Climate Dynamics 16(10-11), 755-774.

Yu, S. C., Mathur, R., Kang, D. W., Schere, K., Eder, B., and Pleirn, J., 2006. Performance and Diagnostic Evaluation of Ozone Predictions by the Eta-Community Multiscale Air Quality Forecast System During the 2002 New England Air Quality Study. Journal of the Air & Waste Management Association 56(10), 1459-1471.

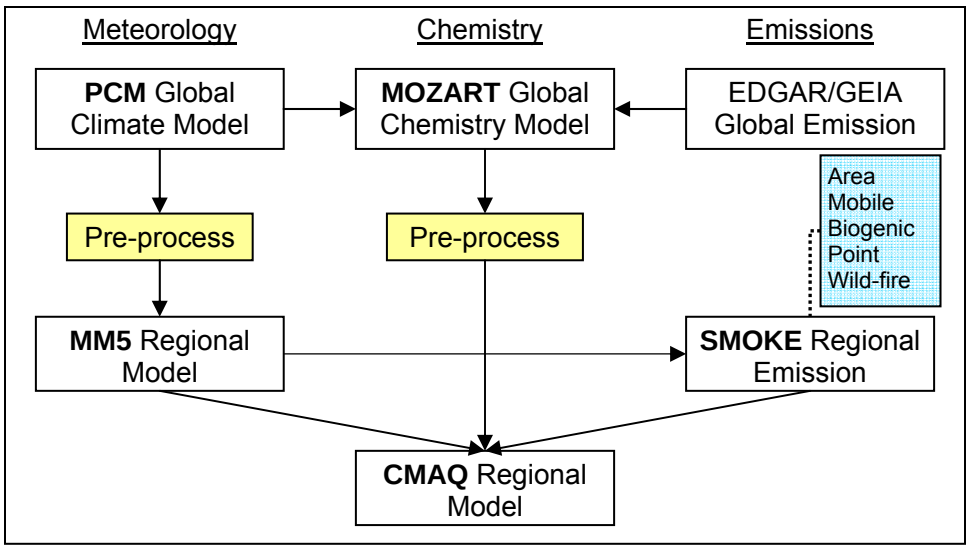

Figure 1: Schematic of the multi-scale modeling framework coupling the large scale global climate and chemistry models with the regional scale meteorology and chemical transport models. Bolded text represents individual model system.

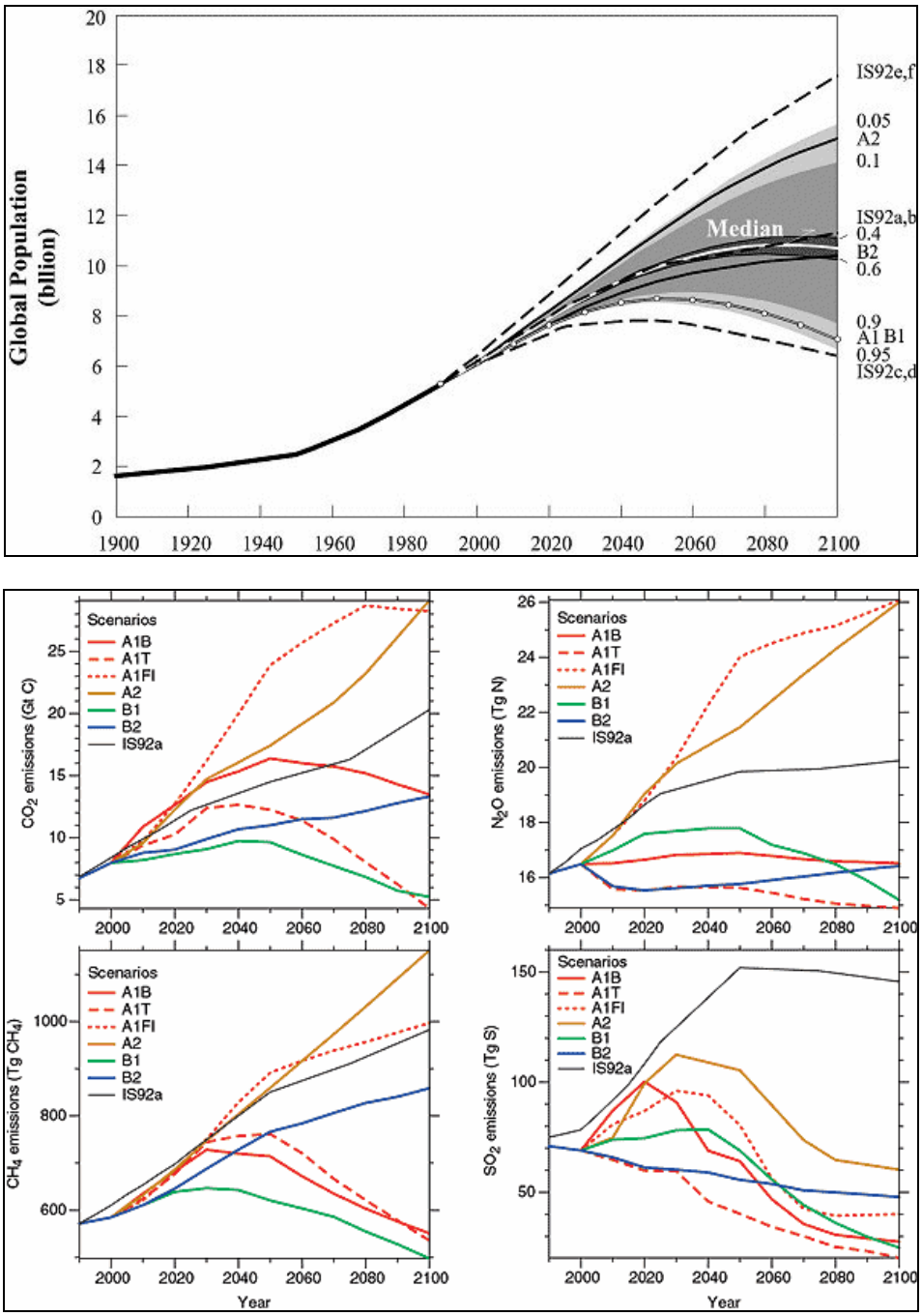

Figure 2: Projected global population growth and estimated future anthropogenic greenhouse gas emissions for CO_2, N_2O, CH_4 and SO_2 by IPCC SRES scenario family. (Figures adapted from 2001 IPCC Assessment – Nakićenović et al., 2000).

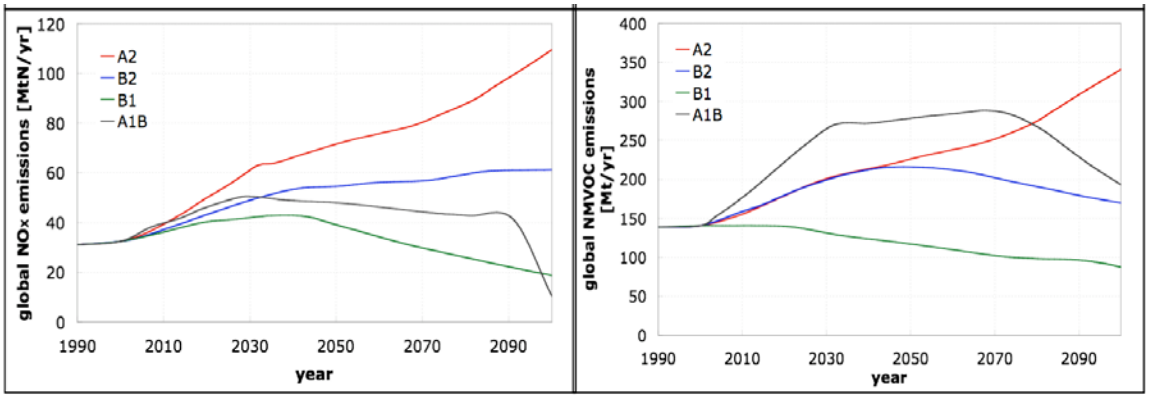

Figure 3: Projected global NOx (left) and non-methane volatile organic compound (right) emissions by IPCC SRES scenario family (Adapted from Prather et al., 2001).

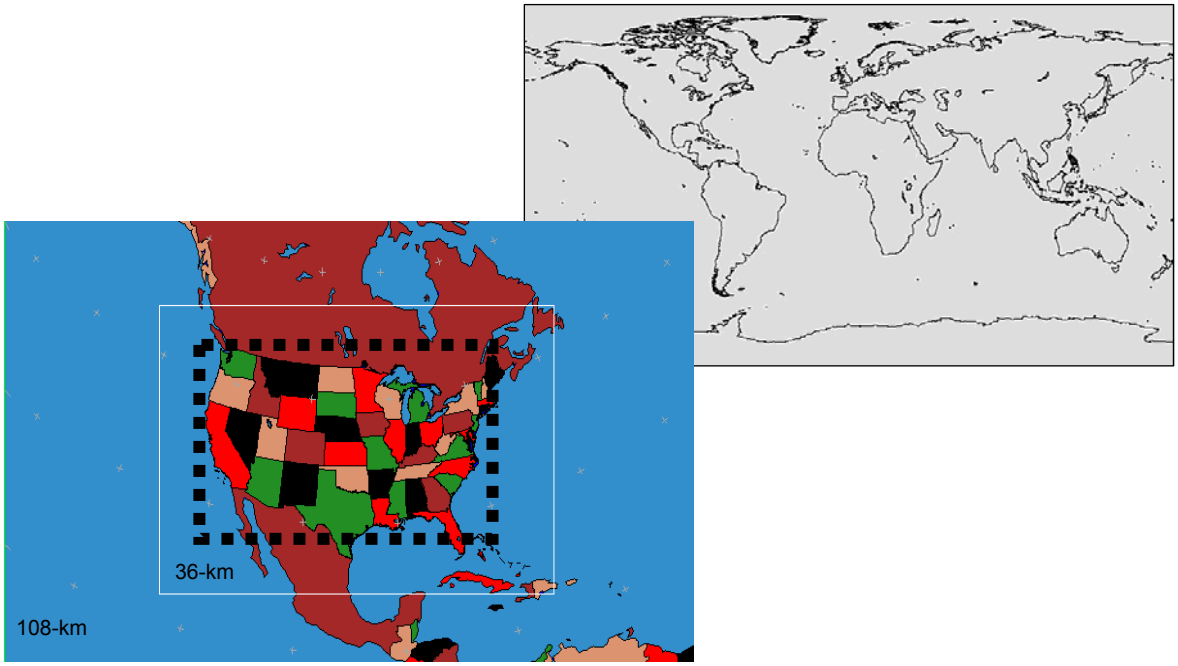

Figure 4: Simulation domain coverage for global models (top) and regional models (bottom). The regional MM5 simulation domains depicted are for 108-km parent domain, and 36-km inner nested domain (white line). The regional CMAQ simulation domain is inside the 36-km MM5 simulation domain (black dotted line).

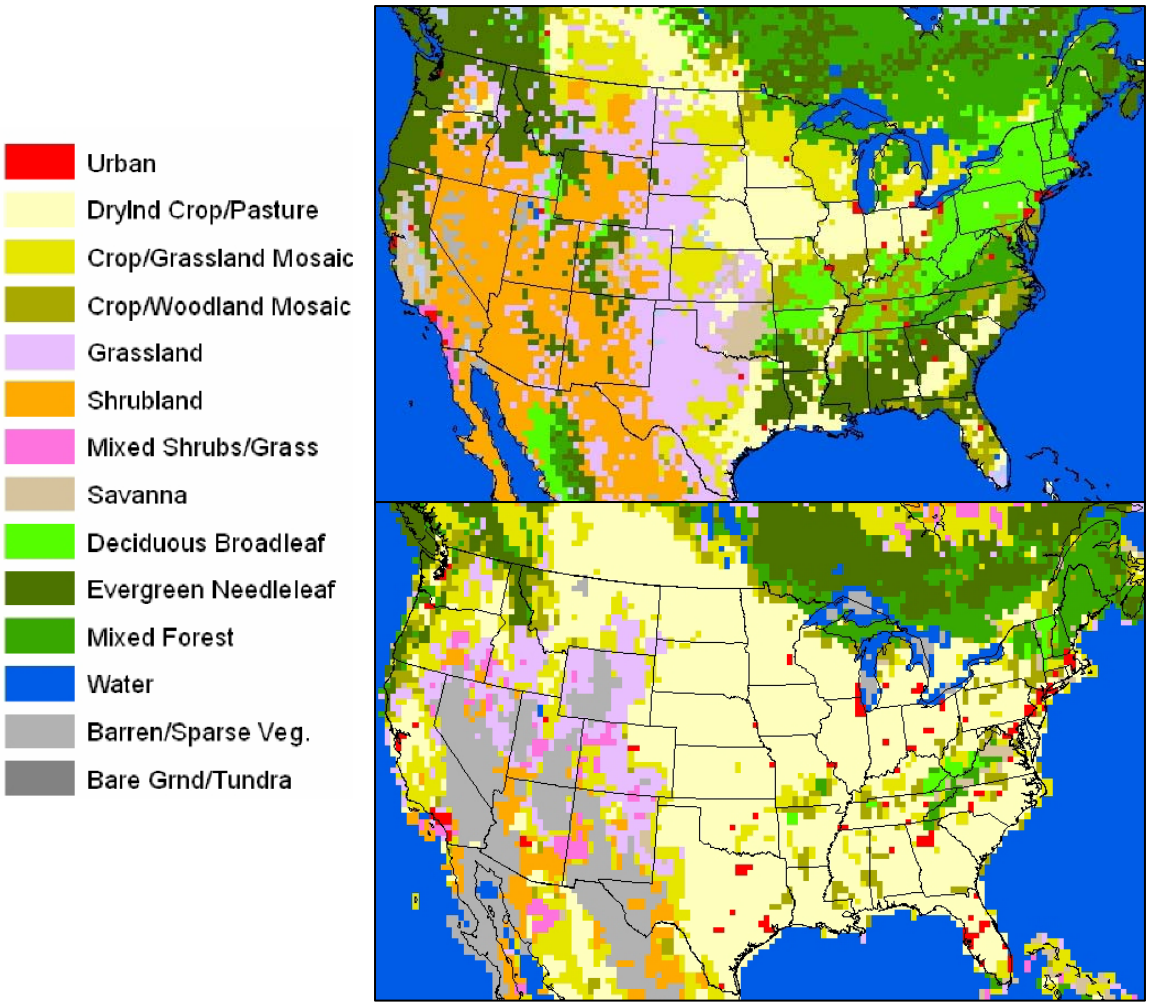

Figure 5: MM5 landuse by USGS categories for the current base-case (top) and the future case (bottom) simulations.

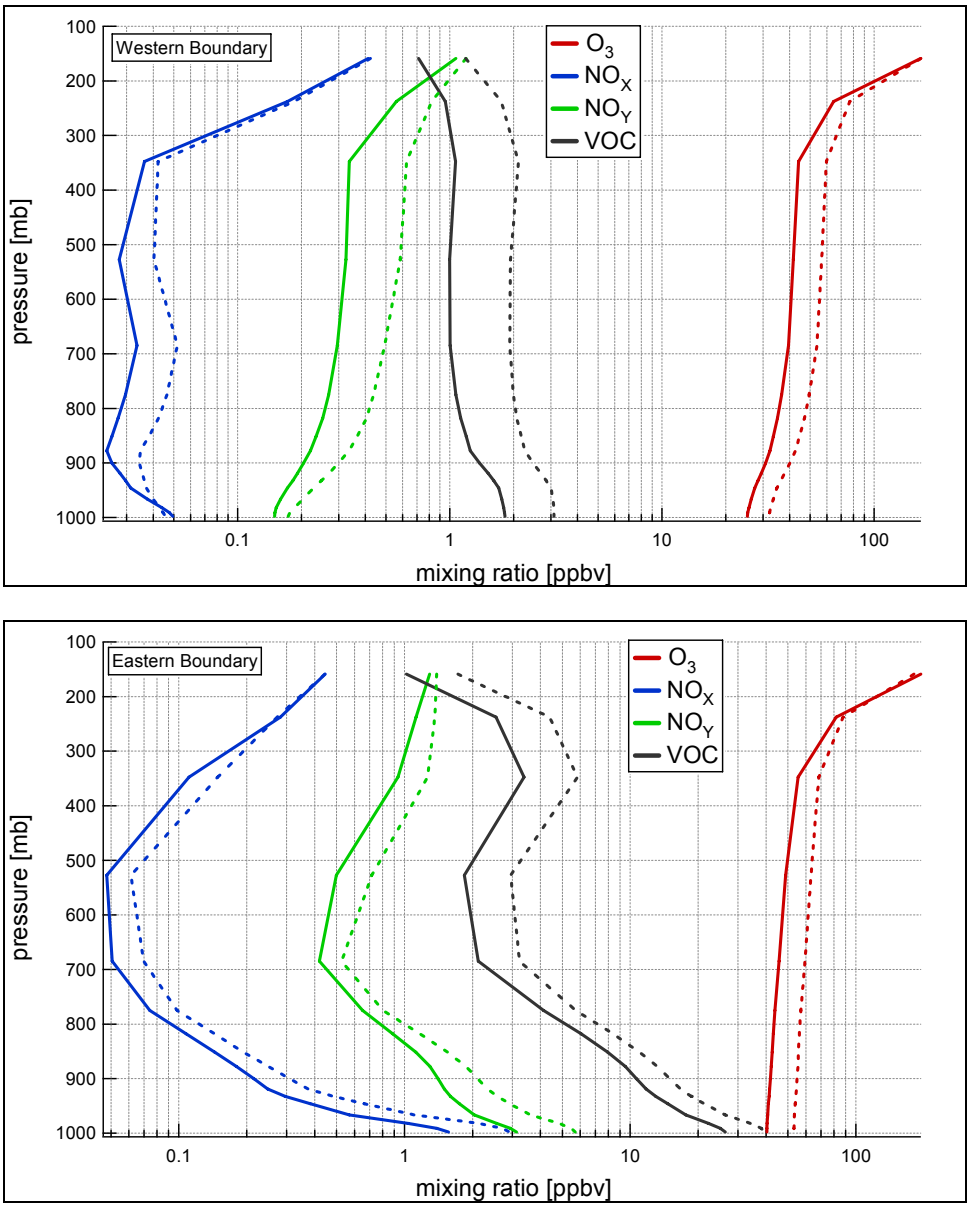

Figure 6: Summary of current decade (solid line) and future decade (dotted line) boundary condition profiles along the western (top) and eastern (bottom) regional model domain. Concentrations were averaged for July months from the MOZART global chemistry model simulation output.

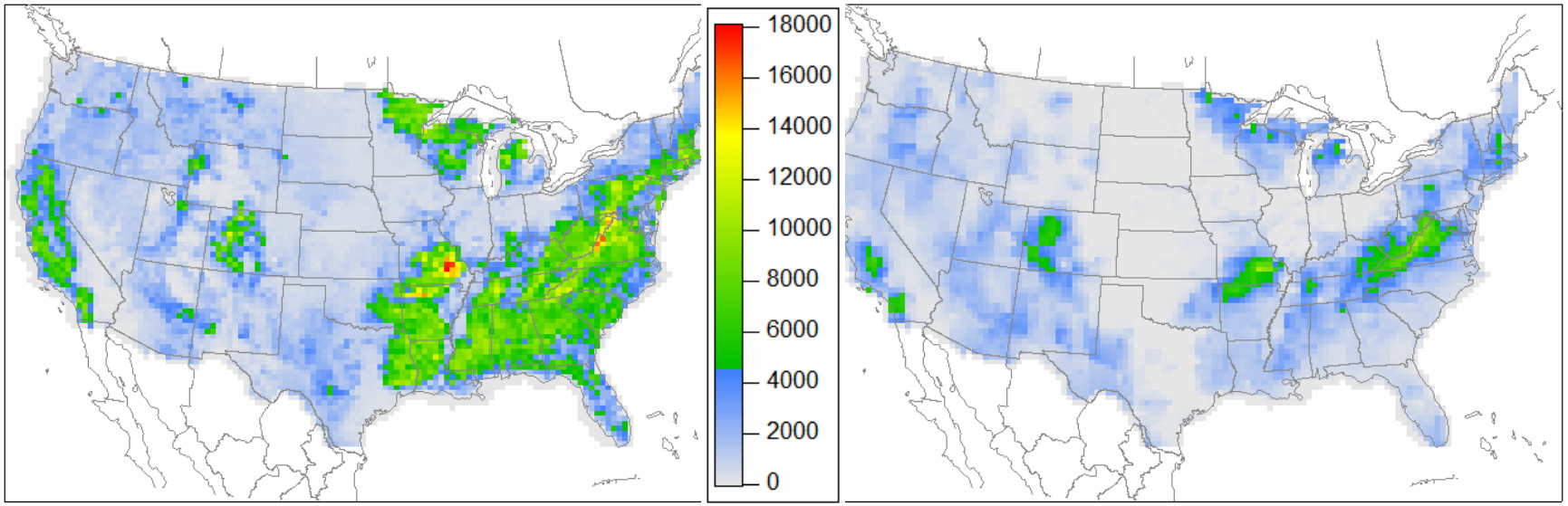

Figure 7: Modeled isoprene emission capacity (µg-Isoprene m-2 hr-1) for July, normalized at 30°C for current base-case (left) and predicted future (right) landcover conditions.

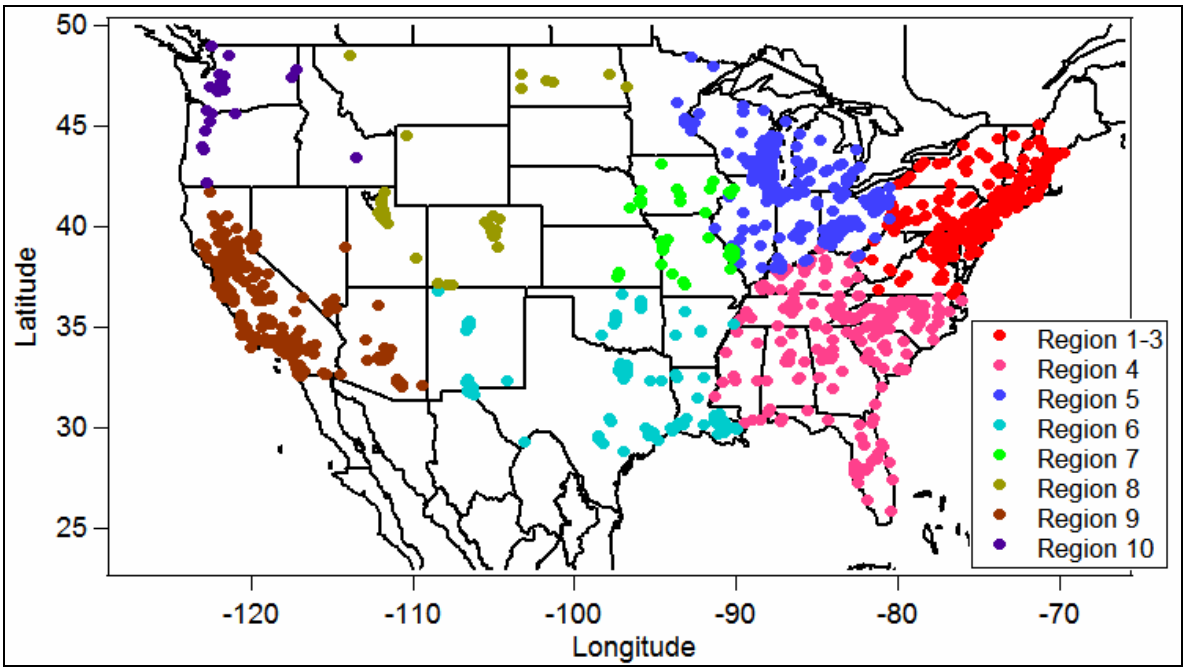

Figure 8: Locations of the EPA AQS ozone monitoring sites with at least 4 summers of measurement data between years 1994 and 2003. Sites are color coded by EPA regions.

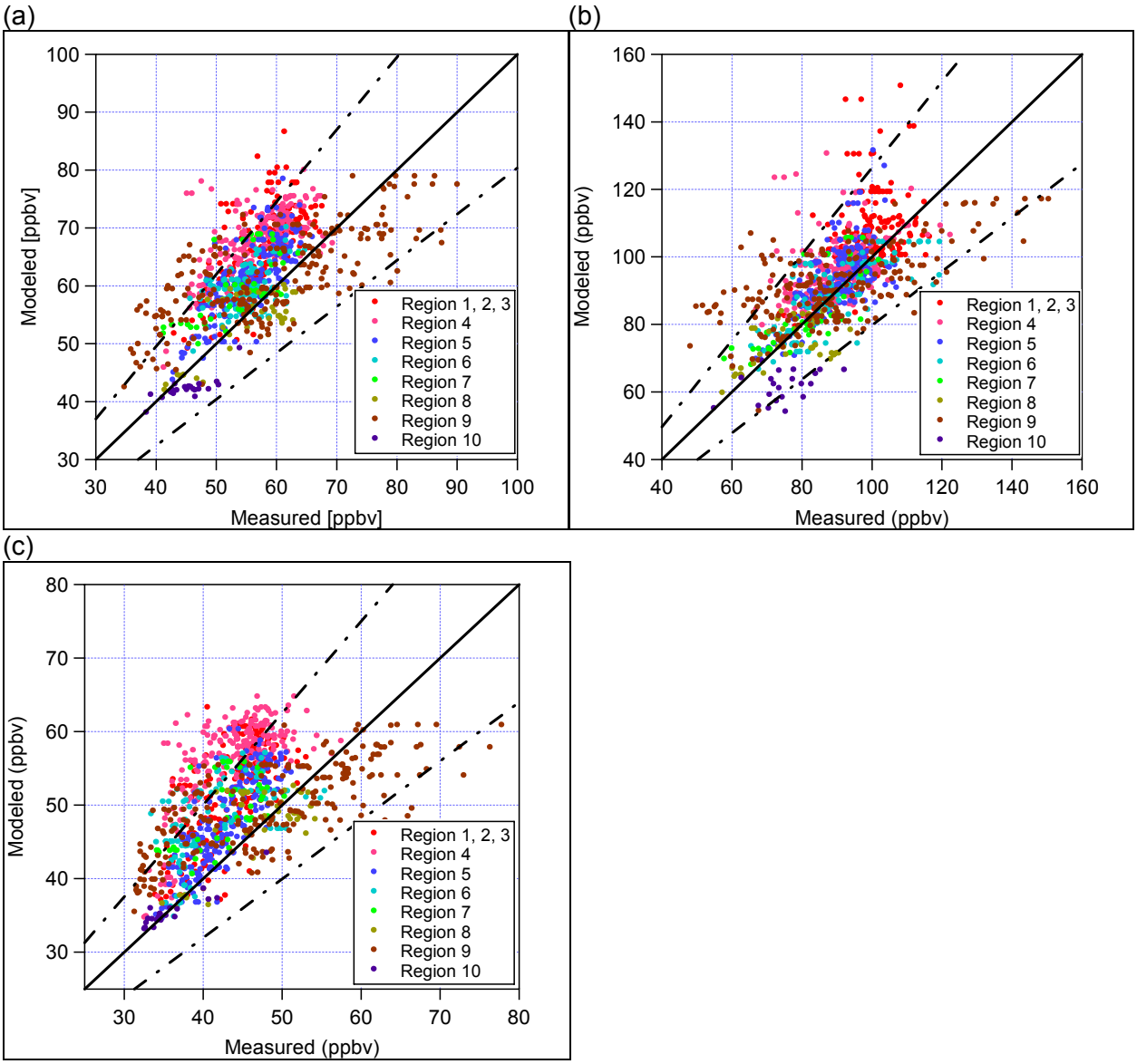

Figure 9: Scatter plot of modeled vs. measured daily maximum 8-hr ozone concentrations by site for (a) overall period average concentrations, (b) episodic (98th percentile) concentrations, and (c) non-episodic (20th percentile) concentrations across the 10 modeled and measured summer periods. The solid reference line indicates 1:1 agreement and dotted reference line indicates 1:1.25 (75%) of measured concentrations.

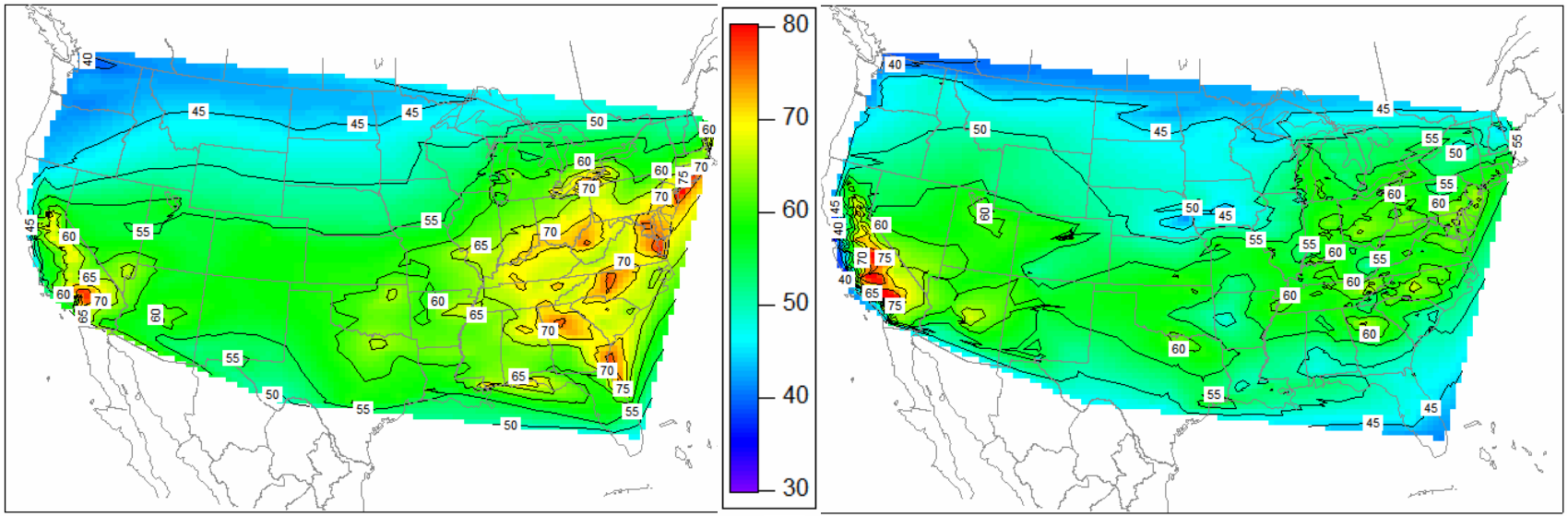

Figure 10: Modeled (left) and measured (right) daily maximum 8-hr ozone concentrations (ppbv) averaged over the 10 modeled and measured summer periods. Contour plots are constructed with ozone concentrations spatially interpolated at observational sites in the domain.

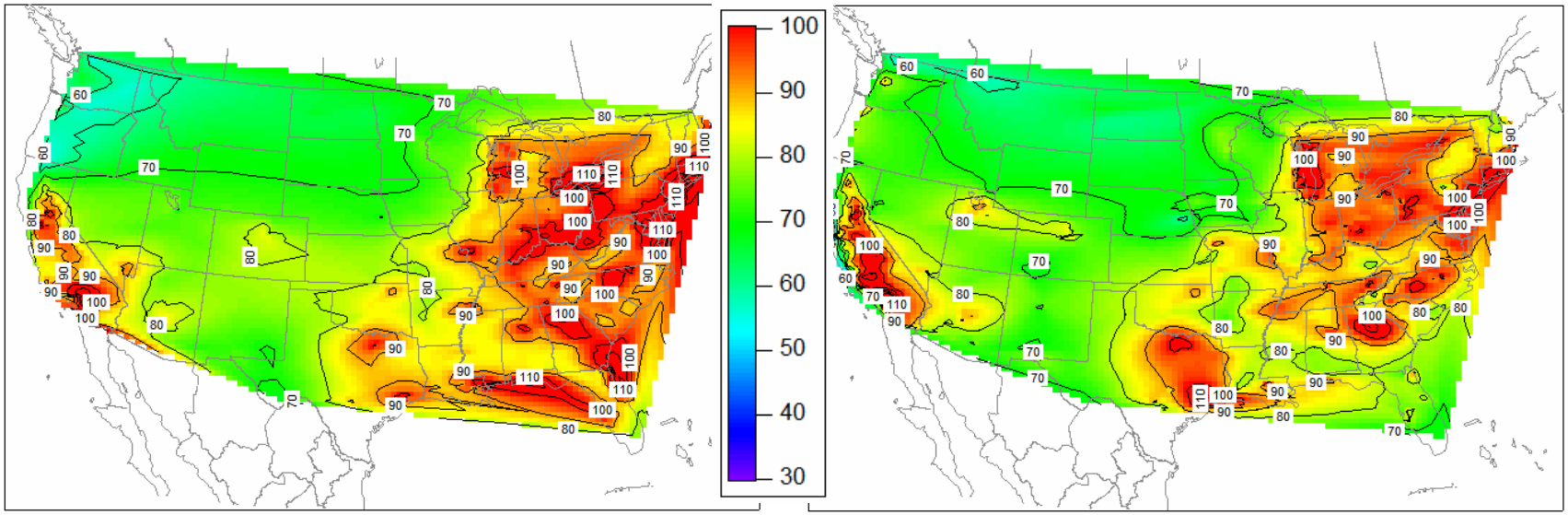

Figure 11: Modeled (left) and measured (right) episodic (98th percentile) daily maximum 8-hr ozone concentrations (ppbv) over the 10 modeled and measured summer periods. Contour plots are constructed with ozone concentrations spatially interpolated at observational sites in the domain.

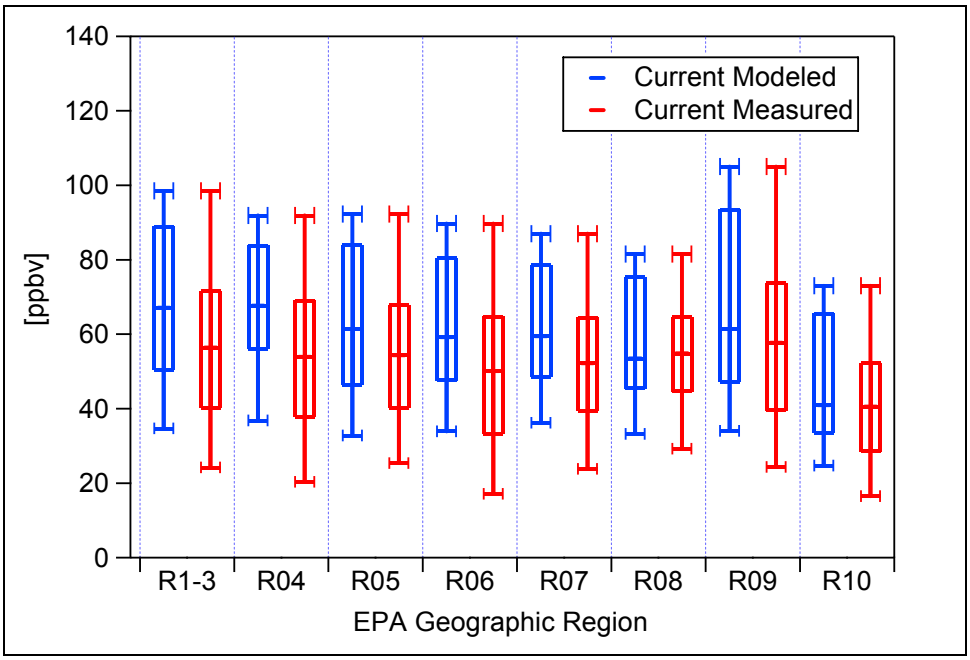

Figure 12: Current base-case modeled (left) and measured (right) daily maximum 8-hr ozone concentration ranges by EPA regions. The top and bottom bars represent 98th and 2nd percentile values, the top and bottom box indicates 80th and 20th percentile values, and the center bar represents overall average concentrations across the region.

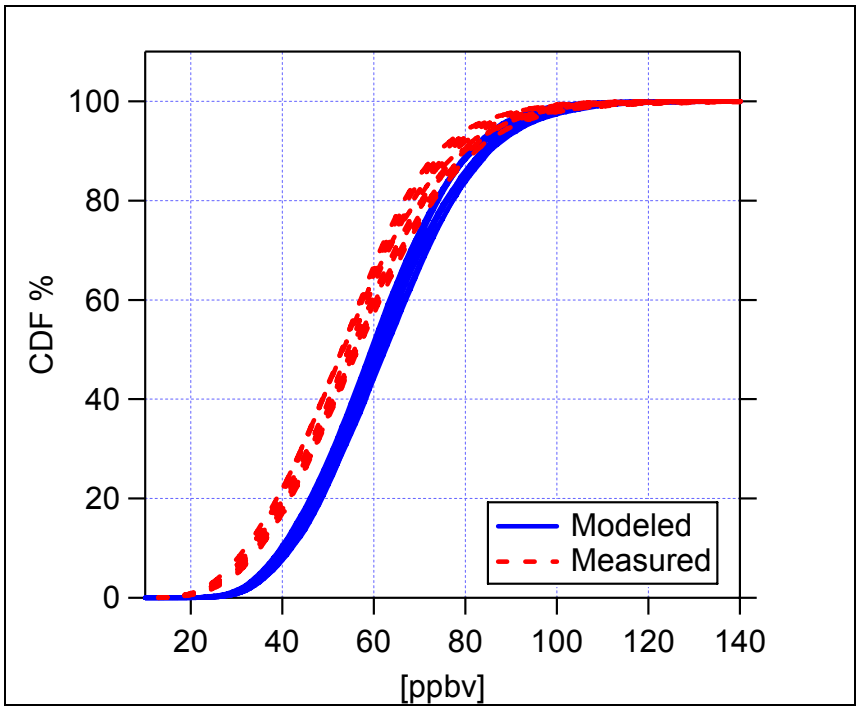

Figure 13: Cumulative distribution functions (CDF) of modeled and measured daily maximum 8-hr ozone concentrations for each summer across all measurement sites in the domain.

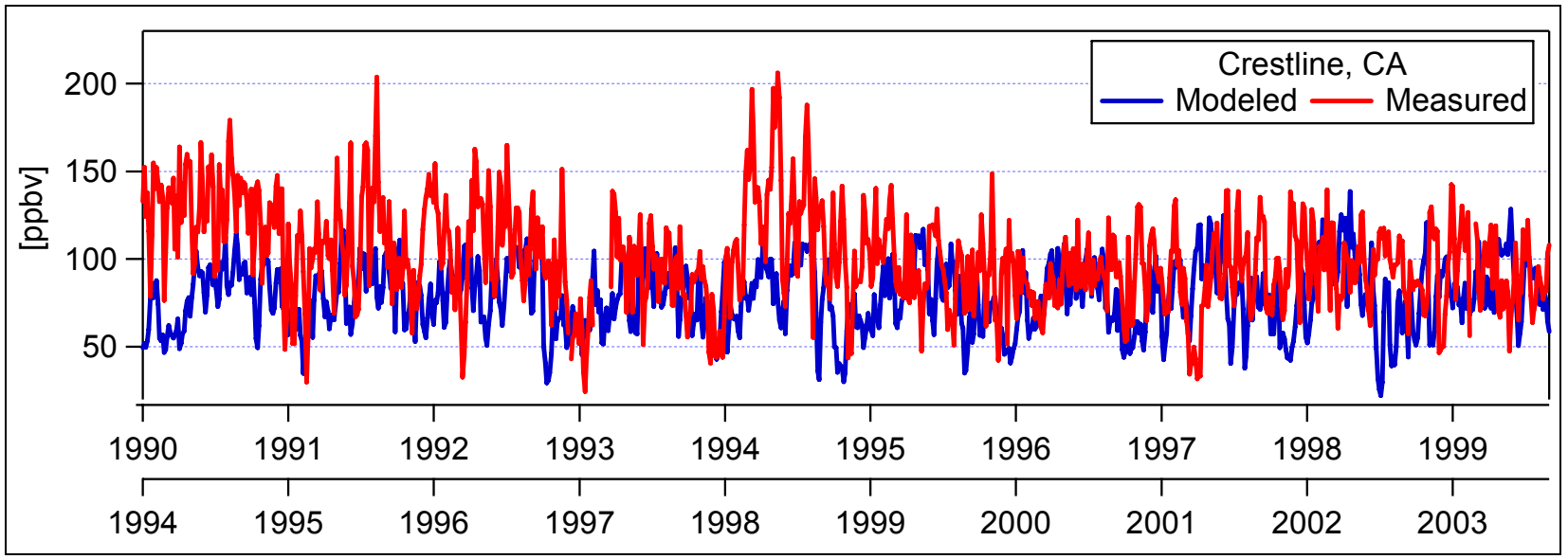

Figure 14: Time series of summer months modeled (1990-1999) and measured (1994-2003) daily maximum 8-hr ozone concentrations for Crestline, CA monitoring site.

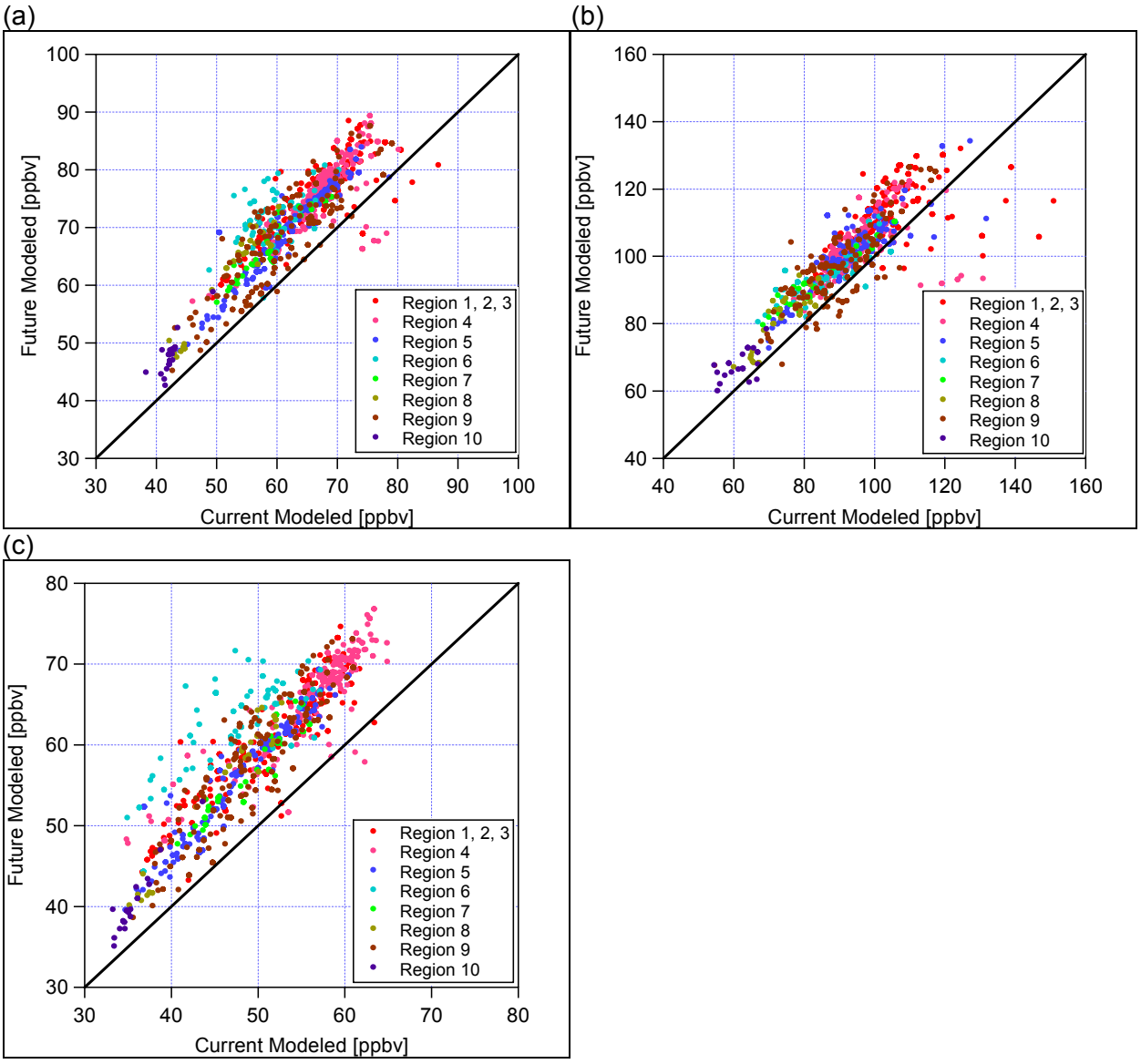

Figure 15: Scatter plot of future case vs. current base-case simulation results of daily maximum 8-hr ozone concentrations by site for (a) overall period average concentrations, (b) episodic (98^{th} percentile) concentrations, and (c) non-episodic (20^{th} percentile) concentrations across the 10 modeled and measured summer periods. The solid reference line indicates 1:1 concentration between future modeled and current modeled cases.

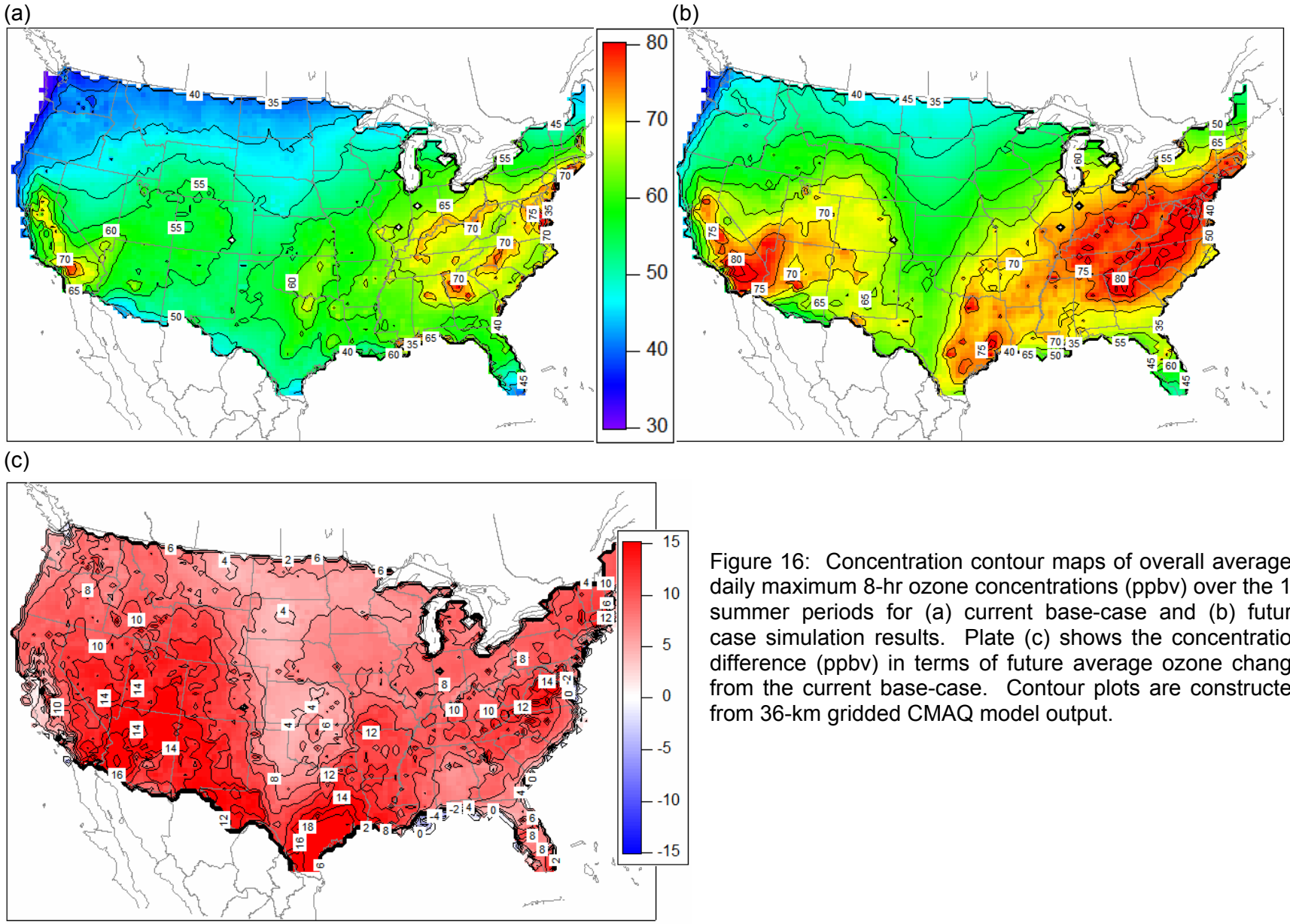

Figure 16: Concentration contour maps of overall averaged daily maximum 8-hr ozone concentrations (ppbv) over the 10 summer periods for (a) current base-case and (b) future case simulation results. Plate (c) shows the concentration difference (ppbv) in terms of future average ozone change from the current base-case. Contour plots are constructed from 36-km gridded CMAQ model output.

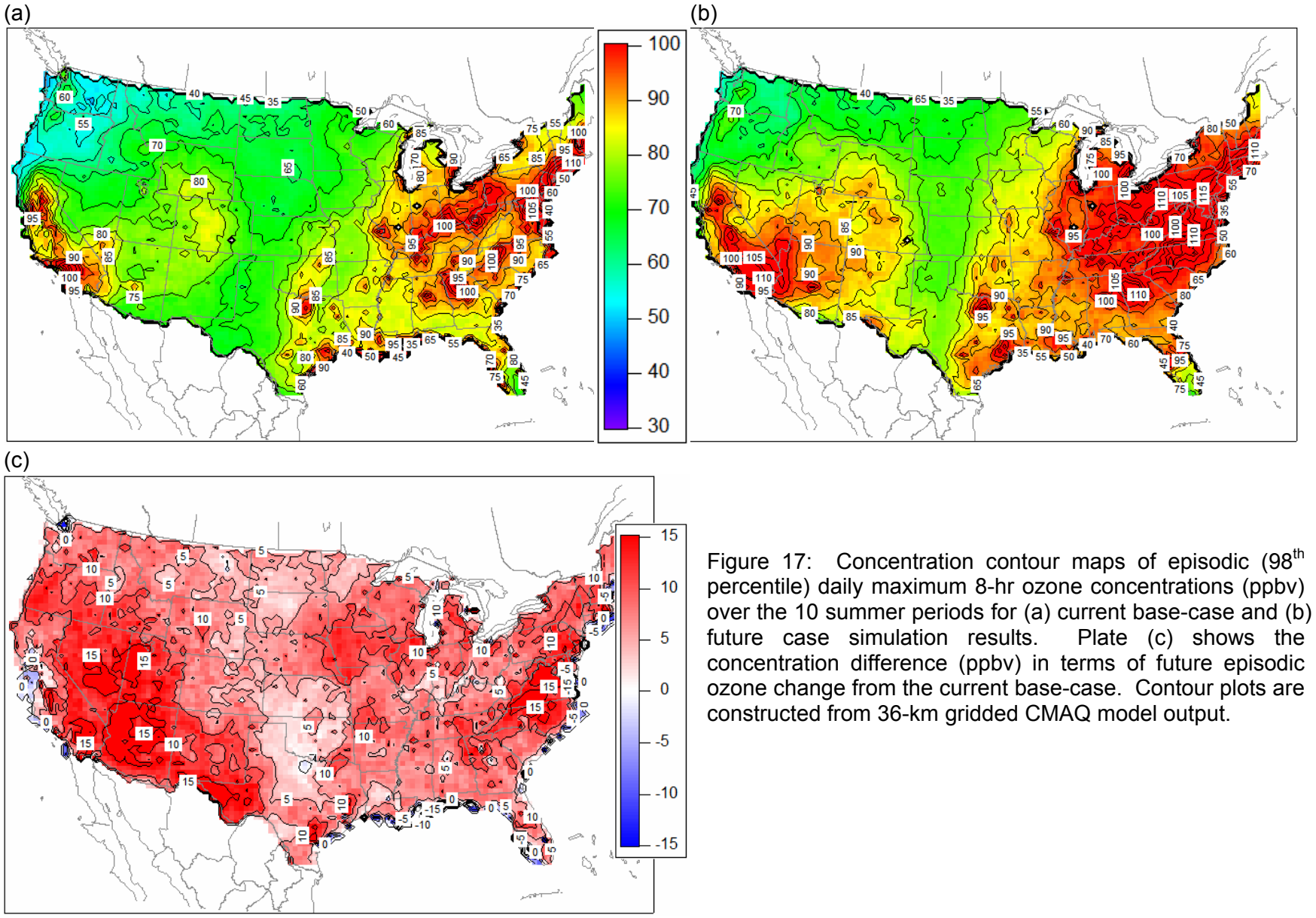

Figure 17: Concentration contour maps of episodic (98th percentile) daily maximum 8-hr ozone concentrations (ppbv) over the 10 summer periods for (a) current base-case and (b) future case simulation results. Plate (c) shows the concentration difference (ppbv) in terms of future episodic ozone change from the current base-case. Contour plots are constructed from 36-km gridded CMAQ model output.

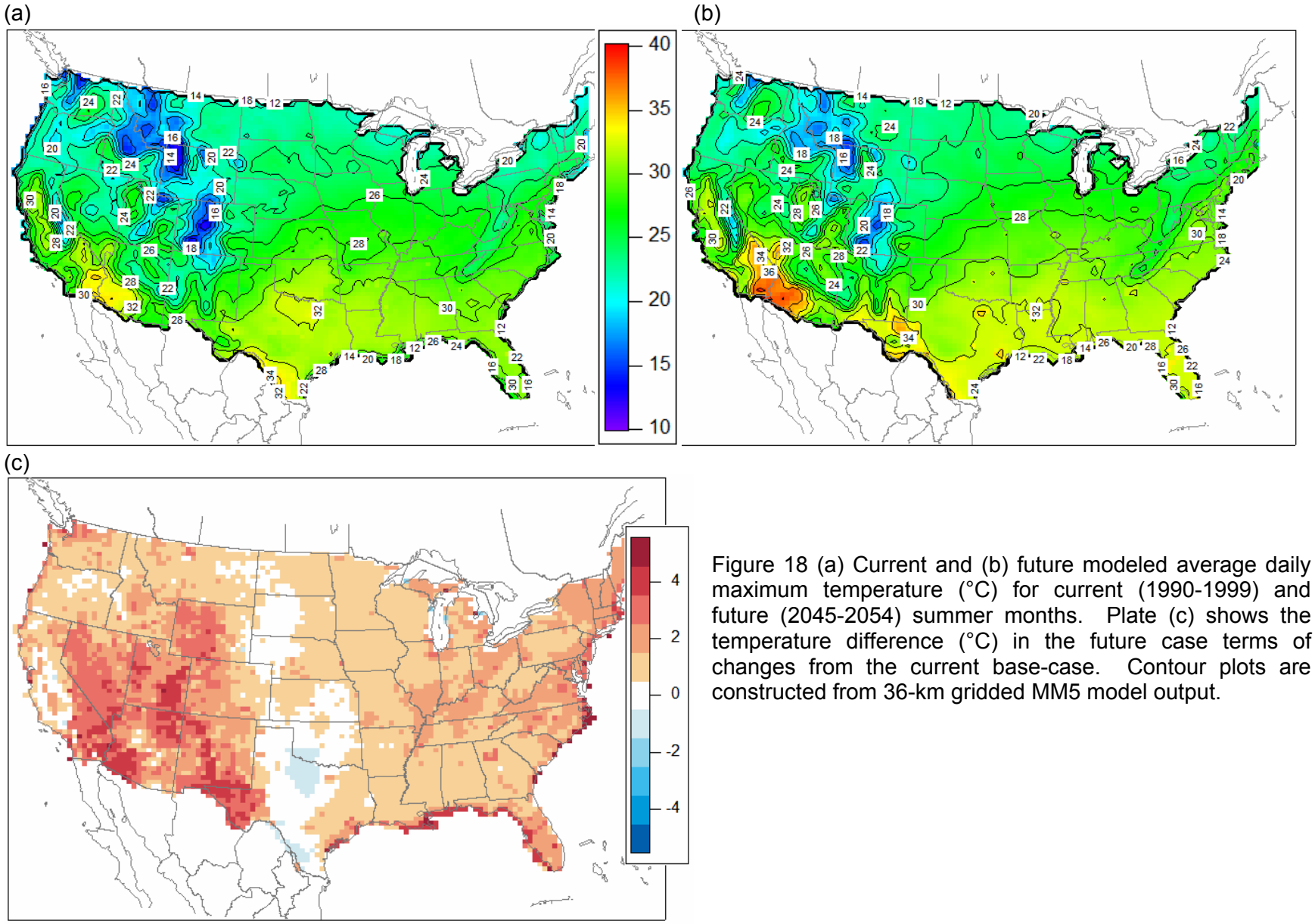

Figure 18 (a) Current and (b) future modeled average daily maximum temperature (°C) for current (1990-1999) and future (2045-2054) summer months. Plate (c) shows the temperature difference (°C) in the future case terms of changes from the current base-case. Contour plots are constructed from 36-km gridded MM5 model output.

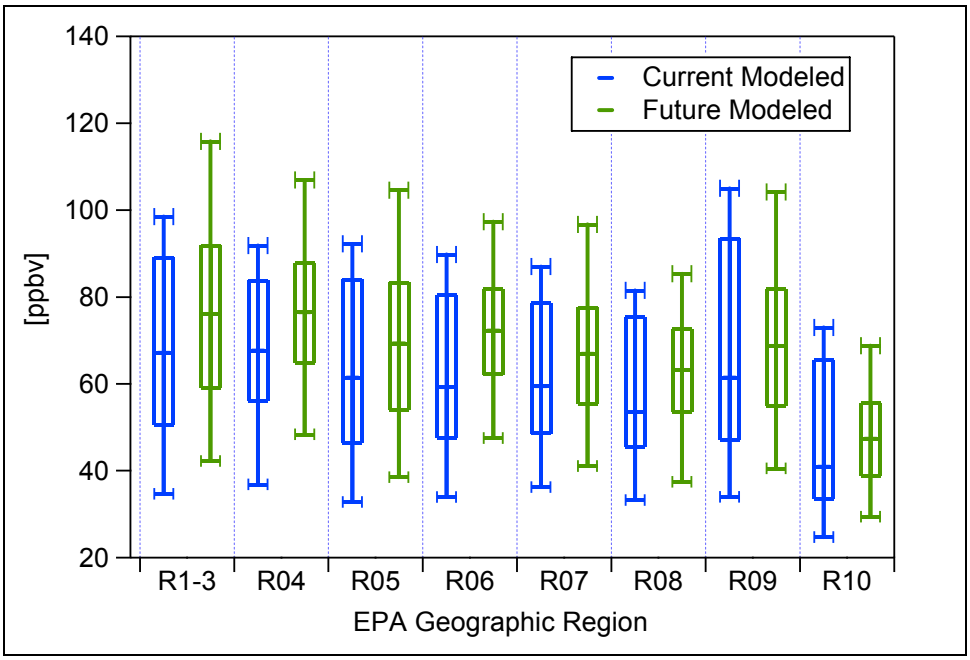

Figure 19: Modeled current base-case (left) and future case (right) daily maximum 8-hr ozone concentration ranges by EPA regions. The top and bottom bars represent 98th and 2nd percentile values, the top and bottom box indicates 80th and 20th percentile values, and the center bar represents overall average concentrations across the region.

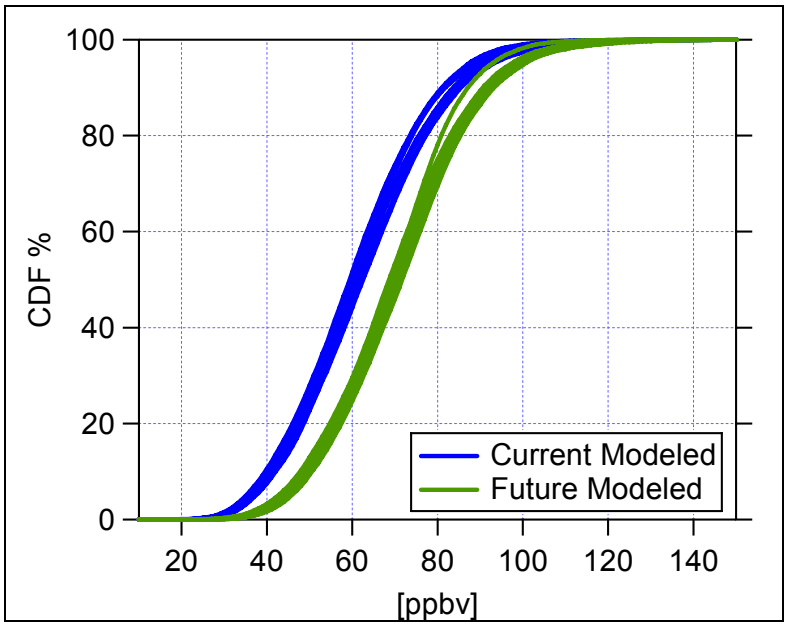

Figure 20: Cumulative distribution functions (CDF) of current base-case and future case modeled results for daily maximum 8-hr ozone concentrations of each summer (current case: 1990-1999 and future case: 2045-2054).

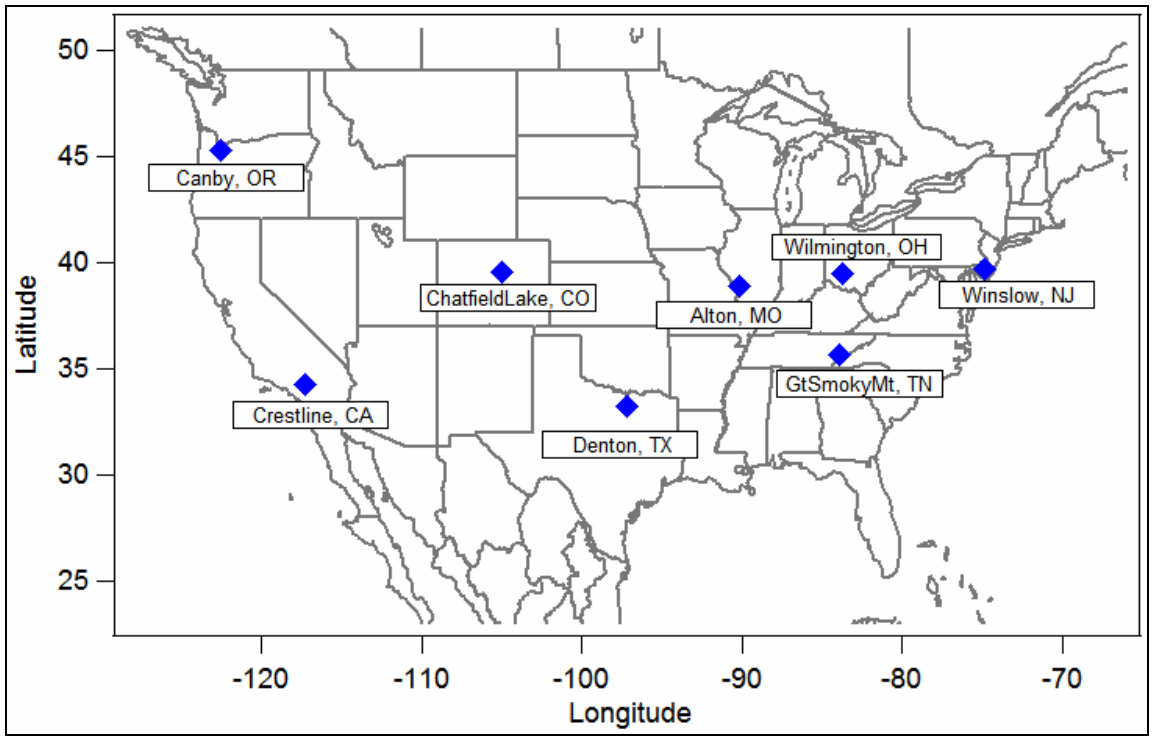

Figure 21: Locations of selected sites with high observed ozone concentrations from EPA geographic regions.

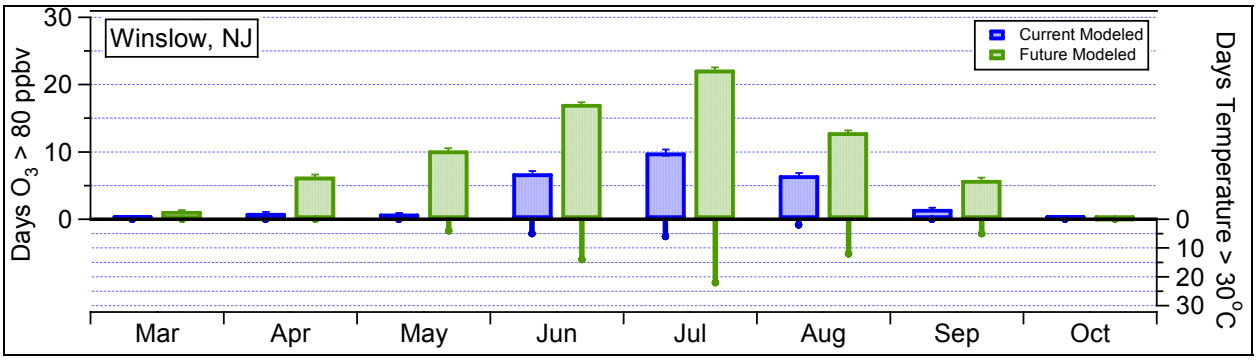
Winslow, NJ
Current Modeled
Future Modeled
Days O_3 > 80 ppbv
Days Temperature > 30°C
0
10
20
30
Mar
Apr
May
Jun
Jul
Aug
Sep
Oct

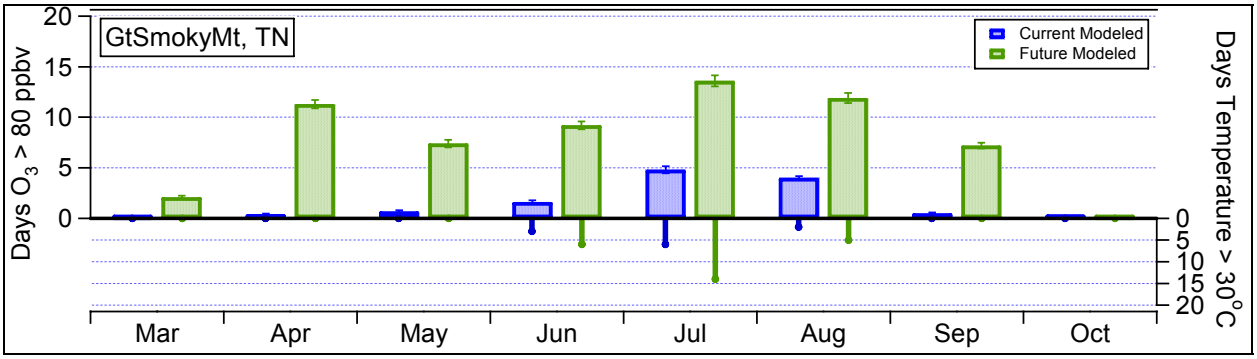
GtSmokyMt, TN
Current Modeled
Future Modeled
Days O_3 > 80 ppbv
Days Temperature > 30°C
0
5
10
15
20
Mar
Apr
May
Jun
Jul
Aug
Sep
Oct

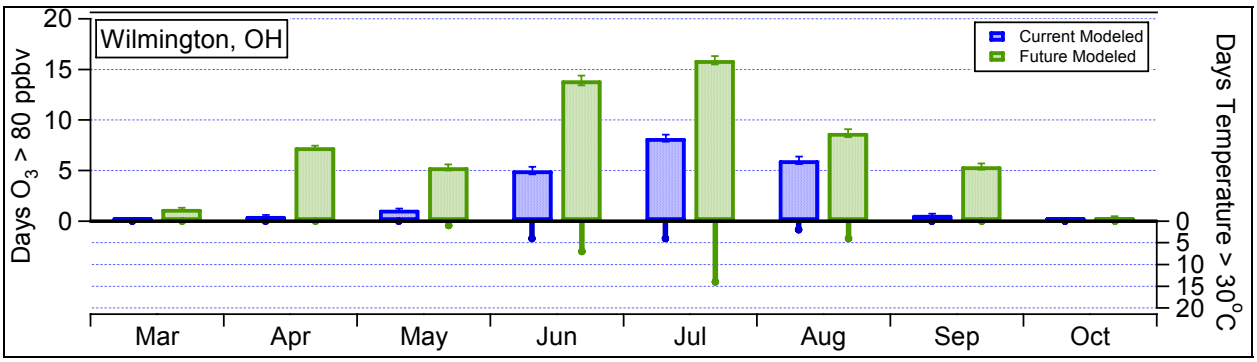
Wilmington, OH
Current Modeled
Future Modeled
Days O_3 > 80 ppbv
Days Temperature > 30°C
0
5
10
15
20
Mar
Apr
May
Jun
Jul
Aug
Sep
Oct

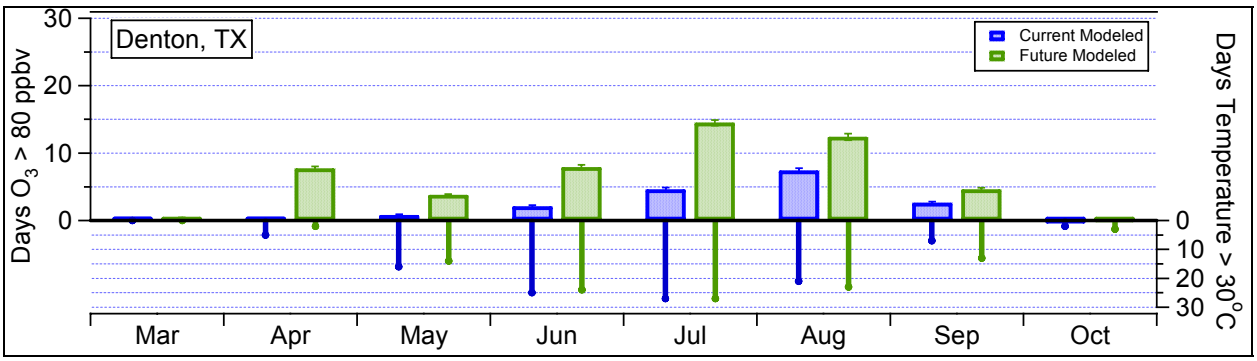
Denton, TX
Current Modeled
Future Modeled
Days O_3 > 80 ppbv
Days Temperature > 30°C
0
10
20
30
Mar
Apr
May
Jun
Jul
Aug
Sep
Oct

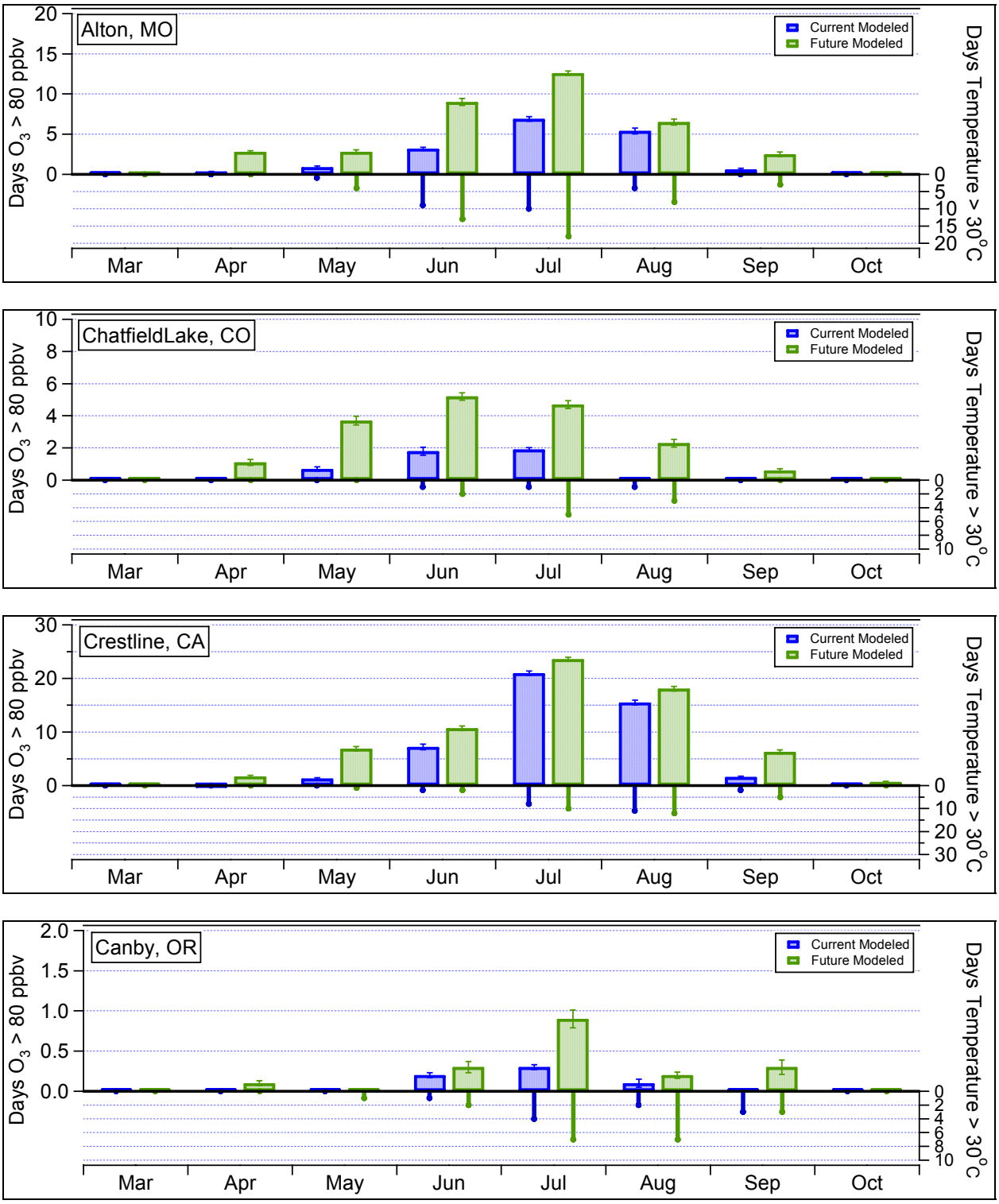

Figure 22: Current base-case and future case average number of days per month maximum daily 8-hr ozone concentrations exceed 80 ppbv over the 10-year simulation periods (current: 1990-1999 and future: 2045-2054) for the selected cities in the US continent. Bottom of each figure shows the average number of days per month maximum daily temperature exceeds 30°C for current base-case and future case simulations.

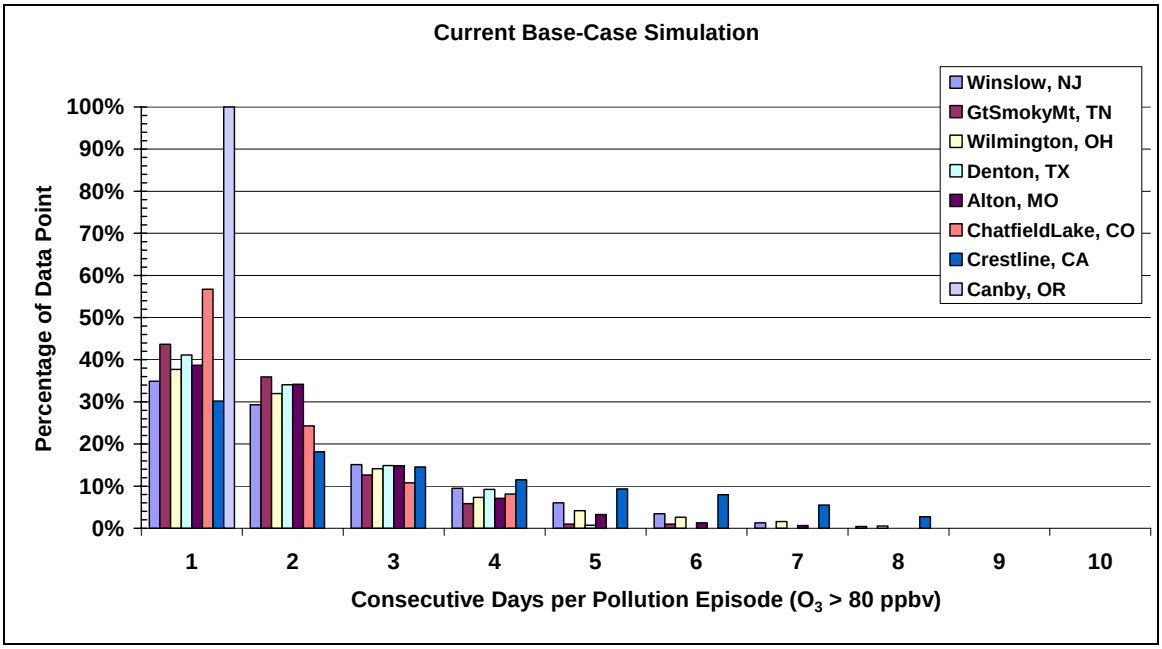

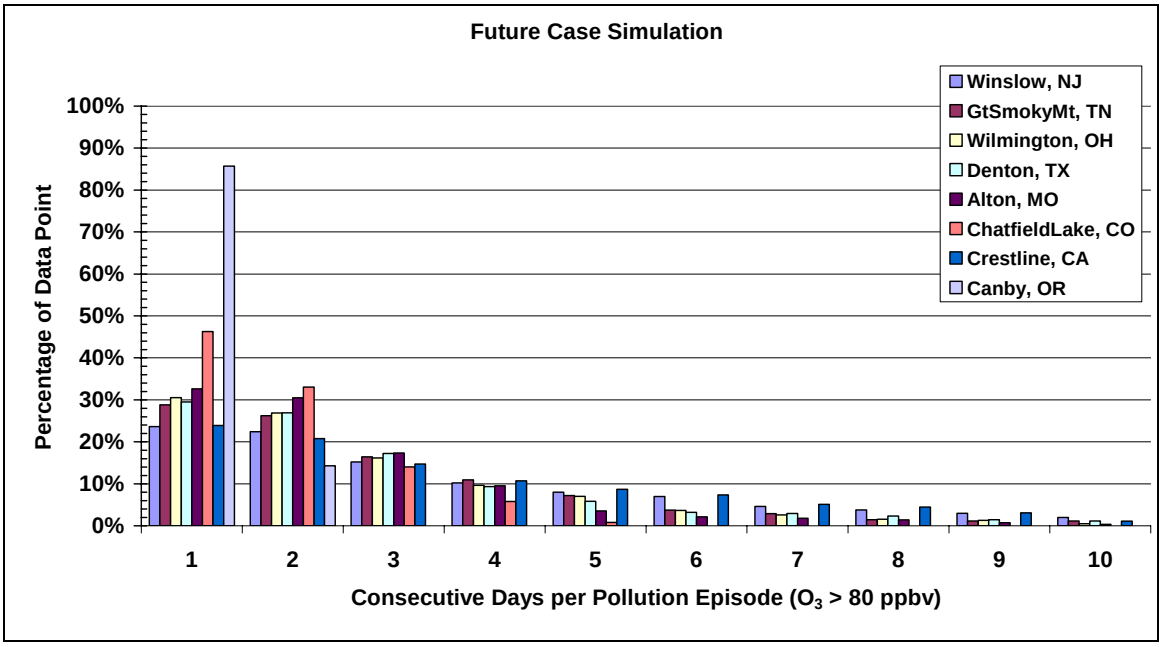

Figure 23: Frequency distributions of current base-case (top) and future case (bottom) duration of ozone episodic events, defined as consecutive days per pollution episode daily maximum 8-hr ozone concentrations exceed 80 ppbv for selected cities in the US continent.

Table 1: Model vertical layer structure and the approximate elevation at layer mid-point for the MM5 and CMAQ regional models (left), and the MOZART and PCM global models (right).

Layer	MM5 Sigma	CMAQ Sigma	Approximate Elevation (m)
28	0.000	0.000	12,670
27	0.131	0.131	10,300
26	0.175	0.175	9,278
25	0.225		8,315
24	0.275		7,450
23	0.325		6,664
22	0.375	0.375	5,942
21	0.425		5,275
20	0.475		4,653
19	0.525		4,070
18	0.575	0.575	3,522
17	0.625		3,004
16	0.675		2,514
15	0.725	0.725	2,047
14	0.775	0.775	1,624
13	0.820	0.820	1,302
12	0.850	0.850	1,061
11	0.878		878
10	0.895	0.878	860
9	0.900	0.900	690
8	0.920	0.920	571
7	0.930	0.930	454
6	0.950	0.950	281
5	0.965		225
4	0.975	0.975	149
3	0.985	0.985	82
2	0.995	0.995	18
1	1.000	1.000	0

Layer	MOZART/PCM Pressure (mbar)	Approximate Elevation (m)
19	0	29,223
18	10	26,216
17	20	22,579
16	50	19,010
15	80	16,430
14	120	14,561
13	160	12,717
12	220	10,923
11	290	9,200
10	370	7,569
9	460	6,052
8	550	4,669
7	650	3,439
6	740	2,380
5	830	1,508
4	900	835
3	960	372
2	990	124
1	1,000	0

Table 2: Quantitative comparison of landuse and land cover changes between the current and future case simulations.

Description	Base Case USGS Map Area (km^2)	Future Case USGS Map Area (km^2)	Percent Change
Mix Shrub/Grass	29808	465264	1461%
Bare Sparse Vegetation	93312	1321920	1317%
Dryland Crop Pasture	1486512	5456160	267%
Urban	55728	169776	205%
Crop/Grass Mosaic	1065312	2011392	89%
Crop/Wood Mosaic	578016	648000	12%
Water Bodies	10465200	9000720	-14%
Grassland	1503360	1049760	-30%
Evergreen Needleleaf	2575152	1664064	-35%
Savanna	251424	149040	-41%
Mixed Forest	1854576	918864	-50%
Shrub land	1999728	575424	-71%
Deciduous Broadleaf	1041984	84240	-92%
Irrigated Crop. Pasture	82944	0	-100%
Evergreen Broadleaf	23328	0	-100%
Wooded Wetland	86832	0	-100%
Wooded Tundra	317520	0	-100%
Mixed Tundra	2592	0	-100%
Snow or Ice	1296	0	-100%

Table 3: Summary of averaged CMAQ boundary conditions extracted from the MOZART model, averaged below 500mb height, and the percentage change between the current and future case simulations for western (left) and eastern (right) domain boundaries.

Western Boundary (ppbv)			
	Current	Future	Change
O_3	38	50	35%
NOx	0.03	0.04	44%
NOy	0.28	0.47	69%
VOC	1.1	2.1	87%

Eastern Boundary (ppbv)			
	Current	Future	Change
O_3	46	59	30%
NOx	0.14	0.22	63%
NOy	0.78	1.16	49%
VOC	5.0	7.3	47%

Table 4: Summary of domain-wide emissions (kilotons/day) for current year, and projected future case emission ratios (future/current) in the US by source category and species. Biogenic emissions are estimated for the month of July. (More detail emission summary and changes by individual states are available in the Appendix.)

	Area	On-Road Mobile	Non-Road Mobile	Point	Wild-Fire	Biogenic (July)
CO	45 / 1.33	184 / 1.02	61 / 1.13	11 / 1.00	1.5 / 1.25	–
NOx	5 / 1.57	23 / 1.02	11 / 1.09	23 / 1.00	–	4.0 / 1.04
VOC	24 / 1.94	15 / 1.02	7 / 1.32	5 / 1.00	0.1 / 1.24	130 / 0.60
SO_2	3 / 1.50	0.8 / 1.00	1.3 / 1.28	42 / 1.00	–	–

Table 5: Summary of model statistics comparing modeled and measured daily maximum 8-hr ozone concentrations across the 10-summer periods.

	Overall Period Average Concentrations	Episodic 98th Percentile Ozone Concentrations	Non-Episodic 20th Percentile Ozone Concentrations
Number of Points	1022	1022	1022
MB (ppbv)	6.3	3.3	7.3
ME (ppbv)	7.8	8.5	8.6
NMB	11%	4%	15%
NME	14%	9%	18%
R	0.62	0.64	0.55
Model Average (ppbv)	63	93	50
Model Standard Deviation (ppbv)	7.9	12	7.1
Measured Average (ppbv)	57	90	44
Measured Standard Deviation (ppbv)	8.0	14	6.9

Table 6: Summary of parameters describing the modeled and measured cumulative distribution functions (Figure 13) in terms of maximum and minimum values across the 10 observed and measure summer periods.

	Measured Minimum	Measured Maximum	Modeled Minimum	Modeled Maximum
Number of Points	71034	89926	93002	95046
Average (ppbv)	53	57	61	64
Variance ($ppbv^2$)	289	361	256	324
Maximum (ppbv)	140	208	144	189
20^{th} Percentile (ppbv)	37	41	47	50
50^{th} Percentile (ppbv)	54	58	60	64
80^{th} Percentile (ppbv)	66	72	73	79
98^{th} Percentile (ppbv)	91	101	95	104

Table 7: Summary of parameters describing the current base-case and future case modeled cumulative distribution functions (Figure 20) in terms of maximum and minimum values across the 10 summer periods.

	Current Modeled Minimum	Current Modeled Maximum	Future Modeled Minimum	Future Modeled Maximum
Number of Points	93002	95046	93002	95046
Average (ppbv)	61	64	70	73
Variance ($ppbv^2$)	256	324	212	295
Maximum (ppbv)	144	189	133	177
20^{th} Percentile (ppbv)	47	50	55	58
50^{th} Percentile (ppbv)	60	64	69	72
80^{th} Percentile (ppbv)	73	79	82	86
98^{th} Percentile (ppbv)	95	104	99	110

Table 8: Summary of 8 selected sites with high observed ozone concentrations from EPA geographic regions.

EPA Region	Site Name	Average Daily Max 8-hr O_3 [ppbv]	98th Percentile Daily Max 8-hr O_3 [ppbv]	Note
1-3	Winslow, NJ	67	109	30km SE of Philadelphia, PA
4	GtSmokyMt, TN	68	99	50km S of Knoxville, TN
5	Wilmington, OH	66	102	80km NE of Cincinnati,OH
6	Denton, TX	65	107	40km N of Dallas, TX
7	Alton, MO	64	102	30km N of St. Louis, MO
8	ChatfieldLake, CO	61	86	20km S of Denver, OR
9	Crestline, CA	101	165	10km N of San Bernadino, CA
10	Canby, OR	43	84	30km S of Portland, OR

CHAPTER FOUR

Impact of Future Land Use and Land Cover Changes on Regional Air Quality in the United States

Jack Chen, Jeremy Avise, Brian Lamb
Washington State University, Department of Civil and Environmental Research

Alex Guenther, Christine Wiedinmyer
National Center for Atmospheric Research

Abstract

A coupled global and regional scale modeling system was implemented to quantify the effects of changing climate and land use, land cover (LULC) on future biogenic emissions, and estimate their impacts on ozone and biogenic secondary organic aerosols (BSOA) in the continental US. The system was applied for five July months for a current base-case (Case 1, 1990 decade) and three future cases (2045 decade). Future case simulations included changes in climate, anthropogenic emissions and global pollutant background concentrations. Additional differences include: Case 2 future climate with present LULC; Case 3 future climate with agricultural expansion, and Case 4 future climate with agricultural expansion plus regions of reforestation for carbon-sequestration. Results show changing future meteorology with present LULC in Case 2 produced an increase of average continental emission rates of 25% and 21% for isoprene and monoterpenes, from the base-case of 9 mg m^{-2} day^{-1} and 2.6 mgC m^{-2} day^{-1}, respectively. However when LULC were changed together with future climate, predicted isoprene and monoterpene emissions decreased and the variability in biogenic emissions also decreased. In Case 3, continental isoprene and monoterpene emissions were reduced by 52% and 31%, and in Case 4, emissions were reduced by 31% and 14%, from the base-case, respectively. For future air quality, all three future cases have 10 ppbv higher US average 8-hr ozone concentrations due to warmer climate, higher global pollution backgrounds and significant increases in regional anthropogenic emissions. Future BSOA concentrations changed between +7% to -41% from the base-case of 0.4 μg m^{-3}. Spatially, concentrations vary by larger magnitudes following the differences in monoterpene emissions. Overall, the results indicate that on a regional basis changes in LULC can offset increases in biogenic emissions due to climate warming and thus, LULC must be considered in projections of future air quality.

Introduction

Natural source emissions such as those from plants are important components in regulating the state of air quality in the atmosphere. Plant emits large quantities of biogenic volatile organic compounds (BVOC). In the continental US, annual BVOC emissions from plants exceed the combined total of anthropogenic VOC emissions (Lamb et al., 1993). Of all the BVOC from plants, isoprene (C_5H_8) is the predominant compound. Isoprene is emitted from most broadleaf trees such as poplar, oak, willow and sycamore. Globally, isoprene represents approximately 44% of total BVOC with estimated annual isoprene emission of 570 Tg $year^{-1}$ (Guenther et al., 1995). Isoprene is highly reactive in the lower atmosphere. It is an important precursor to tropospheric ozone formation (Atkinson, 2000; Fuentes et al., 2000).

In addition to isoprene, monoterpenes ($C_{10}H_{16}$) are also important compounds emitted directly by many coniferous trees. The global emission rate of monoterpenes is estimated to be lower than isoprene, at 130 TgC $year^{-1}$ (Guenther et al., 1995). Although the global burden of monoterpenes is less, their importance in air quality is well known. Monoterpenes are easily oxidized by ozone, hydroxyl radical ($OH\cdot$) and nitrate radical ($NO_3\cdot$) to form low vapor pressure products in the atmosphere. These products readily partition into the aerosol phase and contribute to the formation of biogenic secondary organic aerosols (BSOA) which lead to regional haze and reduced visibility (Yu et al., 1999; Kanakidou et al., 2005). A model study by Tsigaridis et al. (2003) estimated that global BSOA formed from biogenic emissions range from 2.5 to 44.5 Tg $year^{-1}$ compared to anthropogenic SOA which are estimated in the range from 0.05 Tg $year^{-1}$ to 2.62 Tg $year^{-1}$.

Future global changes including large scale climate change, as well as alterations in land use and land cover (LULC), are interrelated factors that can greatly influence future environmental conditions. In order to accurately understand and quantify the impacts of

regional air quality from global changes, it is imperative that we correctly account for variations in the spatial extent and distribution of natural sources. Recently, several studies have examined the global burden of isoprene emissions and the resulting impacts on tropospheric ozone in the future (Sanderson et al., 2003; Wiedinmyer et al., 2006; Lathiere et al., 2005; Hauglustaine et al., 2005). Sanderson et al. (2003) estimated global isoprene emission to increase by 27% in 2090 from the present 549 Tg $year^{-1}$ as result of climate change and the associated vegetation distribution. The consequence on air pollution is 10-20 ppbv increase in global surface ozone. In an alternate scenario where future LULC was unchanged, representing present conditions, the study found even higher isoprene emissions, with 34% increase from the present case, to 731 Tg $year^{-1}$. This resulted in even higher ozone pollution. Similarly, Wiedinmyer et al. (2006) estimated global isoprene to increase in the future by 70% to 889 Tg $year^{-1}$ with combined climate and land cover changes. The increase in biogenic emissions resulted in higher global surface ozone concentrations with increases up to 55 ppbv, and caused more regions to experience poor air quality in the future.

The effects of human-induced LULC changes such as deforestation and increases in agriculture and urban areas are shown to impact future global climate as well as global atmospheric chemistry (Feddema et al., 2005; Foley et al., 2005). Different assumptions to future LULC can extensively affect the estimated changes in future regional environmental conditions. In this study, we focus on future biogenic emission estimates, and the resulting impacts on ground level ozone and BSOA concentrations over the continental US. Unlike previous studies that are based on global models, here, we employed a coupled global and regional scale model to account for the collective impacts from:

- Climate-driven future vegetation land cover changes
- Predicted expansions in future agricultural and urban land use

- Predicted changes in future chemical background concentrations and regional meteorological variations
- Predicted changes in future anthropogenic emissions

This model framework provides much higher spatial and temporal resolution in future air quality simulations that cannot be achieved from global models. In the next sections, we present a brief overview of the model system and future LULC scenarios, followed by analyses of predicted changes in biogenic isoprene and monoterpene emissions, and the resulting impacts on future ground level ozone and BSOA concentrations.

Modeling Approach and Scenario Descriptions

The coupled global and regional model framework is achieved through a one-way nesting technique where global-scale models provide time-stepping, spatial varying boundary conditions for regional-scale models. This system was recently applied to examine the combined effects of global change on US regional air quality 50 years in the future, and in a detailed sensitivity analysis of factors influencing future pollutant concentrations (Chen et al., 2007; Avise et al., 2007). These studies evaluated the system with long-term ozone measurement data, and showed the system performs well in capturing episodic, high ozone conditions. For more detailed descriptions of the modeling system, the readers are referred to the earlier work; only brief overviews are provided here.

The global models that provide current and future climate and atmospheric chemical conditions are the PCM (Parallel Climate Model, Washington et al., 2000), and the MOZART2 (Ozone and Related Chemical Tracers version 2, Horowitz et al., 2003) model, respectively. In the regional scale, the MM5 mesoscale meteorological model (Grell et al., 1994) and the EPA CMAQ (Community Multi-scale Air Quality, Byun et al., 1999) model downscale the global model results for simulations at much higher resolution centered over the continental US. The

regional chemistry model domain is made up of 125 by 84 grids using 36 km x 36 km horizontal grid cells and 18 vertical layers. Hourly output is obtained for all of the simulation periods.

The model system was applied to simulate five July months selected from the global runs for the 1990 decade as a base-case for comparison to results for five July months selected from the 2045 decade. High temperature and high solar insolation in July result in higher biogenic emissions, and poorer regional air quality compared to rest of the year. Multiple July simulations allow the system to capture environmental variability from year to year as driven by the large scale models.

Global and regional meteorology for the current decade are simulated without observational or analyses nudging. They represent present day conditions but have no direct match to specific weather events. Climatology for the 2045 decade is based on the Intergovernment Panel on Climate Change (IPCC) SRES A2 scenario. The A2 storyline has a business as usual pessimistic future outlook. For 2045, the scenario estimates a large global population of 11 billion and 1.5°C higher global mean temperature compared to the present condition (Nakićenović et al., 2000).

The regional anthropogenic emissions for the base-case July simulation are based on the US Environmental Protection Agency (EPA) 1999 National Emissions Inventory (NEI 1999). The inventory includes categories from area, mobile, and point sources. For the future scenarios, anthropogenic emissions are projected to 2045 with region-specific emission factors from the EPA Economic Growth and Analysis System (EGAS, U.S. EPA, 2004). The projection factors account for predicted population and economic growth, but do not include emission reduction strategies, or possible future technological advances influencing regional emissions. On average across the continent, anthropogenic VOC, NOx and CO emissions increased by 50%, 10% and 10%, respectively from the 1990 case. Spatial distributions of future

anthropogenic emissions are updated with results from the Spatially Explicit Regional Growth Model (SERGOM) to reflect population density increases and urban area expansion (Theobald, 2005).

The regional scale biogenic emissions for both present and future scenarios are generated with the simplified version of the MEGAN model (referred as MEGAN-EZ in Guenther et al., 2006). The model estimates hourly isoprene, monoterpene and other BVOC emissions with gridded emission capacities, monthly foliage density, and predicted hourly temperature and ground level shortwave radiations. The model follows the same framework as earlier biogenic emissions models, but has several improvements, including better characterization of vegetation distribution and foliar density, updated leaf energy balance calculations, revised light attenuation algorithms within a forest canopy, and detailed chemical speciation profiles for air quality model mechanisms.

Vegetation inputs to MEGAN for the current period simulation were based upon global satellite observations with 1-km spatial resolution. The data were up-sampled to match the 36-km grid over the regional domain. Meteorological variables for MEGAN were generated from the coupled PCM-MM5 climate-meteorological model.

Future LULC scenarios affecting biogenic emissions are based on the IMAGE 2.2 global model dataset (Strengers et al., 2004). The dataset was used as part of the IPCC assessment, and is consistent with the IPCC A2 climate scenario. Changes in future LULC are due to human induced agricultural expansion, urban area developments, as well as, climate induced changes in vegetation distributions. Figure 1 compares the current and future vegetation coverage for three plant functional types: broadleaf trees, needleleaf trees and croplands. Large differences in plant area coverage are predicted in the future. Most notably is the conversion of current broadleaf and needleleaf forests to agriculture and dry croplands. Significant reductions in

forests occur in the east and coastal Pacific Northwest. Furthermore, much of the current LULC in the eastern states are transformed to agriculture lands. Replacing forests with pasture and cropland can significantly lower isoprene and monoterpene emissions due to decreases in BVOC emitting foliar density.

For comparison with the agricultural dominated future LULC, we examine a second scenario affecting future biogenic emissions. The second future vegetation distribution is modified from a recent study by Jackson et al. (2005) who examined the significant expansion of managed forests for purposes of carbon sequestration, particularly in the northern midwest and Southeast. The reforestation is aimed at future greenhouse gas emissions trading by increased biogenic carbon-sequestration. Future LULC projections were estimated using the Forest and Agriculture Sector Optimization Model-Green House Gases (FASOMGHG) (Adams et al., 1996). The model converted 72 million hectares of non-irrigated agriculture and pasture lands to woody forests based upon the projected costs of carbon trading. Figure 2 depicts the estimated LULC change under this scenario. Significant portions of the Midwest are reforested with hardwood plants such as oak and poplar which have very high isoprene emission capacities. Similarly, regions in the south are reforested with softwood trees such as pine, which generally have higher monoterpene emission capacities than the agricultural lands they replace.

Table 1 summarizes the climate and LULC scenarios considered in this study. The first simulation (Case 1) is the base-case. It represents present-day vegetation distributions and present regional emissions. Meteorology for this case is based on the 1990-1999 climatic conditions. Case 2 focuses on future biogenic emissions and air quality changes due to climate change without considering future LULC. Case 3 and Case 4 are aimed at examining the effects of alternate future LULC changes on future biogenic emissions and air quality. For consistency, all future simulations (Case 2, 3, 4) are performed with the same sets of future

meteorological conditions, future global chemical background conditions, and projected regional anthropogenic emissions in 2045. Comparisons between these cases provide quantitative estimates on LULC effects on future biogenic emissions, and the indirect impacts on regional ozone and BSOA conditions.

Future changes in meteorological conditions such as canopy temperature and surface solar radiation are important variables influencing biogenic emissions. The regional meteorological conditions are simulated using the MM5 model downscaled from the PCM global model. Figure 3 and 4 show simulated present-day and future changes for average July daily maximum temperature and surface solar radiation. The predicted changes conform to the projected IPCC-A2 scenario, with a continental mean temperature increase of 2°C and a solar radiation increase of 17 W/m^2. Spatially, temperature and solar radiation changes vary across the continent. Large temperature increases of 2°C – 6°C are estimated for the southwest US, while smaller increases of 1°C – 3°C are predicted for the entire eastern US. Regions in the Pacific Northwest and the central states have the least temperature change, with central Texas having small decreases of 1°C in July. Slightly different spatial distributions are predicted for ground level solar radiation. Large increases are estimated in the central states, along the west coast and southern Florida. These regions are predicted to have increased energy inputs between 60 W/m^2 to 100 W/m^2. In addition, states in the east coast are predicted to have large decreases from 20 W/m^2 to 60 W/m^2. Smaller decreases are also modeled for inland Northwest, and north central Texas with approximate 20 W/m^2 lower energy input compared to the present condition.

Results and Discussion

Analyses of MEGAN model results show significant differences in predicted isoprene and monoterpene emissions for the different scenarios. These, in turn, result in different air pollution conditions in the future.

Biogenic Emissions

Figure 5 and 6 show, respectively, the modeled isoprene and monoterpene emission rates for the present base-case (plate a) and the magnitudes of changes for the future scenarios (plates b, d, d). The present day continental isoprene and monoterpenes emission rates are similar to results from recent studies using MEGAN, both in magnitude and spatial distributions (Helmig et al., 2007; Palmer et al., 2006). Elevated isoprene emissions are estimated for regions in the southeast, western California and northern midwest. The hot spots of >80 mg m-2 day-1 emissions in the southeast correspond to the high-density oak forests in the Ozarks region in Missouri (Wiedinmyer et al., 2005). The base-case average continental isoprene emission rate is 9 mg m-2 day-1 with a standard deviation of 14 mg m-2 day-1.

In Case 2, the higher predicted future temperatures with present day vegetation distribution cause isoprene and monoterpene emissions to increase significantly. The average continental emission rate is 11 mg m^{-2} day^{-1} with a continental standard deviation of 17 mg m^{-2} day^{-1}. The increases are proportional to the base-case emission rates, such that areas of higher base-case isoprene emissions have higher predicted increases due to generally warmer future climate.

On the contrary, with predicted changes in future LULC, the MEGAN model estimates significantly lower isoprene emissions for both Case 3 and Case 4. Regions of lower emissions rates are estimated for the east and coastal California. The southeast region has the largest emission decrease with 30 mg m^{-2} day^{-1} reductions from the 55 mg m^{-2} day^{-1} for the base-case.

Estimated isoprene emissions for Case 4 are similar to Case 3, except for regions of reforestation. The goal of carbon-sequestration through increased poplar and oak plantations significantly increases isoprene emissions by 5 mg m^{-2} day^{-1} in the southeast Texas and by 10 to 30 mg m^{-2} day^{-1} in the Midwest. The regions of largest increase are in states of Iowa, Illinois and Indiana. Quantitatively, the continental average isoprene emissions for Case 3 and 4 are lower than the base-case at 4.3 mg m^{-2} day^{-1} and 6.2 mg m^{-2} day^{-1}, respectively, and the magnitude of continental emission variability is also lowered, with standard deviation of 7 mg m^{-2} day^{-1} and 10 m^{-2} day^{-1}, respectively.

Estimated monoterpene emissions showed similar changes as isoprene from the base-case, but with lower magnitudes, and slightly different spatial distributions. The base-case results showed high monoterpenes emission rates for regions in the east, northern midwest and Pacific northwest. The high monoterpene emissions in the base-case correspond to high density of coniferous trees. The continental average monoterpene emission for the Case 1 is 2.6 mgC m^{-2} day^{-1} with continental standard deviations of 4.2 mgC m^{-2} day^{-1}.

Significant differences in monoterpene emissions are predicted for different future scenarios. Changing climate without LULC changes in Case 2 resulted in much higher monoterpene emissions. The continental average emission is 3.2 mgC m^{-2} day^{-1} with continental standard deviations of 5.1 mgC m^{-2} day^{-1}. The increases are larger for the southeast due to higher base-case emissions and higher predicted future temperature. For Case 3 and Case 4, the predicted changes in future vegetation distributions significantly alter future monoterpene emissions. In Case 3, decreases in forest lands reduced monoterpene emissions by 2 mgC m^{-2} day^{-1} to 10 mgC m^{-2} day^{-1}, with largest reduction in the southeast. In Case 4, the LULC changes increased monoterpene emissions across the Midwest. Furthermore, there are spots of high monoterpene emissions in the south, with emission rates reaching as high as 25 mgC m^{-2} day^{-1}, from 5 mgC m^{-2} day^{-1} in the base-case. The continental monoterpene emission

average for Case 3 and Case 4 are 1.8 mgC m^{-2} day^{-1} and 2.3 mgC m^{-2} day^{-1}, respectively, with lower continental standard deviations compared to base-case, of 2.5 mgC m^{-2} day^{-1} and 2.8 mgC m^{-2} day^{-1}, respectively.

Alternative ways of analyzing the predicted future emission are to compare their spatial and temporal emission variations for the different cases across the continent. Figure 7 shows the total continental isoprene and monoterpene emission range for the four cases. The variability in each case stems from the changes in predicted daily meteorological conditions across the five July simulations. The concentration ranges illustrate the variability of total biogenic emissions under different July meteorological conditions.

In the base-case, isoprene emissions vary from 50 Gg day^{-1} to 104 Gg day^{-1} with average emission of 75 Gg day^{-1}; and monoterpene emission rates vary from 15 Gg day^{-1} to 28 Gg day^{-1} with average of 22 Gg day^{-1}. For the future cases, Case 2 has the largest overall difference compared to the base-case. It has the highest average emissions, and larger emission variability. Average emissions in Case 2 increased by 26% and 20% for isoprene and monoterpenes, respectively, and the emission variability widened by 58 Gg day^{-1} and 13 Gg day^{-1}, respectively. For Case 3, predicted continental emissions decreased from changing LULC by 52% for isoprene and 31% for monoterpenes. Smaller reductions are estimated for Case 4 with 31% and 14% reductions for isoprene and monoterpene emissions, respectively.

Future climate conditions with present LULC increase biogenic emission variability. However, changing future LULC reduced emission variability across different meteorological conditions over time. This is especially evident for Case 3, with agricultural expansion. Significant decreases in woody plants decreased emissions by 21 Gg day^{-1} for isoprene, and 7 Gg day^{-1} for monoterpene emissions. In Case 4, the re-introduction of forests for carbon-

sequestration caused emission range to increased slightly, but is still less than the base-case, by 32 Gg day^{-1} and 9 Gg day^{-1} for isoprene and monoterpene emissions, respectively.

In terms of spatial variability across the continents, Figure 8 depicts the comparisons by percent area exceedance with respect to estimated emission rates. The functions represent percent area within the continent with daily biogenic emission rates greater than the values defined on the x-axis. The figures clearly show the quantitative differences for the four cases by emission rates. For isoprene, Case 2 has highest percentage of continental regions (9%) with emission rates greater than 40 mg m^{-2} day^{-1}, compare to 6% for the base-case, 1% for Case 3, and 4% for Case 4. Similar trends continue with higher emission rates.

For monoterpene emissions, similar spatial variability is predicted for the four cases, albeit at a much lower magnitude. Case 2 has the largest percentage of continental regions (10%) with emission rates greater than 10 mgC m^{-2} day^{-1}, compared to 7% for Case 1, 2% for Case 3, and 3% for Case 4. The fractional area decreases much rapidly with increase emission rates for Case 3 and Case 4 compared to Case 1 and Case 2 with current vegetation distributions.

These results demonstrate that in addition to changing future climatology, changing LULC have even more significant impacts on future biogenic emissions. Changing future meteorology with present vegetation distributions generally resulted in much higher emissions and larger emission variability due to higher future temperature and more short wave radiation reaching the ground. On average, Case 2 has 25% higher isoprene emissions and 21% higher monoterpene emissions across the continent compared to the base-case. However, considering future changes in LULC together with meteorology, the predicted isoprene and monoterpene emissions decrease, and the emission spatial and temporal variability also decreases. In Case 3 and Case 4, continental isoprene emissions are reduced by 52% and

31%, respectively, and monoterpene emissions are reduced by 31% and 14%, respectively. The lower emission variability is likely due to the more homogeneous predicted future LULC compare to present case. Larger regions of analogous vegetation in the future cause emissions to be more similar, thus lower the chances of extreme emission events with changing future meteorology. The reforestation scenario in Case 4 generally gives rise to higher emissions compared to Case 3, and resulted in slightly larger spatial and temporal emission variability than Case 3, but the overall changes are still less than cases with present LULC.

Future Regional Air Quality Implications

Changing biogenic emissions can significantly influence future air quality estimates. This section focuses on the ozone and BSOA impacts from the combined changes in future LULC, meteorological conditions and predicted regional emissions. Ground level ozone and fine particulate matter (PM) are atmospheric pollutants known to cause health problems in human and adversely affect the environment. These pollutants are regulated by the US Environment Protection Agency (EPA) following the National Ambient Air Quality Standards (NAAQS). The current NAAQS for ozone is 80 ppbv 8-hr average concentration, and for $PM_{2.5}$, the NAAQS is 35 $\mu g/m^3$ 24-hr average concentration.

Ozone and BSOA concentrations are analyzed from the output of the CMAQ model simulations. CMAQ has been evaluated and demonstrated good performance in simulating the formation and fate of ozone and PM in many recent studies (Eder et al., 2006; O'Neill et al., 2006; Smyth et al., 2006). In this work, the CMAQ simulations are applied with the same configurations for the four cases. The only differences are in the input emissions data and MM5 regional meteorology. For consistency, the same MM5 meteorology fields used in MEGAN are also used in CMAQ.

Ground Level Ozone

Figure 9 depicts the period average daily maximum 8-hr ozone concentrations for the base-case (plate a) and the concentration differences of the three future cases from that of the base-case (plates b, b, d). Simulation results for the base-case have been evaluated against available ozone measurements in earlier studies (Chen et al., 2007, Avise et al., 2007). Here, we focus on the ozone concentration changes in the future due to changes in biogenic emissions from the LULC scenarios. CMAQ predicted much higher ozone concentrations in the future throughout the continent. The three future cases have approximately 10 ppbv higher regional averaged ozone concentrations compared to the current base-case simulation at 56 ppbv. Spatially, the increases are larger along costal urban areas than in central states inland. The simulated future ozone increases are due to the combine effects of warmer temperature, higher projected future anthropogenic emissions, and higher global pollutant background concentrations.

Between the three future cases, ozone pollution is slightly worse for Case 2 than Case 3 or Case 4. Case 2 with the highest biogenic isoprene emissions has the largest area of elevated daily maximum 8-hr ozone concentrations. In Case 2, ozone levels are higher over larger areas near Boston, New York, Philadelphia, and Washington DC along the east coast. The higher estimated isoprene emissions in this case aid the ozone production downwind of these cities. For Case 3 and 4, the magnitude of ozone increases is slightly less due to estimated reductions in future isoprene emissions from LULC change. Concentration changes for Case 3 and Case 4 are very similar except for regions of reforestation in Case 4. Higher isoprene emissions in Midwest cause future ozone concentrations in the region to be slightly higher.

Figure 10 shows the percent area exceedance with respect to modeled daily maximum 8-hr ozone concentrations. The percent area exceeding the 80 ppbv NAQQS threshold is

different among the four cases. Case 1, with the current emission and climate scenario, has the smallest area exceeding the NAAQS standard at 6% of the total continental US. Among the three future cases, Case 2 has highest percent area exceeding the NAAQS ozone standard, with 20% of the continental US. For Case 3 and Case 4, when future LULC shift towards agricultural coverage and decreased isoprene emissions, the area where the daily maxima exceed the standard is less. Case 3 has 17% of total US area exceeding 80 ppbv, and Case 4, with slightly higher isoprene emission in the Midwest, has 18% of total US continent exceeding the NAAQS 80 ppbv standard.

Figure 11 shows continental averaged ozone concentration ranges across the five simulate July months for the four cases. The range of concentration variability among the current base-case and the three future cases are very similar, but the magnitudes of concentrations differ. For the current base-case, the domain averaged ozone concentration varied from 64 ppbv to 47 ppbv with overall average of 56 ppbv. For the three future cases, despite the large differences in biogenic emissions, predicted ozone concentrations and concentration variability are similar. The three future cases have domain averaged ozone concentrations ranging from 57 ppbv to 78 ppbv with overall average between 66 ppbv and 67 ppbv. The insensitivity in simulated future ozone condition to changes in LULC is largely due to the increases in predicted future anthropogenic emissions, as well as large spatial averaging over the entire continental domain.

To more explicitly illustrate the effects of changing LULC and the associated biogenic emissions on future ozone, Figure 12 depicts the average daily maximum 8-hr ozone concentration difference of Case 3 and Case 4 from Case 2. The results show that changing LULC in the future significantly decreases the future ozone conditions compared to Case 2, when LULC is unchanged. For both future LULC scenarios, averaged daily maximum 8-hr ozone concentrations decreased from 1 ppbv to 5 ppbv due to changing biogenic emissions

alone. In Case 3, the conversion of broadleaf forests to agriculture lands decreased predicted future ozone significantly for areas in the east and California compared to Case 2. For the reforestation scenario, Case 4, higher isoprene emissions increased the predicted future ozone distinctly for the states of Iowa, Illinois and Indiana. Ozone concentrations in these regions increased by 1 ppbv to 5 ppbv when compared with future estimates using current LULC scenario.

Biogenic Secondary Organic Aerosol

The CMAQ secondary organic aerosol science algorithm follows the approach of Schell et al., (2001). The model simulates SOA as function of VOC oxidation from ozone, OH· and NO_3· radicals. For BSOA, the precursor gas-phase compounds are monoterpenes. Although reports from several recent studies indicate observed BSOA formation from isoprene oxidation (Claeys et al., 2004), CMAQ does not currently include these SOA production mechanisms.

Figure 13 depicts the average 24-hr BSOA concentrations for the base-case (plate a) and the concentration changes for the future cases (plates b, c, d). Elevated BSOA are estimated for regions with high monoterpene emissions, such as the east, northern midwest, and the Pacific northwest. In the base-case, peak continental BSOA levels of approximately 2.0 μg m^{-3} occur in the southwest near Atlanta, GA and Birmingham, AL urban areas. The model also simulated high BSOA for regions along the Pacific northwest with average BSOA concentrations ranging from 0.5 μg m^{-3} to 1.5 μg m^{-3}. The average continental 24-hr BSOA for the base-case is 0.4 μg m^{-3}. Elevated BSOA generally occur in areas of high monoterpene emissions and high atmospheric oxidant concentrations (O_3, OH·, NO_3·) that drive the BSOA formation chemistry.

Among the three future cases, BSOA concentrations generally vary in proportion with the estimated changes in future biogenic monoterpene emissions. Case 2 with highest

continental monoterpene emissions and predicted future ozone concentrations has higher overall BSOA concentrations. Under present LULC and future climate conditions, the mean continental 24-hr BSOA increased by 7% from the base-case to 0.43 μg m^{-3}. BSOA concentration changes range from -0.2 μg m^{-3} to +0.8 μg m^{-3}. Large BSOA concentration increases occur in the east and Pacific northwest. Slight decreases in BSOA concentrations are predicted in the southeast compared to the base-case. This is largely due to reductions in lower atmospheric oxidant concentrations, which lower BSOA production at night. The large nighttime BSOA reductions decreased the mean 24-hr BSOA levels compared to the base-case.

When LULC is changed with predicted future climate in Case 3 and Case 4, BSOA concentrations changed significantly from the resulting changes in monoterpene emissions. In Case 3, where broadleaf and needleleaf forests are converted to dry and irrigated croplands, predicted BSOA concentrations decrease for regions in the southeast and Pacific northwest. The largest change occurs in Mississippi, Alabama and Georgia where reductions as large as 1.3 μg m^{-3} in BSOA concentrations are simulated compared to the base-case. Averaged across the entire continent, the estimated 24-hr BSOA decreased by 41% from the base-case to 0.24 μg m^{-3}.

Estimated BSOA increased slightly for Case 4 with the future reforestation scenario when compared to Case 3. The increases in broadleaf plantations in the Midwest and south eastern Texas indirectly increased future BSOA concentrations. The increases ranged from 0.2 μg m^{-3} to 0.8 μg m^{-3} when compared to the present base-case results. The mean continental 24-hr BSOA concentration for the reforestation scenario is 0.29 μg m^{-3}. This represents a 30% reduction from the base-case due to diminishing broadleaf forests, but a 21% increase from Case 3, due to reforestation.

Spatial distributions of BSOA for the four cases were slightly different, but matches with the estimated monoterpene emission changes. Figure 14 shows the percent area exceedance with respect to modeled average 24-hr BSOA concentrations. Case 1 and 2 with higher BSOA concentrations have more areas with higher BSOA concentrations compared to Case 3 and 4 with future LULC changes. For Case 1, BSOA levels exceed 1 ug/m3 over 11% of the continental US, compared to 12% for Case 2, 4% for Case 3 and 5% for Case 4.

The average continental BSOA concentration ranges across the five July months also vary for the four scenarios. As shown in Figure 15, the average continental BSOA concentration was highest for Case 2 and lowest for Case 3. The changes are similar to that of estimated monoterpene emissions albeit at much lower magnitudes. In terms of BSOA concentration variability across the five July meteorological conditions, Case 1 and Case 2 with present LULC have a larger BSOA concentration range compared to Case 3 and Case 4. This is mostly due to the more homogeneous LULC distributions estimated for the future cases compare to the present. More uniform LULC in the future decreases the range of monoterpene emissions and results in lower BSOA concentration variability.

Conclusions

Climate change and human perturbations in the future can significantly affect the dominant vegetation species and alter LULC. Changing vegetation distributions accompanied with variable meteorological conditions can considerably influence the magnitude and spatial distribution of biogenic isoprene and monoterpenes emissions. These, in turn, can impact the formation of secondary atmosphere pollutants.

In this study, we implemented a coupled global and regional scale modeling system to quantify the effects of changing LULC on future biogenic emissions, and their indirect effects on

future ground level ozone and biogenic secondary organic aerosols (BSOA). The system was applied for four different scenarios: Case 1 is the current base-case with 1990 conditions; Case 2 represents future simulations in 2045, but with current LULC scenario; Case 3 assumes future agriculture dominated LULC with vegetation species driven by future climate, and Case 4 considers the effect of reforestation aimed at carbon-sequestrations in the Midwest and southwest regions. For each case, the model simulates biogenic emissions and air quality conditions for five July months over the continental US domain.

Results show isoprene and monoterpene emissions increase as expected under warmer future climatology. However, changing LULC showed even more significant effects on the magnitude and spatial distribution of future biogenic emissions. Warmer temperatures and higher solar insolation in the future increase future biogenic emissions, but when LULC are changed together, the reductions in forests decrease isoprene and monoterpene emissions by even larger amounts.

Average continental isoprene and monoterpene emission rates for the current base-case, Case 1, are estimated to be 9 mg m^{-2} day^{-1} and 2.6 mgC m^{-2} day^{-1}, respectively. In Case 2, isoprene and monoterpene emission rates increase by 25% and 21%, respectively, from the base-case. In Case 3, significant reductions of forest area reduce isoprene and monoterpene emission rates by 52% and 31%. The reductions are less in Case 4 with 31% and 14% due to reforestation for regions in the Midwest and southeast.

In addition to lower overall emission rates, changing LULC in Case 3 and Case 4 also resulted in lower emission spatial and temporal variability compared to Case 1 and Case 2 with current LULC. Larger regions of homogeneous vegetation in the future cause the biogenic emission rates to be more similar. This lowers the occurrences of extreme emission events due to changes in future meteorology.

In terms of future regional air quality, all three future cases estimated approximately 10 ppbv higher continental mean daily maximum 8-hr ozone concentrations compared to the current base-case, at 56 ppbv. The large homogeneous change across the three future scenarios is primarily due to the combined effects of warmer temperature, higher projected anthropogenic emissions and higher global pollution background concentrations. However, when compared with Case 2, future ozone concentrations differ spatially by -5 ppbv to +5 ppbv from changing LULC in Case 3 and Case 4. Lower ozone concentrations are estimated for regions in the east and California due to lower future isoprene emissions. In Case 4, the higher estimated future isoprene emissions from reforestation increase future ozone concentrations for states of Iowa, Illinois, and Indiana.

Changing future LULC has slightly larger impact on future BSOA concentrations. Future BSOA concentrations generally vary in proportion with the estimated changes in future biogenic monoterpene emissions. Elevated BSOA occur in areas of high monoterpene emissions, generally in the east, northern midwest and the Pacific Northwest. Future average 24-hr BSOA concentrations vary by +7% to -41% from the base-case concentration of 0.4 μg m^{-3}. Case 2 with higher monoterpene emission is predicted to increase BSOA by 7%. Average BSOA concentrations decrease in Case 3 and Case 4 with lower monoterpene emissions compared to current base-case. Case 3 with largest reduction in monoterpene emissions decrease BSOA by 41% to 0.24 μg m^{-3}. In Case 4, the reforestation LULC resulted in 21% increases from Case 3, but still represents 30% reductions in average BSOA concentrations when compared with the base-case. The large BSOA reductions in the south dominated the BSOA increases in the reforested Midwest regions.

References

Adams, D. M., Alig, R. J., Callaway, J. M., McCarl, B. A., and Winnett, S. M., 1996. The Forest and Agricultural Sector Optimization Model (FASOM): Model Structure and Policy Applications. USDA Forest Service Research Paper, PNW-495, Pacific Northwest Research Station, Portland, Oregon.

Atkinson, R., 2000. Atmospheric Chemistry of VOCs and NOx. Atmospheric Environment 34(12-14), 2063-2101.

Avise, J., Chen, J., Lamb, B., Mass, C., Salathe, E., Guenther, A., Wiedinmyer, C., Larkin, N., McKenzie, D., and O'Neill, S., 2007. Contribution of Global Changes in Climate, Emissions, and Chemical Boundary Conditions to Changes in Regional Air Quality. Manuscript in preparation.

Strengers, B., Leemans, R., Eickhout, B., de Vries, B., and Bouwman, L., 2004. The Land-use Projections and Resulting Emissions in the IPCC SRES Scenarios as Simulated by the IMAGE 2.2 Model. 61(4), 381-393.

Byun, D. W. and Ching, J. K. S., 1999. Science Algorithms of the EPA Models-3 Community Multiscale Air Quality (CMAQ) Modeling System. U.S. Environmental Protection Agency, EPA/600/R-99/030.

Chen, J., Avise, J., Lamb, B., Mass, C., Salathe, E., Guenther, A., Wiedinmyer, C., Larkin, N., McKenzie, D., and O'Neill, S., 2007. Global Change Impacts on Regional Air Quality in the United States. Manuscript in preparation.

Claeys, M., Graham, B., Vas, G., Wang, W., Vermeylen, R., Pashynska, V., Cafmeyer, J., Guyon, P., Andreae, M. O., Artaxo, P., and Maenhaut, W., 2004. Formation of Secondary Organic Aerosols through Photooxidation of Isoprene. Science 303(5661), 1173-1176.

Eder, B. and Yu, S. C., 2006. A Performance Evaluation of the 2004 Release of Models-3 CMAQ. Atmospheric Environment 40(26), 4811-4824.

Feddema, J. J., Oleson, K. W., Bonan, G. B., Mearns, L. O., Buja, L. E., Meehl, G. A., and Washington, W. M., 2005. The Importance of Land-Cover Change in Simulating Future Climates. Science 310(5754), 1674-1678.

Foley, J. A., DeFries, R., Asner, G. P., Barford, C., Bonan, G., Carpenter, S. R., Chapin, F. S., Coe, M. T., Daily, G. C., Gibbs, H. K., Helkowski, J. H., Holloway, T., Howard, E. A., Kucharik, C. J., Monfreda, C., Patz, J. A., Prentice, I. C., Ramankutty, N. n, and Snyder, P. K., 2005. Global Consequences of Land Use. Science 309(5734), 570-574.

Fuentes, J. D., Lerdau, M., Atkinson, R., Baldocchi, D., Bottenheim, J. W., Ciccioli, P., Lamb, B., Geron, C., Gu, L., Guenther, A., Sharkey, T. D., and Stockwell, W., 2000. Biogenic Hydrocarbons in the Atmospheric Boundary Layer: a Review. Bulletin of the American Meteorological Society 81(7), 1537-1575.

Grell, A. G., Dudhia, J., and Stauffer, D. R., 1994. A description of the fifth-generation Penn State/NCAR Mesoscale Model (MM5). National Center for Atmospheric Research, NCAR Technical Note NCAR/TN-398+STR.

Guenther, A., Hewitt, C. N., Erickson, D., Fall, R., Geron, C., Graedel, T., Harley, P., Klinger, L., Lerdau, M., Mckay, W. A., Pierce, T., Scholes, B., Steinbrecher, R., Tallamraju, R., Taylor, J., and Zimmerman, P., 1995. A Global-Model of Natural Volatile Organic-Compound Emissions. Journal

of Geophysical Research-Atmospheres 100(D5), 8873-8892.

Guenther, A., Karl, T., Harley, P., Wiedinmyer, C., Palmer, P. I., and Geron, C., 2006. Estimates of Global Terrestrial Isoprene Emissions Using MEGAN (Model of Emissions of Gases and Aerosols from Nature). Atmospheric Chemistry and Physics Discussions 6107-173.

Hauglustaine, D. A., Lathiere, J., Szopa, S., and Folberth, G. A., 2005. Future Tropospheric Ozone Simulated With a Climate-Chemistry-Biosphere Model. Geophysical Research Letters 32(24), doi:10.1029/2005GL024031.

Helmig, D., Ortega, J., Duhl, T., Tanner, D., Guenther, A., Harley, P., Wiedinmyer, C., Milford, J., and Sakulyanontvittaya, T., 2007. Sesquiterpene Emissions from Pine Trees - Identifications, Emission Rates and Flux Estimates for the Contiguous United States. Environmental Science & Technology 41(5), 1545-1553.

Horowitz, L. W., Walters, S., Mauzerall, D. L., Emmons, L. K., Rasch, P. J., Granier, C., Tie, X. X., Lamarque, J. F., Schultz, M. G., Tyndall, G. S., Orlando, J. J., and Brasseur, G. P., 2003. A Global Simulation of Tropospheric Ozone and Related Tracers: Description and Evaluation of Mozart, Version 2. Journal of Geophysical Research-Atmospheres 108(D24), doi:10.1029/2002JD002853.

Jackson, R. B., Jobbagy, E. G., Avissar, R., Roy, S. B., Barrett, D. J., Cook, C. W., Farley, K. A., Le Maitre, D. C., Mccarl, B. A., and Murray, B. C., 2005. Trading Water for Carbon with Biological Sequestration. Science 310(5756), 1944-1947.

Kanakidou, M., Seinfeld, J. H., Pandis, S. N., Barnes, I., Dentener, F. J., Facchini, M. C., Van Dingenen, R., Ervens, B., Nenes, A., Nielsen, C. J., Swietlicki, E., Putaud, J. P., Balkanski, Y., Fuzzi, S., Horth, J., Moortgat, G. K., Winterhalter, R., Myhre, C. E. L., Tsigaridis, K., Vignati, E., Stephanou, E. G., and Wilson, J., 2005. Organic Aerosol and Global Climate Modelling: a Review. Atmospheric Chemistry and Physics 51053-1123.

Lamb, B., Gay, D., Westberg, H., and Pierce, T., 1993. A Biogenic Hydrocarbon Emission Inventory for the USA Using a Simple Forest Canopy Model. Atmospheric Environment Part a-General Topics 27(11), 1673-1690.

Lathiere, J., Hauglustaine, D. A., De Noblet-Ducoudre, N., Krinner, G., and Folberth, G. A., 2005. Past and Future Changes in Biogenic Volatile Organic Compound Emissions Simulated With a Global Dynamic Vegetation Model. Geophysical Research Letters 32(20), doi:10.1029/2005GL024164.

Nakićenović, N., J. Alcamo, G. Davis, B. de Vries, B. Fenhann, S. Gaffin, Gregory K., A. Grübler, T. Y. Jung, T. Kram, E. L. La Rovere, E. L. Michaelis, S. Mori, T. Morita, W. Pepper, H. Pitcher, L. Price, K. Raihi, A. Roehrl, H.-H. Rogner, A. Sankovski, M. Schlesinger, P. Shukla, S. Smith, R. Swart, S. van Rooijen, N. Victor, and Z. Dadi, IPCC Special Report on Emissions Scenarios, Cambridge University Press, Cambridge, United Kingdom and New York, NY, USA, 2000.

O'Neill, S. M., Lamb, B. K., Chen, J., Claiborn, C., Finn, D., Otterson, S., Figueroa, C., Bowman, C., Boyer, M., Wilson, R., Arnold, J., Aalbers, S., Stocum, J., Swab, C., Stoll, M., Dubois, M., and Anderson, M., 2006. Modeling Ozone and Aerosol Formation and Transport in the Pacific Northwest with the Community Multi-Scale Air Quality (CMAQ) Modeling System. Environmental Science & Technology 40(4), 1286-1299.

Palmer, P. I., Abbot, D. S., Fu, T. M., Jacob, D. J., Chance, K., Kurosu, T. P., Guenther, A., Wiedinmyer, C., Stanton, J. C., Pilling, M. J., Pressley, S. N., Lamb, B., and Sumner, A. L., 2006. Quantifying the Seasonal and Interannual Variability of North American Isoprene Emissions Using Satellite Observations of the Formaldehyde Column. Journal of Geophysical Research-Atmospheres

111(D12), doi:10.1029/2005JD006689.

Sanderson, M. G., Jones, C. D., Collins, W. J., Johnson, C. E., and Derwent, R. G., 2003. Effect of Climate Change on Isoprene Emissions and Surface Ozone Levels. Geophysical Research Letters 30(18), doi:10.1029/2003GL017642.

Schell, B., Ackermann, I. J., Hass, H., Binkowski, F. S., and Ebel, A., 2001. Modeling the Formation of Secondary Organic Aerosol Within a Comprehensive Air Quality Model System. Journal of Geophysical Research-Atmospheres 106(D22), 28275-28293.

Smyth, S. C., Jiang, W. M., Yin, D. Z., Roth, H., and Giroux, T., 2006. Evaluation of CMAQ O_3 and $PM_{2.5}$ Performance Using Pacific 2001 Measurement Data. Atmospheric Environment 40(15), 2735-2749.

Theobald, D. M., 2005. Landscape Patterns of Exurban Growth in the Usa From 1980 to 2020. Ecology and Society 10(1), [online] http://www.ecologyandsociety.org/vol10/iss1/art32/.

Tsigaridis, K. and Kanakidou, M., 2003. Global Modelling of Secondary Organic Aerosol in the Troposphere: a Sensitivity Analysis. Atmospheric Chemistry and Physics 31849-1869.

U.S. EPA, 2004. Economic Growth Analysis System (EGAS) version 5.0 User Manual. U.S. Environmental Protection Agency, [online] http://www.epa.gov/ttn/ecas/egas5.htm.

Washington, W. M., Weatherly, J. W., Meehl, G. A., Semtner, A. J., Bettge, T. W., Craig, A. P., Strand, W. G., Arblaster, J., Wayland, V. B., James, R., and Zhang, Y., 2000. Parallel Climate Model (PCM) Control and Transient Simulations. Climate Dynamics 16(10-11), 755-774.

Wiedinmyer, C., Greenberg, J., Guenther, A., Hopkins, B., Baker, K., Geron, C., Palmer, P. I., Long, B. P., Turner, J. R., Petron, G., Harley, P., Pierce, T. E., Lamb, B., Westberg, H., Baugh, W., Koerber, M. , and Janssen, M., 2005. Ozarks Isoprene Experiment (Ozie): Measurements and Modeling of the "Isoprene Volcano". Journal of Geophysical Research-Atmospheres 110(D18), doi:10.1029/2005JD005800.

Wiedinmyer, C., Tie, X. X., Guenther, A., Neilson, R., and Granier, C., 2006. Future Changes in Biogenic Isoprene Emissions: How Might They Affect Regional and Global Atmospheric Chemistry? Earth Interactions 10doi:10.1175/EI174.1.

Yu, J. Z., Griffin, R. J., Cocker, D. R., Flagan, R. C., Seinfeld, J. H., and Blanchard, P., 1999. Observation of Gaseous and Particulate Products of Monoterpene Oxidation in Forest Atmospheres. Geophysical Research Letters 26(8), 1145-1148.

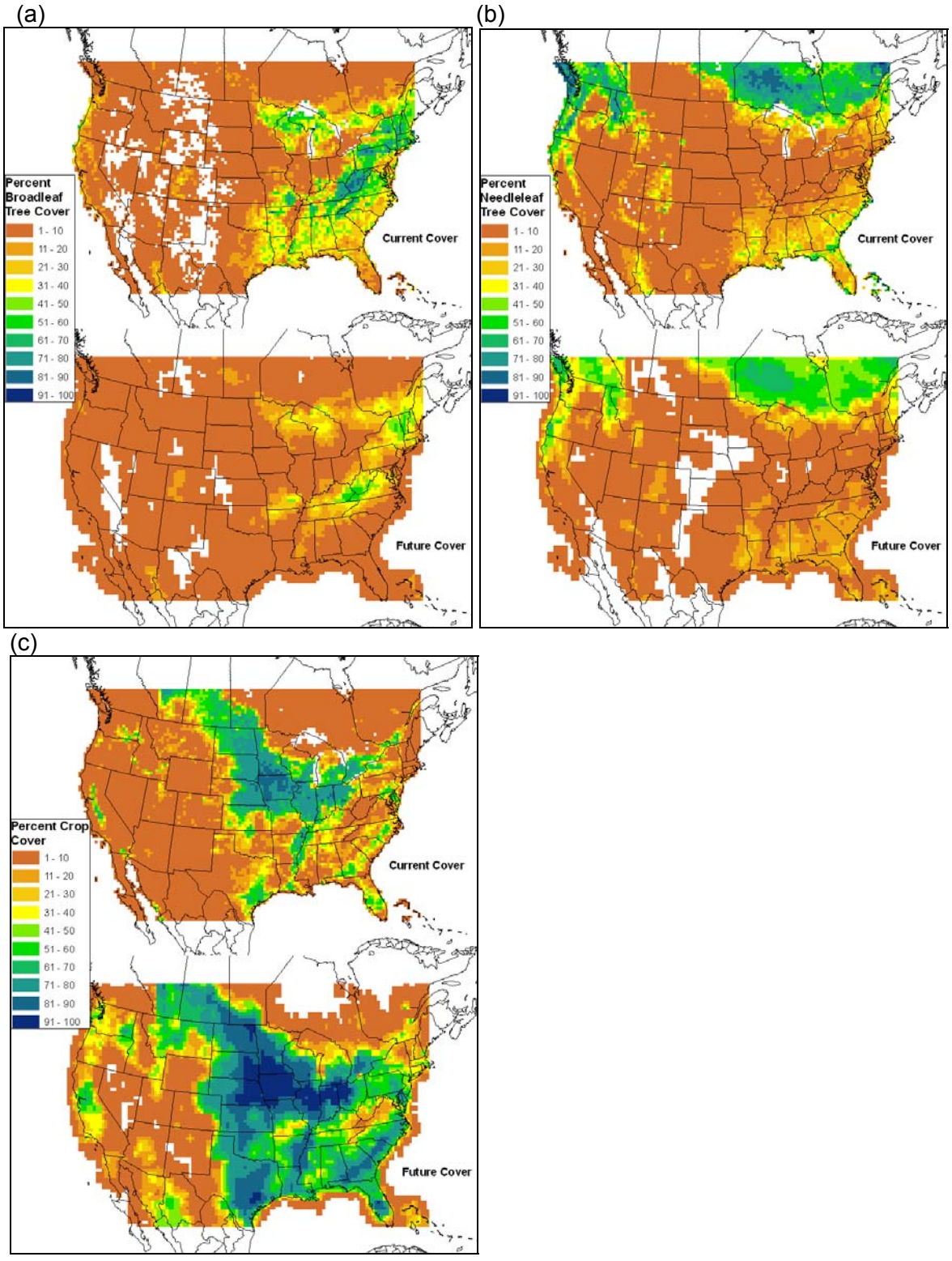

Figure 1: Estimated percent land cover for current (top) and future (bottom) scenario for (a) broadleaf trees, (b) needleleaf trees and (c) cropland.

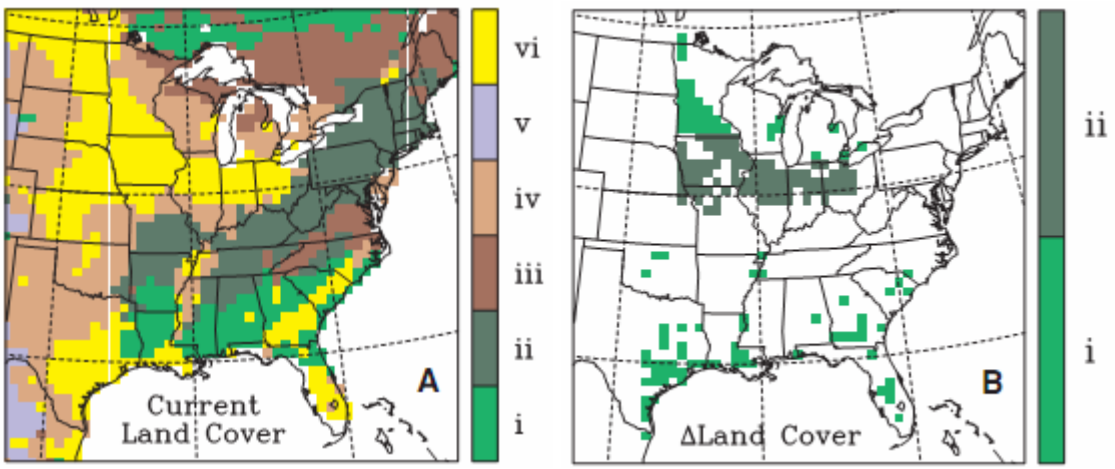

Figure 2: Estimated changes in future LULC by plant functional types. The afforestation scenario in Figure (B) is used in Case 4. Figure (A), shows current LULC for (i) evergreen needleleaf forest, (ii) deciduous broadleaf forest, (iii) other forest, (iv) grass/shrubland, (v) desert/semi-desert, and (vi) farmland. Figure (B), depicts regions where crops and pasture are replaced by (i) softwood and (ii) hardwood plantations (Figure adapted from Jackson et al. 2005).

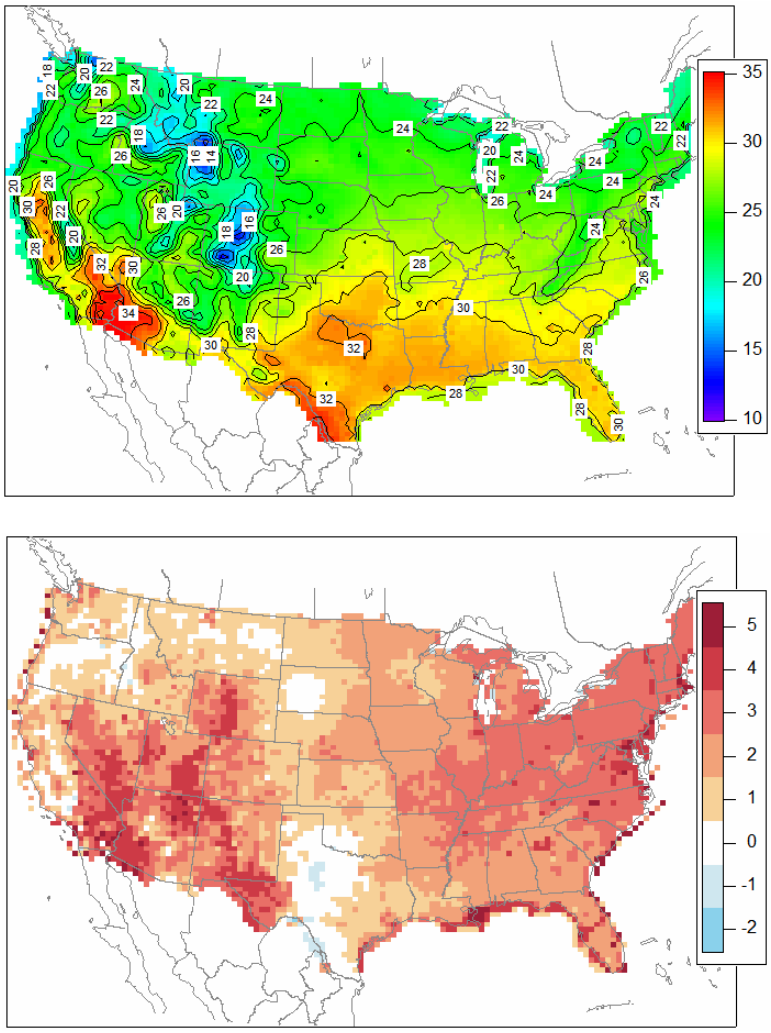

Figure 3: Simulated mean July daily maximum ground level temperature (top) and simulated temperature change from 2000 to 2045 (°C)

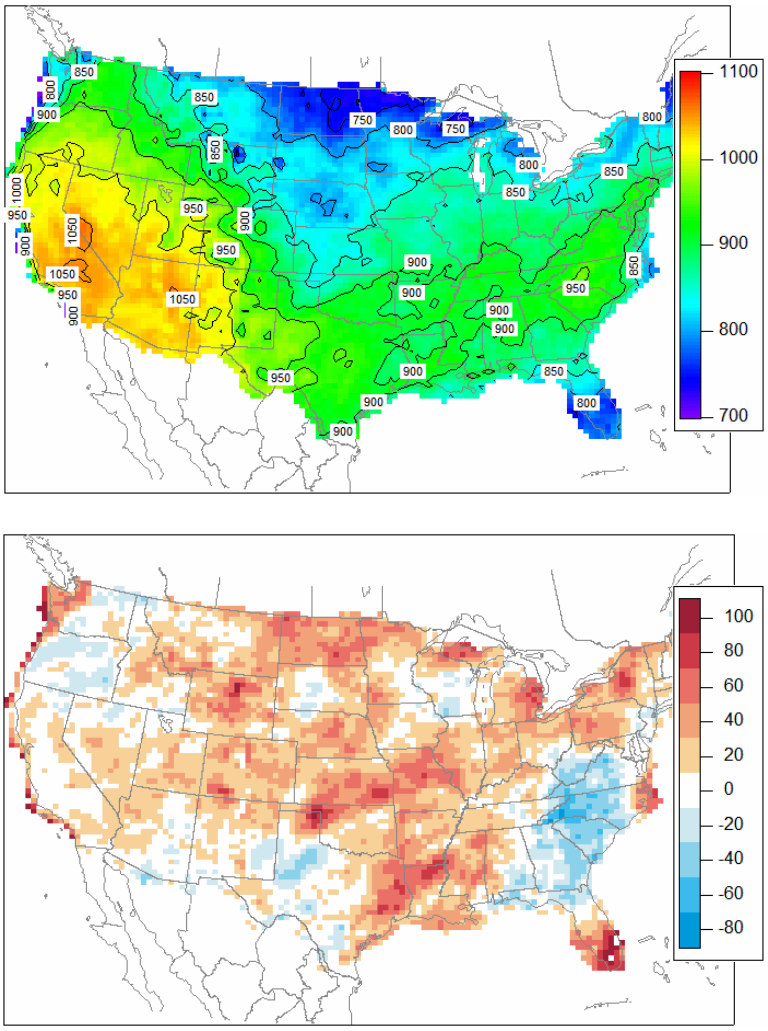

Figure 4: Simulated mean July daily maximum ground level solar radiation (top) and simulated change in ground level solar radiation from 2000 to 2045 (W/m^2)

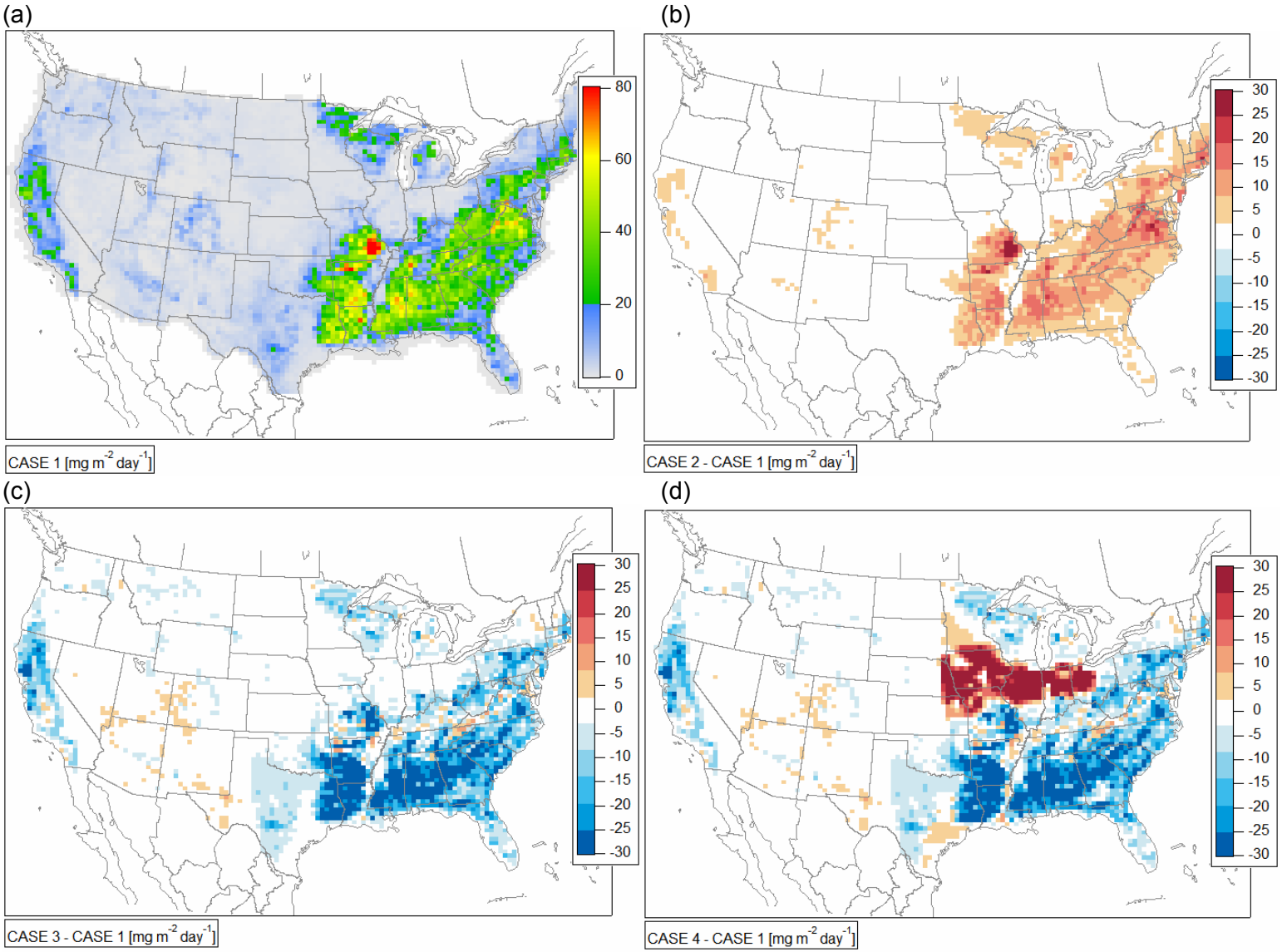

Figure 5: Mean July daily isoprene emissions for the current base-case (Plate a) and magnitude of emission differences between future cases and the current base-case (Plates b, d and d).

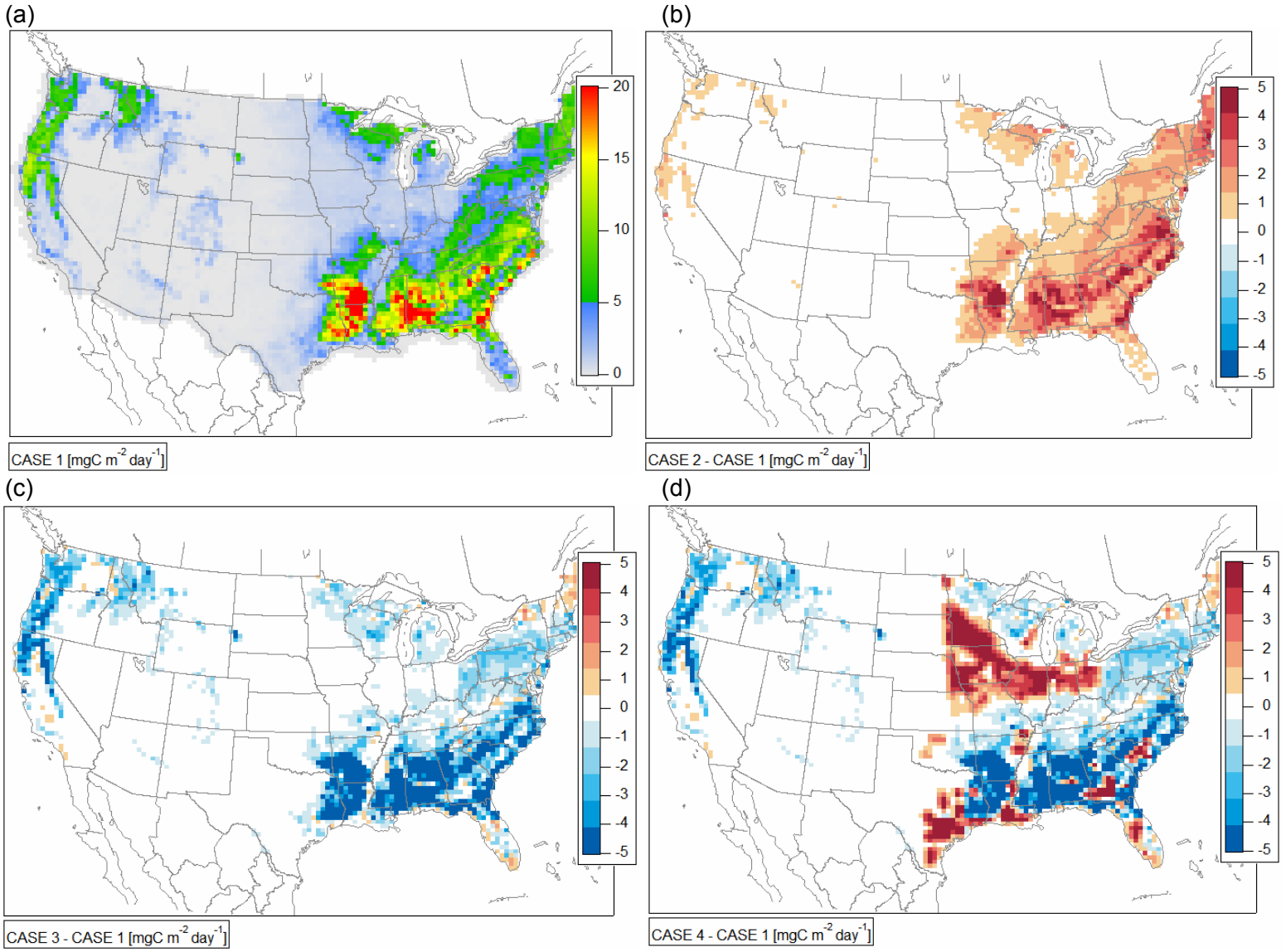

Figure 6: Mean July daily monoterpene emissions for the current base-case (Plate a) and magnitude of emission differences between future cases and the current base-case (Plates b, c and d).

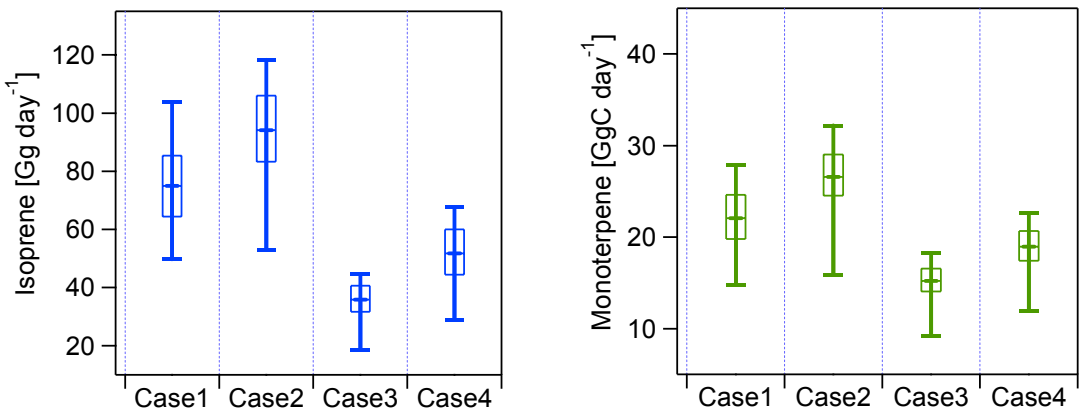

Figure 7: Total US continental emissions and the emission variability across the simulated July months for isoprene (left) and monoterpene (right). The top and bottom whiskers represent maximum and minimum values, the box indicates 80th, and 20th percentile values with overall average marked by the middle.

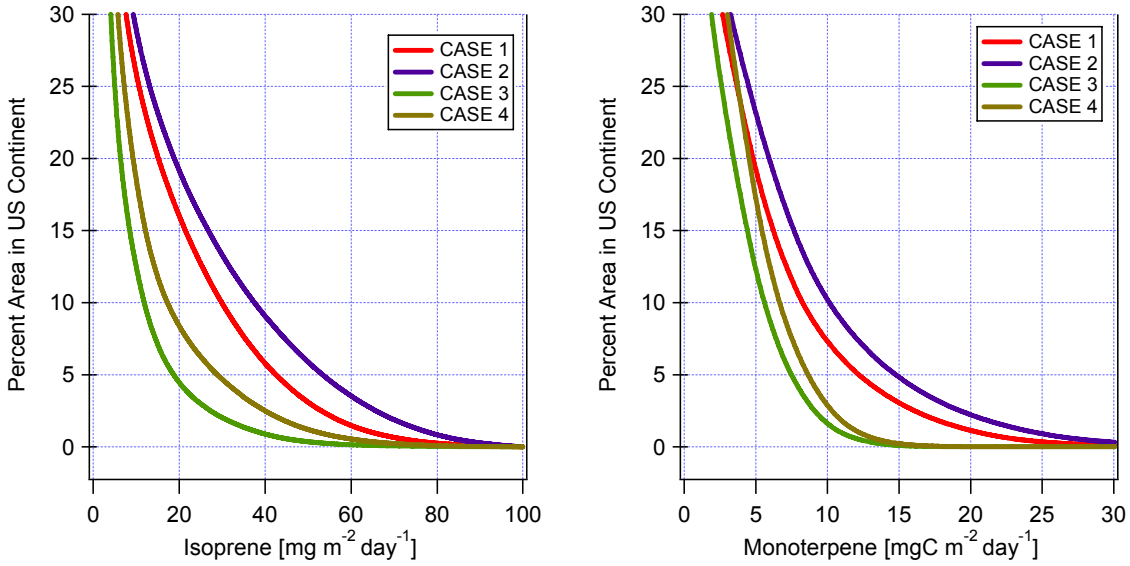

Figure 8: Percent area in US continent with daily isoprene (left) and monoterpene (right) emission rates exceeding values on the x-axis for the four cases.

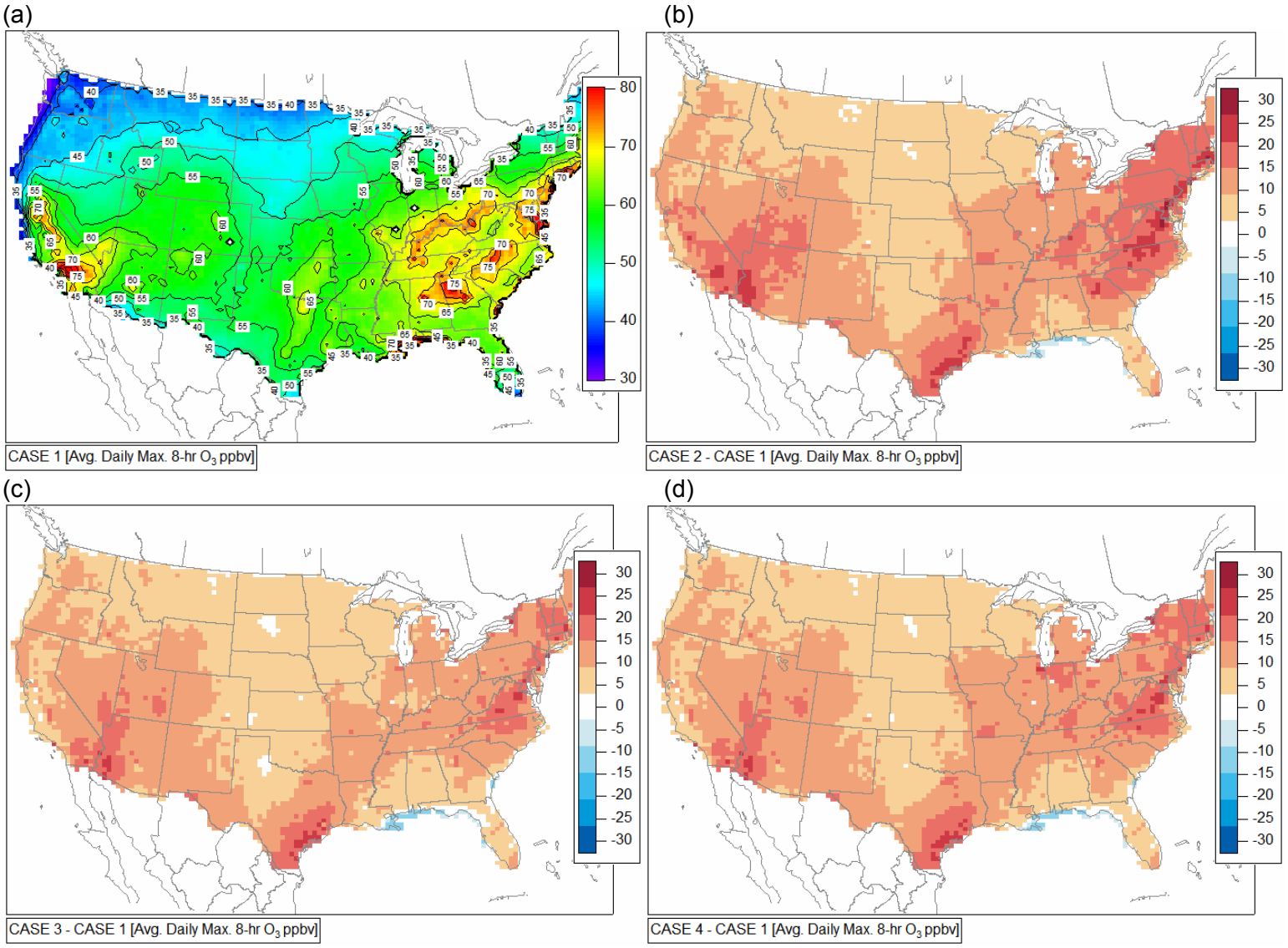

Figure 9: Mean July daily maximum 8-hr ozone concentrations for the current base-case (Plate a) and differences between future cases and the current base-case (Plates b, c and d).

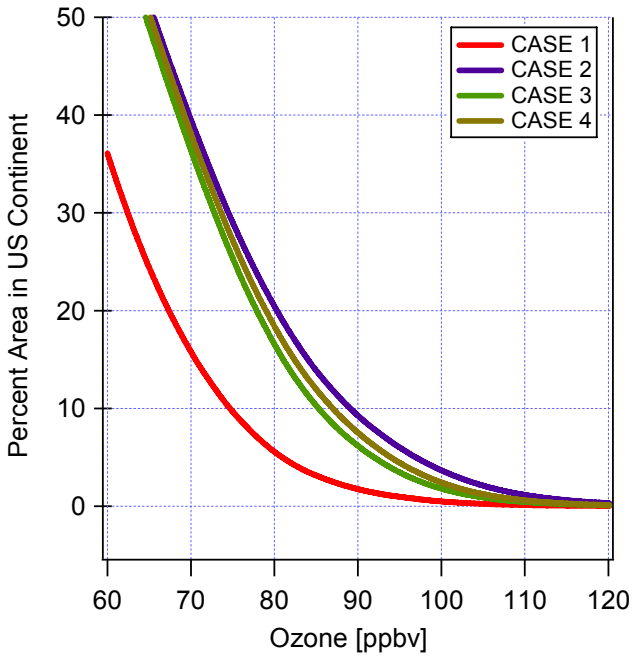

Figure 10: Percent area in US continent with modeled daily maximum 8-hr ozone concentrations exceeding values on the x-axis for the four cases.

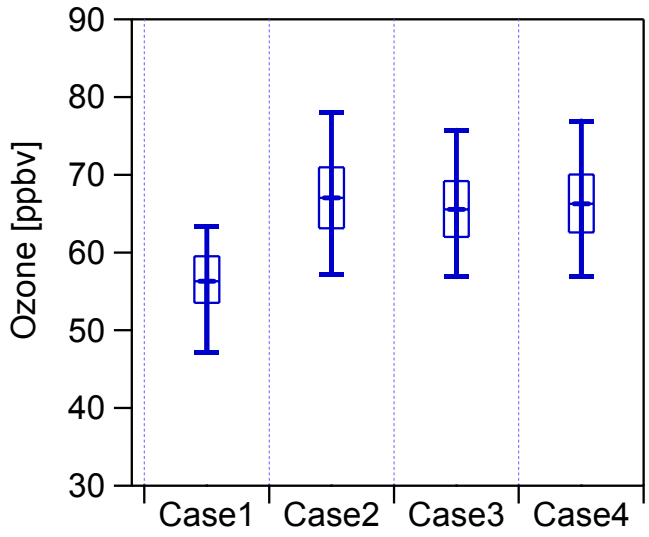

Figure 11: Continental averaged daily maximum 8-hr ozone concentration ranges across the five simulate July months for the four cases. The top and bottom whiskers represent maximum and minimum values, the box indicates 80th, and 20th percentile values with overall average marked by the middle.

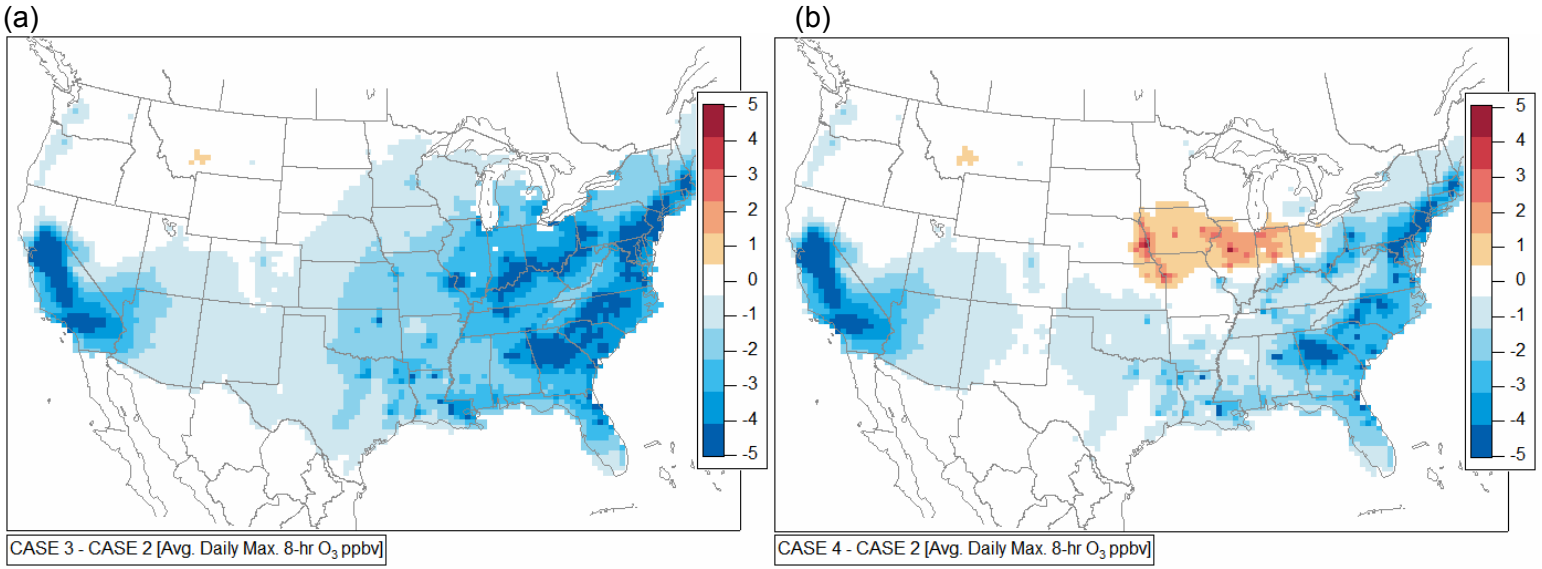

Figure 12: Mean July daily maximum 8-hr ozone concentration differences between Case 3 and Case 2 (Plate a), and Case 4 and Case 2 (Plate b).

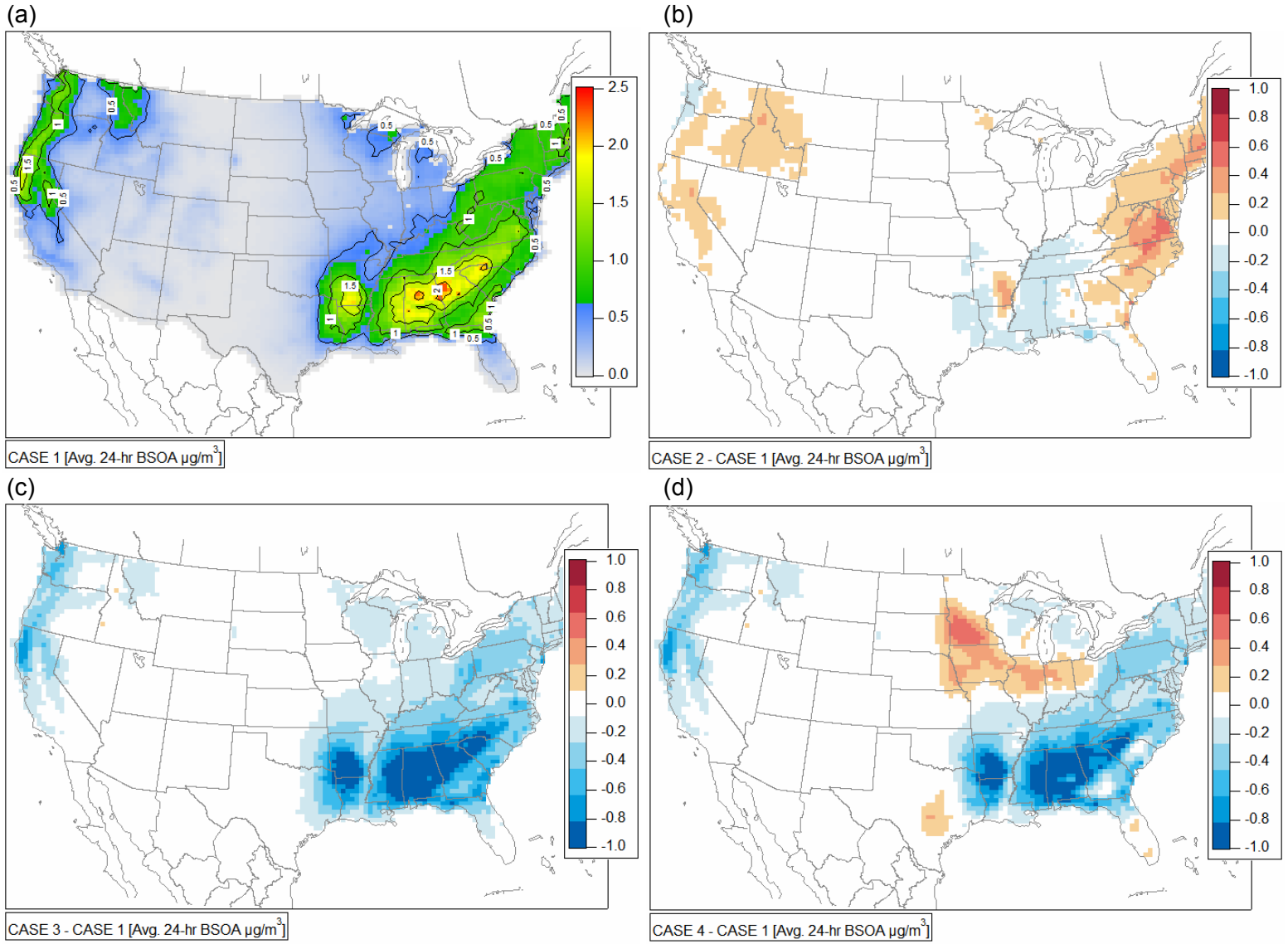

Figure 13: Mean July 24-hr BSOA concentrations for the current base-case (Plate a) and differences between future cases and the current base-case (Plates b, c and d).

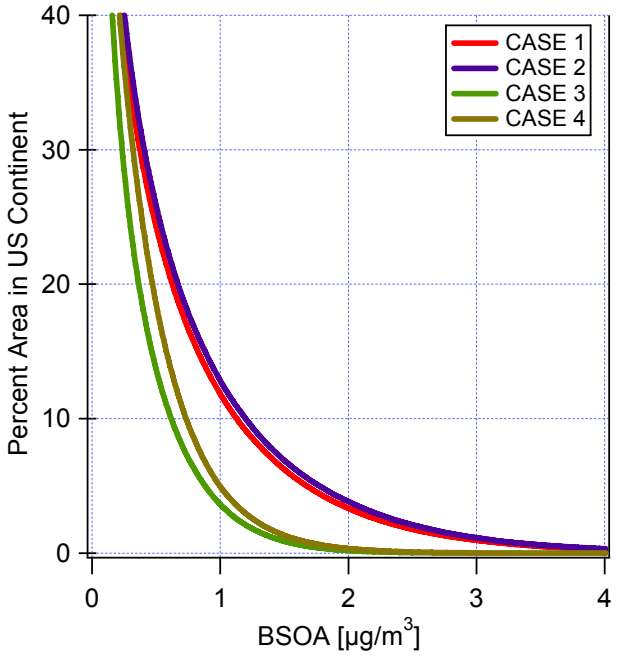

Figure 14: Percent area in US continent with modeled average 24-hr BSOA concentrations exceeding values on the x-axis for the four cases.

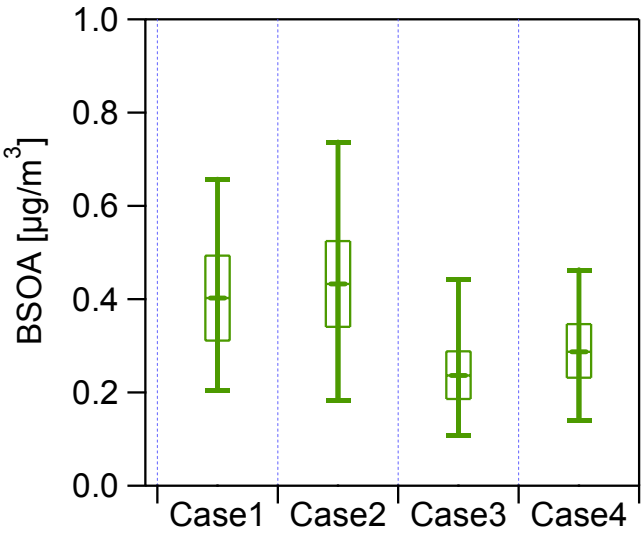

Figure 15: Continental averaged 24-hr BSOA concentration ranges across the five simulate July months for the four cases. The top and bottom whiskers represent maximum and minimum values, the box indicates 80th, and 20th percentile values with overall average marked by the middle.

Table 1: Summary of climate and LULC model scenarios

Case Name	Anthropogenic Emissions	Meteorology Condition	Land Use and Land Cover	Remark
Case 1	Current	Current	Current	Present base-case
Case 2	Future	Future	Current	Future meteorology driven biogenic emissions
Case 3	Future	Future	Future	IPCC A2 agriculture scenario
Case 4	Future	Future	Future	Afforestation scenario for carbon sequestration

CHAPTER FIVE

Summary and Conclusions

This research implemented and evaluated two numerical air quality forecast systems. The first was designed for short-term daily forecasts of air pollution concentrations for Pacific Northwest. The second was a long-range prediction system to assess the effects of global change upon US regional air quality 50 years into the future.

Development, Implementation, and Evaluation of Short-Term Air Quality Forecast System

As a significant upgrade to the existing AIRPACT-2 air quality forecast system, a new real-time numerical air quality, modeling framework was successfully developed, implemented, and evaluated. The new system, AIRPACT-3, used the MM5/SMOKE/CMAQ model framework with the latest scientific algorithms and improved model inputs. The new system produces hourly ozone and fine particulate matter (PM) concentration forecasts for Washington, Oregon and Idaho states, and their bordering areas on a daily basis.

The AIRPACT-3 forecast system was evaluated for the August – November 2004 period and compared with available observational data for the Pacific Northwest. Results showed that the system performed well for ground level ozone and $PM_{2.5}$ concentrations. AIRPACT-3 was competent in predicting a broad range of episodic ozone concentrations. The system, however, systematically over-predicted at low concentrations. The system accurately predicted the timing of daily peak ozone concentrations to within 3 hours of the observed daily maximum. For $PM_{2.5}$ forecasts, the system correctly predicted variations in total mass concentrations between urban

and rural regions. Moreover, the system captured speciated fine PM component characteristics, especially for nitrate and ammonium fine aerosols. Due to insufficient model resolution for resolving complex regional topography in the Columbia River Gorge, the system performed poorly for speciated PM at sites in this region.

Overall, the new AIRPACT-3 system outperformed the existing short-range air quality forecast system. The model enhancements offered by the AIRPACT-3 system included the following:

- The inclusion of emissions processing with real-time wild and prescribed fire emissions from the Bluesky system.
- The incorporation of updated anthropogenic emissions based on the EPA NEI-2002 inventory and with emission data projected to 2005.
- The addition of a dynamic dairy ammonia emissions module.
- The improvement of dynamic boundary conditions from long-term averaged global chemical model.
- The introduction of dynamic initial conditions to enhance model continuity.
- The integration of explicit PM treatment with chemistry for inorganic and organic secondary aerosols.

Long-Range Prediction of US Regional Air Quality Using Coupled Global and Regional Scale Modeling Systems

The coupling of global and regional scale modeling systems was developed for the first time to study and quantify the US regional air quality from the impacts of global changes 50 years in the future. The model approach was novel in the following ways:

- The entire modeling system was driven by a single global climate model designed explicitly for scenario consistency.
- The interface between the global climate model and the regional meteorological model effectively captured the global climate influence on regional meteorology.
- The boundary conditions for the regional air quality model, provided by the global chemistry model, represented realistic changes in general global pollution concentrations.

- The projections of land use and land cover, based on future climate change and probable anthropogenic perturbations, were accounted for in the modeling system.
- Regional anthropogenic emissions were projected to the future based on predicted economic and population growth, as well as estimated expansion in urban areas.
- Biogenic emissions were generated from predicted changes in vegetation distributions and future regional meteorology.
- The entire model system was applied for two 10-year periods: 1990-1999 as base-case and 2045-2054 as future-case. The long-term simulations captured large-scale signals from global change, while minimizing the inter-annual variability irrespective of climate.

The system was first evaluated with 10-year measurement ozone records across the US continent. The system adequately captured the episodic ozone conditions and the spatial distribution of ozone pollution across the continent.

The long term simulations were based upon the Intergovernmental Panel on Climate Change (IPCC) A2, business-as-usual, global emissions scenario. For this case and using projected US anthropogenic emissions from the EPA Economic Growth Analysis System (EGAS), results showed deteriorating ozone conditions, with higher 8-hr ozone concentrations, for both episodic and non-episodic pollution events. Spatially, the system predicted expansion of urban air pollution footprints over much wider rural regions. For selected sites downwind of urban cities, episodic ozone occurrences were predicted to begin earlier and end later in the year. Furthermore, the duration of each pollution event was predicted to lengthen, with more consecutive days which ozone concentrations exceed the EPA 80 ppbv national standard.

Application of Long-Range Forecast System

Biogenic VOC are significant precursors to regional air pollution. Future changes in land use and land cover (LULC) can substantially affect the level of biogenic emissions and thus regional air quality. However, the effects of future LULC on regional air quality are seldom examined.

The long-range forecast system was applied to study the effects of future LULC scenarios on estimated biogenic emissions and future air pollution conditions. The system was applied to five July months for each of the four cases studied. The results of the three future cases in 2045 were compared to a base-case, Case 1, in 1990. Results showed the future case with current LULC and future climate (Case 2) to have the highest isoprene and monoterpene emission rates. However, if agriculture land use were to dominate the US continent in the future, biogenic isoprene and monoterpene emissions are reduced significantly (Cases 3 and 4) with respect to the base-case.

Inferior future regional air quality was forecasted for all three future cases irrespective of future LULC, with higher continental mean daily maximum 8-hr ozone concentrations with respect to the base-case. The large increase of ozone concentration was due to the combined effects of future warmer temperature, higher projected anthropogenic emissions, and elevated global pollution background concentrations. Future biogenic secondary organic aerosol (BSOA) was dependent largely on monoterpene emissions and thus, on future LULC. A reduction in future monoterpene emission (Cases 3 and 4) caused a decrease in the mean 24-hr BSOA concentrations, with respect to the base-case; while a higher future monoterpene emission was predicted to increase the level of BSOA (Case 2). These results of the long-range forecast system demonstrated the strong interconnectivity of global change and anthropogenic influences towards biogenic emissions and regional air pollution.

Future Directions

The evaluation of AIRPACT-3 short-range forecast system showed satisfactory performance. AIRPACT-3, being an operational forecast system, requires systematic and continuous evaluations in concert with input data assessments. Maintaining long-term records of model performance will provide more accurate performance evaluations including seasonal

forecast variability, and performance changes associated with model configurations. Furthermore, evaluating forecast performance together with input data, such as the MM5 meteorology, can provide valuable information on sources of the error in the overall model framework. Additional improvements to AIRPACT-3 may also include nested model simulations over regions of complex topography. By nesting down to 4-km grid resolution within the current 12-km domain, the system can take advantage of the available high resolution MM5 forecasts to better resolve complex pollution transport from the initial 12-km forecast.

The long-range air quality forecast system was applied to study the impact of global change on regional quality. Evaluation showed the system captured the high ozone pollutions, but were less effective in capturing the lower ozone concentrations. Additional sensitivity simulations can be applied to improve the base-case simulation through better representations of past regional emissions. Since ozone pollution is highly sensitive to changes in emission and global pollution background, multiple future scenarios based on varying climate, LULC, and emission projections, are necessary to address the range of possible future air quality conditions, and to provide degree of uncertainty to the current pollution estimate.

The sensitivity of LULC scenarios on future emission estimates and secondary pollution conditions was demonstrated using the long-range forecast system. Overall confidence in the model results would improve with the increase number of scenarios. The forecast system would benefit from the development of future LULC scenario driven by potential future global climate conditions. A well-established future LULC should be used to drive regional simulations, including regional meteorology and emission estimates, for consistent representations of future environments. Only through these fundamental and consistent adjustments to model input can one improve representation of the tightly coupled biosphere-atmosphere interactions.

APPENDIX

Appendix A: Supplementary Material for Chapter One

SAPRC-99 gas-phase chemical mechanism species and their descriptions (adapted from Carter, 2000)

Mechanism Species	Species Descriptions
NO2	Nitrogen dioxide
NO	Nitric oxide
O3P	Ground state oxygen atoms
O3	Ozone
NO3	Nitrate radical
N2O5	Nitrogen pentoxide
HNO3	Nitric acide
O1D2	Excited oxygen atom
HO	Hydroxyl radicals
HONO	Nitrous acid
HO2	Hydroperoxide radicals
CO	Carbon monoxide
HNO4	Peroxynitric acid
HO2H	Hydrogen peroxide
SO2	Sulfer dioxide
SULF	Sulfates (SO_3 or H_2SO_4)
C_O2	Methyl peroxy radicals
HCHO	Formaldehyde
COOH	Methyl hydroperoxide
MEOH	Methanol
RO2_R	Peroxy radical operator representing NO to NO_2 conversion with HO_2 formation
ROOH	Lumped higher organic hydroperoxides
R2O2	Peroxy radical operator representing NO to NO_2 conversion without HO_2 formation
RO2_N	Peroxy radical operator representing NO consumption with organic nitrate formation
RNO3	Lumped Organic Nitrates
MEK	Ketones and other non-aldehyde oxygenated products which react with OH radicals slower than 5E-12 cm^3 $molec^{-2}$ sec^{-1}
PROD2	Ketones and other non-aldehyde oxygenated products which react with OH radicals faster than 5E-12 cm^3 $molec^{-2}$ sec^{-1}
CCO_O2	Acetyl peroxy radicals
PAN	Peroxy acetyl nitrate
CCO_OOH	Peroxy acetic acid
CCO_OH	Acetic acid
RCO_O2	Peroxy propionyl and higher peroxy acyl radicals
PAN2	Peroxypropionyl nitrate and other higher alkyl PAN analogues
CCHO	Acetaldehyde
RCO_OOH	Higher organic peroxy acids
RCO_OH	Higher organic acids
BZCO_O2	Peroxyacyl radical formed from aromatic aldehydes
PBZN	PAN analogues formed from aromatic aldehydes

BZ_O	Phenoxy radicals
MA_RCO3	Peroxyacyl radicals formed from methacrolein and other acroleins
MA_PAN	PAN analogue formed from methacrolein
TBU_O	t-Butoxy radicals
ACET	Acetone
NPHE	Nitrophenols
PHEN	Phenol
BZNO2_O	Nitro-substituted phenoxy radical
HOCOO	Radical formed when Formaldehyde reacts with HO_2
HCOOH	Formic acid
RCHO	Lumped C3+ aldehydes
GLY	Glyoxal
MGLY	Methyl glyoxal
BACL	Biacetyl
CRES	Cresols
BALD	Aromatic aldehydes (e.g., benzaldehyde)
METHACRO	Methacrolein
MVK	Methyl Vinyl Ketone
ISOPROD	Lumped isoprene product species
DCB1	Reactive aromatic fragmentation products that do not undergo significant photodecomposition to radicals
DCB2	Reactive aromatic fragmentation products which photolyze with alpha-dicarbonyl-like action spectrum
DCB3	Reactive aromatic fragmentation products which photolyze with acrolein action spectrum
ETHENE	Ethene
ISOPRENE	Isoprene
TRP1	Terpenes
ALK1	Alkanes and other non-aromatic compounds that react only with OH, and have kOH < 5E2 ppm^{-1} min^{-1}. (Primarily ethane)
ALK2	Alkanes and other non-aromatic compounds that react only with OH, and have kOH between 5E2 and 2.5E3 ppm^{-1} min^{-1}. (Primarily propane and acetylene)
ALK3	Alkanes and other non-aromatic compounds that react only with OH, and have kOH between 2.5E3 and 5E3 ppm^{-1} min^{-1}
ALK4	Alkanes and other non-aromatic compounds that react only with OH, and have kOH between 5E3 and 1E4 ppm^{-1} min^{-1}
ALK5	Alkanes and other non-aromatic compounds that react only with OH, and have kOH greater than 1E4 ppm^{-1} min^{-1}
ARO1	Aromatics with kOH < 2E4 ppm^{-1} min^{-1}
ARO2	Aromatics with kOH > 2E4 ppm^{-1} min^{-1}
OLE1	Alkenes (other than ethene) with kOH < 7E4 ppm^{-1} min^{-1}
OLE2	Alkenes (other than ethene) with kOH > 7E4 ppm^{-1} min^{-1}
ALK5AER	Oxidized ALK5 for secondary organic aerosol module
ARO1AER	Oxidized ARO1 for secondary organic aerosol module
ARO2AER	Oxidized ARO2 for secondary organic aerosol module
OLE2AER	Oxidized OLE2 for secondary organic aerosol module
SULAER	Oxidized SULF for secondary organic aerosol module
TRP1AER	Oxidized TRP1 for secondary organic aerosol module
CRESAER	Oxidized CRES for secondary organic aerosol module

Appendix B: Supplementary Material for Chapter Two

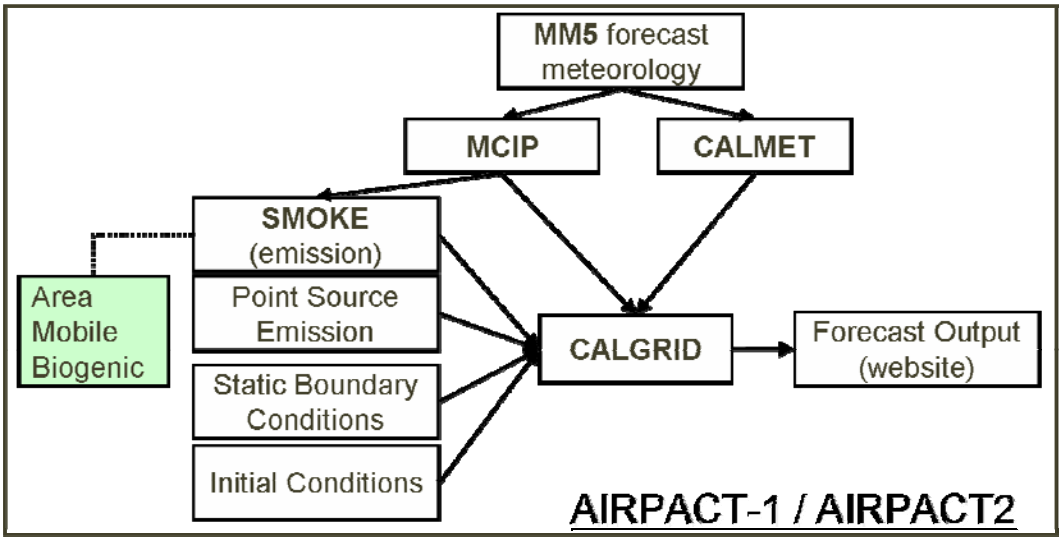

Schematics of the old AIRPACT-1 and AIRPACT-2 short-range air quality forecast system model framework

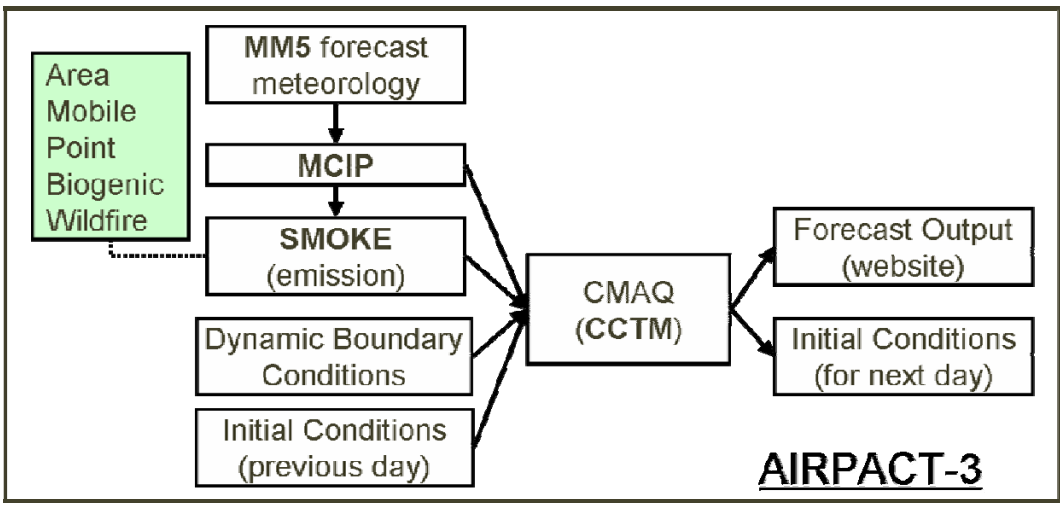

Schematics of the new AIRPACT-3 short-range air quality forecast system model framework

Equations of Model Performance Statistics

Statistics	Formula
Mean Bias (MB)	$\frac{1}{N}\sum_{i=1}^{N}\left(C_{\mathrm{mod}i}-C_{\mathrm{obs}i}\right)$
Mean Error (ME)	$\frac{1}{N}\sum_{i=1}^{N}\left\lvert C_{\mathrm{mod}i}-C_{\mathrm{obs}i}\right\rvert$
Normalized Mean Bias (NMB) (%)	$\frac{1}{N}\frac{\sum_{i=1}^{N}\left(C_{\mathrm{mod}i}-C_{\mathrm{obs}i}\right)}{\sum_{i=1}^{N}C_{\mathrm{obs}i}}$
Normalized Mean Error (NME) (%)	$\frac{1}{N}\frac{\sum_{i=1}^{N}\left\lvert C_{\mathrm{mod}i}-C_{\mathrm{obs}i}\right\rvert}{\sum_{i=1}^{N}C_{\mathrm{obs}i}}$
Fractional Bias (FB) (%)	$\frac{1}{N}\sum_{i=1}^{N}\frac{\left(C_{\mathrm{mod}i}-C_{\mathrm{obs}i}\right)}{0.5\left(C_{\mathrm{mod}i}+C_{\mathrm{obs}i}\right)}$
Fractional Error (FE) (%)	$\frac{1}{N}\sum_{i=1}^{N}\frac{\left\lvert\left(C_{\mathrm{mod}i}-C_{\mathrm{obs}i}\right)\right\rvert}{0.5\left(C_{\mathrm{mod}i}+C_{\mathrm{obs}i}\right)}$
Correlation Coefficient (R)	$\frac{\sum_{i=1}^{N}\left(C_{\mathrm{mod}i}-\overline{C_{\mathrm{mod}}}\right)\left(C_{\mathrm{obs}i}-\overline{C_{\mathrm{obs}}}\right)}{\left[\sum_{i=1}^{N}\left(C_{\mathrm{mod}i}-\overline{C_{\mathrm{mod}}}\right)^{2}\cdot\sum_{i=1}^{n}\left(C_{\mathrm{obs}i}-\overline{C_{\mathrm{obs}}}\right)^{2}\right]^{1/2}}$
Root Mean Square Error (RMSE)	$\left[\frac{1}{N}\sum_{i=1}^{n}\left(C_{\mathrm{mod}i}-C_{\mathrm{obs}i}\right)^{2}\right]^{1/2}$

N = Total number of paired data

$C_{\mathrm{mod}i}$ = modeled concentration

$C_{\mathrm{obs}i}$ = observed concentration

$$\overline{C_{\mathrm{mod}}}=\frac{\sum_{i=1}^{N}C_{\mathrm{mod}i}}{N}$$

$$\overline{C_{\mathrm{obs}}}=\frac{\sum_{i=1}^{N}C_{\mathrm{obs}i}}{N}$$

Appendix C: Supplementary Material for Chapter Three

Regional emission summary by source categories

Anthropogenic Emissions

	kilotons/year		kilotons/day		
Area	**1990**	**2045**	**1990**	**2045**	**Ratio**
CO	16367	21482	45	59	1.31
NOX	1704	2682	5	7	1.57
VOC	8601	17299	24	47	2.01
SO2	1265	1929	4	5	1.52

Non-road Mobile	**1990**	**2045**	**1990**	**2045**	**Ratio**
CO	22092	25220	61	69	1.14
NOX	3978	4413	11	12	1.11
VOC	2526	3426	7	9	1.36
SO2	462	638	1	2	1.38

On-road Mobile	**1990**	**2045**	**1990**	**2045**	**Ratio**
CO	67022	66455	184	182	0.99
NOX	8196	8132	23	22	0.99
VOC	5534	5439	15	15	0.98
SO2	294	291	1	1	0.99

Point	**1990**	**2045**	**1990**	**2045**	**Ratio**
CO	4117	4117	11	11	1.00
NOX	8426	8426	23	23	1.00
VOC	1642	1642	5	5	1.00
SO2	15250	15250	42	42	1.00

Natural Sources Emissions

	kilotons/year		kilotons/day		
Wild-Fire	**1990**	**2045**	**1990**	**2045**	**Ratio**
CO	535	666	1.5	2	1.25
TOG	43	53	0.1	0.2	1.24

Biogenic	**kilotons/July**		**kilotons/day**		
	1990	**2045**	**1990**	**2045**	**Ratio**
ISOPRENE	2269	943	73	30	0.42
MONOTERPENE	734	462	23	15	0.63
OVOC	1024	994	33	32	0.97
Total BVOC	4027	2399	130	77	0.60
NO	116	121	4	4	1.04

Summary of point source emissions by state in the regional domain for the current base-case (left), and the projected future case to current case emission ratios (right).

	Point Source Emission					Future/Current Emission Ratio				
(Kilotons/year)	CO	NOX	VOC	NH3	SO2	CO	NOX	VOC	NH3	SO2
Alabama	168	288	70	1	651	1.0	1.0	1.0	1.0	1.0
Arizona	13	118	9	0	106	1.0	1.0	1.0	1.0	1.0
Arkansas	106	103	31	1	134	1.0	1.0	1.0	1.0	1.0
California	93	123	65	14	42	1.0	1.0	1.0	1.0	1.0
Colorado	43	112	38	0	102	1.0	1.0	1.0	1.0	1.0
Connecticut	6	19	6	0	48	1.0	1.0	1.0	1.0	1.0
Delaware	21	20	6	1	77	1.0	1.0	1.0	1.0	1.0
Washington DC	0	1	0	0	2	1.0	1.0	1.0	1.0	1.0
Florida	171	390	49	2	813	1.0	1.0	1.0	1.0	1.0
Georgia	207	280	41	5	595	1.0	1.0	1.0	1.0	1.0
Idaho	25	11	4	1	17	1.0	1.0	1.0	1.0	1.0
Illinois	121	407	99	9	956	1.0	1.0	1.0	1.0	1.0
Indiana	439	437	74	3	1048	1.0	1.0	1.0	1.0	1.0
Iowa	12	109	11	4	249	1.0	1.0	1.0	1.0	1.0
Kansas	99	178	31	1	134	1.0	1.0	1.0	1.0	1.0
Kentucky	105	359	67	1	700	1.0	1.0	1.0	1.0	1.0
Louisiana	201	347	91	11	294	1.0	1.0	1.0	1.0	1.0
Maine	9	16	3	0	33	1.0	1.0	1.0	1.0	1.0
Maryland	116	133	8	0	318	1.0	1.0	1.0	1.0	1.0
Massachusetts	12	60	11	0	147	1.0	1.0	1.0	1.0	1.0
Michigan	92	302	53	0	481	1.0	1.0	1.0	1.0	1.0
Minnesota	29	150	27	1	124	1.0	1.0	1.0	1.0	1.0
Mississippi	70	184	61	1	213	1.0	1.0	1.0	1.0	1.0
Missouri	104	221	33	4	374	1.0	1.0	1.0	1.0	1.0
Montana	51	58	7	0	47	1.0	1.0	1.0	1.0	1.0
Nebraska	10	56	8	0	67	1.0	1.0	1.0	1.0	1.0
Nevada	17	46	1	0	49	1.0	1.0	1.0	1.0	1.0
New Hampshire	5	16	3	0	61	1.0	1.0	1.0	1.0	1.0
New Jersey	15	56	23	0	63	1.0	1.0	1.0	1.0	1.0
New Mexico	40	164	15	0	144	1.0	1.0	1.0	1.0	1.0
New York	57	142	8	2	353	1.0	1.0	1.0	1.0	1.0
North Carolina	82	268	80	2	531	1.0	1.0	1.0	1.0	1.0
North Dakota	11	87	1	0	253	1.0	1.0	1.0	1.0	1.0
Ohio	255	509	44	3	1443	1.0	1.0	1.0	1.0	1.0
Oklahoma	72	197	38	4	140	1.0	1.0	1.0	1.0	1.0
Oregon	55	26	17	0	25	1.0	1.0	1.0	1.0	1.0
Pennsylvania	121	313	48	1	1094	1.0	1.0	1.0	1.0	1.0
Rhode Island	3	3	3	0	2	1.0	1.0	1.0	1.0	1.0
South Carolina	61	135	33	1	268	1.0	1.0	1.0	1.0	1.0
South Dakota	1	29	2	0	28	1.0	1.0	1.0	1.0	1.0
Tennessee	128	271	95	2	539	1.0	1.0	1.0	1.0	1.0
Texas	403	861	187	2	977	1.0	1.0	1.0	1.0	1.0
Utah	41	99	9	1	42	1.0	1.0	1.0	1.0	1.0
Vermont	2	1	2	0	1	1.0	1.0	1.0	1.0	1.0
Virginia	76	174	50	1	303	1.0	1.0	1.0	1.0	1.0
Washington	187	55	19	4	127	1.0	1.0	1.0	1.0	1.0
West Virginia	112	338	21	0	753	1.0	1.0	1.0	1.0	1.0
Wisconsin	52	151	40	1	281	1.0	1.0	1.0	1.0	1.0
Wyoming	54	131	17	1	137	1.0	1.0	1.0	1.0	1.0

Summary of mobile source emissions by state in the regional domain for the current base-case (left), and the projected future case to current case emission ratios (right).

	Mobile Source Emission					Future/Current Emission Ratio				
(Kilotons/year)	CO	NOX	VOC	NH3	SO2	CO	NOX	VOC	NH3	SO2
Alabama	1402	162	120	5	6	1.0	1.0	1.0	1.0	1.0
Arizona	1010	161	93	5	6	1.0	1.0	1.0	1.0	1.0
Arkansas	793	100	64	3	4	1.0	1.0	1.0	1.0	1.0
California	5648	697	562	28	11	1.0	1.0	1.0	1.0	1.0
Colorado	1177	123	84	4	5	1.0	1.0	1.0	1.0	1.0
Connecticut	721	88	53	3	3	1.0	1.0	1.0	1.0	1.0
Delaware	191	26	16	1	1	1.0	1.0	1.0	1.0	1.0
Washington DC	83	9	7	0	0	1.0	1.0	1.0	1.0	1.0
Florida	3331	419	324	14	16	0.9	0.9	0.8	0.9	0.9
Georgia	2508	311	206	10	12	1.0	1.0	1.0	1.0	1.0
Idaho	389	49	29	1	2	1.0	1.0	1.0	1.0	1.0
Illinois	2658	317	213	10	12	1.0	1.0	1.0	1.0	1.0
Indiana	1903	233	150	7	9	1.0	1.0	1.0	1.0	1.0
Iowa	850	102	62	3	4	1.0	1.0	1.0	1.0	1.0
Kansas	763	93	58	3	3	1.0	1.0	1.0	1.0	1.0
Kentucky	1218	161	97	5	6	1.0	1.0	1.0	1.0	1.0
Louisiana	1070	137	91	4	5	1.0	1.0	1.0	1.0	1.0
Maine	285	28	19	1	1	1.1	1.1	1.1	1.1	1.1
Maryland	1184	149	91	5	6	1.0	1.0	1.0	1.0	1.0
Massachusetts	1316	153	100	5	6	1.0	1.0	1.0	1.0	1.0
Michigan	2824	309	211	9	11	1.0	1.0	1.0	1.0	1.0
Minnesota	1473	171	106	5	6	1.0	1.0	1.0	1.0	1.0
Mississippi	826	126	74	3	4	1.0	1.0	1.0	1.0	1.0
Missouri	1658	215	137	7	8	1.0	1.0	1.0	1.0	1.0
Montana	289	36	20	1	1	1.0	1.0	1.0	1.0	1.0
Nebraska	516	63	38	2	2	1.0	1.0	1.0	1.0	1.0
Nevada	452	53	40	2	2	1.0	1.0	1.0	1.0	1.0
New Hampshire	343	42	24	1	1	1.0	1.0	1.0	1.0	1.0
New Jersey	1478	191	124	7	7	1.0	1.0	1.0	1.0	1.0
New Mexico	669	77	51	2	3	1.0	1.0	1.0	1.0	1.0
New York	3345	385	258	12	15	1.0	1.0	1.0	1.0	1.0
North Carolina	2237	284	186	9	11	1.0	1.0	1.0	1.0	1.0
North Dakota	228	27	16	1	1	1.0	1.0	1.0	1.0	1.0
Ohio	2894	333	218	10	13	1.0	1.0	1.0	1.0	1.0
Oklahoma	1115	138	95	4	5	1.0	1.0	1.0	1.0	1.0
Oregon	1009	137	96	3	4	0.9	0.9	0.9	0.9	0.9
Pennsylvania	2735	330	209	10	12	1.0	1.0	1.0	1.0	1.0
Rhode Island	199	24	16	1	1	1.0	1.0	1.0	1.0	1.0
South Carolina	1200	153	97	4	6	1.0	1.0	1.0	1.0	1.0
South Dakota	242	30	17	1	1	1.0	1.0	1.0	1.0	1.0
Tennessee	1685	210	138	6	8	1.0	1.0	1.0	1.0	1.0
Texas	4746	622	445	20	24	1.0	1.0	0.9	1.0	1.0
Utah	622	66	47	2	3	1.0	1.0	1.0	1.0	1.0
Vermont	216	24	15	1	1	1.0	1.0	1.0	1.0	1.0
Virginia	1881	194	147	7	8	1.0	1.0	1.0	1.0	1.0
Washington	1365	161	102	5	6	1.0	1.0	1.0	1.0	1.0
West Virginia	493	57	37	2	2	1.0	1.0	1.0	1.0	1.0
Wisconsin	1542	189	114	6	7	1.0	1.0	1.0	1.0	1.0
Wyoming	238	29	16	1	1	1.0	1.0	1.0	1.0	1.0

Summary of non-road mobile source emissions by state in the regional domain for the current base-case (left), and the projected future case to current case emission ratios (right).

	Non-Road Mobile Source Emission					Future/Current Emission Ratio				
(Kilotons/year)	CO	NOX	VOC	NH3	SO2	CO	NOX	VOC	NH3	SO2
Alabama	357	57	46	0	7	1.2	1.0	1.5	1.1	1.5
Arizona	478	54	45	0	5	1.1	1.0	1.3	1.1	1.0
Arkansas	216	65	30	0	7	1.2	1.0	1.4	1.1	1.3
California	1150	362	173	0	53	1.5	1.1	1.6	1.1	1.2
Colorado	383	52	37	0	5	1.1	1.0	1.2	1.0	1.1
Connecticut	289	23	29	0	2	1.1	1.2	1.4	1.1	1.3
Delaware	78	9	11	0	2	1.2	1.3	1.6	1.2	1.6
Washington DC	15	3	1	0	0	1.1	1.0	1.3	1.0	1.0
Florida	1642	141	188	0	17	1.2	1.3	1.5	1.2	1.5
Georgia	686	91	67	0	8	1.1	1.2	1.3	1.1	1.2
Idaho	136	26	21	0	2	1.1	0.9	1.3	1.1	1.0
Illinois	997	191	97	0	20	1.1	1.1	1.3	1.0	1.2
Indiana	532	109	49	0	12	1.1	1.1	1.2	1.0	1.3
Iowa	312	87	36	0	9	1.1	1.0	1.2	1.0	1.0
Kansas	264	85	25	0	8	1.1	0.9	1.2	1.0	0.9
Kentucky	282	91	34	0	12	1.2	1.2	1.4	1.1	1.9
Louisiana	383	238	57	0	34	1.2	1.5	1.6	1.2	2.3
Maine	96	12	16	0	2	1.1	1.3	1.2	1.1	1.7
Maryland	441	44	46	0	5	1.1	1.2	1.4	1.1	1.4
Massachusetts	476	66	44	0	8	1.1	1.1	1.3	1.0	1.2
Michigan	963	82	141	0	13	1.1	1.1	1.3	1.1	1.4
Minnesota	556	115	100	0	13	1.2	1.1	1.3	1.1	1.2
Mississippi	207	73	31	0	10	1.2	1.2	1.5	1.1	1.9
Missouri	482	121	56	0	12	1.1	1.1	1.4	1.1	1.3
Montana	92	66	13	0	5	1.1	0.8	1.1	1.0	0.9
Nebraska	184	95	20	0	8	1.1	0.9	1.2	1.0	0.9
Nevada	163	26	17	0	3	1.1	1.1	1.3	1.1	1.1
New Hampshire	123	9	18	0	1	1.2	1.2	1.4	1.2	1.2
New Jersey	696	57	70	0	6	1.1	1.2	1.4	1.1	1.4
New Mexico	117	40	13	0	3	1.1	0.8	1.2	1.1	0.9
New York	1215	156	134	0	18	1.1	1.2	1.4	1.1	1.3
North Carolina	707	76	72	0	7	1.1	1.1	1.4	1.1	1.1
North Dakota	102	58	14	0	6	1.1	0.9	1.1	1.0	1.0
Ohio	1027	167	101	0	18	1.1	1.1	1.3	1.1	1.4
Oklahoma	284	54	31	0	5	1.1	0.9	1.4	1.1	1.0
Oregon	327	50	37	0	6	1.1	1.1	1.3	1.1	1.4
Pennsylvania	918	124	88	0	13	1.1	1.1	1.2	1.1	1.3
Rhode Island	75	6	7	0	1	1.1	1.3	1.4	1.1	1.5
South Carolina	363	44	42	0	5	1.2	1.1	1.5	1.1	1.4
South Dakota	90	32	12	0	3	1.1	1.0	1.2	1.0	1.0
Tennessee	437	90	50	0	10	1.1	1.1	1.4	1.1	1.5
Texas	1696	297	152	0	41	1.1	1.1	1.3	1.1	1.5
Utah	192	41	25	0	4	1.1	1.0	1.3	1.0	1.0
Vermont	59	4	9	0	0	1.1	1.1	1.2	1.1	1.1
Virginia	576	58	58	0	9	1.1	1.1	1.4	1.1	1.3
Washington	509	91	59	0	10	1.1	1.2	1.4	1.1	1.5
West Virginia	114	41	15	0	5	1.1	1.2	1.3	1.1	1.8
Wisconsin	549	66	80	0	7	1.1	1.0	1.3	1.1	1.1
Wyoming	56	31	9	0	2	1.1	0.8	1.2	1.1	0.8

Summary of area source emissions by state in the regional domain for the current base-case (left), and the projected future case to current case emission ratios (right).

	Area Source Emission					Future/Current Emission Ratio				
(Kilotons/year)	CO	NOX	VOC	NH3	SO2	CO	NOX	VOC	NH3	SO2
Alabama	1071	39	327	81	44	1.10	1.27	1.65	2.50	0.98
Arizona	495	64	123	30	6	1.16	1.66	1.86	2.28	1.05
Arkansas	172	37	109	144	18	1.16	1.68	2.07	2.52	2.61
California	1263	161	516	190	25	1.37	1.65	2.33	2.43	1.33
Colorado	187	14	101	108	2	1.09	1.47	1.59	2.26	1.68
Connecticut	187	15	100	5	12	1.02	1.28	1.63	2.29	0.96
Delaware	23	4	15	10	10	1.76	2.13	2.38	2.50	2.60
Washington DC	6	2	10	1	6	1.75	2.11	1.88	1.80	1.87
Florida	2185	76	417	79	48	1.16	1.41	2.04	2.36	2.38
Georgia	757	42	239	87	7	1.38	1.70	2.11	2.48	1.70
Idaho	829	46	274	71	6	1.66	2.09	2.71	2.46	1.22
Illinois	137	39	304	117	38	1.69	1.61	2.25	2.52	2.23
Indiana	213	44	250	94	9	1.66	1.36	2.35	2.52	1.25
Iowa	76	29	132	291	23	1.07	1.68	1.87	2.57	1.14
Kansas	95	15	98	226	4	1.62	1.58	1.88	2.53	1.66
Kentucky	242	77	135	90	55	1.36	1.58	1.95	2.51	1.13
Louisiana	226	95	126	66	81	1.35	1.73	1.95	2.82	2.50
Maine	21	7	34	4	11	0.98	1.05	2.77	2.41	1.20
Maryland	119	17	136	23	39	1.78	1.77	1.96	2.50	2.06
Massachusetts	267	28	160	8	63	1.22	1.43	1.86	2.17	1.82
Michigan	173	49	336	60	32	1.41	1.55	1.85	2.49	1.53
Minnesota	425	24	183	188	6	1.02	1.41	1.65	2.53	1.31
Mississippi	264	9	145	72	1	1.45	1.60	2.04	2.51	1.23
Missouri	261	39	255	194	32	1.09	1.30	1.50	2.54	1.38
Montana	166	15	53	94	2	1.13	1.77	1.63	2.51	1.10
Nebraska	48	14	74	243	9	1.05	1.69	1.83	2.53	2.12
Nevada	648	21	65	18	7	1.04	1.22	1.49	2.07	1.40
New Hampshire	78	6	56	2	10	1.18	1.29	1.50	2.39	1.27
New Jersey	181	39	175	9	46	1.23	1.30	1.87	2.20	1.37
New Mexico	282	30	63	49	9	1.12	1.86	1.97	2.49	0.81
New York	455	64	412	59	148	1.16	1.11	1.71	2.40	1.09
North Carolina	794	29	311	182	32	1.53	1.51	1.97	2.52	1.29
North Dakota	50	19	62	91	54	0.97	1.36	1.42	2.53	0.98
Ohio	220	61	303	72	63	1.56	1.46	2.28	2.51	1.43
Oklahoma	141	35	141	207	5	1.17	1.54	2.08	2.57	1.90
Oregon	356	30	317	63	21	1.35	1.65	1.98	2.46	1.42
Pennsylvania	339	56	301	80	91	1.23	1.40	1.89	2.48	1.34
Rhode Island	8	5	34	0	5	1.37	1.70	1.13	2.31	1.12
South Carolina	473	25	194	30	15	1.58	1.59	2.28	2.49	1.22
South Dakota	78	7	44	145	19	0.98	1.25	1.48	2.52	1.18
Tennessee	185	26	214	77	41	1.70	1.79	2.39	2.54	1.48
Texas	727	49	561	489	7	1.27	1.56	2.09	2.51	1.76
Utah	396	27	83	36	11	1.38	1.85	2.15	2.48	1.18
Vermont	52	4	29	9	7	1.06	1.47	1.59	2.51	1.64
Virginia	253	46	159	67	15	1.71	1.61	2.03	2.51	1.60
Washington	229	20	126	48	3	1.69	1.80	2.30	2.56	1.20
West Virginia	119	14	87	17	12	1.37	1.69	1.84	2.51	1.47
Wisconsin	293	30	187	101	41	1.79	1.45	2.36	2.52	2.10
Wyoming	100	62	23	53	15	1.18	2.02	1.63	2.52	1.09

Summary of wild-fire emissions by state in the regional domain for the current base-case (left), and the projected future case to current case emission ratios (right).

	Wild Fire Source Emission		Future/Current Emission Ratio	
(Kilotons/year)	CO	VOC	CO	VOC
Alabama	0.6	0.0	1.0	1.0
Arizona	49.6	4.1	0.1	0.1
Arkansas	0.6	0.1	1.0	1.0
California	294.7	23.9	0.2	0.2
Colorado	6.6	0.5	1.3	1.3
Connecticut	0.0	0.0		
Delaware	0.0	0.0		
Washington DC	0.0	0.0		
Florida	45.1	3.5	1.0	0.9
Georgia	0.5	0.0	1.0	1.0
Idaho	23.1	1.8	2.5	2.5
Illinois	0.1	0.0	1.0	1.0
Indiana	0.0	0.0	1.0	1.0
Iowa	0.1	0.0	1.0	1.0
Kansas	0.2	0.0	1.0	1.0
Kentucky	1.0	0.1	1.0	1.0
Louisiana	0.5	0.0	1.0	1.0
Maine	0.0	0.0	1.0	1.0
Maryland	0.0	0.0	1.0	1.0
Massachusetts	0.0	0.0		
Michigan	0.3	0.0	0.9	0.9
Minnesota	12.6	0.8	0.9	1.0
Mississippi	1.4	0.1	1.0	1.0
Missouri	1.2	0.1	1.0	1.0
Montana	4.9	0.4	11.6	12.7
Nebraska	0.1	0.0	3.5	3.6
Nevada	27.4	2.2	0.3	0.3
New Hampshire	0.0	0.0	1.3	1.4
New Jersey	0.0	0.0	1.0	1.0
New Mexico	20.3	1.7	0.4	0.4
New York	0.0	0.0	1.0	1.0
North Carolina	0.6	0.1	1.0	1.0
North Dakota	0.8	0.1	0.2	0.2
Ohio	0.1	0.0	1.0	1.0
Oklahoma	1.8	0.2	1.0	1.0
Oregon	18.7	1.5	12.2	12.1
Pennsylvania	0.1	0.0	1.0	1.0
Rhode Island	0.0	0.0		
South Carolina	0.4	0.0	1.0	1.0
South Dakota	1.7	0.1	0.1	0.1
Tennessee	0.5	0.0	1.0	1.0
Texas	1.6	0.1	0.8	0.8
Utah	11.1	0.9	1.3	1.3
Vermont	0.0	0.0	1.3	1.4
Virginia	0.9	0.1	1.0	1.0
Washington	2.8	0.2	45.7	47.2
West Virginia	0.0	0.0	1.0	1.0
Wisconsin	0.1	0.0	1.1	1.1
Wyoming	2.7	0.2	3.4	3.6

Summary of July biogenic emissions by state in the regional domain for the current base-case (left), and the projected future case to current case emission ratios (right).

	Biogenic Source Emission					Future/Current Emission Ratio				
(Kilotons//July)	ISO	MTP	OVOC	NO	VOC	ISO	MTP	OVOC	NO	VOC
Alabama	147	65	59	1.2	270	0.2	0.5	0.9	1.0	0.4
Arkansas	166	55	58	1.9	279	0.3	0.4	0.8	1.0	0.4
Arizona	25	2	7	1.8	34	1.1	1.1	0.8	1.0	1.0
California	109	26	31	3.9	166	0.4	0.6	0.9	1.0	0.5
Colorado	29	4	9	2.7	42	0.8	0.8	0.9	1.0	0.8
Connecticut	6	1	2	0.0	10	0.6	0.7	1.0	1.1	0.7
Washington DC	0	0	0	0.0	0					
Delaware	2	1	1	0.1	3	0.5	0.6	1.1	1.1	0.7
Florida	36	20	20	2.3	76	0.3	0.7	1.1	1.0	0.6
Georgia	119	55	51	1.9	226	0.2	0.5	0.9	1.0	0.5
Iowa	7	4	15	5.2	27	0.3	1.2	1.2	1.1	0.9
Idaho	12	9	12	1.5	33	0.7	0.8	1.0	1.1	0.8
Illinois	29	8	21	4.8	58	0.3	0.8	1.1	1.1	0.7
Indiana	18	6	15	2.9	39	0.3	0.7	1.0	1.1	0.6
Kansas	13	3	11	6.9	27	0.1	1.3	1.1	1.0	0.6
Kentucky	72	15	34	1.8	120	0.6	0.7	1.0	1.0	0.7
Louisiana	86	36	33	1.6	155	0.2	0.5	0.9	1.0	0.4
Massachusetts	16	4	6	0.1	27	0.5	0.7	1.0	1.1	0.7
Maryland	20	4	7	0.3	31	0.6	0.6	1.1	1.1	0.7
Maine	6	9	9	0.1	24	0.8	1.1	1.3	1.2	1.1
Michigan	32	13	20	1.6	65	0.7	0.8	1.2	1.2	0.9
Minnesota	37	12	23	4.1	72	0.5	0.8	1.1	1.1	0.8
Missouri	139	17	44	3.5	200	0.5	0.8	1.0	1.1	0.7
Mississippi	115	41	44	1.7	200	0.3	0.6	1.0	1.0	0.5
Montana	21	14	17	4.2	53	0.3	0.6	0.9	1.1	0.6
North Carolina	108	44	46	1.4	198	0.3	0.5	0.9	1.0	0.5
North Dakota	5	2	7	4.3	14	0.1	1.2	1.3	1.1	0.8
Nebraska	7	2	9	5.8	18	0.1	1.5	1.3	1.1	0.8
New Hampshire	11	7	7	0.1	25	0.7	0.8	1.1	1.1	0.9
New Jersey	11	3	5	0.2	20	0.3	0.5	0.9	1.1	0.5
New Mexico	24	2	7	2.8	33	1.0	0.9	0.7	1.0	1.0
Nevada	11	1	3	1.0	16	1.3	0.9	0.7	1.0	1.1
New York	31	19	30	0.9	80	0.7	0.8	1.1	1.1	0.8
Ohio	30	10	21	2.2	60	0.3	0.6	1.0	1.1	0.6
Oklahoma	58	11	23	4.8	92	0.3	0.6	0.9	1.0	0.5
Oregon	23	20	24	1.1	67	0.7	0.7	0.9	1.0	0.7
Pennsylvania	78	20	34	1.2	132	0.3	0.5	0.9	1.1	0.5
Puerto Rico	0	0	0	0.0	0					
Rhode Island	1	0	0	0.0	1	1.0	0.7	1.3	1.1	1.0
South Carolina	66	30	27	1.0	123	0.2	0.5	0.9	1.0	0.4
South Dakota	8	3	7	4.6	18	0.1	1.0	1.3	1.1	0.7
Tennessee	97	20	36	1.5	153	0.5	0.6	0.9	1.0	0.6
Texas	155	35	64	19.6	254	0.3	0.7	0.9	1.0	0.5
Utah	13	1	4	0.9	17	1.2	1.1	0.9	1.0	1.1
Virginia	133	29	42	1.0	204	0.6	0.6	1.0	1.0	0.7
Vermont	4	4	6	0.1	14	0.8	0.9	1.2	1.1	1.0
Washington	15	17	22	1.5	54	0.6	0.6	0.9	1.1	0.7
Wisconsin	34	12	21	2.6	67	0.6	0.8	1.1	1.1	0.8
West Virginia	73	11	24	0.3	109	0.5	0.7	0.9	1.0	0.6